Fuel cell combined cycles

Comparative analysis of diesel- and methanol-fuelled SOFC-ICE and SOFC-GT combined cycles for application on naval surface combatants

R. Wijnker

TU Delft

DAMEN NAVAL

Thesis for the degree of MSc in Marine Technology in the specializations of Marine Engineering and Ship Design

Fuel cell combined cycles

Comparative analysis of diesel- and methanol-fuelled SOFC-ICE and SOFC-GT combined cycles for application on naval surface combatants

by

R. Wijnker

Performed at

Damen Naval

This thesis (MT.24/25.040.M) is classified as confidential in accordance with the general conditions for projects performed by the TUDelft

23-06-2025

Company supervisors

Daily supervisor:	Ir. S. Knegt
Daily Supervisor:	Ir. G.J. Meijn

Thesis exam committee

Chair:	Dr. ir. L. van Biert
Staff Member:	N.G.H. Goselink, MSc, BA
Staff Member:	Dr. ir. P. de Vos
Company Member:	Ir. G.J. Meijn
Company Member:	Ir. S. Knegt

Author Details

Studynumber:	4588800
Author contact e-mail:	

Cover Image: SIGMA Class Multi-Mission Frigate, adapted from [1]

An electronic version of this thesis is available at https://repository.tudelft.nl/

TU Delft

DAMEN NAVAL

Preface

Before you lies my thesis for the degree of Master of Science in Marine Technology, marking the end of my time as a student at Delft University of Technology. After nine years of studying, I am proud to finally take the next step into my professional career. This thesis could not have been written without the support of many individuals, and I would like to express my sincere gratitude to everyone who contributed in any way.

First and foremost, I would like to thank my supervisors at Damen Naval, Sander Knegt and Gert-Jan Meijn, for their excellent guidance throughout the research process. What began as a vague idea without a clear end goal gradually took shape thanks to their valuable feedback and advice, ultimately resulting in the work presented here.

I am also grateful to my academic supervisors at Delft University of Technology, Lindert van Biert and Niek Goselink, for their time, insights, and constructive feedback. A special thanks to Niek for helping me understand Cycle-Tempo. Before this research, I was unfamiliar with the software, and his experience and advice were extremely helpful in learning how to use it and in developing the combined cycle models. I would also like to thank Peter de Vos for being part of my thesis assessment committee.

Special thanks go to Simon Bedert, Pieter Maljaars, Johan van der Vorst, Arno Berghuis, Sander Knegt, and Gert-Jan Meijn for sharing their expert opinions through the survey conducted at Damen Naval. Their input was invaluable in identifying the most suitable fuels for this research.

I would also like to thank my fellow interns at Damen Naval for the great company and shared laughs, which brought some much-needed balance to the long days of thesis writing.

Finally, to you, the reader — thank you for your interest in my thesis. I hope it provides the insights and information you are looking for.

R. Wijnker
Delft, June 2025

Summary

Throughout current literature, different combinations between fuel cell type, heat engine type and fuel have been considered. Most studies focus on one combination, and operating conditions (fuel cell temperature, fuel cell pressure, cell voltage, fuel utilization factor, etc.) vary throughout these studies. Due to these variations in operating conditions, as well as differences in integration strategy, it is difficult to select a single combination to be the most suitable for marine applications. Additionally, current literature primarily focusses on maximizing system efficiency. Other factors such as system size, weight, IR signature and acoustic emissions are less frequently discussed in current literature. System size and weight are important factors for the feasibility of the combined cycles in current vessel designs, and the IR signature and acoustic emissions are important criteria for naval applications.

In this thesis, a solid oxide fuel cell (SOFC) is combined with an internal combustion engine (ICE) or a gas turbine (GT), and the system is fuelled by diesel or methanol (MeOH). This results in the following four combined cycles:

- Diesel-fuelled SOFC-ICE
- Diesel-fuelled SOFC-GT
- MeOH-fuelled SOFC-ICE
- MeOH-fuelled SOFC-GT

These combinations are compared for naval surface combatants based on system efficiency, annual energy consumption, annual CO_2 emissions, exhaust gas temperature, total system weight and total system volume. Additionally, the combined cycles are compared to the current power generation system of a SIGMA surface combatant to determine the relative performance of the combined cycles to a conventional heat engine.

To determine the annual energy consumption, CO_2 emissions and exhaust temperature, the combined cycles are modelled in Cycle-Tempo. The SOFC, ICE and GT are modelled as individual models and validated with available reference data. These individual models are then combined into a single model for each combined cycle, which is validated by comparing the results with results from current literature. The size and weight of the system is then obtained by selecting readily available components and summing their dimensions and weights.

For each comparison criteria, a different combined cycle performs the best. To minimize annual energy consumption, total system weight and total system volume, the diesel-fuelled SOFC-ICE combined cycle performs the best. To minimize exhaust gas temperature, the diesel-fuelled SOFC-GT combined cycle is the best choice. To minimize annual CO_2 emissions, the MeOH-fuelled SOFC-ICE combined cycle is preferred. The exact performance of the combined cycles for these comparison criteria, depends on the power split between the SOFC and the heat engine. The annual energy consumption for the diesel-fuelled SOFC-ICE is between 4.4% (for a power split of 4.6-95.4) and 18.2% (for a power split of 25-75) lower than the current system of the SIGMA. The weight of this system is between 1.5% lighter (for a power split of 4.6-95.4) and 51.6% heavier (for a power split of 30-70) compared to the current system. For both the diesel-fuelled combined cycles, the exhaust temperature at silent speed can be reduced by 212 °C, which is a reduction of 58.3% compared to the current system. At cruising speed, the diesel-fuelled SOFC-GT can reduce the exhaust temperature with up to 207 °C at a power split of 30-70, which is a reduction of 65.8% compared to the current system. When using the MeOH-fuelled SOFC-ICE combined cycle, the annual CO_2 emissions can be reduced by up to 25.9% compared to the current system for a power split of 25-75.

Depending on the preferred comparison criteria (annual energy consumption, emissions, exhaust temperature or system weight and volume), a different combined cycle and power split is preferred. There is no single solution that performs best for all criteria. It is therefore up to the designer to choose which criteria is most important and select the combined cycle accordingly. For this thesis, annual energy consumption and total system weight and volume are considered most important. For the combined cycles, a trade-off needs to be made between these criteria. A higher power split results generally in a lower annual energy consumption, but this also leads to a higher system weight and volume. To select the best power split for the SIGMA, a utopian solution is defined. This solution consists of the lowest annual energy consumption and the lowest system weight. This solution is

impossible to reach, and the combined cycle and power split that lies closest to this utopian solution is deemed the best. This best solution is the diesel-fuelled SOFC-ICE combined cycle with a power split of 8.4-91.6 in favour of the ICE.

The diesel-fuelled SOFC-ICE combined cycle is implemented in the general arrangement plan of the SIGMA to assess the feasibility of this system in terms of system volume. The current power generation system (ICEs and diesel gensets) are removed, and the new components for the combined cycles are placed in the newly available space in the vessel. In the current general arrangement of the vessel, a maximum power split of 7.8-92.2 in favour of the ICE can be placed without having to change the design of the vessel. This power split is slightly lower than the ideal power split of 8.4-91.6. This lower power split results in a slightly higher annual energy consumption and slightly lower system weight and volume compared to the ideal power split. Compared to the current system of the SIGMA, the diesel-fuelled SOFC-ICE combined cycle with a power split of 7.8-91.2 can reduce the annual energy consumption and CO_2 emissions by about 6%. The exhaust temperature at silent speed reduces by about 212 °C (about 58%) and by about 80 °C (about 25%) at cruising speed. This reduction in energy consumption, CO_2 emissions and exhaust temperature comes at the cost of a 4% increase in total system weight.

Overall, fuel cell combined cycles can help in reducing the fuel consumption and GHG emissions of the marine sector. Nevertheless, the implementation of fuel cell combined cycles alone is insufficient to reach the net-zero targets set by the IMO as outlined in [2]. For naval surface combatants, the combined cycles only reach a small reduction in fuel consumption and CO_2 emissions (6%). The main benefit for these vessels lies in the reduction in exhaust gas temperature. A significant reduction in exhaust gas temperature (58% at silent speed and 25% at cruising speed), and therefore a reduced IR-signature, is possible with a system small enough to still fit in the current design of the SIGMA.

Contents

List of Figures

List of Tables

Nomenclature

Abbreviations

AAW	anti-aircraft warfare
AC	alternating current
AOG	anode off-gas
Ar	argon
ASuW	anti-surface warfare
ASW	anti-submarine warfare
CH_4	methane
CI	compression ignition
CO	carbon monoxide
CO_2	carbon dioxide
COG	cathode off-gas
CT	Cycle-Tempo
DC	direct current
DIR	direct internal reforming
GHG	greenhouse gas
GT	gas turbine
H_2	hydrogen
H_2O	water
HCCI	homogeneous charge compression ignition
HEX	heat exchangers
HSC	high-end surface combatant
HVO	hydrotreated vegetable oil
ICE	internal combustion engine
IIR	indirect internal reforming
IMO	International Maritime Organisation
IR	infra-red
LHV	lower heating value
LNG	liquefied natural gas
LPD	landing platform dock
LPG	liquefied petroleum gas
MCFC	molten carbonate fuel cell
MeOH	methanol
N_2	nitrogen
NATO	North Atlantic Treaty Organization
NG	natural gas
NH_3	ammonia
NO_x	nitrogen oxide
O_2	oxygen
OPV	oceangoing patrol vessel
ORC	organic Rankine cycle
PEMFC	proton exchange membrane fuel cell
PM	particulate matter
RO	reverse osmosis
SOFC	solid oxide fuel cell
SO_x	sulphur oxide
SRC	steam Rankine cycle
TRL	technology readiness level
UHC	unburnt hydrocarbons

Symbols

Symbol	Definition	Unit
A/F	Air-to-fuel ratio	-
c_p	Specific heat	kJ/kgK
E	Energy	kJ/s
m	Mass	ton
$\dot{m}$	Mass flow	kg/s
M	Molar mass	kmol/kg
n	Polytropic exponent	-
p	Pressure	bar
P	Power	kW
R	Range	NM
t	Time spent	s/year
T	Temperature	°C
TR	Temperature ratio	-
u_f	Fuel utilization factor	-
v	Ship speed	NM/hr
V	Volume	m^3
x	Molar fraction	-
Δ	Difference	-
η	Efficiency	-
λ	Air-excess ratio	-
Π	Pressure ratio	-
ρ	Density	ton/m^3

Subscript	Definition
an	Anode
ca	Cathode
$cell$	Individual fuel cell
$comb$	Combined
$compr$	Compressor
$cruising$	Cruising speed
$e-motor$	Electric motor
exh	Exhaust
HEX	Heat exchanger
in	Input
is	Isentropic
m	Mechanical
out	Output
$reform$	Reformer
$silent$	Silent operation
$stack$	Fuel cell stack
$stoich$	Stoichiometric
top	Top speed
$turb$	Turbine

1

Introduction

Shipping contributes to about 3% of the global greenhouse gas (GHG) emissions [3]. To reduce this contribution, the International Maritime Organisation (IMO) has set targets to reduce the GHG emissions from shipping to net-zero in 2050 [2]. To reach this target, technological innovation and supportive policies are necessary [4]. Among the technical innovations, fuel cells are considered as promising for the marine sector due to their higher efficiencies compared to conventional diesel engines and gas turbines [5]. Besides higher efficiencies, fuel cells offer the possibility to reduce noise and vibrations due to a reduction in moving components compared to conventional heat engines [5, 6]. Compared to a conventional diesel generator, fuel cells can reduce the acoustic emissions by 50 dB [7], making them particularly interesting for naval vessels. In these vessels, acoustic emissions need to be minimized to avoid detection by enemy vessels [8]. Additionally, fuel cells can contribute to a reduction in infra-red (IR)-signature of the vessel through waste heat recovery [6]. This reduction in IR-signature decreases the likelyhood of detection by enemy vessels, and decreases the risk of being hit by enemy missiles using IR-targeting [8].

However, there are a few drawbacks to using fuel cells. The main issues are the power density and transient load response [5, 9, 10]. When pairing high-temperature fuel cells with heat engines, the transient load response improves and the power density of the system increases [10]. Additionally, the system efficiency of these combined cycles can reach values surpassing 70% [11, 12]. If waste heat is recovered in the combined cycle system, the IR-signature of the vessel can also be reduced. However, these combined cycles still include conventional heat engines, reducing the benefits in terms of acoustic emissions.

The high system efficiency, increased power density, improved transient load response, and possibility for waste heat recovery make fuel cell combined cycles an interesting solution to reduce the fuel consumption, GHG emissions and IR-signature of naval vessels. The focus of this thesis is therefore to compare fuel cell combined cycles with current solutions, and determine the relative performance gain in terms of fuel consumption and vessel signature (GHG emissions and IR-signature).

1.1. Problem definition

Numerous studies have been conducted on the performance of fuel cell combined cycles. Different fuel cells (proton exchange membrane fuel cell (PEMFC), solid oxide fuel cell (SOFC) and molten carbonate fuel cell (MCFC)) are combined with different heat engines (internal combustion engine (ICE), gas turbine (GT), organic Rankine cycle (ORC) and steam Rankine cycle (SRC)), and many different fuels are considered (diesel, methanol (MeOH), liquefied natural gas (LNG), natural gas (NG), methane (CH_4), hydrogen (H_2), ammonia (NH_3)). However, many of these studies focus only on one combination of fuel and combined cycle, and each study has slight differences in integration strategy and operating parameters (temperature, pressure, fuel utilization, cell voltage, etc.). These differences make it challenging to compare the different studies with each other, and to determine which combination of combined cycle and fuel is most promising for the maritime sector. Additionally, the research on combined cycles focussing on naval vessels is limited, and important factors for these vessels such as IR-signature and acoustic emissions are not considered in current literature.

Moreover, the combined cycles are typically optimized for system performance, and the sizing of the system is often ignored. Some studies [13–15] state that the size and weight of the system increase compared to

conventional heat engines, but these studies often ignore the effect of this increase on the design and operation of the vessel. Combined cycles can reach net electrical efficiencies of up to 70% [12], whereas conventional heat engines only reach up to 50% [16]. However, these efficiencies are obtained for a large contribution of the fuel cell to the total power, which results in a large and heavy system. An increase in system weight and volume may mean that the overall weight of size of the vessel increasses when accomodating the combined cycle. This increase in weight or size of the vessel may lead to an increase in ship resistance, and therefore fuel consumption, (partly) negating the improved efficiency of the combined cycles.

1.2. Research objective

Due to the lack of research on combined cycles for naval vessels, this thesis focusses on the application of combined cycles on these type of vessels. Different combinations of combined cycles and fuels are evaluated at the same operating conditions and integration strategy, and these combinations are compared based on system efficiency, annual energy consumption, annual GHG emissions, IR-signature, system weight and volume. By using the same integration strategy and operating conditions for each combined cycle and fuel, a direct comparison between the systems can be made, and the best system can be selected for naval vessels. To check whether the considered combinations are actually beneficial for naval vessels, the combinations are also compared to the current power plant of a reference vessel. After comparing the systems with the current power plant, the best performing solution is determined, and then drawn in the general arrangement of the reference vessel. This implementation step ensures the feasibility of the best system in terms of available space in the vessel.

1.3. Scope

The goal of this thesis is to compare different combinations of fuel and combined cycles for application on naval surface combatants. In the timeframe of the master thesis, it is not possible to evaluate every possible combined cycle and fuel. For this thesis, only diesel and MeOH and only the combined cycles where an SOFC is combined with an ICE or GT are considered, and these combinations are shown in Table 1.1. For a detailed explanation on why these fuels and combined cycles are chosen, the reader is directed to chapter 2.

In naval vessels operated by North Atlantic Treaty Organization (NATO) members, the diesel is standardized as NATO F-76 fuel. This fuel contains a maximum of 0.5% sulphur, which has significant poisoning effects on the fuel cell [5, 17]. Several desulphurization processess are possible, but, to the extent of the authors knowledge, none of these processess are available as onboard systems. For the purpose of this thesis, the desulphurization process is assumed to take place onshore, and desulphurized diesel enters the fuel tanks of the vessel.

Table 1.1: Combinations of combined cycle and fuel considered in this thesis

Combined cycle	Fuel
SOFC-ICE	Diesel
	MeOH
SOFC-GT	Diesel
	MeOH

To reach a complete picture of the performance of the different systems, they have to be evaluated for every possible operating mode of the vessel. These operating modes are generally captured in an operational profile of a vessel, in which the power demand is related to operating time. In the timeframe of the master thesis, it is not feasible to evaluate the four diffferent combinations for every operating mode of the vessel. The operational profile is therefore simplified to only contain three operating modes: silent operation at low speed, sailing at cruising speed and sailing at top speed. The different combinations of combined cycles are evaluated, and conclusions are drawn, based on these three operating modes. The performance of each system is evaluated for different criteria: net electrical efficiency (i.e. fuel consumption), IR signature (i.e. exhaust temperature), GHG emissions (i.e. CO_2 emissions), size and weight. Based on these criteria a best performing system is selected, which will then be drawn in the general arrangement of a naval surface combatant.

1.4. Research questions

The aim of this thesis is to determine how different combined cycles perform compared to eachother, and to implement the best performing system into the design of a naval surface combatant. For this purpose, the following main research question is formulated:

> *How do different combinations of fuel and combined cycle perform in terms of system efficiency, size, weight, IR signature and GHG emissions for a naval surface combatant, how do they compare to the current power generation system of a reference surface combatant, and how can the best-performing system be integrated in the general arrangement of this reference vessel?*

This main research question contains multiple different aspects, and to ensure that every aspect is adressed it is divided into multiple sub-questions:

1. What is the power requirement for the different operating points, and how should this power requirement be split among the fuel cell and the heat engine?
2. What is the overall efficiency and fuel consumption of the different combinations of fuel and combined cycle?
3. How does each combination affect the IR signature and GHG emissions of the vessel?
4. What is the size and weight of each combination?
5. How do the different combinations compare to the current power plant of the vessel, and which system performs the best?
6. How can the best-performing system be implemented in the general arrangement of the vessel?

After answering all of the sub-questions, all of the necessary information is available to write a comprehensive and complete answer to the main research question.

1.4.1. Hypothesis

Based on current literature on combined cycles, a hypothesis for the main research question can be formulated. The combined cycles are evaluated on different criteria, and depending on the criteria a different combined cycle or fuel may be better.

In terms of system efficiency, efficiencies for SOFC-ICE systems are slightly higher than the SOFC-GT systems. Between diesel and MeOH, the reported efficiencies lie close together, and no clear winner can be chosen at this time. For sizing and weight of the systems, GTs offer better power density compared to ICEs. It is therefore expected that the SOFC-GT system outperforms the SOFC-ICE system. Additionally, the energy density of diesel is about twice the energy density of MeOH. If the energy input is kept constant over the different combined cycles, it is expected that the diesel systems perform better in terms of weight. Due to the lower energy density of MeOH, the fuel storage onboard would be twice as large compared to diesel, which increases the overal weight of the system.

The IR-signature of the vessel depends on many factors and the largest contributors are the waste heat and reaction products of the main machinery. The waste heat from the main machinery heats the surrounding steel, creating a hotspot in the ships hull. The reaction products leave the ship through large exhaust funnels, creating a hotspot at the exhaust of the ship. Lastly, the actual exhaust gasses can heat surrounding equipment after leaving the exhaust funnel, creating additional hotspots [18]. Implementing fuel cells in the power plant can help in reducing the temperature of the exhaust gasses leaving the ship, which has a positive impact on the IR-signature of the vessel. Exhaust temperatures for ICEs are generally lower than exhaust temperatures for GTs. It is therefore expected that the SOFC-ICE system performs the best regarding IR-signature. Additionally, MeOH has a lower flame temperature than diesel, which reduces the exhaust temperature for MeOH compared to diesel operation.

GHG emissions largely depend on type of fuel and the amount of fuel used by the system. ICEs have a higher thermal efficiency than GTs, meaning that the ICE consumes less fuel compared to the GT. MeOH produces less GHG when combusted compared to diesel. For this reason it is expected that the MeOH-fuelled SOFC-ICE performs the best in terms of GHG emissions.

Overall, the system efficiency and system weight are the most important criteria in selecting the best system. GHG emissions are directly related to fuel consumption (system efficiency), and IR-signature is highly dependent

on waste heat utilization. IR-signature can also be suppressed by cooling the exhaust gasses before they leave the vessel. A lower exhaust temperature necessitates less cooling, and is therefore favourable for naval vessels. When mostly considering system efficiency and weight and volume, it is expected that the SOFC-ICE system running on diesel will be the best solution due to the higher energy density of the fuel resulting in less fuel storage weight and volume, and the higher efficiency of the ICE compared to a GT.

Lastly, a higher power share of the SOFC is expected to increase the system efficiency, but also increase the system weight. Sapra et al. [13] optimize a SOFC-ICE system running on LNG, and find an optimal power split of 28-72 in favour of the ICE for an oceangoing patrol vessel (OPV). With this power split, the system will be about twice the volume and about 8% heavier compared to a conventional power plant. Due to the large increase in system volume, it is expected that this power split will not fit in a reference vessel. To fit the vessel, it is expected that a lower power split is necessary to be feasible for implementation in a reference vessel. However, it is expected that the combined cycle at this lower power split will still improve the system efficiency, IR signature and GHG emissions compared to a conventional power plant, albeit less than the optimal power split calculated by Sapra et al.

1.5. Outline of the report

Throughout this report, the previously mentioned research questions are answered. First, current literature on SOFC combined cycles is briefly discussed in chapter 2. This chapter also compares the different fuels for these combined cycles for naval application. Next, chapter 3 discusses how the performance of the different combined cycles is assessed. Then, in chapter 4, the models to calculate the performance are created. The performance of the different combined cycles and their performance with respect to the current system is discussed in chapter 5. This chapter also draws conclusions on the best sytem for naval surface combatants. The best system is then drawn in the general arrangment plan of a reference vessel in chapter 6. Lastly, the final conclusions and recommendations are stated in chapter 7 and chapter 8 respectively.

2

SOFC combined cycles in current literature

In current literature, solid oxide fuel cell (SOFC) combined cycles are studied extensively, both for stationary applications and marine applications. In this thesis, combined cycles with a gas turbine (GT) or an internal combustion engine (ICE) are evaluated. These combined cycles (SOFC-GT and SOFC-ICE) are discussed in section 2.1 and section 2.2 respectively. Next, in section 2.3, the different fuels for these combined cycles are addressed, and the most suitable fuels for naval surface combatants are selected.

2.1. SOFC-GT

In current literature, two main system layouts can be identified: pressurized and atmospheric systems (Figure 2.1) [19]. In pressurized systems, also referred to as direct systems, the SOFC is located between the compressor and the turbine of the GT, and operates at elevated pressures. In these systems, the airflow through the compressor of the GT is generally equal to the airflow necessary for the SOFC, resulting in large SOFC power shares (between 80-90%) [20, 21]. This high SOFC power share results in high system efficiencies (up to 80% [22]), but also increase the system weight and volume due to the relatively low energy density of the SOFC compared to the GT.

Atmospheric systems, or indirect systems, operate the SOFC at atmospheric conditions. Waste heat from the SOFC exhaust gas is used to increase the temperature of the air between the compressor and turbine of the GT. Additional fuel can be supplied in a combustor to further increase the turbine inlet temperature and increase the power production of this turbine. In this system, the airflow into the SOFC does not need to match the airflow through the compressor, and smaller SOFC power shares can be used in this system. A lower SOFC power share increases the energy density of the system, but this comes at the cost of a lower system efficiency.

Various studies focus on the performance of pressurized or atmospheric systems, and some are briefly discussed below.

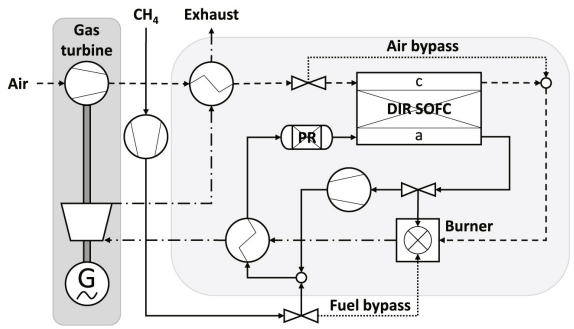

(a) Pressurized SOFC-GT combined cycle

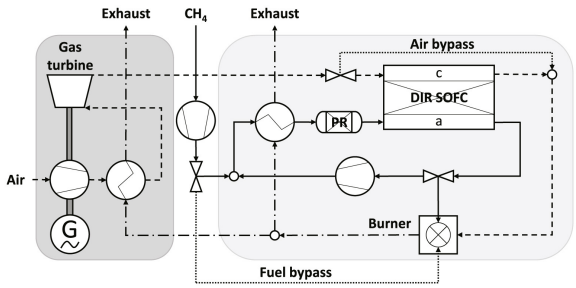

(b) Atmospheric SOFC-GT combined cycle

Figure 2.1: Different SOFC-GT integration strategies [19]

Chan et al. [20] model a pressurized SOFC-GT combined cycle running on NG. In their system, the NG is internally reformed at the anode of the SOFC, and the SOFC produces 80.5% of the total power of the system. With their system, an elctrical efficiency of 61.9% is obtained. When including the heat recovery in the system, the overall system efficiency (electrical+heat) rises to 86.4%.

Zhao et al. [23] model an atmospheric SOFC-GT combined cycle running on syngas produced from coal. With this system, the authors report an electrical efficiency of 57%. This efficiency is slightly lower than the efficiency reported by Chan et al. [20] in the pressurized system. When an SOFC is operated at elevated pressures, the open cell voltage increases. This in turn leads to a higher cell voltage, which increases the electrical efficiency of the fuel cell [24]. This in turn raises the system efficiency of the combined cycle.

Park and Kim [21] compare the performance of a pressurized system with an atmospheric system running on methane (CH_4). The authors report an electrical efficiency of 66.5% for the atmospheric system and an electrical efficiency of 72.5% for the pressurized system. The higher system efficiency for the pressurized system is due to the higher SOFC efficiency at elevated pressures.

Gandiglio et al. [25] also compare the performance of a pressurized and an atmospheric system. Their systems run on NG instead of pure CH_4, resulting in electrical efficiencies of 64.6% and 71.9% for the atmospheric and pressurized system respectively. These values are slighly lower than the reported efficiencies by Park and Kim [21]. This can be explained by a difference in fuel utilization factor of the fuel cell, and differences in mechanical and generator efficiency in the system.

Lastly, van Biert et al. [19] compare the performance of pressurized and atmospheric systems running on CH_4 for different fuel utilization factors, cell voltages, stack temperatures and compression ratios. The authors find that for the pressurized system, a net electrical efficiency of 75.5% can be achieved. When running the same cell voltage and stack tempertature as Park and Kim [21], van Biert et al. obtain system efficiencies differing by 2.4%, which they attribute to differences in fuel utilization, GT power fraction and fuel cell stack power density.

An overview of these studies (and other identified research focusing on SOFC-GT combined cycles) is given in Appendix A. In the studies focussing on SOFC-GT combined cycles, integration strategies, operating parameters and fuel vary. This makes it difficult to compare the different integration strategies and fuels with each other, and to determine which combination is best for shipping applications.

2.2. SOFC-ICE

SOFC-ICE combined cycles are a more recent development, and these cycles are mainly studied due to lower capital costs, longer lifetime, reduced sensitivity to ambient conditions and increased efficiency of an ICE compared to a GT [26, 27]. There are two main integration strategies present in current literature: coupled and decoupled systems (see Figure 2.2). In both strategies, anode off-gas (AOG) from the SOFC is combusted in the ICE for additional power generation. In coupled systems, the ICE runs only on AOG. In this configuration, the SOFC has the highest contribution to the total power, resulting in a high system efficiency. However, this also means that the power density of the system is relatively low due to the low power density of the fuel cell. In decoupled systems the ICE runs on a mixture of AOG and additional fuel. The possibility to direct additional fuel to the ICE means that the power share of the ICE can increase compared to the coupled system, which improves the power density of the system. However, due to the addition of extra fuel, the system efficiency is lower compared to the coupled system.

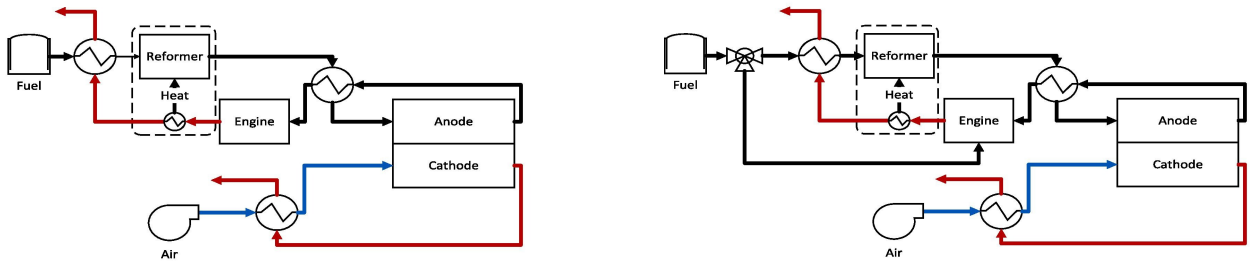

(a) Coupled SOFC-ICE combined cycle

(b) Decoupled SOFC-ICE combined cycle

Figure 2.2: Different SOFC-ICE integration strategies [28]

Various studies focus on SOFC-ICE combined cycles, and a few of these studies are discussed briefly below.

Park et al. [29] integrate a homogeneous charge compression ignition (HCCI) ICE with an SOFC into a coupled system. In this combined cycle, AOG from a pressurized SOFC running on externally reformed NG is combusted in the HCCI engine. The SOFC produces 86.9% of the total power, and the system has a net electrical efficiency of 59.5%. Additionally, waste heat is recovered through steam generation, resulting in a total system efficiency (electrical + heat) of 71.1%.

Chuahy and Kokjohn [12] analyze a diesel-fuelled SOFC-ICE combined cycle. In their system, the fuel cell operates at elevated pressures, and diesel can be directly fed into a HCCI engine resulting in a decoupled system. The SOFC generates 85.3% of the total power, resulting in a system electrical efficiency of 70.9%.

Sapra et al. [13] study an atmospheric decoupled system for application on naval vessels. The system efficiency and sizing are optimized for three different vessel types: oceangoing patrol vessel (OPV), landing platform dock (LPD) and high-end surface combatant (HSC). The ideal power split based on system efficiency and sizing is 28-72 for the OPV, 55-45 for the LPD and 27-73 for the HSC. With these power splits, the authors report a system efficiency of 51.9% for the OPV, 59.1% for the LPD and 51.9% for the HSC.

Another study by Sapra et al. [10] evaluates a decoupled system running on NG. In this system, the SOFC operates at atmospheric pressure, and different power splits are evaluated (33-67, 50-50 and 67-33). The performance of these power splits is compared to a standalone, NG-fuelled marine engine. Each power split achieves a higher system efficiency than the standalone engine. The higher power split (67-33) obtains the highest efficiency improvement of 8.4%. The lowest power split achieves a 5.2% improvement compared to the standalone engine. The authors then look at the power density and transient load response of the system, and conclude that the lower power split (33-67) is beneficial for marine applications.

An overview of these studies (and other identified research focusing on SOFC-ICE combined cycles) is given in Appendix A. For this combined cycle, different integration strategies, operating parameters and fuels are used in current literature, making it difficult to compare the studies and select the best combination of fuel and system layout for marine applications.

2.3. Fuels

For the previously presented combined cycles, different fuels are used in current literature. Diesel, MeOH, NG, LNG, CH_4, NH_3 and H_2 have all been considered [19, 30–35]. Most studies focus on NG, either in its gaseous form, liquified as LNG, or simplified to pure CH_4. For each fuel, reported system efficiencies lie between 50-70%. However, a direct comparison between the different fuels is difficult due to differences in integration strategy and operating conditions.

Due to time constraints for the thesis, not all of the different fuels can be considered. For this reason, a selection of fuels is made by evaluating the different fuels for suitability on naval surface combatants. To determine which fuel is most suitable for these vessels, a multi criteria analysis is performed. Each fuel is ranked based on flash-point, toxicity, explosive limits in air, energy density, storage and handling conditions, availability, technology readiness level (TRL), and emissions such as carbon dioxide (CO_2), nitrogen oxide (NO_x), sulphur oxide (SO_x), unburnt hydrocarbons (UHC) and particulate matter (PM), and an overview of all the fuel properties regarding these criteria is given in Table 2.1.

For the multi criteria analysis, the properties from Table 2.1 are transformed to a score between 1 (bad) and 5 (good). Each criteria is also given a weight factor. These weight factors are based on a small survey conducted within Damen Naval. Representatives from different departments were asked to score the different criteria between 1 (low importance) and 5 (high importance) for two operating times; times of peace and times of war. The results from this survey were averaged, leading to the different weight factors for peacetime and wartime. During times of war, the vessel is likely to be targeted by missiles, torpedoes and naval guns, increasing the risk of a fuel leak. The safety of the fuel is therefore very important. Low flash-point and high explosive limits can be catastrophic to the vessel and toxicity can be catastrophic to the crew. The weight factors for safety are therefore high for times of war. During peacetimes, the vessel is less likely to be damaged, meaning that the risk of a fuel leak decreases, posing less risk to the ship and crew. While still important parameters, the weight factors of the safety criteria are therefore reduced for peacetime.

Table 2.1: Overview of the properties of each fuel for the different comparison criteria [7, 36–63]

Criteria		**Fuel**					
		Diesel	**hydrotreated vegetable oil (HVO)**	**MeOH**	**NH_3**	**LNG**	**H_2**
Safety	Flash-point	>52 °C	>61 °C	9.7 °C	N/A	<-188 °C	N/A
	Toxicity	Low	Low	Low	High	Non-toxic	Non-toxic
	Explosive limits	0.6-6.5%	0.6-7.5%	5.5-44%	16-25%	4-15%	4-76%
Operational	Energy Density	45.8 MJ/kg, 38.2 GJ/m^3	44.0 MJ/kg, 34.4 GJ/m^3	19.9 MJ/kg, 15.8 GJ/m^3	18.6 MJ/kg, 12.7 GJ/m^3	55.2 MJ/kg, 25.5 GJ/m^3	120 MJ/kg, 9.6 GJ/m^3
	Storage and Handling	Ambient	Ambient	Ambient	-34 °C or 17 bar	-162 °C	-253 °C or 250 bar
	Availability	Good	Medium, but steadily increasing	Good	Medium-Low	Good	Low
	TRL	Mature	Mature	Available	Testing	Mature	Research
Environmental	CO_2 emissions	0.2701 kg/kWh	0.0405 kg/kWh	0.2486 kg/kWh	N/A	0.2061 kg/kWh	N/A
	Other emissions	SO_x, NO_x, PM, UHC	NO_x, PM, UHC	NO_x, PM	NO_x,PM	SO_x, NO_x, PM, CH_4	NO_x

The energy density and availability of the fuel are important characteristics during wartime. These characteristics directly influence the refuelling intervals and refuelling locations of the vessel, which have a significant impact on the operational deployability of the vessel. While these factors are also important during times of peace, changing course for refuelling and shorter refuelling intervals are not as bad as during times of war. Storage and handling conditions of the fuel influence the complexity of the fuel system onboard. A simpler system is always better regardless of operating times, due to due to easier maintenance and reduced system costs. The TRL becomes more important depending on the desired time of implementation. When this lies further in the future, this becomes less relevant.

While GHG emissions are important characteristics for commercial vessels, this is less the case for naval vessels. Global GHG emissions are a serious problem, and governments also try to reduce the emissions for government operated vessels, such as surface combatants. For this reason, the GHG emissions associated with the fuel are somewhat important. However, during times of war the GHG emissions of the vessel are of reduced importance. More important are the operational capabilities of the vessel, which should not be limited by the use of alternative fuels just because they have lower GHG emissions.

For operation during times of peace, HVO performs the best. Followed by diesel, MeOH and LNG respectively. Ammonia (NH_3) and hydrogen (H_2) score the worst out of all the fuels, making them undesirable for use on naval surface combatants. For wartime operation, the fuels rank about equal to peacetime operation. The only difference being that LNG and MeOH swapped places. Another interesting thing to note is the significant increase in score for diesel. This is explained by the low weight factor of environmental performance of the fuel for wartime operation. On the other criteria, diesel and HVO score almost identical, which decreases the score difference compared to peacetime operation.

Interesting to note is that one respondent of the survey pointed out that, due to the current geopolitical climate, upcoming new-build projects will all be designed exclusively around wartime scenarios. For this reason, only the results for wartime operation are taken for the selection of the fuels, making the preferred fuel for combined cycles in naval surface combatants diesel or HVO. Due to the better availability of diesel, this fuel is preferred for short term implementation. When looking at implementation further in the future, availability of HVO will be better, and HVO will be the preferred choice due to its better environmental performance.

Table 2.2: Multi-criteria analysis of the different fuels for use in naval surface combatants operating during times of peace and times of war. For peacetime the total possible score is 154, and for wartime the total possible score is 163.5

Criteria		Weight		Fuel					
		Peace	**War**	**Diesel**	**HVO**	**MeOH**	**NH_3**	**LNG**	**H_2**
Safety	Flammability	2.7	4.2	3	3	2	5	1	1
	Toxicity	4.0	4.5	4	4	4	1	5	5
	Explosiveness	2.8	4.3	4	4	2	3	4	1
Operational	Energy Density	3.8	4.6	5	5	3	3	4	1
	Storage and Handling	3.7	3.5	5	5	5	3	1	1
	Availability	4.3	5.0	5	3	5	2	5	1
	TRL	3.0	3.7	5	5	4	3	5	2
Environmental	CO_2 emissions	2.7	1.3	1	4	2	5	3	5
	Other emissions	3.8	1.5	1	3	4	4	2	5
Total	**Peacetime**	30.8	-	115.8	122.9	111.0	94.7	105.0	75.8
	Wartime	-	32.7	135.1	132.0	115.0	96.6	116.6	65.6

MeOH and LNG may also be interesting for naval applications. In wartime, these two fuels score almost identical, with a marginal preference for LNG. When peacetime operation returns in the design of surface combatants, it is interesting to also include these fuels in the comparison. In this thesis, only diesel and MeOH are considered for the combined cycles. Diesel and HVO have almost identical properties, with the main difference in GHG emissions and availability of the fuel. For naval vessels, availability of the fuel is more important than GHG emissions, and diesel is preferred over HVO due to the better short-term availability. Additionally, extensive research is already performed on combined cycles using LNG (or NG) as fuel. For this reason, this fuel is also left out in this thesis.

When combining these fuels with the combined cycles discussed in the beginning of this chapter, the following combinations are considered in this thesis:

- Diesel-fuelled SOFC-ICE
- Diesel-fuelled SOFC-GT
- MeOH-fuelled SOFC-ICE
- MeOH-fuelled SOFC-GT

For these combinations, the performance indicators are given in chapter 3. Next, the models to asses these combinations are given in chapter 4, and the results are discussed in chapter 5.

3

Performance metrics

This chapter explains how the different combined cycles are evaluated. First, in section 3.1, a reference vessel is selected to determine the power output for the systems. In section 3.2 the modelling software for the combined cycles is discussed. This section also addresses the calculation of the performance indicators (efficiency, fuel consumption, emissions, etc.) to compare the different combined cycles.

3.1. Reference vessel

The combined cycles in this thesis are studied for application on naval surface combatants. For these vessels, the power output of the combined cycle depends on the ship resistance (which varies with ship speed, displacement, sea state and hull fouling) and amount of power needed to run all the electrical systems onboard. For this power output, there is no single answer for all surface combatants. Smaller surface combants will have a lower power output than the larger variants. Additionally, surface combatants designed for stealth operations have a vastly different power demand that surface combatants designed for anti-aircraft warfare (AAW). For this thesis, a reference vessel is selected from the vessel portfolio of Damen Naval. Due to the military nature of these vessels, the available vessels for this thesis are limited. These vessels are generally designed for foreign or domestic governments, which means that most information regarding these vessels is classified and cannot be shared for this thesis. Besides custom designed vessels for governments, Damen Naval also offers a standardized modular design for the export market. Thise export vessels are part of the SIGMA class surface combatant, and data-sheets for these vessels can be publicly accessed from the Damen Naval website. For this reason, the SIGMA is chosen as the reference vessel for this thesis. Different sized vessels are available in the SIGMA range, and for this thesis the SIGMA 10514 is taken as the reference vessel. Additional information about this vessel can be found in Appendix C.

3.1.1. Power output

The power output for the combined cycles is calculated using the available data for the SIGMA. This power output needs to be high enough to overcome the resistance of the vessel, and also power the electrical systems onboard the ship. For the SIGMA, a power-speed curve and a hotel load of 0.5 MWe are provided by Damen Naval. The power-speed curve (Figure 3.1) shows the required engine power for different ship speeds at a design draught of 4 m, sea state 3 and clean hull conditions. This engine power is equal to the power output of the main drivers, which is higher than the power that is actually delivered to the propeller. When transferring the engine power to the propeller, some losses are induced by the gearbox and shaft bearings. The actual power delivered to the propellers is not part of the scope of this thesis, and the power given by the power-speed curve is taken as the propulsion power needed from the combined cycles.

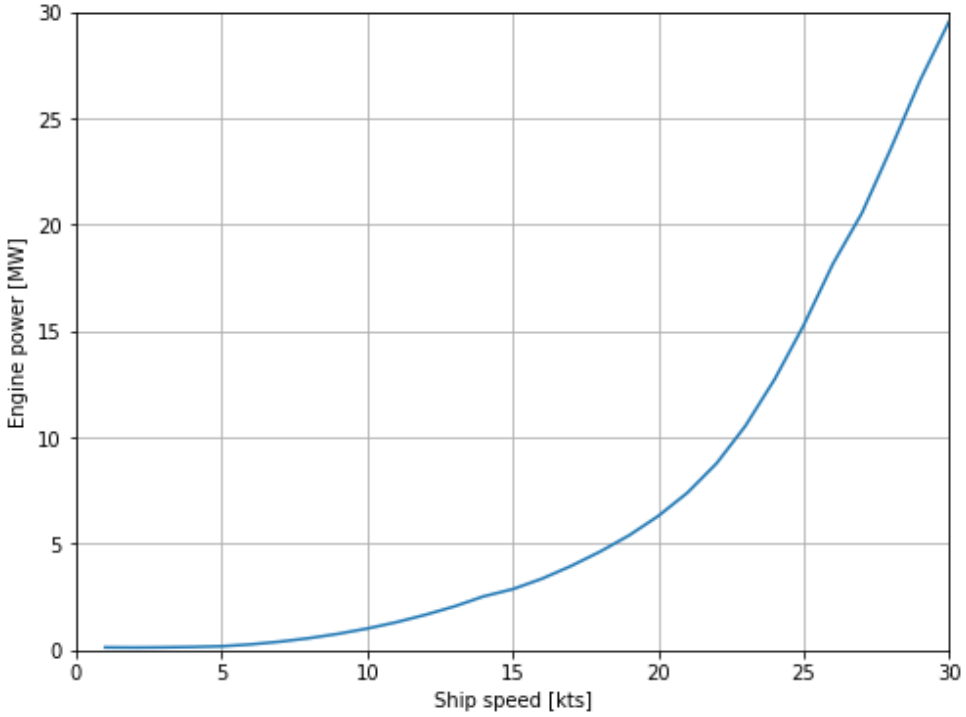

Figure 3.1: Power-speed curve of the reference vessel for 4 meter draught, sea state 3 and clean hull conditions

The engine power (P_{engine}) from Figure 3.1 cannot be used directly as the power output for the combined cycles. In this figure, the engine power is given in mechanical power (MW). In the combined cycles (part of) the power is produced as electrical power (MWe). This electrical power needs to be converted to mechanical power before it can be used to drive the propellers of the reference vessel. In this conversion, energy losses are introduced. An electric motor converts electric power into rotational mechanical power. During this conversion, some power is lost in the motor due to friction and heat. Depending on the type of electric motor, these losses are between 4-30% [64]. Additionally, the electric power coming from the combined cycle may not match the input power of the electric motor (alternating current (AC), direct current (DC), voltage, current, etc.). To match these properties, an electric conversion step may be necessary. Depending on the conversion step (AC-AC, AC-DC, DC-DC or DC-AC conversion) losses are between 5-20% [65–67].

This means that the electric power output of the combined cycles needs to be higher than the mechanical power stated in Figure 3.1. For this thesis, a conversion step efficiency ($\eta_{conversion}$) and motor efficiency ($\eta_{e-motor}$ of 95% are assumed. To obtain the electric power output of the combined cycle ($P_{cc,el}$), the engine power from Figure 3.1 is divided by the conversion step efficiency and motor efficiency (Equation 3.1). The total power output of the combined cycle (P_{tot}) is then obtained by summing the electric propulsion power and the hotel load (P_{hotel}), as shown in Equation 3.2. This total power is plotted against the different ship speeds in Figure 3.2, showing the total electric power that needs to be produced by the combined cycle to operate the vessel at a given ship speed.

$$P_{cc,el} = \frac{P_{engine}}{\eta_{conversion} * \eta_{e-motor}} \tag{3.1}$$

$$P_{tot} = P_{cc,el} + P_{hotel} \tag{3.2}$$

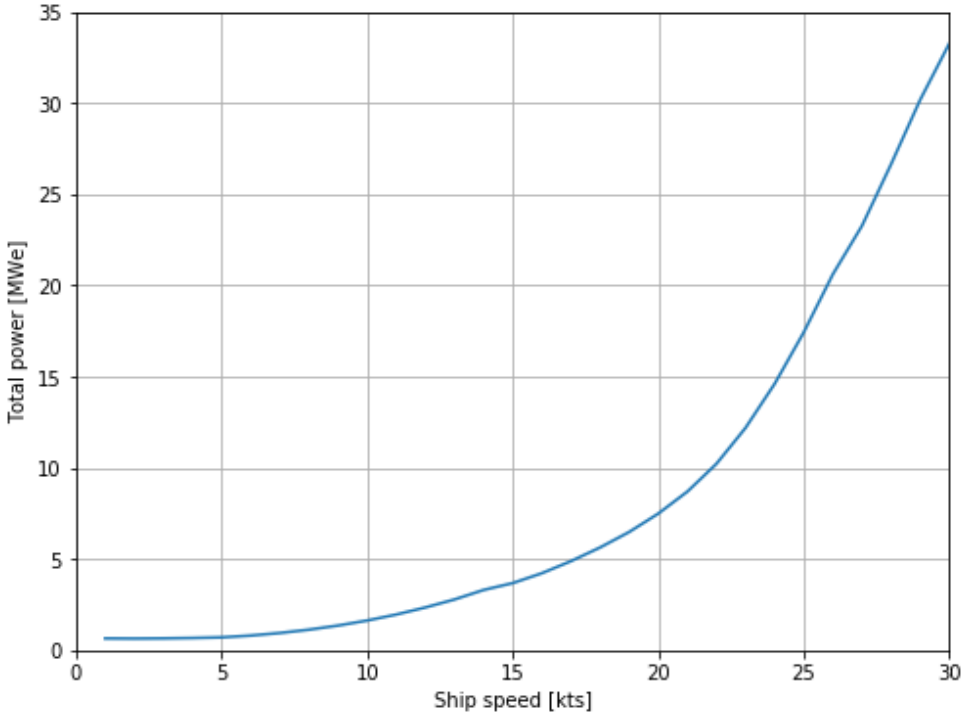

Figure 3.2: Electric power output for the combined cycles at different ship speeds, for 4 meter draught, sea state 3 and clean hull conditions

In the power-speed curves, ship speeds ranging from 1 to 30 kts are given. However, due to ttime constraints, not all of these ship speeds can be considered in this thesis. For the analysis of the different combined cycles, only three ship speeds are considered: silent speed at 6 kts, cruising speed at 18 kts and top speed at 27 kts. The total electric power output for these ship speeds is taken from Figure 3.2, and stated in Table 3.1. This power output is the total required power when all of the power is generated as electrical power. This means that the heat engine of the combined cycle is connected to a generator, which converts mechanical engine power to electrical power. This generator also induces energy losses of about 3% [68], meaning that the engine power needs to be slightly higher than the electric power from the generator. Another option is to mechanically couple the heat engine to a gearbox (Figure 3.4). This way, less power is needed to drive the vessel as there are less losses in the conversion from mechanical to electrical and back to mechanical power. In this thesis, both the electric propulsion and hybrid propulsion are considered in the sizing of the system. To ensure that the models created in chapter 4 provide enough power to operate the vessel, the power output for electric propulsion is taken. This means that for the hybrid propulsion, the system produces slightly more power than necessary for the operation of the vessel. This results in a slight overestimation of the fuel consumption for the hybrid solutions compared to the fully electric solutions.

Table 3.1: Electric power output of the combined cycle for the three operating speeds of the reference vessel

Operating mode	Ship speed	Electric power output
Silent	6 kts	0.8 MWe
Cruising	18 kts	5.6 MWe
Top	27 kts	23.3 MWe

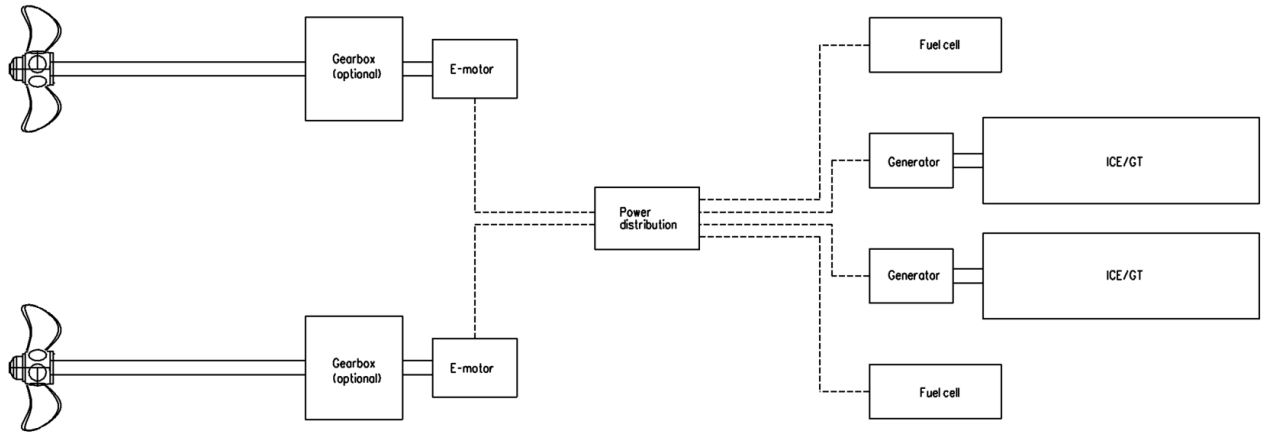

Figure 3.3: Fully electric power plant. The propeller is driven by an electric motor, either directly or through a reduction gearbox, and the electric power for the electric motor is generated by the fuel cells and gensets

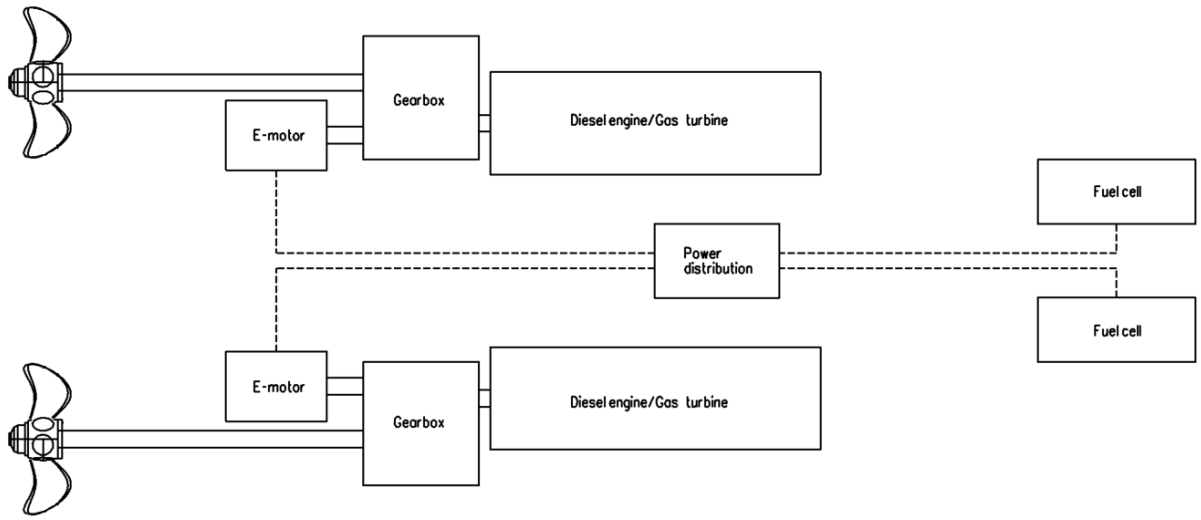

Figure 3.4: Hybrid power plant. The propeller is driven by an electric motor and a heat engine through a gearbox. The electric power for the electric motor is generated by the fuel cell

3.1.2. Operational profile

With the power demand for the different operating modes, the fuel consumption and CO_2 emissions can be calculated for each operating mode. However, the vessel does not always operate at the same operating mode. To compare the fuel consumption and emissions for a combination of operating modes, they need to be converted to an annual fuel consumption and annual CO_2 emissions. To calculate the annual fuel consumption and emissions, an operational profile is used. This operational profile relates the different operating modes with the annual time spent at this ship speed. For frigates, a typical operational profile is given by Klein Woud and Stapersma [69], and this operational profile is shown in Figure 3.5. In this operational profile, three different missions are shown: towed array mission, general purpose mission and carrier escort mission. For each mission, the time spent at the ship speeds between 0 and 30 kts are given.

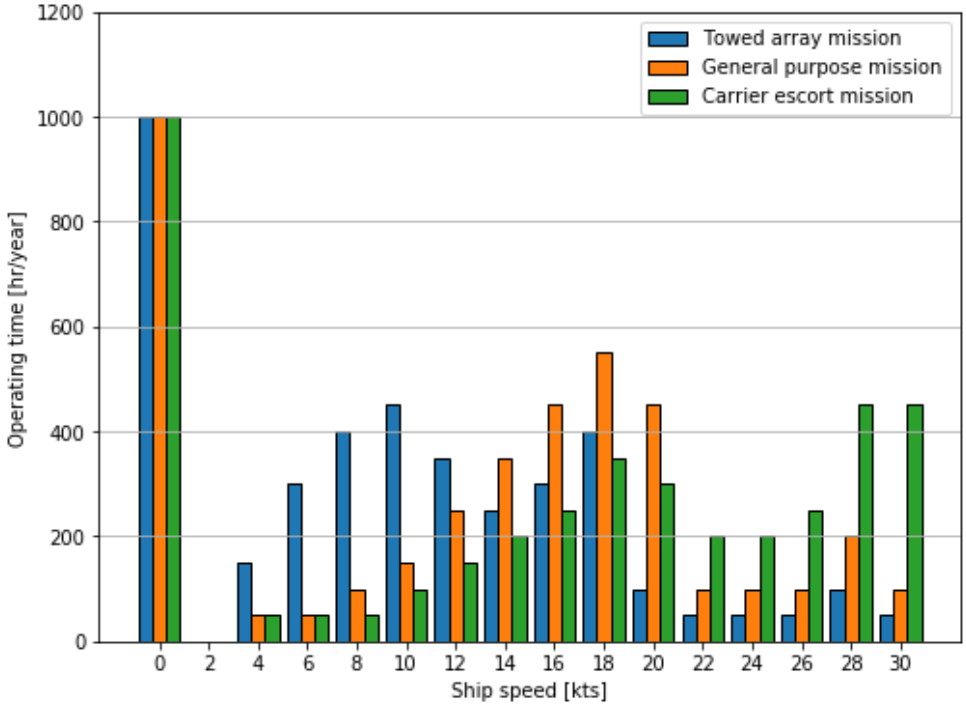

Figure 3.5: Typical operating profile of a frigate for different missions [69]

For an accurate calculation of the annual fuel consumption and emissions, all of the ship speeds and missions should be considered. However, this is not feasible in the timeframe of this thesis, and only three ship speeds are considered (6, 18 and 27 kts). The operational profile given by Klein Woud and Stapersma is therefore simplified for this thesis to only contain these three ship speeds. The ship speeds present in the original operating profile are assigned to the three operating modes based on the absolute distance of the original speed to the simplified speed, with the exception of 0 knots. For 0 knots, the ship is assumed to be laying in the harbour, where it obtains its power from the shore. For this ship speed the onboard power plant is not running, and this ship speed does not contribute to the fuel consumption and emissions of the vessel. The ship speeds from 2 to 10 knots are assigned to silent operation, 12 to 22 knots to cruising speed and 24 to 30 knots to top speed. For each mission in the operational profile (towed array, general purpose and carrier escort) the time spent at each operating mode is obtained. Next, it is assumed that the reference vessel spends an equal time on each mission (i.e. 33% towed array, 33% general purpose and 33% carrier escort). The time spent at each operating mode is therefore equal to the average value of the different missions, which is calculated using Equation 3.3 to Equation 3.5. This results in the simplified operational profile given in Figure 3.6.

$$t_{silent} = \frac{\sum_{i=2\text{kts}}^{10\text{kts}} t_i^{\text{towed array}} + \sum_{i=2\text{kts}}^{10\text{kts}} t_i^{\text{general purpose}} + \sum_{i=2\text{kts}}^{10\text{kts}} t_i^{\text{carrier escort}}}{3} \tag{3.3}$$

$$t_{cruising} = \frac{\sum_{i=12\text{kts}}^{22\text{kts}} t_i^{\text{towed array}} + \sum_{i=12\text{kts}}^{22\text{kts}} t_i^{\text{general purpose}} + \sum_{i=12\text{kts}}^{22\text{kts}} t_i^{\text{carrier escort}}}{3} \tag{3.4}$$

$$t_{top} = \frac{\sum_{i=24\text{kts}}^{30\text{kts}} t_i^{\text{towed array}} + \sum_{i=24\text{kts}}^{30\text{kts}} t_i^{\text{general purpose}} + \sum_{i=24\text{kts}}^{30\text{kts}} t_i^{\text{carrier escort}}}{3} \tag{3.5}$$

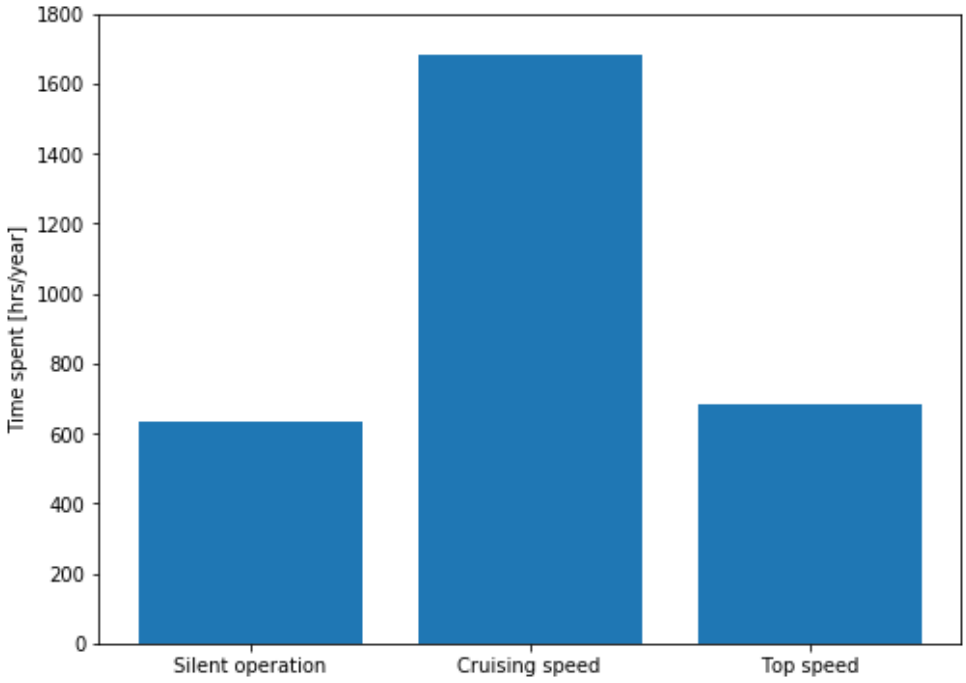

Figure 3.6: Simplified operational profile considered in this thesis

3.2. Performance indicators

The performance of the different combined cycles is assessed on system efficiency, GHG emissions, IR-signature, system weight and system volume. First, the modelling software to obtain these performance indicators is discussed. Next, for each these performance indicators the calculation method is briefly discussed.

3.2.1. Modelling software

To obtain the fuel consumption, CO_2 emissions and exhaust temperature, Cycle-Tempo (CT) is used. CT is a thermodynamic flow modelling software for the thermodynamic analysis of energy conversion systems [70]. CT contains a component library with (among others) heat exchangers (HEX), pumps, compressors, turbines, fuel cells and reformers, which correspond to the necessary components for the combined cycles. With these components, a system matrix of energy and mass equations is generated, from which the relevant mass and energy flows are calculated. CT gives temperature, pressure, mass flow and composition of the different streams, as well as the energy output and efficiency of the entire system. CT is used in current literature to assess the performance of SOFCs with different fuels by [71]. Additionally, SOFC combined cycles are analysed using CT by Aravind et al. [22] and van Biert et al. [19]. This shows the suitability of this software for the analysis of the different combined cycles in this thesis. In chapter 4 the development and working principles of the different combined cycle models are discussed in detail.

3.2.2. Power split

An important aspect of the combined cycles is the power split. This power split gives the contribution of the SOFC and heat engine to the total power. A larger contribution of the SOFC leads to a higher system efficiency. However, this also leads to an increase in size and weight of the entire system due to the lower power density of the SOFC compared to the heat engine. In this thesis, the power split will be varied to see the exact influence on efficiency and sizing of the system based on the following boundary conditions:

- At silent operations, all of the required power is delivered by the SOFC to reduce acoustic emissions of the vessel.
- At cruising speed, the power production is shared between the SOFC and heat engine.
- At top speed, the total installed power equals the power demand of the vessel.

The exact power split for the combined cycles and how it is defined is discussed in detail in chapter 5.

3.2.3. Part-load operation

Depending on the evaluated power splits and installed power of the components, the heat engine and fuel cell operate at either full-load or part-load at the different operating modes. The efficiency of the ICE, GT and SOFC changes depending on the operating load of the component, which is shown in Figure 3.7. For the marine ICE, available data for the MAN 20V20/33D STC diesel engine is used [72]. The marine GT is the efficiency curve of the GE LM2500+ [73]. Lastly, the SOFC performance curve is given for a SolydEra fuel cell module [74] fuelled by hydrogen and NG. Here, it can be seen that the part-load operation of these components significantly influences the efficiency of the component. For the ICE, a maximum can be observed between 75-90% load. For the GT and SOFC this maximum lies at 100% and 75% load respectively. To maximize the efficiency of the combined cycles, these different components should be operated at or close to their respective maximum efficiency. However, this may not be possible for all operating modes, and this depends on the available power output of commercial systems, the number and size of the installed components, and the power demand of the vessel at the different operating modes. If for example a single GT that can deliver the power for top speed operation is installed, it will operate at part-load for the other operating modes. If however the total power is split between multiple engines, a single engine can be operated for cruising speed, while the other engines are only used for top speed. This improves the efficiency of the system by running the engine closer to its maximum efficiency.

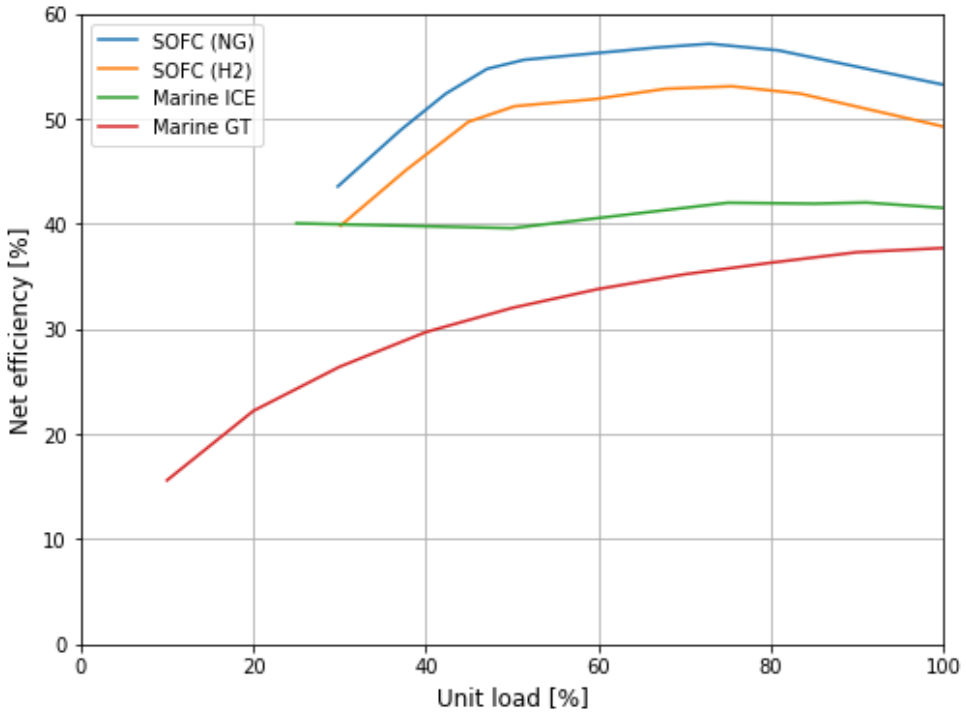

Figure 3.7: Part load efficiency curves of an SOFC running on NG and H_2 [74], marine ICE [72] and marine GT [73]. The curves for the SOFC show the net electrical efficiency, and the curves for the ICE and GT show the net thermal efficiency

3.2.4. System efficiency

For each combined cycle, the system efficiency is calculated by CT as the net power output of the system divided by the energy input of the fuel (Equation 3.6). This parameter gives a good indication of which combined cycle performs the best for a given operating mode, but it cannot be used to compare the different combined cycles over the entire operating profile of the reference vessel. For this reason, the annual energy consumption is used to compare the different combined cycles instead. For each operating mode, the CT model calculates a mass flow of fuel in kg/s. This is converted into an annual energy consumption using Equation 3.7. The fuel mass flow is multiplied with the lower heating value (LHV) of the fuel, and the time spent at this operating mode per year. The annual energy consumption is then obtained by summing the energy consumption of each operating mode.

$$\eta = \frac{P_{net}}{E_{in,fuel}} = \frac{P_{net}}{\dot{m}_{fuel} \cdot LHV_{fuel}} \tag{3.6}$$

$$E_{in}^{year} = \dot{m}_{fuel} \cdot LHV_{fuel} \cdot t_i, \text{ where i = silent, cruising, top} \tag{3.7}$$

3.2.5. GHG emissions

GHG emissions for marine power plants include CO_2, carbon monoxide (CO), UHC, NO_x, SO_x and PM. In CT, not all of these components are taken into account. The CT models assume a full conversion of the fuel into CO_2 and water (H_2O). This means that there will be no CO, UHC and PM present in the exhaust gas of the models. Additionally, in this thesis the fuels contain no sulphur, which means that SO_x emissions are also not present in the CT models. Lastly, NO_x emissions are also not calculated in the CT models.

This means that only CO_2 emissions can be calculated using the CT models. In CT, the exhaust gas composition is calculated in molar fractions, and is a mixture of intake air (77.29% N_2, 20.75% O_2, 1.01% H_2O, 0.03% CO_2 and 0.92% Ar based on volume), and CO_2 and H_2O from oxidizing the fuel. The annual CO_2 emissions are obtained by calculating the mass flow of CO_2 in the exhaust gas, and subtracting the mass flow of CO_2 already present in the intake air Equation 3.8. The mass flow of CO_2 is obtained by multiplying the mass flow of the exhaust gas ($\dot{m}_{exhaust}$) with its average molar mass ($M_{exhaust}$) and the molar fraction of CO_2 in the exhaust gas (x_{CO_2}). This is then divided by the molar mass of CO_2 to obtain a mass flow in kg/s. The mass flow of CO_2 in the intake are is calculated the same way, but by using the average molar mass and molar fraction of CO_2 for the intake air. These two values are then subtracted to obtain the CO_2 emissions from oxidizing the fuel. Next, this value is converted to an annual CO_2 emission by multiplying with the time spent at the different operating modes (t_i) and dividing by 1000 kg/ton.

$$CO_2^{year} = \left(\frac{\dot{m}_{exhaust} \cdot M_{exhaust} \cdot x_{exhaust}^{CO_2}}{M_{CO_2}} - \frac{\dot{m}_{air,in} \cdot M_{air,in} \cdot x_{air,in}^{CO_2}}{M_{CO_2}} \right) \cdot \frac{t_i}{1000}, \text{ where i = silent, cruising, top} \tag{3.8}$$

3.2.6. IR-signature

The IR-signature of the vessel is determined by both internal and external factors. From the internal factors, the main machinery has by far the highest contribution. Hot exhaust gasses coming from the engine, as well as heat radiated to the steel hull from the main machinery create visible hot-spots in the IR spectrum. External factors are heating of the hull due to radiated heat from the sun, both directly absorbed by the hull, or reflected by the sea water to the hull. [18]

With the CT models, only the temperature of the exhaust gasses can be determined. Of the internal factors, the exhaust temperature has the most significant contribution to the IR-signature [18]. In this thesis, radiated heat from the machinery and sun are not taken into account, and the IR-signature only consists of the hot exhaust gasses leaving the system.

3.2.7. System weight and volume

The weight and volume of the system are determined by selecting off-the-shelf components meeting the power output (for heat engine, e-motor and fuel cell), power consumption and fluid flow (blowers and pumps) and transmitted heat (HEXs). Additionally, the fuel storage weight and volume is taken into account. For the calculation of the fuel storage, the range of the reference vessel is used. This range is calculated with Equation 3.9 by multiplying the fuel storage weight (m_{fuel} in ton) with the ship speed (v_{ship} in NM/hr) and then dividing this value by the fuel consumption at this ship speed ($\dot{m}_{fuel}$ in ton/hr). It should be noted that this calculation is a simplification of the range calculation for the actual vessel. In reality, the range also depends on e.g. tank filling factors. For the sake of comparing the different combined cycles, this simplified range is sufficient as long as all the combined cycles are calculated in the same way. The ship speed and fuel consumption are taken for cruising speed (18 NM/hr), resulting in a range of the reference vessel of 5700 NM. This range is used to calculate the fuel storage weight for each combined cycle in chapter 5.

$$R = \frac{m_{fuel} \cdot v_{ship}}{\dot{m}_{fuel}} \tag{3.9}$$

4

Cycle-Tempo models

For the modelling of the different combined cycles, Cycle-Tempo (CT) software is used. The first step is to create a standalone model for the ICE, GT and SOFC. These standalone models are created in section 4.1 for operation on diesel fuel and in section 4.2 for operation on MeOH fuel. These models are created to ensure that the results from CT are the same as the reference data for these components. Next, in section 4.3, the standalone models are combined into a single model to represent the SOFC-ICE and SOFC-GT combined cycles. Just like the standalone models, the combined cycle models are created for both diesel and MeOH fuel. Lastly, section 4.4 gives some concluding remarks about the combined cycle models.

4.1. Diesel

First, the models of the ICE, GT and SOFC running on diesel are created. In this thesis, the combined cycles will be implemented in naval vessels. For these vessels, fuels are standardized for NATO members to ensure the performance of the fuel when refuelling at different locations. NATO F-76 diesel fuel is the standardized version of marine diesel, and this fuel is used for this thesis. NATO F-76 diesel, hereafter referred to as diesel, has an average chemical formula of $C_{14.8}H_{26.9}$ [17]. The heaviest hydrocarbon available in CT is C_6H_{14}, which is much lighter than diesel. Diesel can therefore not be chosen in CT as a predefined fuel, and it needs to be approximated by mixing carbon (C) and hydrogen (H) atoms. To be able to mix the diesel with AOG in the combined cycle, these two streams must be of the same type. AOG is a so-called Gas Mixture, which means that diesel also needs to be a Gas Mixture. For a Gas Mixture, the composition of the stream is set based on molar percentages. For diesel, the molar H/C ratio is 1.82 [17], which leads to a mixture containing 35.46% C and 64.54% H. CT calculates the LHV of a Gas Mixture, which is 44231 kJ/kg for the given molar ratio. This value is slightly different than the LHV for diesel, which is 42700 kJ/kg [17]. This means that in the CT model, the fuel mass flow will be slightly different than the actual mass flow of diesel with the correct LHV. However, as the combined cycles are compared based on energy flow and not fuel mass flow, it does not really matter, and the ICE, GT and SOFC models are created using the LHV as calculated by CT.

4.1.1. Internal combustion engine

The thermodynamic cycle of an ICE consists of a compression stroke, heat addition through combustion, and an expansion stroke. In thermodynamics, this process is approximated by the Diesel, Otto or Seiliger cycle. These cycles consist of adiabatic compression, heat addition, adiabatic expansion and heat release. The main difference between the different cycles is in the heat addition. For diesel engines (which start the combustion of the fuel through compression ignition (CI)), the Diesel cycle is commonly used, where the heat addition takes place at constant pressure [75]. For this thesis, the Diesel cycle is also assumed. The modelling in CT is done by connecting standard components. For the ICE, no standard component is available, and the thermodynamic cycle needs to be approximated using the available components. These available components are the compressor, combustor and turbine, which are used to approximate a Diesel cycle for the ICE. First, air is compressed in the compressor, and then fed into the combustor. In the combustor, diesel is added and combusted with the compressed air, which raises the temperature. Next, the reaction products from the combustor are expanded in the turbine. To check whether the CT model can predict the thermal efficiency, fuel consumption and exhaust temperature accurately, test data for a marine diesel engine is used. The engine used for this thesis is the MAN

20V28/33D STC, which is a sequentially turbocharged, intercooled marine diesel engine. For this engine, test data for different engine loads is available from the paper by Geertsma et al. [72]. Besides modelling the cylinder as compressor-combustor-turbine, an additional compressor, turbine and HEX are included to represent the turbocharger and intercooler. Addtionally, a pump provides the cooling water for the intercooler, and another pump is added to represent the fuel pump. The layout of the ICE model is shown in Figure 4.1.

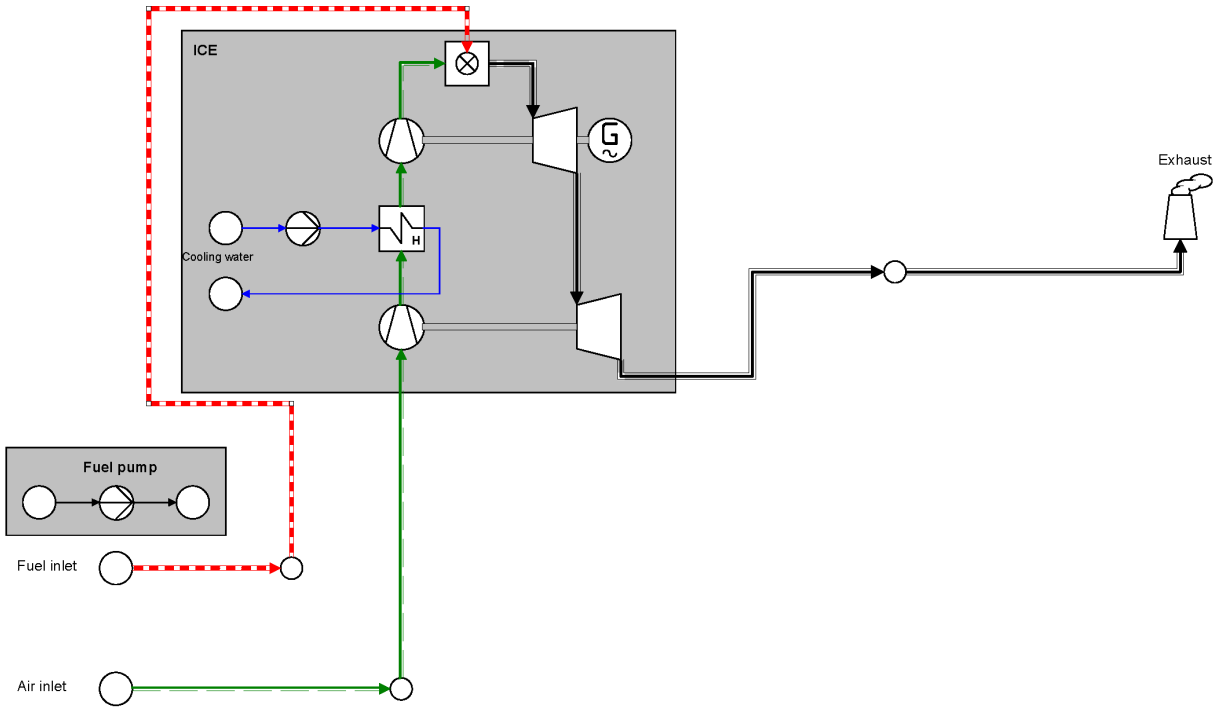

Figure 4.1: CT model for the ICE

With the main layout of the model set, the parameters of the different components need to be determined. First, the ambient conditions of the model need to be set. In the available test data for the engine, ambient pressure is 0.97 bar and ambient temperature is 25 °C. These conditions are set for the air inlet, fuel inlet and cooling water inlet. Next, the air is compressed in the turbocharger. The pressure ratio and isentropic efficiency of the turbocharger compressor are set to match the outlet pressure and temperature of the engine data. After the turbocharger compressor, the air is cooled in the intercooler. In the intercooler, the temperature difference and pressure loss are set to match the intake conditions of the engine. Next, the air enters the cylinder, where it is compressed. The pressure after the compression stroke is not given in the engine data, and needs to be calculated. For this calculation, Equation 4.1 and Equation 4.2 for adiabatic, polytropic compression are used [76]. These equations relate the pressure and volume at the beginning and end of the compression stroke for a standard Diesel cycle. Here, the pressure ratio of the compression is calculated with the geometric compression ratio of the engine (v_1/v_2) and a polytropic exponent (n). These parameters are given by Geertsma et al. [72] for this specific engine, and are 13.8 and 1.38 respectively. Using these values gives a pressure ratio (Π_{compr}) of 37.41 and a temperature ratio (TR) of 2.71. In CT, these values are used to match the pressure and temperature at the outlet of the compressor. The pressure ratio is set in the compressor as an input variable, and the TR is used to match the outlet temperature of the compressor by varying the isentropic efficiency of the compressor in CT. In this case, setting an isentropic efficiency of 1 in the compressor results in an outlet temperature equal to the expected TR from Equation 4.2.

$$\Pi_{compr} = \frac{p_2}{p_1} = \left(\frac{v_1}{v_2}\right)^n \tag{4.1}$$

$$TR = \frac{T_2}{T_1} = \left(\frac{V_1}{V_2}\right)^{n-1} \tag{4.2}$$

Next, the pressure after the combustor is taken equal as the pressure before the combustor. This is in line with the Diesel cycle, where combustion takes place at constant pressure. The pressure after the turbine is given in the engine data, and the pressure ratio of the turbine is then set accordingly. The isentropic efficiency of the turbine is taken equal to the compressor (which is 1), resulting in a temperature after the turbine as calculated by CT. To match this temperature with the engine data, the air-excess ratio (λ) of the combustor is set. Lastly, the pressure ratio and isentropic efficiency of the turbocharger turbine are set to match the exhaust pressure and temperature of the engine data. Now that all the pressures and temperatures are set correctly, the power of the turbocharger compressor needs to be matched with the power of the turbocharger turbine. This is achieved by lowering the mechanical efficiency from 1 until both powers are equal. Lastly, the mechanical efficiency of the cylinder compressor and turbine are set to match the output power and thermal efficiency of the engine with the reference data. The operating parameters for each component are shown in Table 4.1 for full load of the engine, and these parameters are compared to values present in current literature. For the part-load parameters, the reader is directed to Appendix D. In this table, it can be seen that only the air-excess ratio differs from the value presented by Geertsma et al. [72] for this engine. This means that in the model, the air consumption of the engine is underestimated. This influences the composition of the exhaust gas, which will give different fractions for each molecule than the actual exhaust gas of the real engine. If λ is taken equal to the value presented by Geertsma, the exhaust temperature would become way lower than the temperature in the reference data. For the different combined cycles, exhaust temperature is one of the performance indicators in the comparison. For this reason, an accurate calculation of exhaust temperature is given a higher priority than an accurate exhaust gas composition. While exhaust gas composition is also important for the CO_2 emissions of the combined cycle, the CO_2 produced by oxidizing the fuel (in kg/s) is not affected by the exhaust gas composition. Figure 4.2 shows how the efficiency and exhaust temperature of the CT model compare to the reference data for full- and part-load operation of the engine. Here it can be seen that the model predicts the engine efficiency and exhaust temperature accurately, and this model can be used for the calculations of the combined cycles.

Table 4.1: CT parameters for the ICE model at 100% load

Component	Parameter		CT Value		Reference value		Reference
Turbocharger	Isentropic efficiency compressor	$\eta_{is,compr}$	0.79	-	0.8	-	[12]
	Pressure ratio compressor	Π_{compr}	4.752	-	4.752	-	[72]
	Mechanical efficiency compressor	$\eta_{m,compr}$	0.956	-		-	
	Isentropic efficiency turbine	$\eta_{is,turb}$	0.855	-	0.8	-	[12]
	Pressure ratio turbine	Π_{turb}	3.468	-	3.468	-	[72]
	Mechanical efficiency turbine	$\eta_{m,turb}$	0.956	-		-	
Intercooler	Pressure drop	Δp_{loss}	0.049	bar	0.049	bar	[72]
	Temperature drop	ΔT	186	°C	186	°C	[72]
Cylinder	Isentropic efficiency compressor	$\eta_{is,compr}$	1	-	-	-	
	Pressure ratio compressor	Π_{compr}	37.41	-	-	-	
	Mechanical efficiency compressor	$\eta_{m,compr}$	0.8568	-	0.85-0.9	-	[77, 78]
	Air excess ratio combustor	λ	1.95	-	2.4	-	[72]
	Isentropic efficiency turbine	$\eta_{is,turb}$	1	-	-	-	
	Pressure ratio turbine	Π_{turb}	49.29	-	-	-	
	Mechanical efficiency turbine	$\eta_{m,turb}$	0.8568	-	0.85-0.9	-	[77, 78]
Generator	Generator efficiency	η_{gen}	0.97	-	0.95-0.97	-	[68]
Pumps	Isentropic efficiency	η_{is}	0.85	-	0.7-0.85	-	[19, 71]
	Mechanical efficiency	η_m	0.8	-	0.6-0.9	-	[19, 71]
Overall	Power output	P_{out}	10000	kW	9997	kW	[72]
	Energy consumption	E_{in}	8411.25	kJ/kWh	8411.90	kJ/kWh	[72]
	Exhaust temperature	T_{exh}	386.79	°C	387	°C	[72]

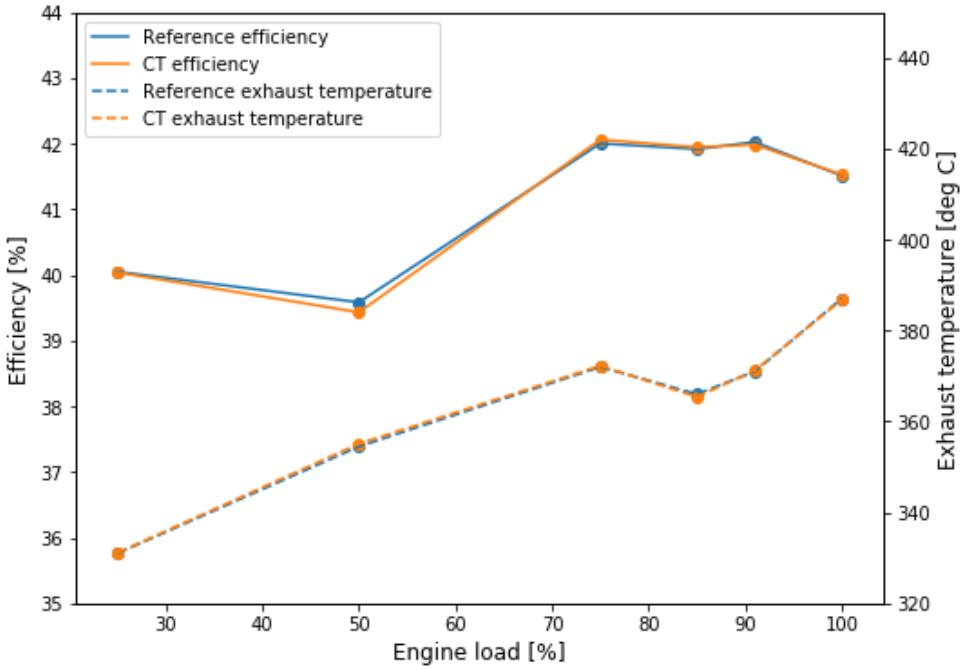

Figure 4.2: Comparison of exhaust temperature and efficiency of the ICE model and the reference values [72] at different operating loads

4.1.2. Gas turbine

Similar to the ICE model, the GT is modelled using standard components. In CT a gas turbine component is available. However, with this component, there is no freedom regarding the intake fuel or integrating the GT into a combined cycle. This means that this component is not suitable for this thesis, and the GT needs to be modelled using a compressor, combustor and turbine. Just like the ICE model, the GT model is created taking reference data into account. For the GT model, reference data for a General Electric LM2500+ marine gas turbine is used, and performance data of this GT is given in Table 4.2 [73].

Table 4.2: Performance data for the General Electric LM2500+ marine gas turbine [73]

Load [%]	Electric power output [MWe]	Generator efficiency [%]	Inlet airflow [kg/s]	Fuel flow [kg/s]	Thermal efficiency [%]	Pressure ratio compressor [-]	Exhaust temperature [°C]	Combustion chamber pressure loss [%]
100	31.2	97.5	88.4	1.87	37.7	23.54	534	3
90	28.1	97.5	84.7	1.70	37.3	22.14	515	3
80	24.9	97.4	80.3	1.55	36.3	20.69	504	3
70	21.8	97.3	75.5	1.40	35.2	19.17	493	3
60	18.6	97.0	70.4	1.25	33.8	17.72	484	3
50	15.5	96.6	65.5	1.09	32	16.05	474	3
40	12.3	96	59.8	0.94	29.7	14.46	464	3
30	9.1	95	53.2	0.78	26.4	12.61	458	3
20	6.0	93	46.3	0.61	22.2	10.62	447	3
10	2.8	87.4	38.5	0.41	15.6	8.38	426	3

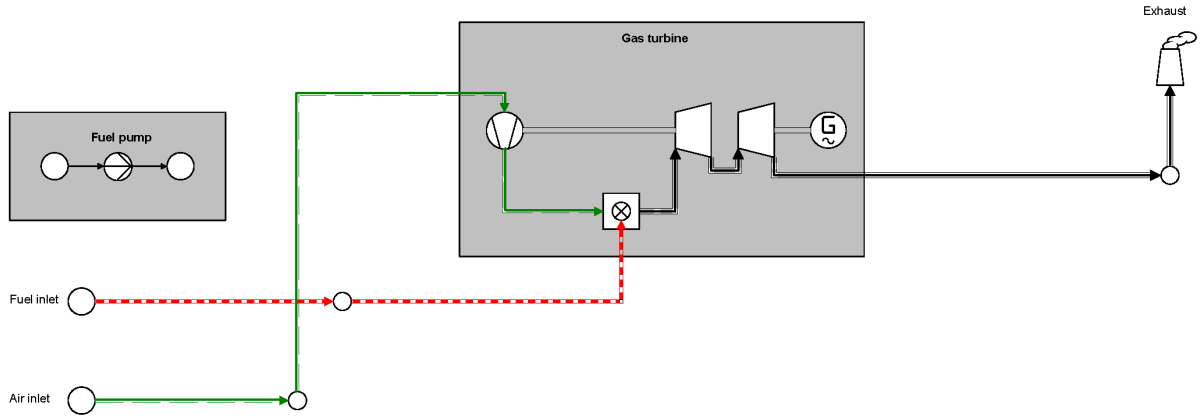

Figure 4.3: CT model for the GT

The LM2500+ consists of a single compressor, and two turbines. One turbine produces just enough power to drive the compressor, and the other turbine produces the output power. This layout is also adopted in the CT model, and is shown in Figure 4.3. Just like the ICE model, the parameters for each component are set to match the reference data. While Table 4.2 gives most of the necessary information, this is not sufficient to fully set the model parameters. For the model to run correctly, the isentropic efficiency of the compressor and both turbines, as well as the pressure ratio of both turbines needs to be determined. In the paper by Haglind and Elmegaard [73], compressor maps are given for the LM2500+. These compressor maps show the relation between corrected mass flow, pressure ratio and isentropic efficiency of the compressor. The corrected mass flow is calculated with Equation 4.3 [79]. In this case, the corrected mass flow is equal to the actual mass flow. This is because the inlet temperature and pressure of the compressor are equal to ambient conditions, which simplifies the corrected mass flow equation to just the mass flow. When taking the mass flow and pressure ratio of the compressor given in Table 4.2, the operating line of the compressor can be plotted in the compressor map of Figure 4.4a. This figure is then used to determine the normalized speed for each operating point, which is then used to plot a second operating line in Figure 4.4b. From this figure, the isentropic efficiency of the compressor at the different operating points is read.

$$\dot{m}_{corr} = \dot{m} \cdot \sqrt{\frac{T_{in}}{T_{amb}}} \cdot \frac{p_{amb}}{p_{in}} \tag{4.3}$$

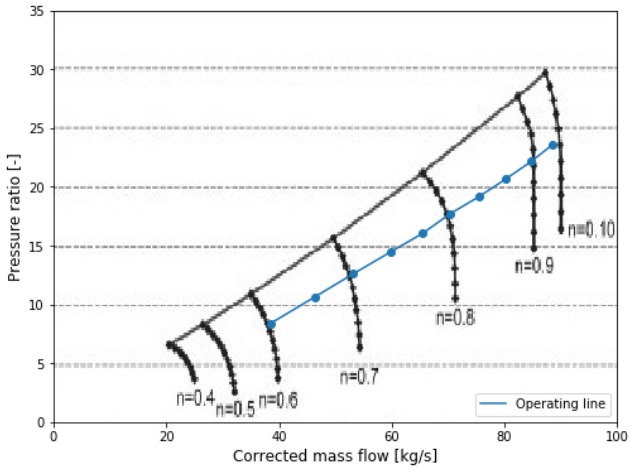

(a) Relation between corrected mass flow, pressure ratio and normalized speed

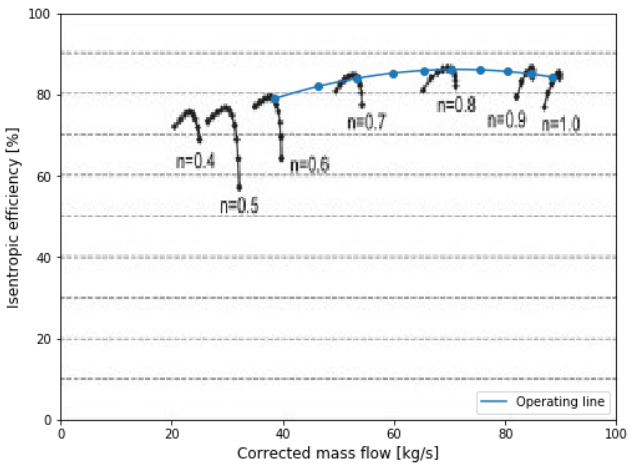

(b) Relation between corrected mass flow, isentropic efficiency and normalized speed

Figure 4.4: Compressor map for the General Electric LM2500+ marine gas turbine [73], with the operating line plotted on top

First, the pressure ratio and isentropic efficiency of the compressor are set in the model. Next, the pressure loss and air-excess ratio are set in the combustor. This gives a pressure and temperature of the exhaust gasses entering the first turbine. Next, the pressure ratio and isentropic efficiency of the two turbines are varied to match the first turbine with the compressor power, and the exhaust temperature of the model with the reference data. Lastly, the mechanical efficiency of the compressor and turbines are set to match the thermal efficiency of the reference data. The parameters used for the full-load model, as well as a comparison to values presented in literature, are shown in Table 4.3. For full-load and part-load operation of the GT, the reference data and the results from the model are compared in Figure 4.5. In this figure, it can be seen that the model predicts the exhaust temperature and efficiency correctly for loads higher than 60%. At loads between 30%-60%, the model slighly underestimates both the exhaust temperature and thermal efficiency. This difference is however minimal, and is not expected to impact the system performance of the combined cycles significantly. However, at loads lower than 30%, the model can no longer predict the system efficiency correctly. This can be explained by the design of the actual GT. The GE LM2500+ is a so-called variable geometry gas turbine. This means that the angle of the inlet guide vanes can be controlled and changed during operation. This change in inlet guide vane angle influences the inlet flow of the gas turbine, and has a positive impact on the performance of the gas turbine. In CT, this change in inlet guide vane angle cannot be captured by the model. This means that at low loads, where the inlet guide vane angle is changed the most, the model can no longer predict the performance of the GT correctly.

Table 4.3: CT parameters for the GT model at 100% load

Component	Parameter		CT Value		Reference value		Reference
Compressor	Isentropic efficiency	η_{is}	0.843	-	0.78	-	[19]
	Pressure ratio	Π	23.54	-	23.54	-	[73]
	Mechanical efficiency	η_m	0.997	-	0.99	-	[73]
Turbine	Isentropic efficiency	η_{is}	0.865	-	0.82	-	[19]
	Pressure ratio	Π	4.80	-		-	
	Mechanical efficiency	η_m	0.997	-	0.99	-	[73]
Power turbine	Isentropic efficiency	η_{is}	0.86	-		-	
	Pressure ratio	Π	4.76	-	-	-	
	Mechanical efficiency	η_m	0.996	-	0.99	-	[73]
Generator	Generator efficiency	η_{gen}	0.975	-	0.975	-	[73]
Pumps	Isentropic efficiency	η_{is}	0.85	-	0.7-0.85	-	[19, 71]
	Mechanical efficiency	η_m	0.8	-	0.6-0.9	-	[19, 71]
Overall	Power output	P_{out}	31.28	MW	31.21	MW	[73]
	Energy consumption	E_{in}	9530.6	kJ/kWh	9549.1	kJ/kWh	[73]
	Exhaust temperature	T_{exh}	533.8	°C	533.8	°C	[73]

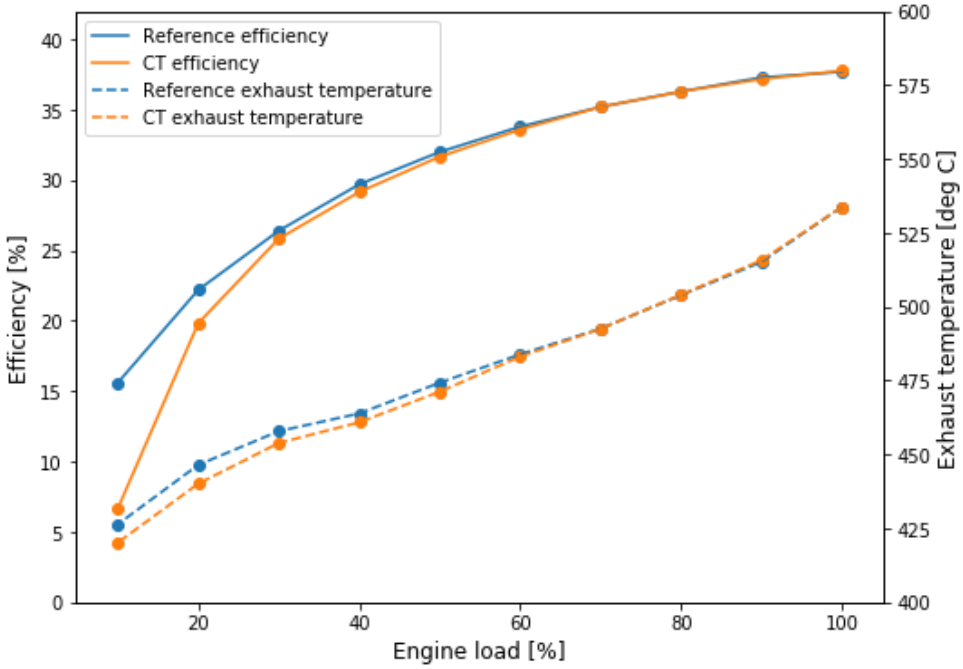

Figure 4.5: Comparison of exhaust temperature and efficiency of the GT model and the reference values [73] for different engine loads

4.1.3. Solid oxide fuel cell

The SOFC can be implemented in the model using the fuel cell component. In this component, there are three options regarding SOFCs. The first option is the standard SOFC. Using this option, only H_2 and CO can be fed into the fuel cell. When using diesel fuel, this fuel needs to be reformed by an external fuel reformer into a mixture of H_2 and CO. However, during this reforming, some H_2 and CO react back into CH_4 in a so-called methanation reaction [80, 81]. This means that a small amount of CH_4 will also enter the fuel cell, and the standard SOFC cannot be used in the model. The other options are indirect internal reforming (IIR)- and direct internal reforming (DIR)-SOFC. With these options, any CH_4 entering the fuel cell will be reformed into H_2 and CO in an internal reformer (IIR) or directly at the anode (DIR). For this thesis, the DIR-SOFC is chosen for the models.

In CT, the mass flow into the anode, and the oxygen flow from the cathode to the anode are calculated using Equation 4.4 and Equation 4.5 respectively [22]. The mass flow into the anode is calculated using the molar mass of the anode intake gas (M_{an}), the total current (I), the Faraday constant (F), the fuel utilization factor (u_f) and the molar fractions of H_2, CO and CH_4 in the anode intake gas. The oxygen flow is calculated using the molar mass of oxygen (M_{O_2}), total current and the Faraday constant. In the CT model, the outlet temperature of the SOFC is an input variable. Using this outlet temperature, the energy balance determines the mass flow of air into the cathode [22].

$$m_{an}^{in} = \frac{I \cdot M_{an}}{2 \cdot F \cdot \left(y_{H_2}^{in} + y_{CO}^{in} + y_{CH_4}^{in}\right) \cdot u_f} \tag{4.4}$$

$$m_{O_2} = M_{O_2} \frac{I}{4F} \tag{4.5}$$

SOFCs have a high operating temperature (600-1000 °C [82]), which means that the incoming air and fuel for the fuel cell need to be heated to this operating temperature. The heat necessary for this heating can be taken from the exhaust gasses (AOG and cathode off-gas (COG)) of the fuel cell. In the AOG, some unreacted H_2 and CO are still present. To raise the exhaust gas temperature, this AOG can be mixed with COG and combusted in a combustor. By combusting the AOG, extra heat is generated that can be used to heat the incoming streams. By heating the incoming streams with HEXs, some pressure loss is introduced. This pressure loss needs to be compensated by the fuel pump, air blower and exhaust blower. Lastly, the diesel needs to be reformed before it can enter the fuel cell. This is achieved by feeding the diesel into a gasifier. This gasifier takes fuel and steam as

input, and reacts them to form H_2 and CO. This reformed gas can then be fed into the fuel cell. This reforming reaction is an endothermic reaction, and a heat source is necessary. In the model, this heat is also taken from the exhaust gas of the fuel cell. To minimize the number of components in the system, each stream only contains one HEX, with the exception of the water stream going into the fuel reformer. The HEXs heating the water to steam are split in an economizer (heating the water to the boiling point), an evaporator (evaporating the water into steam at the same temperature) and a superheater (heating the steam to the reformer inlet temperature). The exhaust gas is directed through each HEX in such a way that the inlet temperature of the hot fluid is higher than the outlet temperature of the cold fluid. An overview of the system is shown in Figure 4.6. In this figure, it may seem that the inlet air of the SOFC is heated by low temperature exhaust gas. The exhaust gas and inlet air of the SOFC have about the same mass flow, with the exhaust gas being slightly larger. If the inlet air of the SOFC is heated first, the exhaust gas temperature will be lower than the outlet temperature of the other streams, and it can no longer heat these streams to the desired temperature. The other streams are small compared to the exhaust gas stream, which means that the temperature difference between the exhaust blower and inlet air heater is fairly small. The exhaust gas entering the inlet air heater still has a temperature of around 750 °C, which is sufficient to heat the inlet air to the SOFC inlet temperature (700 °C).

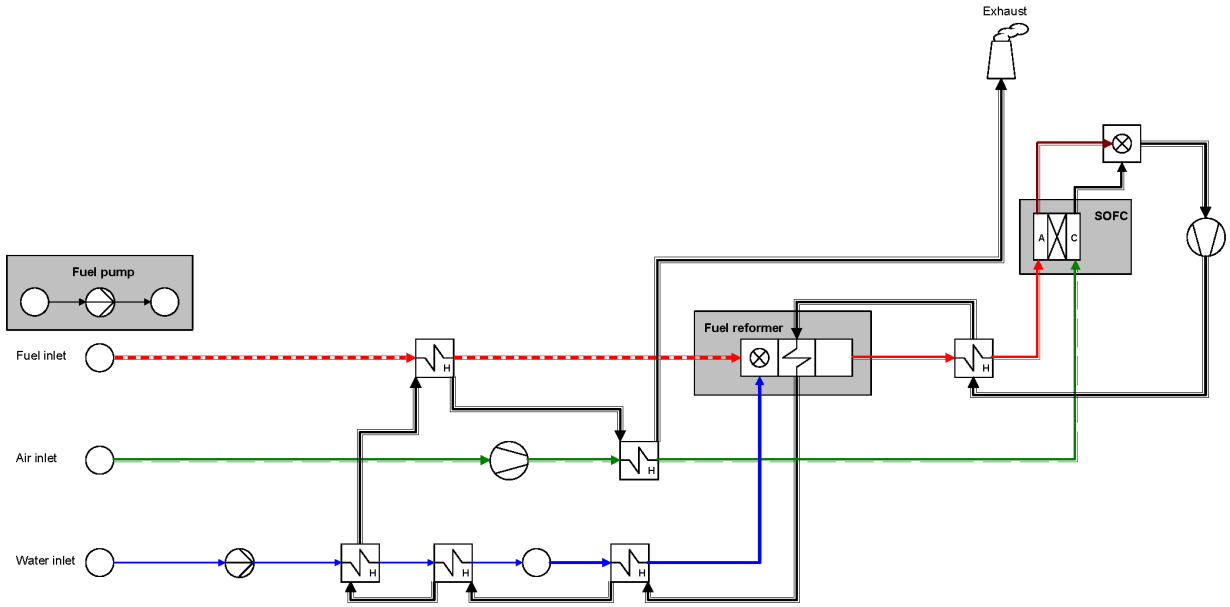

Figure 4.6: CT model for the SOFC

For the model to run correctly, some parameters are necessary. First of all, the operating temperature, pressure, cell voltage and fuel utilization need to be set for the fuel cell. For these parameters, the SolydEra fuel cell module (FCM) is used. This fuel cell consists of the SolydEra G8 stack with 70 cells [74]. The relation between output power, stack voltage and stack current for this fuel cell is given in Figure 4.7. This curve is given for a temperature of 750 °C, which is taken as the fuel cell operating temperature. The operating pressure for these curves is not provided by SolydEra, and it is assumed that the fuel cell operates at atmospheric pressure. The cell voltage can be calculated by dividing the stack voltage by the number of cells in the stack. Lastly, the fuel utilization factor is determined by matching the model efficiency with the reported efficiency by SolydEra [74].

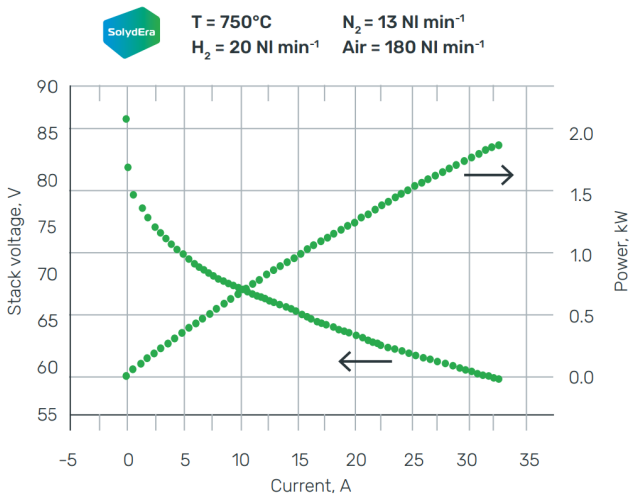

Figure 4.7: Relation between power, current and stack voltage for the SolydEra G8 stack [83]

The efficiency reported by SolydEra [74] is for operation on hydrogen or NG. The model is therefore run with both these fuels to assess the performance. For operation on hydrogen, the fuel reformer is bypassed, and no steam enters the system. For operation on NG, the fuel reformer is used to convert the NG to a mixture of H_2 and CO. For this reformer, a reforming temperature of 600 °C [84] and a steam to fuel (S/F) ratio of 2.3 kg/kg are used [71]. Lastly, a pressure loss of 0.01 bar is assumed for every HEX. The efficiency of the CT model is plotted against the reported efficiency by SolydEra in Figure 4.8. In this figure, it can be seen that the CT model gives results close to the actual performance of this fuel cell for operation on either NG or hydrogen. The CT models are only run for loads between 75% and 100%. At 75%, the efficiency of the SOFC reaches its maximum value. Operating the fuel cell at this load may increase the efficiency of the combined cycles. Lowering the load of the SOFC will reduce its efficiency again, which means that this lower load is not beneficial for the system efficiency of the combined cycles. Loads lower than 75% are therefore not considered in the validation of this model.

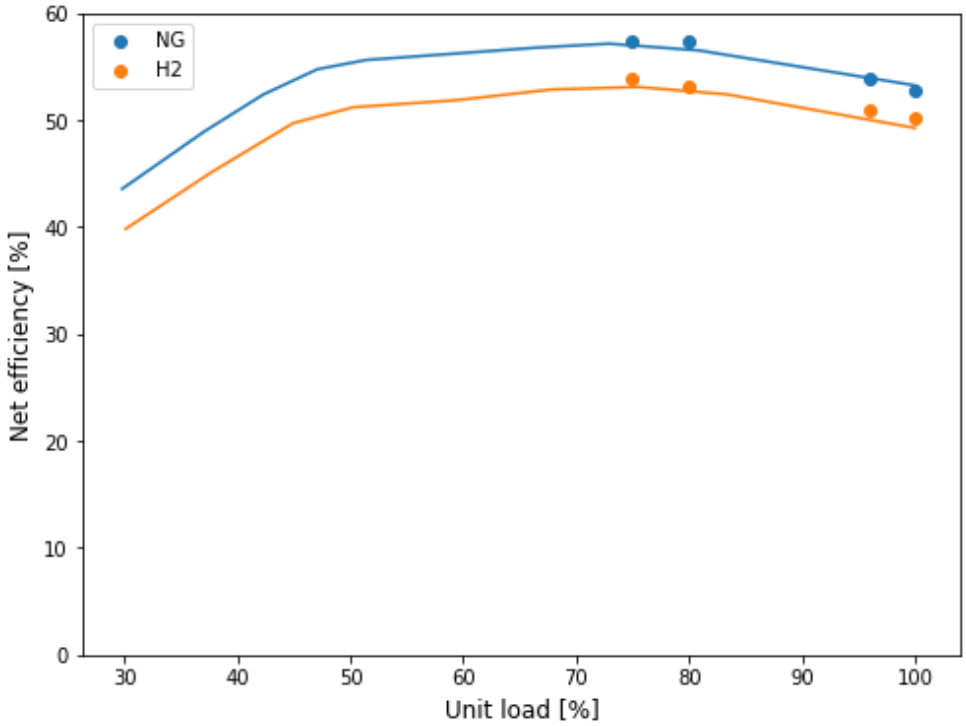

Figure 4.8: Efficiency of the SOFC model compared to the efficiency curve reported by SolydEra [74]. The continuous line is the reported efficiency, and the markers are the obtained efficiency from the CT models

Next, the fuel is changed from NG to diesel. The fuel reformer temperature is set at 600 °C [84], which is the same as the reforming temperature used for NG. The fuel cell temperature, pressure, cell voltage and fuel utilization are also kept constant. For this model, the S/F ratio is changed. The S/F ratio is calculated using the minimal steam to carbon (S/C) ratio needed to avoid coking of the reformer. For steam reforming of diesel, the minimal S/C ratio is 2 kmol/kmol [85]. In CT, a S/F ratio in kg/kg is needed as input, which means that the S/C ratio needs to be converted to a S/F ratio. This is achieved by using Equation 4.10, which is derived from Equation 4.6 to Equation 4.9. Here, the S/F ratio is calculated by multiplying the S/C ratio with the ratio of molar mass between steam and the fuel ($\frac{M_{steam}}{M_{fuel}}$) and the total kmol carbon per kmol fuel ($n_{carbon,fuel}$). For diesel ($C_{14.8}H_{26.9}$), this results in a S/F ratio of 2.61 kg/kg.

$$S/C = \frac{n_{steam}}{n_{carbon}} \tag{4.6}$$

$$S/F = \frac{m_{steam}}{m_{fuel}} \tag{4.7}$$

$$S/F = \frac{n_{steam} \cdot M_{steam}}{n_{fuel} \cdot M_{fuel}} \tag{4.8}$$

$$S/F = \frac{n_{steam} \cdot M_{steam}}{\frac{n_{carbon}}{n_{carbon,fuel}} \cdot M_{fuel}} \tag{4.9}$$

$$S/F = S/C \cdot \frac{M_{steam}}{M_{fuel}} \cdot n_{carbon,fuel} \tag{4.10}$$

The efficiency of the model is then calculated for the same loads as for the NG and hydrogen models. This results in the efficiencies as shown in Figure 4.9. Here it can be seen that the efficiency of the fuel cell operating on diesel slightly decreases compared to running on NG. This can be explained by the different LHV of the fuels. CT calculates a mass flow into the anode based on the composition of this stream (Equation 4.4). This composition is a result from the steam reforming reaction and S/F ratio. This in turn determines the mass flow of fuel into the system. For both NG and diesel, this mass flow is 0.012 kg/s and 0.013 kg/s respectively for a gross power output of 325 kWe of the SOFC. The mass flow for each fuel is about the same, but the energy content of the fuel is different. When multiplying these mass flows with the LHV of the respective fuels, an energy flow into the system is obtained (497.5 kW for NG and 530.8 kW for diesel). For NG less energy input is necessary for the same power output, resulting in a higher efficiency ($\eta = P_{out}/E_{in}$).

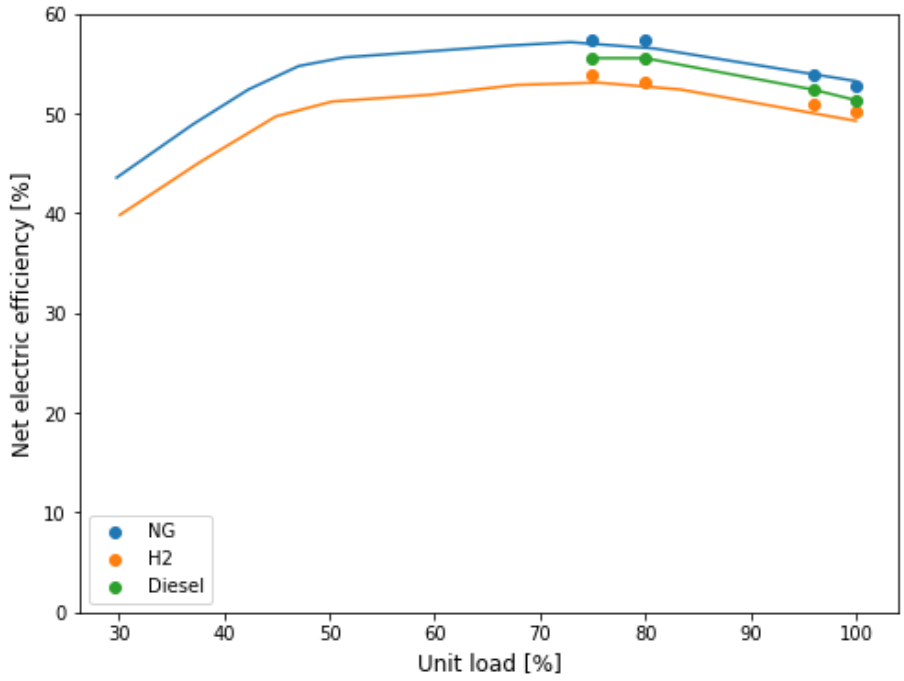

Figure 4.9: Efficiency of the SOFC model running on diesel, compared to running on NG and hydrogen as reported by SolydEra [74]

In a study by van Veldhuizen et al. [71], operation of an SOFC on both diesel, methane and hydrogen are compared. In this study, the efficiency of the diesel fuelled SOFC also lies between the methane and hydrogen fuelled SOFC. Ezgi et al. [7] also model an atmospheric SOFC running on reformed diesel. The authors report a net efficiency of 55.28%, which is only slightly lower than the maximum net efficiency reached by the CT model (55.39%). This shows that the model can predict the performance of the SOFC fuelled by diesel correctly.

Lastly, the exhaust temperature of the system is compared to the value reported by SolydEra [74] in Table 4.4. Here it can be seen that the exhaust temperature for NG lies between the range reported by SolydEra. For diesel operation, no exhaust temperature is available. The exhaust temperature for diesel operation is higher than operation on NG. This can be explained in a few ways. First of all, the airflow into the fuel cell is larger for operation on NG. This is explained by a difference in anode inlet stream composition. The fractions of H_2, CO and CH_4 are different between NG- and diesel-operation. This difference leads to a different (lower) mass flow into the anode, which in turn influences the energy balance of the fuel cell. This different energy balance means that the airflow into the cathode decreases for diesel-operation. Since both the fuel flow into the anode and the air flow into the cathode are lower for diesel operation, less heat is extracted from the exhaust gas to reach the intake temperatures. Lastly, the c_p for the diesel exhaust gas is slightly higher than that of the NG exhaust gas. The temperature difference in the HEX is calculated using Equation 4.11 [86] by dividing the transferred heat (Q) with the mass flow ($\dot{m}$) and the specific heat (c_p). For NG, the transferred heat and mass flow are both about 4% higher. Additionally, the c_p for the NG exhaust gas is slightly lower compared to diesel exhaust gas. In the equation, this results in a larger ΔT for NG, which corresponds to a lower exhaust temperature leaving the system.

$$Q = m \cdot c_p \cdot \Delta T \tag{4.11}$$

Table 4.4: Exhaust temperature for the SOFC model operating on NG or diesel

	Exhaust temperature	Reference value
Diesel	148.7 °C	-
NG	125.5 °C	120-140 °C [74]

The parameters used for the different components of the SOFC model are given in Table 4.5 for 100% load. For each parameter, a reference value in current literature is also provided. For part-load operation, only the cell voltage is changed (0.85 V for 100% and 0.89 V for 75%). It should be noted that in part load, the performance of the blowers and pumps also changes. However, no performance data for part-load regarding the blowers and pumps is available, and the performance of these components is assumed to be constant regardless of part-load or full-load operation. An overview of all the parameters for the part-load models is given in Appendix D.

Table 4.5: CT parameters for the SOFC model at 100% load

Component	Parameter		CT Value		Reference value		Reference
SOFC	Fuel utilization factor	u_f	0.8	-	0.8	-	[71]
	Cell voltage	V_{cell}	0.85	V	0.85	V	[74]
	Stack temperature	T_{stack}	750	°C	750	°C	[74]
	Inlet temperature	T_{in}	700	°C	$T_{stack} - 75$ - $T_{stack} - 40$	°C	[19, 71]
	Outlet temperature	T_{out}	790	°C	$T_{stack} + 25$ - $T_{stack} + 40$	°C	[19, 71]
	Anode pressure drop	Δp_{an}	0.02	bar	0.02	bar	[71]
	Cathode pressure drop	Δp_{ca}	0.02	bar	0.015	bar	[71]
Fuel reformer	Reformer temperature	T_{reform}	600	°C	600	°C	[84]
	Steam to carbon ratio	S/C	2	kmol/kmol	2	kmol/kmol	[85]
	Steam to fuel ratio	S/F	2.61	kg/kg	-	-	-
	Pressure drop	Δp	0.01	bar	0.01	bar	[71]
Heat exchangers	Pressure drop	Δp	0.01	bar	0.01	bar	[71]
Pumps	Isentropic efficiency	η_{is}	0.85	-	0.7-0.85	-	[19, 71]
	Mechanical efficiency	η_m	0.8	-	0.6-0.9	-	[19, 71]
Blowers	Isentropic efficiency	η_{is}	0.85	-	0.7-0.85	-	[19, 71]
	Mechanical efficiency	η_m	0.8	-	0.6-0.9	-	[19, 71]

4.2. Methanol

MeOH has different fuel properties than diesel, and this influences the performance of the different components. Table 4.6 shows an overview of the different fuel properties between diesel and MeOH. First of all, the LHV of MeOH is about half of the LHV of diesel, which means that for the same energy input in the system, about twice as much MeOH is needed in terms of weight. For the heat engines this means that the fuel injection system needs to be altered to accomodate this increase in fuel flow. Next, the stoichiometric air-to-fuel ratio of MeOH is significantly lower. This ratio shows how much air is necessary for complete combustion of the fuel, and less air is necessary to combust 1 kg of MeOH compared to 1 kg of diesel. MeOH also has a lower flame temperature than diesel. This means that when combusting the fuel at stoichiometric conditions, the temperature after combustion is lower for MeOH, which in turn lowers the temperature of the exhaust gasses compared to diesel.

Table 4.6: Difference in fuel properties between diesel and MeOH [87]

Property	Diesel	MeOH
LHV [kJ/kg]	42700	20100
A/F_{stoich} [-]	14.6	6.5
Flame temperature [°C]	2054	1890

Due to the differences in fuel properties, the performance of the components change in terms of efficiency and exhaust temperature. For each model, the necessary changes to run on MeOH are discussed in the sections below.

4.2.1. Internal combustion engine

The conversion of the ICE model to run on MeOH necessitates a few changes. First of all, the fuel type needs to be changed from diesel to MeOH. For the model, it is assumed that the same amount of energy enters the system, i.e. the energy input from the fuel is equal for diesel and MeOH. This means that the fuel mass flow needs to increase for MeOH due to the lower LHV. This increased fuel mass flow, together with a lower A/F_{stoich}, means that the airflow into the engine also changes when the air-excess ratio is kept the same in the engine. The turbocharger for the reference ICE is designed for a specific air flow, and if the airflow changes for operation on MeOH, this requires a different turbocharger for the engine. A different turbocharger may have differences in mechanical and isentropic efficiency, and this data is unavailable for MeOH engines. Due to a lack of reference data for MeOH-fuelled turbocharged engines, the mechanical and isentropic effficiencies of the turbocharger are kept the same as for the diesel-fuelled model. To match the power output of the turbocharger turbine with the turbocharger compressor, the air excess ratio (λ) in the combustor is changed compared to diesel operation. The difference in λ, in addition to a different fuel composition, influences the composition of the exhaust gas, which has a direct influence on the power produced by the turbocharger turbine. The in-cylinder process is modeled as a Diesel cycle in CT, which means that the power of the expansion stroke can be calculated using Equation 4.12. When the power necessary for compression of the air is subtracted, the net power output of the cycle is obtained. For MeOH operation, the mass flow through the turbine increases slightly, mainly due to an increase in fuel flow into the engine. Due to a difference in exhaust gas composition and a lower temperature after combustion (which is a result from the lower flame temperature of MeOH), the ΔT in this equation changes. Lastly, c_p changes due to a difference in exhaust gas composition. These changes lead to an increase in power output for MeOH operation, which in turn increases the efficiency of the system compared to diesel operation (as the energy input in the system is kept constant for both fuels). The lower temperature after combustion also lowers the exhaust gas temperature leaving the system. The engine efficiency and exhaust gas temperature of the converted model to MeOH operation compared to diesel operation are shown in Figure 4.10. From the model, an increase in engine efficiency of about 2% and a decrease in exhaust temperature of about 30 °C can be observed.

$$P_{turb} = \dot{m} \cdot c_p \cdot \Delta T \tag{4.12}$$

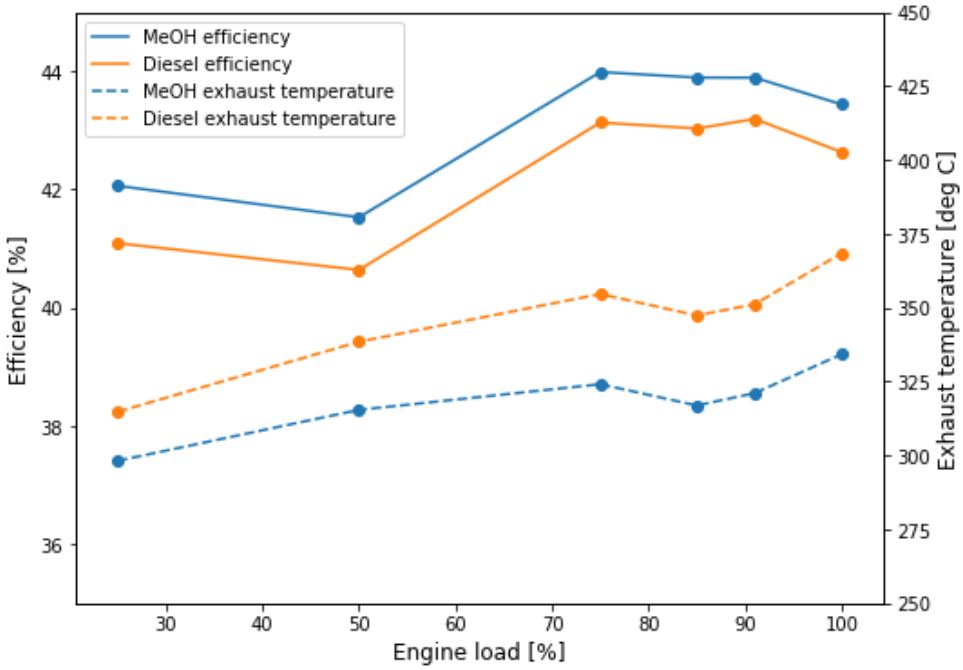

Figure 4.10: Efficiency and exhaust temperature for MeOH operation compared to diesel operation of the ICE model

Currently, MAN and Wärtsilä both offer MeOH engines for the marine sector [88, 89], but no performance data is given by either manufacturer in terms of engine efficiency and exhaust temperature. Nordhavn Power Solutions [90] offer small marine engines (200-400 kW) running on so-called MD97 fuel, which is a mixture of MeOH and "ignition enhancer". These engines are based on the Scania marine diesel engines, and a peak efficiency of 45% is reached at about 80% load. When comparing this value for the MeOH engine [91] to its diesel counterpart [92], an increase in efficiency is observed (43% for diesel and 45% for MeOH). For these engines however, no data is available regarding exhaust gas temperatures.

In current literature, various studies are performed on the performance of MeOH engines. Tol [93] experimentally studies the effect of MeOH-diesel blends of 0%, 10% and 20% MeOH in terms of energy, which equals to a mass percentage of 0%, 18.9% and 34.4% MeOH for the respective fuels, in a MAN 4L20/27 diesel engine. In his experiments, Tol found that the thermal efficiency of the different fuel blends are within 0.25% of eachother. Additionally, he measured the exhaust gas temperature of the different fuel blends, and found that the exhaust temperature decreases for increasing MeOH content. Yusaf et al. [94] study MeOH-diesel fuel blends of up to 30% MeOH based on volume. In their research, they found that the thermal efficiency of the MeOH-diesel blends increased compared to operation on pure diesel. Similar to the research by Tol, Yusef et al. found that the exhaust temperature of the engine decreased when operating on MeOH blends compared to pure diesel operation. Hassan et al. [95] evaluate the engine performance and exhaust temperature of a four-stroke CI engine for MeOH-diesel blends up to 21 vol.% MeOH. They find that the thermal efficiency of the engine increased for MeOH fractions up to 14%, and decreased for the 21% mixture. The exhaust temperature decreased for increasing MeOH fractions. A recent study by Karvounis et al. [96], investigates two types of MeOH injection in a Wärtsilä 9L46C marine diesel engine. The authors find that for direct injection of MeOH, the engine can run knock-free for a MeOH energy fraction of 95% (or a mass fraction of 97.6%). At this MeOH fraction, they observe a thermal efficiency increase of the engine of 4.2% compared to operation on diesel, which is attributed to faster combustion and lower compression work and heat losses when running on high MeOH fractions.

When comparing the results from the CT model with the abovementioned studies, the same trends can be observed. Most of the abovementioned studies agree that the efficiency of the engine increases for increasing MeOH fractions. These results are available for MeOH fractions up to 97 mass%. For exhaust temperature, the studies also agree that for an increase in MeOH fraction, the temperature decreases. However, these studies only look at a maximum MeOH fraction of 34.4 mass%. When extrapolating to 100% MeOH, it is expected that the exhaust temperature decreases compared to diesel, but data for high MeOH fractions is still unavailable in current literature.

4.2.2. Gas turbine

Similar changes are made to the GT model as to the ICE model. The fuel is changed, fuel mass flow is increased and λ is increased to match the intake air flow of the diesel model. The result of these changes on thermal efficiency and exhaust gas temperature are shown in Figure 4.11. Just like the ICE model, the thermal efficiency of the GT increases, and the exhaust temperature decreases. This effect is also observed in experimental tests by Siemens [97]. Siemens has experimentally tested the effect of converting the Siemens Energy SGT-A20 gas turbine from diesel to MeOH. The changes made to the GT by Siemens are limited to the fuel system, and the the compressor and turbines are kept the same. In their experiments, they found that the thermal efficiency of the GT increased with about 4%, and the exhaust temperature reduces by about 25 °C. While these numbers are valid for the SGT-A20 gas turbine, they may not directly apply to the modelled GE LM2500+. However, the trend of increased efficiency and reduced exhaust temperature can be applied to the modelled gas turbine. In the case of the CT model, the thermal efficiency increased by about 1.5%, and the exhaust temperature reduces by about 30 °C, meaning that the model shows the same behaviour as the converted GT by Siemens.

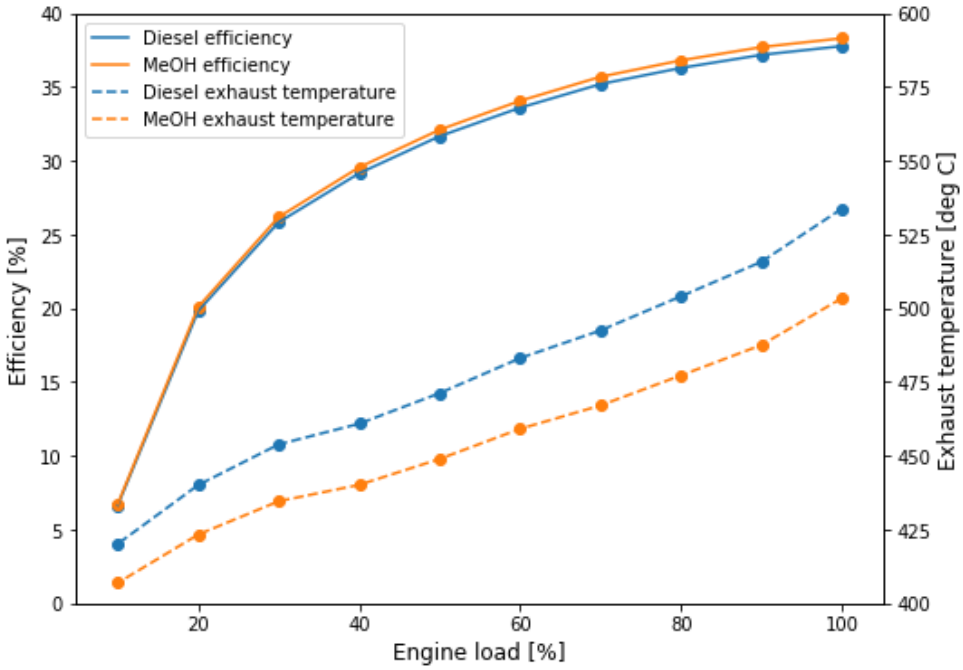

Figure 4.11: Efficiency and exhaust temperature for MeOH operation compared to diesel operation of the GT model

4.2.3. Solid oxide fuel cell

For the SOFC model, the changes are slightly different. MeOH can be reformed internally in the SOFC, which eliminates the need for an external reformer [15]. However, to reduce thermal stresses on the SOFC, many studies still implement an external reformer [71], and an external reformer is also included in the model for this thesis. All of the MeOH can be reformed into H_2 and CO at a temperature of 300 °C. However, at this temperature, a portion of the H_2 and CO react to form CH_4 [81]. To reduce the amount of methanation, the reformer temperature is kept at 600°C (equal to the diesel operation). For the steam reforming reaction of MeOH, a minimal S/C ratio of 1.2 is necessary to avoid coking of the reformer [98]. When using Equation 4.10, this results in a S/F ratio of 0.68 kg/kg.

The efficiency of the fuel cell running on MeOH is shown in Figure 4.12. Compared to operation on diesel, the efficiency of the fuel cell decreases when running on MeOH. This is explained by a large difference in S/F ratio. For both fuels, the mass flow into the anode is about equal (0.043 kg/s for diesel and 0.044 kg/s for MeOH). However, the mass flow of fuel changes from 0.012 kg/s for diesel to 0.026 kg/s for MeOH for a gross SOFC power of 325 kWe. For MeOH, this results in an energy flow into the system of 548.7 kW, which is higher than the energy flow for diesel (530.8 kW). This higher energy flow into the system results in a lower system efficiency. In a study by van Veldhuizen et al. [71], operation of an SOFC on both MeOH and diesel is compared. In this study, the efficiency of the MeOH fuelled SOFC decreases compared to operation on diesel, similar to the results from the CT models in this thesis.

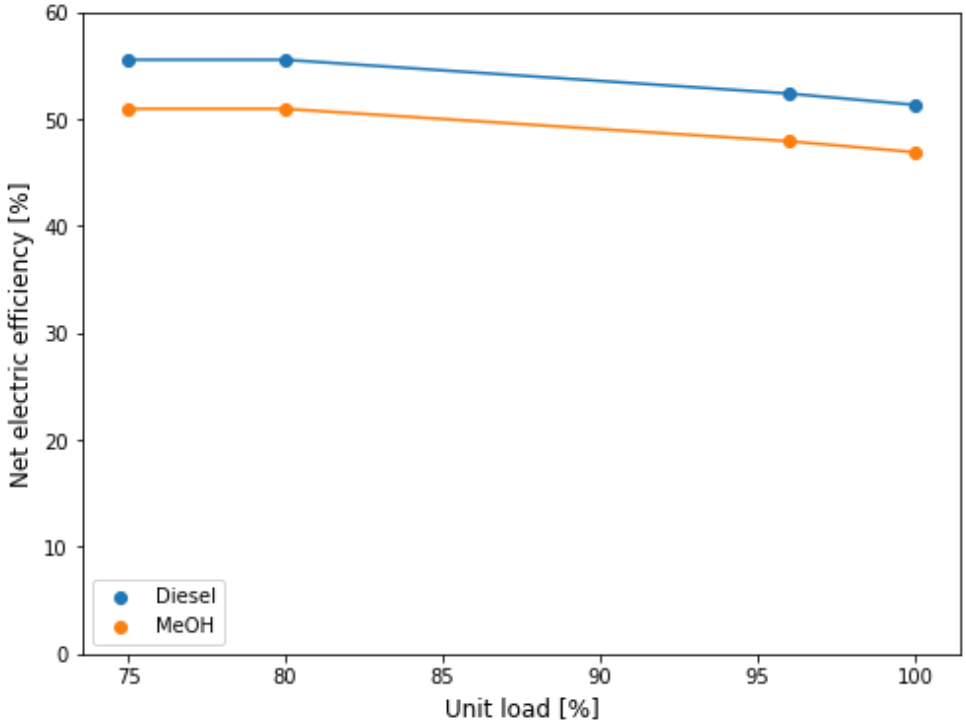

Figure 4.12: Efficiency of the SOFC model running on MeOH, compared to running on diesel

The exhaust temperature for MeOH operation increases compared to diesel operation (shown in Table 4.7). This can mostly be explained by a decrease in steam mass flow for MeOH operation. The lower S/F ratio reduces the steam flow of the system from 0.031 kg/s for diesel to 0.018 kg/s for MeOH. This lower mass flow of steam means that less heat is extracted from the exhaust gas in the economizer, evaporator and superheater. In both systems, the exhaust flow is about equal (1.199 kg/s for diesel and 1.194 kg/s for MeOH), which means that the temperature difference over these three HEXs is lower for MeOH operation, resulting in a higher exhaust gas temperature leaving the system.

Table 4.7: Exhaust temperature SOFC model operating on MeOH or diesel

	Exhaust temperature
Diesel	148.7 °C
MeOH	202.0 °C

4.3. Combined cycle models

Using the models for the standalone ICE, GT and SOFC, the combined cycle models are created. First, the SOFC and the ICE models are combined into the SOFC-ICE model, and the model is validated with results from current literature. Next, the SOFC and GT model are combined into the SOFC-GT model, which is again validated by comparing the results with current literature.

4.3.1. SOFC-ICE

As already mentioned in chapter 3, there are two integration strategies in current literature: coupled and decoupled. For this thesis, the decoupled configuration is chosen for the combined cycles. In naval vessels, redundancy is an important factor in the system design. When using coupled systems, the ICE can no longer produce power if the SOFC is lost due to damage or flooding. This leaves the vessel vulnerable to enemy ships, as it can no longer generate power to flee the area. Additionally, the power demand of the reference vessel is fairly large. This means that for a coupled system, due to a large power share of the SOFC, the power plant would become very large and would no longer fit in current design of the vessel. The decoupled system improves the redundancy of the system by allowing for individual operation of the SOFC and ICE, and also allows for power

splits that could fit on the current design of the reference vessel. However, this does come at the cost of a lower system efficiency, and therefore higher fuel consumption compared to the coupled system.

To create the CT model for the parallel configuration, the standalone SOFC and ICE models need to be integrated into a single model. This integration is performed in two steps. First, the SOFC and ICE model are placed in a single model, without integrating these systems. In this model, both the SOFC and ICE operate independently from each other, and only share a fuel inlet, air inlet and exhaust gas outlet. This independend operation model is shown in Figure 4.13. In this figure it can be seen that the intake air and fuel are split into two streams. One enters the ICE and the other enters the SOFC. The exhaust gasses of both systems are then combined into a single stream leaving the system. The independent operation model is created to ensure that combining both standalone models into a single model does not give any strange results. For the verification of this model, the system efficiency in CT is compared to an expected efficiency resulting from Equation 4.13. This equation calculates the system efficiency by dividing the total output power with the total energy input of the system. The total output power is the sum of the ICE power and the SOFC power. The energy input of the system is the sum of the ICE energy input and the SOFC energy input, which is calculated by dividing the power of the component with the efficiency of this component.

$$\eta_{comb} = \frac{P_{ICE/GT} + P_{SOFC}}{E_{in,ICE/GT} + E_{in,SOFC}} = \frac{P_{ICE/GT} + P_{SOFC}}{\frac{P_{ICE/GT}}{\eta_{ICE/GT}} + \frac{P_{SOFC}}{\eta_{SOFC}}} \tag{4.13}$$

The combined efficiency from the CT model, and the expected combined efficiency from Equation 4.13 is given in Table 4.8. In this table it can be seen that the independent operation model gives the same efficiency as the expected values, which means that combining the two standalone models into a single model does not give any unexpected results, and this independent operation model can be used as a starting point to create the combined cycle model.

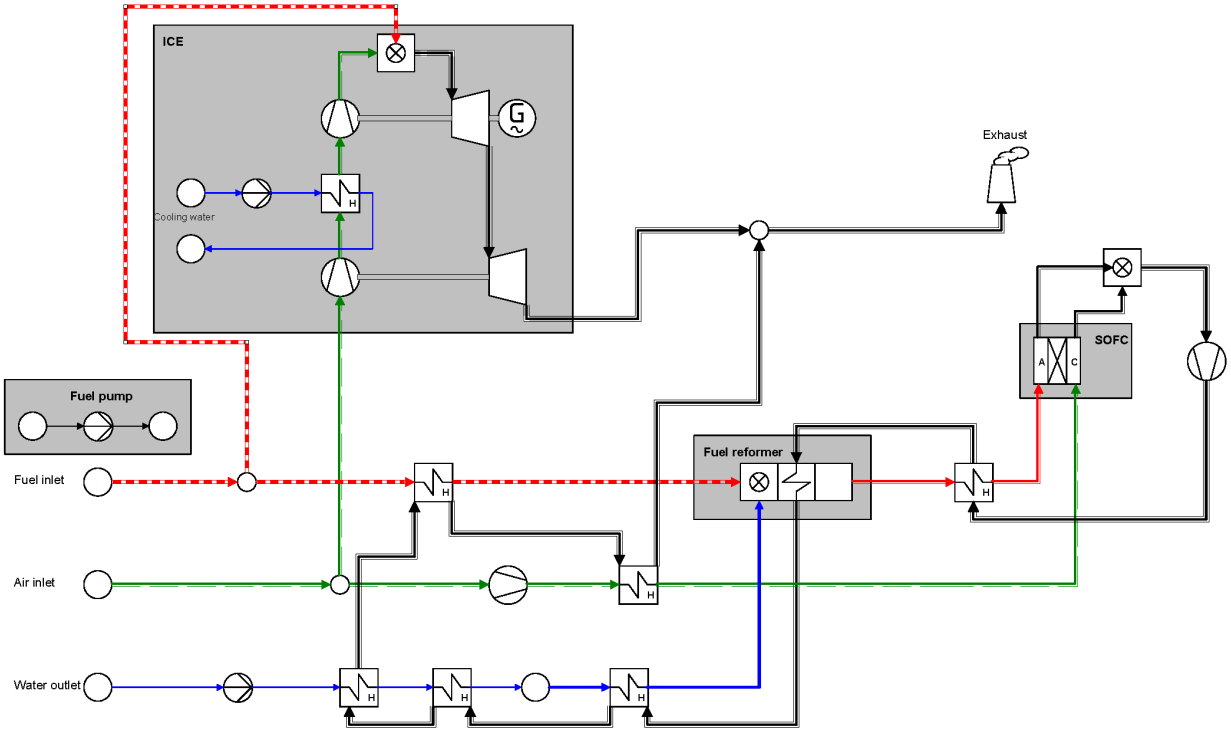

Figure 4.13: Combined model of the ICE and SOFC operating independently

Table 4.8: Combined efficiency from the CT model and the expected value for independent operation of the ICE and SOFC on diesel fuel

Power split	Expected efficiency	Combined efficiency
0-100	42.7%	42.7%
25-75	44.5%	44.5%
50-50	46.5%	46.5%
75-25	48.6%	48.6%
100-0	51.0%	51.0%

The second step in creating the SOFC-ICE combined cycle model is integrating the SOFC and ICE from the independent operation model (Figure 4.13) into a combined cycle. In the chosen configuration (decoupled), the AOG is mixed with diesel fuel and fed into the ICE. However, the AOG contains water vapour, which acts as a diluent if this AOG is to be used as fuel in the ICE, meaning that less energy enters the system per kg of AOG. This water vapour is removed from the AOG by adding a moisture separator. In this moisture separator, the AOG is cooled with ambient air until the water vapour condenses. The dry AOG is then mixed with the diesel fuel, before it enters the combustion chamber of the ICE. The COG is used to pre heat the different intake streams of the SOFC. However, this COG has a lower temperature compared to the exhaust gas used in the independent operation, as it is no longer combusted with AOG to raise the temperature. In the original routing of the SOFC exhaust gas, this no leads to crossing temperature profiles in some HEXs. A crossing temperature profile means that the outlet temperature of the cold fluid is higher than the inlet temperature of the hot fluid. In reality this will mean that the set outlet temperature of the cold fluid can never be reached, and the routing of the COG needs to be changed to avoid crossing temperature profiles. For this rerouting, an extra HEX is added to the air intake stream of the SOFC. This extra HEX results in an additional pressure drop in the inlet stream, which has to be compensated by the blowers in the system. In this layout, the blowers consume additional power, resulting in a slightly lower system efficiency compared to the independent operation model. Lastly, a bypass valve is added into the AOG and COG streams. Using these valves, AOG and COG can be directed towards a combustor, which allows for independent operation of the SOFC for the silent mode of the reference vessel. The entire combined cycle system is shown in Figure 4.14.

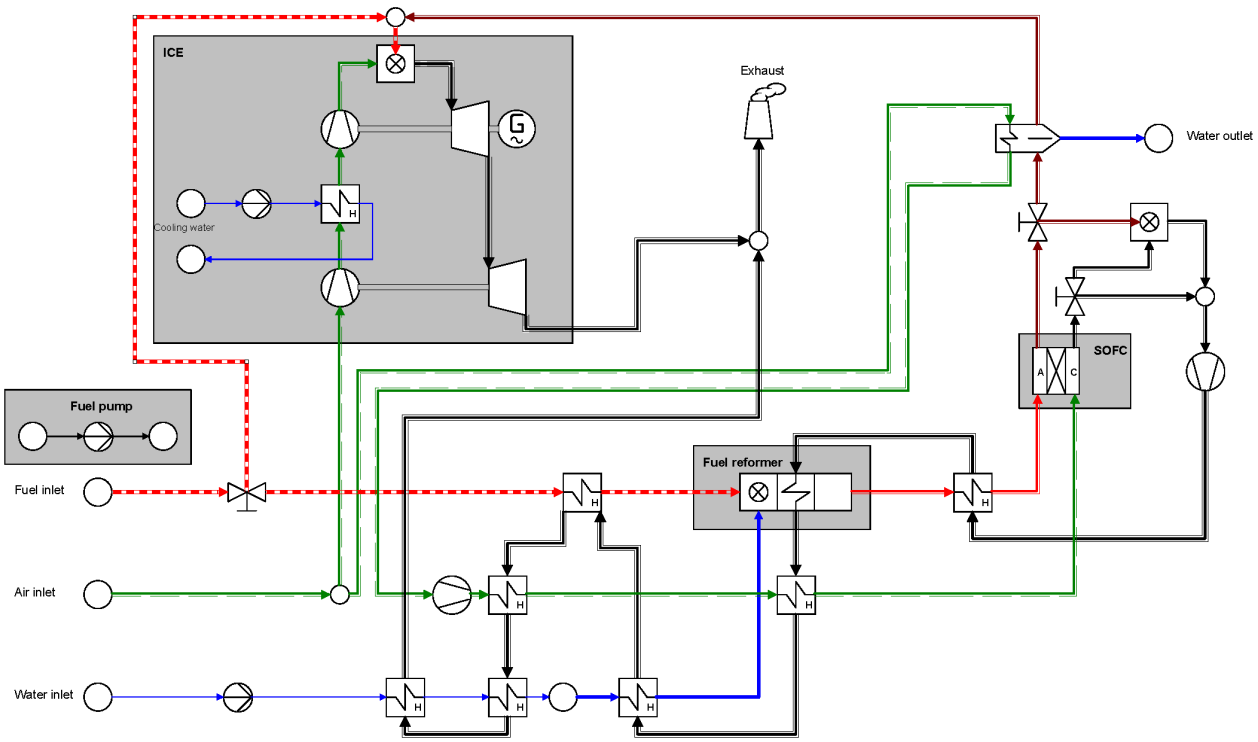

Figure 4.14: CT model of the SOFC-ICE combined cycle

To check whether the combined cycle model gives accurate results, the performance is compared to results from

current literature. In current literature, studies on diesel- and MeOH-fuelled SOFC-ICE with a similar layout to this thesis are extremely limited. For diesel, Chuahy and Kokjohn [12] model a similar system layout as in this thesis, with the main difference being the operating pressure of the SOFC. In this thesis, the SOFC is operated at atmospheric pressure, whereas Chuahy and Kokjohn operate the SOFC at an elevated pressure (>3 bar). Their optimized system has a power share of the SOFC of 85.3%, and the ICE runs on AOG with an addition of 1.08% diesel fuel. With this system, they obtain an electrical efficiency of 70.9%. When running the CT model with the same power split and diesel addition, an electrical efficiency of 61.1% is obtained when both components run at full load, and an efficiency of 65.3% is obtained when the SOFC runs at its maximum effficiency (75% load). For both cases the system efficiency is lower compared to the reported efficiency by Chuahy and Kokjohn. This difference can be explained by the elevated operating pressure of the fuel cell, leading to a higher efficiency of the SOFC. Increasing the operating pressure of the SOFC improves the efficiency of the fuel cell by increasing the open-cell voltage and reducing activation overpotential [99]. Chuahy and Kokjohn report an SOFC efficiency of 64.4%, whereas the fuel cell operates at a maximum efficiency of 55.4% in this thesis.

Li et al. [15] model a SOFC-ICE cycle running on MeOH. In this system, MeOH is fed into the SOFC where it is internally reformed. The ICE runs entirely on AOG, resulting in a power split of 81.6-18.4 in favour of the SOFC. With this system, they obtain an efficiency of 56.1%. While the system by Li et al. is almost identical to the CT model, there is one major difference. Li et al. feed the MeOH directly to the SOFC, whereas the CT model includes an external reformer. To compare the results of the CT model with the results obtained by Li et al., the external reformer is bypassed. When bypassing the external reformer, and setting the same power split as Li et al., the CT model obtains an efficiency of 56.6%. This efficiency is slightly higher than the efficiency reported by Li et al., which can be explained by a difference in fuel utilization factor. Li et al. use a fuel utilization factor of 0.75, whereas it is 0.8 in this thesis. A higher fuel utilization factor means that less unreacted fuel leaves the system, resulting in a higher SOFC efficiency. This higher SOFC efficiency in turn increases the total system efficiency. Next, the external reformer is again included in the CT model, which results in an efficiency of 59.3%. With the external reformer, the system efficiency increases. Li et al. also report this behaviour, and attribute this higher efficiency to a higher partial pressure of H_2 at the anode, which increases the output voltage of the SOFC, resulting in a higher system efficiency.

Table 4.9 shows the results from the CT model compared to the current literature. In this table, it can be seen that the results from the CT model differ slightly from the systems in current literature, and these differences can be attributed to differences in integration strategies or operating parameters. While the results from the CT model are not exactly equal to the results in literature, the model still gives results in the same range as the current literature, and the CT models can be used to compare the different fuels for the SOFC-ICE combined cycles.

Table 4.9: Results of the SOFC-ICE combined cycle model compared to current literature

Fuel	Reference	System performance	Remark
Diesel	Chuahy and Kokjohn [12]	70.9%	SOFC operates at elevated pressure
	This thesis	65.3%	SOFC operates at atmospheric pressure
MeOH	Li et al. [15]	56.1%	Internal fuel reforming Power split: 81.6-18.4
	This thesis	56.6%	Internal fuel reforming Power split: 81.6-18.4
	This thesis	59.3%	External fuel reforming Power split: 81.6-18.4

4.3.2. SOFC-GT

In current literature, the SOFC-GT combined cycles use the waste heat from the SOFC for heat addition in the GT. This results in high system efficiencies, but limits the ability to operate the GT without also running the SOFC. For the naval surface combatant, it is important that both the SOFC and GT are able to operate independently. At silent operations, only the SOFC is running, which means that the heat integration of the combined cycle needs to allow the SOFC to operate without the need for waste heat from the GT. In addition, if the SOFC fails to operate due to damage or flooding, the GT needs to be able to operate independently to still provide the ship with power. This limits the possibility of fully integrating the SOFC and GT into a single system similar to Figure 2.1. In this thesis, it is therefore chosen to integrate the GT and SOFC in a similar fashion as the SOFC-ICE system. Instead of using waste heat from the SOFC for heat addition in the GT, AOG is mixed with additional fuel and

combusted in the combustion chamber of the GT.

Just like with the SOFC-ICE combined cycle, the first step in creating the SOFC-GT combined cycle is placing the standalone SOFC and GT model into a single model. The performance of this independent operation model (Figure 4.15) is checked by comparing it with the expected value for system efficiency from Equation 4.13. This model is checked for the same power splits as the SOFC-ICE models was checked (i.e. 0-100, 25-75, 50-50, 75-25 and 100-0). Table 4.10 shows the obtained efficiency from the CT model compared to the expected efficiency from Equation 4.13. Here it can be seen that the CT model does not produce unexpected results when combining the two standalone models, and this model can be used to create the combined cycle model.

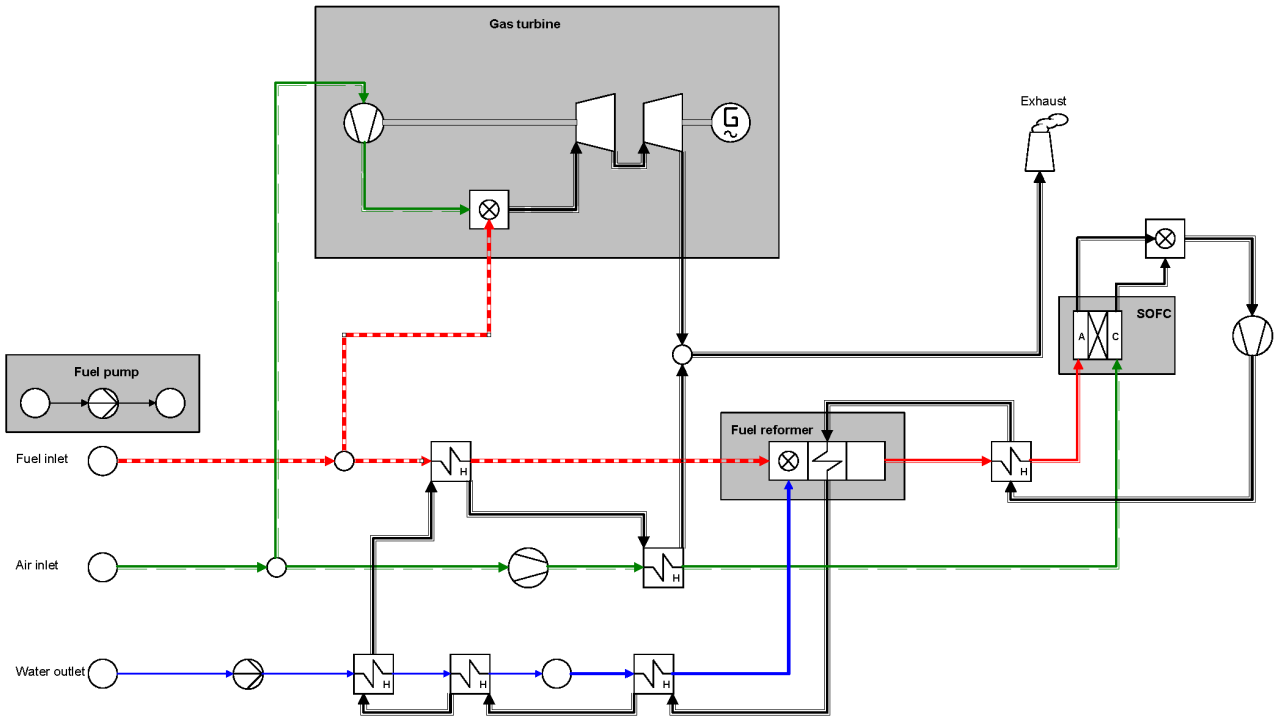

Figure 4.15: Cycle-Tempo model for the independent operation model of the SOFC-GT combined cycle

Table 4.10: Combined efficiency from the CT model and the expected value for independent operation of the GT and SOFC on diesel fuel

Power split	Expected efficiency	Combined efficiency
0-100	37.6%	37.6%
25-75	40.2%	40.0%
50-50	43.3%	43.3%
75-25	46.8%	46.8%
100-0	51.0%	51.0%

When running in combined cycle mode, AOG is directed towards the combustor of the GT, in similar fashion to the combustion of AOG in the SOFC-ICE system. Now that the AOG is no longer combusted with COG to provide heat for the SOFC system, GT exhaust gas is used to preheat the airflow into the cathode. Without the GT exhaust gas, insufficient heat is available from the COG to heat all the streams. Within the system, bypass valves are implemented to allow the SOFC and GT to be decoupled. These bypass valves are located in the AOG, COG and GT exhaust streams. This system is shown in Figure 4.16.

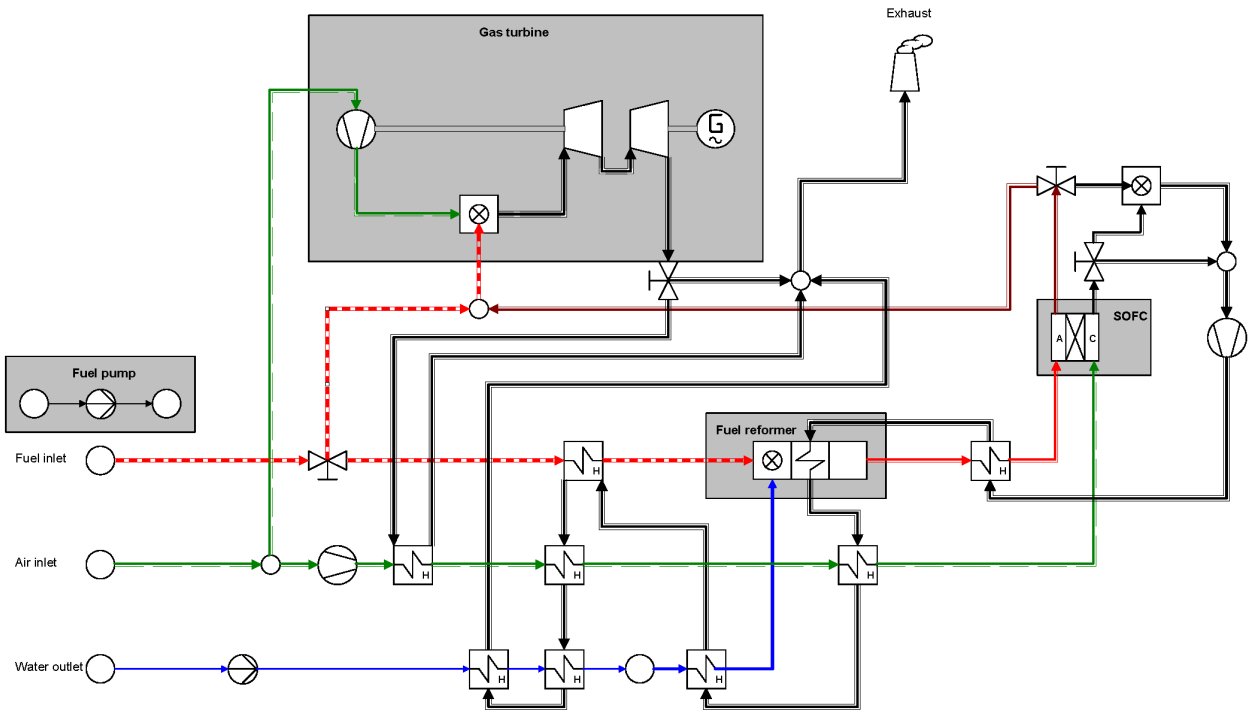

Figure 4.16: Cycle-Tempo model for the SOFC-GT combined cycle

Next, the combined operation is compared to SOFC-GT cycles present in literature. Unfortunately, the integration strategy from this thesis has not yet been considered in current literature, making validation of the CT model difficult; the results from current literature may not directly transfer to the integration strategy of this thesis. Instead of comparing the results from CT directly to the values presented in current literature, the values from the literature are used to determine whether the CT results are in the correct order of magnitude. If for example the literature states a system effficiency of about 60%, and the CT model only gives an efficiency of about 40%, the CT results cannot be valid. If however the CT model also gives an efficiency close to 60%, the results are valid.

Just like with the SOFC-ICE cycle, SOFC-GT cycles running on diesel are scarce. Liu et al. [100] compare a pressurized SOFC-GT cycle using different fuels. Among these fuels is n-decene ($C_{10}H_{22}$). This fuel contains 85% carbon by weight, which is similar to the diesel used in this thesis. In the system by Liu et al., air is compressed by a compressor. The compressed air is then pre-heated by the GT exhaust gas before it enters the fuel cell. AOG and COG are mixed and combusted, after which the exhaust gas is expanded in a turbine. With a power split of 60-40, the authors report system efficiency between 62-68%, depending on the air-to-fuel ratio used (A/F = 3.5 results in 63%, and A/F=3.5 results in 68%). Zhao et al. [23] model an atmospheric SOFC-GT system running on syngas produced from coal. A HEX transfers the heat from the SOFC exhaust gas to the airflow through the GT. With their system, they report a maximum efficiency of around 57%. While both studies model a SOFC-GT combined cycle, the integration strategy is different. Liu et al. implement a pressurized SOFC, which means that the efficiency of the SOFC is higher than an SOFC running at atmospheric pressures. This results in a higher combined cycle efficiency compared to the atmospheric SOFC-GT cycle. The efficiency of the system presented by Liu et al. will therefore be higher than the efficiency of the CT model from this thesis. Zhao et al. present an atmospheric SOFC-GT cycle, which is similar to the CT model. This means that the efficiency of the CT model should be relatively close to the efficiency of the system by Zhao et al. However, the efficiency will not be equal due to a different syngas composition. The results for the CT model are deemed valid if the efficiency is lower than the system by Liu et al., and comparable to the system by Zhao et al.

When running the CT model with a power split of 60-40, which is equal to the power split by Liu et al., a system efficiency of 61.5% is obtained. This is lower than the efficiency of 63-68% reported by Liu et al. [100], and in line with the expectations described above. Zhao et al. [23] do not specify at which power split their system runs, which makes it difficult to determine an appropriate power split to compare the results. In their system, all the heat into the GT is provided by the SOFC exhaust gas, and no additional fuel is added. When running the CT

model without adding additonal fuel to the GT, a power split of 83.8-16.2 is obtained. With this power split the system runs at an efficiency of 60.6%, which is higher than the efficiency reported by Zhao et al. (57%). As it is unclear whether the system by Zhao et al. runs at a similar power split, these values cannot be compared directly. However, it can be said that the efficiencies are of an equal magnitude. This shows that the results produced by the CT model follow the expectations as described earlier, which proves the validity of the results.

Li et al. [15] model a SOFC-GT cycle running on MeOH. In their system, the MeOH is internally reformed in the SOFC, and AOG is combusted with COG to generate heat for the GT. In the GT, the air from the compressor is heated by the SOFC exhaust gas with a HEX, and the heated air is expanded in a turbine. This system has a power split of 86.3-13.7, and an efficiency of 53.0%. In the CT model, the external reformer is bypassed, and the same power split is set. With this system, the CT model gives an efficiency of 52.0%. Just like the MeOH fuelled SOFC-ICE cycle, the efficiency is slightly lower than reported by Li et al. Again, this can be attributed to the lower operating temperature of the SOFC in the CT model. Next, the external reformer is included in the system, which results in a system efficiency of 55.4%. Compared to internal reforming, the efficiency increases when an external reformer is included. Li et al. [15] also report this behaviour. They state that the internal reforming system has an efficiency about 3% lower compared to the external reforming system.

Table 4.11 shows the results from the CT model compared to the current literature. In this table, it can be seen that the results from the CT model differ slightly from the systems in current literature, and these differences can be attributed to differences in integration strategies or operating parameters. While the results from the CT model are not equal to the results in literature, the model still gives results in the same range as the current literature, and the CT models can be used to compare the different fuels for the SOFC-GT combined cycles.

Table 4.11: Results of the SOFC-GT combined cycle model compared to current literature

Fuel	Reference	System performance	Remark
Diesel	Liu et al. [100]	62-68%	SOFC operates at elevated pressure Power split: 60-40
	Zhao et al. [23]	57%	SOFC operates at atmospheric pressure Power split is not given System runs on syngas produced from coal
	This thesis	61.5%	SOFC operates at atmospheric pressure Power split: 60-40
MeOH	Li et al. [15]	53.0%	Internal reforming Power split: 86.3-13.7
	This thesis	52.0%	Internal reforming Power split: 86.3-13.7
	This thesis	55.4%	External reforming Power split: 86.3-13.7

4.4. Conclusion

In this chapter, the combined cycle models were created in Cycle-Tempo (CT) software. First, standalone models for the SOFC, ICE and GT were created using reference data for these components. Next, the SOFC, ICE and GT models were combined into the SOFC-ICE and SOFC-GT combined cycles. These combined cycles were then validated by comparing the results with combined cycles from current literature. Both the SOFC-ICE and the SOFC-GT combined cycle models give results in the same range as the combined cycles in current literature. There are some differences in system efficiency, and these can be explained by a difference in integration strategy or operational parameters such as temperature and pressure. The created models are used in chapter 5 to calculate the energy consumption, CO_2 emissions and exhaust temperature for the different operating modes of the reference vessel.

5

System comparison

With the models described in chapter 4, the performance of the different combined cycles is calculated. First, in section 5.1, a baseline performance is determined using the current installed system of the reference vessel. For the performance of the combined cycles, different power splits are considered, which are discussed in section 5.2. Next, the system efficiency, energy consumption, CO_2 emissions, exhaust temperature, size and weight of the combined cycles are determined in section 5.3, section 5.4, section 5.5, section 5.6 and section 5.7 respectively. The best performing system is then chosen in section 5.8. Lastly, section 5.9 gives a short conclusion of this chapter.

5.1. Current power plant

The current power plant of the reference vessel is used as a baseline to compare the different combined cycles with. The current system consists of two large diesel ICEs (10 MW each) and four diesel generator sets (0.94 MWe each). The diesel generator sets provide electric power to drive two electric motors. The e-motors and the diesel engines drive the propeller shafts through a gearbox. A schematic of this system is shown in Figure 5.1.

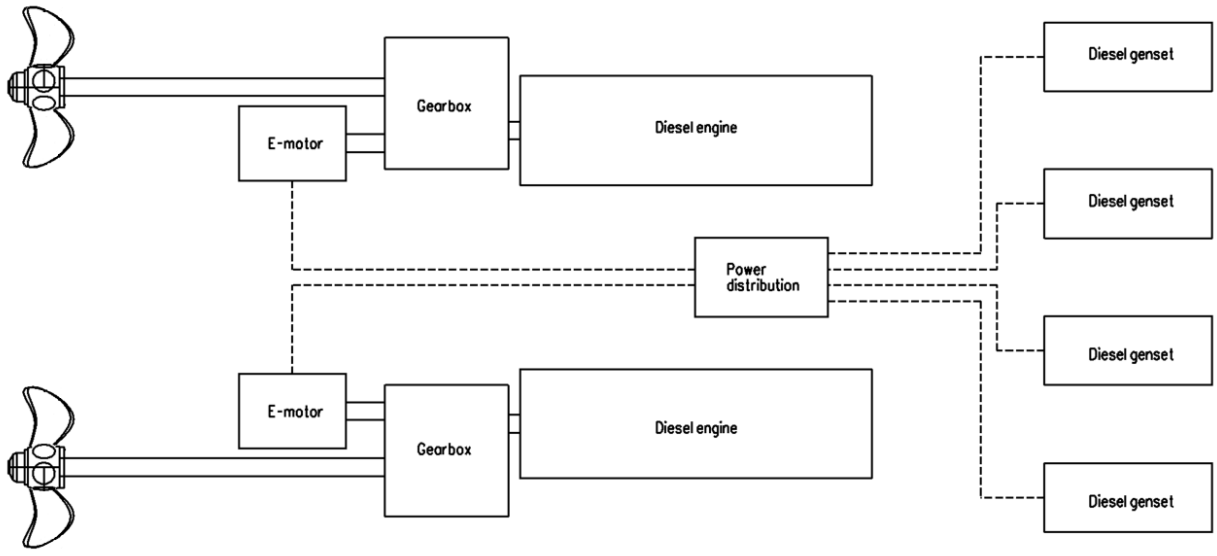

Figure 5.1: Schematic layout of the current power plant. The propeller is driven by the diesel engine and electric motor through a gearbox, and the diesel generators provide the electric power necessary to for the electric motor

The performance of the current system is determined by using the standalone ICE models developed in chapter 4. At top speed, the diesel engines run at 100% load. At cruising speed, the diesel engines run at 25% load, and at silent speed, two of the four diesel generators operate at 75% load, and the other two are switched off. Using these load conditions, and the power demand for these operating modes, the energy consumption, CO_2 emissions and exhaust temperature can be calculated with the ICE model. Additionally, the weight of the system is available for the reference vessel, and the volume of this system can be determined with the dimensions of the different components. The results for the current system are shown in Table 5.1, and these values will be used to determine the relative performance of the combined cycles compared to the current system in section 5.8.

Table 5.1: Energy consumption, exhaust temperature and CO_2 emission for the current power plant

	Energy consumption [kJ/year]	Exhaust temperature [°C]	CO_2 emissions [ton/year]	Component weight [ton]	Component volume [m^3]	Fuel weight [ton]
Silent operation	4.24*10^9	364.8	304.6	-	-	-
Cruising speed	8.20*10^{10}	314.8	5905.5	-	-	-
Top speed	1.34*10^{11}	368.0	9631.6	-	-	-
Total	2.20*10^{11}	-	15841.7	199.4	264.3	351.1

5.2. Power split

The power split between the SOFC and heat engine has a significant impact on the performance of the combined cycles, and different power splits are evaluated in this thesis. The power split is defined as the ratio between SOFC power and heat engine power based on the total installed power for top speed. A power split of 30-70 means that 30% of the total power required for top speed can be delivered by the SOFC operating at 100% load, and 70% of the total power is delivered by the heat engine at 100% load.

For silent operations, all of the power needs to be delivered by the SOFC. To maximize system efficiency at this operating mode, the SOFC needs to be operated at 75% load. When the SOFC at 75% load generates the necessary power for silent speed (0.8 MWe), it can produce a net power of 1.07 MWe at full load. This power output corresponds to 4.6% of the total net power needed to reach top speed (23.3 MWe). This means that the lower boundary for the power split is 4.6-95.4 in favour of the heat engine.

To determine the upper boundary for the power split, the operational profile of the vessel is taken into account. A large portion of the time (56%), the vessel sails at cruising speed, which means that this operating mode has a large impact on the annual fuel consumption of the vessel. Additionally, this operating mode is used to determine the range of the vessel. For these reasons, it is beneficial to maximize the system efficiency at this operating mode. When the power split increases, at a certain point the SOFC becomes large enough to be able to generate all the necessary power for cruising speed. At this point, the system efficiency becomes equal to the efficiency of the SOFC, as no additional power needs to be generated by the heat engine. The system efficiency becomes equal to the efficiency of the SOFC, which is lower than the system efficiency of the combined cycle. Further increasing the power split is then no longer beneficial for the system efficiency at cruising speed, and these power splits are no longer considered. At cruising speed, the system needs a power output 5.6 MWe to operate the vessel. Just like the silent operation, the SOFC needs to generate this power at 75% load to maximize its efficiency. At full load, this means that the SOFC can generate a net power of 7.47 MWe. This corresponds to 32.1% of the total net power for top speed, resulting in a power split of 32.1-67.9 favouring the heat engine. In this thesis, the SOFC power share is therefore varied between 4.6%–30% in 5% intervals. At net power splits above 4.6-95.4, the SOFC can deliver more power than necessary for silent operation. This means that the SOFC either run at loads lower than 75%, or some SOFCs need to be turned off. To ensure maximum efficiency at silent operation, it is chosen to keep running the SOFCs at 75% load, and to turn off any additional SOFCs at the higher power splits.

At top speed, both the SOFC and heat engine are running at full load, to ensure that the power plant is not any larger than it needs to be to deliver the required power. At cruising speed, multiple operating loads are considered. First, the SOFC is operated at its maximum efficiency (75%), and the remaining power is generated by a heat engine operating at part load. Next, the fuel cell is operated at full load, resulting in a larger power

share of the SOFC at cruising speed, which may positively influence the system efficiency despite the fuel cell having a slightly lower efficiency compared to part-load operation.

For the SOFC-ICE system, the total ICE power is generated by two large engines (8–10 MWe each, depending on the power split). At cruising speed, this means that the ICE is operated at 20-50% load, depending on the power split and installed engine power. To maximize the system efficiency, an additional cruising engine may be considered. This cruising engine can then be operated at 80% load, which is where the ICE is most efficient (see chapter 3). However, this also increases the system size and weight, for which space is limited in naval surface combatants. In chapter 3 it can be seen that the part-load efficiency of the ICE is slightly lower at 20-50% load compared to 80% load. However, this difference is fairly small, which means that the system efficiency is not significantly influenced by operating the ICE at this lower load. To reduce the system size, it is therefore chosen to operate the large engine at a low load, instead of including an additional smaller engine for cruising speed.

For the SOFC-GT systems, the part load operation of the GT is dictated by the available marine GTs in the current market. Currently, there are two large marine GT manufacturers; General Electric and Rolls-Royce. Both these manufacturers offer a small GT (around 4.6 MW) and a larger GT (>25 MW). In the power range between 4.6-25 MW, no marine GTs are currently on the market. In the SOFC-GT cycle, this limits the choice of GT to either one large engine or multiple small engines. The GT has poor part-load performance, which means that multiple small GTs are preferred with respect to cruising speed. At this operating mode, one small GT can operate at a relatively high part-load, and the other GTs can be turned off.

Using these system layouts and power splits, the system efficiency, energy consumption, CO_2 emissions, exhaust temperatures and system volume and weight are determined in the sections below.

5.3. System efficiency

The first performance indicator is the system efficiency. Here, the system efficiency is calculated by dividing the net power output with the energy input of the fuel (see chapter 3). For the different combined cycles, the system efficiency for silent operation, cruising speed and top speed is discussed below.

5.3.1. SOFC-ICE diesel

The system efficiency for the different operating modes is shown in Figure 5.2. The efficiency at silent operation is constant regardless of the power split. This is explained by the assumption that at this operating mode, the SOFC is always operated at 75% load. When the power split increases, any additional SOFCs are turned off, resulting in a constant system efficiency for all the power splits. At top speed, the system efficiency steadily increases for increasing power splits. The SOFC has a higher efficiency compared to the ICE. For an increasing power split, the contribution of the SOFC increases, which improves the efficiency of the combined system. Additionally, a larger flow of AOG is available for combustion in the ICE at increasing power splits. This means that more power can be extracted from the AOG, and less diesel needs to be directed to the ICE. This in also increases the system efficiency for larger power splits.

For cruising speed, two operating conditions are evaluated: the SOFC at 75% load or at 100% load. When the SOFC runs at 75%, the efficiency increases up until a power split of 25-75. This has the same explanation as the increase in efficiency for top speed. An increase in SOFC power means more power is generated at the higher efficiency of the SOFC, and more AOG can be combusted in the ICE resulting in less additional diesel usage. When the power share is increased to 30-70, the system efficiency decreases again. This is because at this power split, the ICE produces more power than necessary when only combusting AOG. i.e. no additional diesel is fed into the ICE, and the total power of the system is larger than the power demand at cruising speed. At this power split, only part of the AOG is combusted in the ICE, and the rest is combusted in the SOFC combustor, resulting in a heat loss in the exhaust gas.

When the SOFC is operated at 100% load, AOG is combusted up to a power split of 20-80. At 25-75, the SOFC is large enough to produce all the necessary power for cruising speed. This means that the efficiency at this powers split is equal to the efficiency of the standalone SOFC. At this power split, the unreacted fuel in the AOG is lost as waste heat in the exhaust gas. In the 20-80 power split, it is still used to produce additional power in the ICE, which raises the system efficiency. Lastly, when the power split is further increased to 30-70, the SOFC is large enough to produce the necessary power at about 80% load. At this load, the SOFC has a higher efficiency compared to 100% load, which is visible as an increase in system efficiency in Figure 5.2.

Lastly, it can be seen that, for cruising speed, operating the SOFC at 100% is beneficial for power splits up to 20-80. This is because the efficiency of the SOFC is higher than the efficiency of the ICE. When the SOFC is

operated at 100% load, more power is generated by the fuel cell compared to operation at 75%. This means that more power is produced at the efficiency level of the SOFC, which increases the total system efficiency. For power splits larger than 20-80, it is beneficial to operate the SOFC at 75% instead of 100%. At these high power splits, running the SOFC at lower loads means that the AOG can still be combusted in the ICE without surpassing the power demand. This increases the system efficiency compared to operating the SOFC at 100% load, where no AOG is combusted in the ICE.

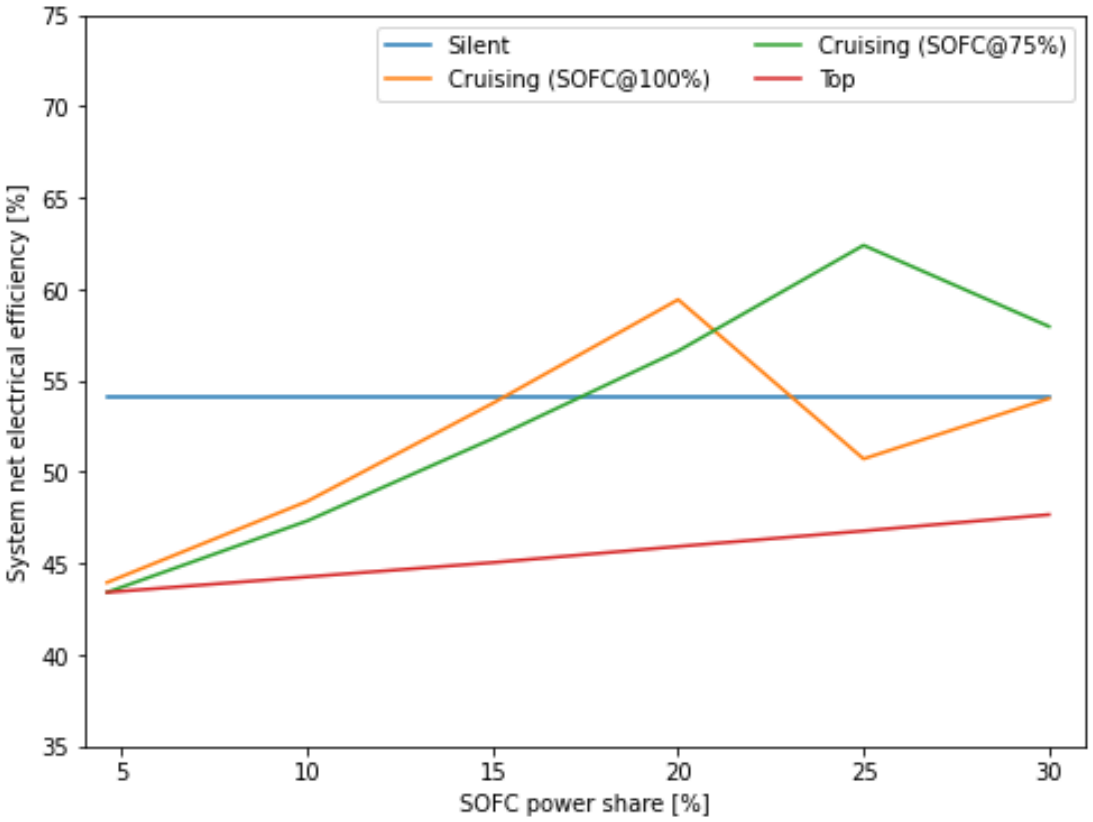

Figure 5.2: Net electrical efficiency for the diesel-fuelled SOFC-ICE combined cycle

5.3.2. SOFC-GT diesel

The system efficiency for the different operating modes is shown in Figure 5.3. Again, the system efficiency for silent operation is constant for each power split, and the system efficiency increases for increasing power splits at top speed. This has the same explanation as the diesel-fuelled SOFC-ICE combined cycle. At silent speed, the SOFC always runs at 75% load and the GT is turned off. At top speed, the larger power split means that more AOG can be combusted in the GT, and less additional diesel is required to achieve the required power output of the GT.

At cruising speed, operating the SOFC at 100% load is beneficial for the system efficiency up to a power split of 15-85. When the power split is increased further, operating the SOFC at 75% load becomes beneficial. This has a few reasons. When the SOFC is operated at 100% load, all the AOG is combusted up to a power split of 15-85. At 20-80, 10% of the AOG is necessary for the heating of the inlet streams of the SOFC. This means that less AOG is combusted in the GT, and additional fuel is necessary to reach the required power output. Additionally, the GT runs at 20% load in this power split. The thermal efficiency of the GT at this load is fairly low (about 20%). This low GT efficiency combined with less AOG directed to the GT result in a drop in system efficiency compared to the 15-85 power split. When the power split is increased to 25-75, the SOFC becomes large enough to produce all the necessary power at full load. This means that the GT does not produce additional power from the AOG, which results in a system efficiency equal to the standalone SOFC. This efficiency is lower than the combined cycle efficiency at the 20-80 power split. When increasing the power split to 30-70, the SOFC can produce the necessary power at about 80%, where its efficiency increases compared to full load.

When operating the SOFC at 75% load, the system efficiency is lower than operating at 100% load. This is

because more power is generated at the lower GT efficiency, which lowers the system efficiency. At the 20-80 power split, the system efficiency is higher compared to operating the fuel cell at full load. This is explained by the part-load of the GT. For part-load operation of the SOFC, the GT runs at 50% load. Here, the GT efficiency is significantly higher compared to the GT running at 20% load (about 32% efficiency compared to about 20% efficiency). Additionally, no AOG is needed for the heating of the SOFC inlet streams for the SOFC running at 75% load. Lastly, the efficiency of the SOFC itself is higher for part-load operation compared to full load. These three factors result in a higher system efficiency for operating the SOFC at part-load for the power split of 20-80. The system efficiency reaches a maximum at the 25-75 power split. Here, 28% of the AOG is needed for the SOFC heat integration, and the rest is combusted in the GT running at 30% load. Further increasing the power split reduces the system efficiency again. Here, 35% of the AOG is needed for heat integration, and the GT runs at 10% load, resulting in a very low thermal efficiency of the GT (about 7%). This lower AOG flow to the GT combined with a lower thermal efficiency of the GT results in a lower system efficiency for the 30-70 powers split compared to the 25-75 power split.

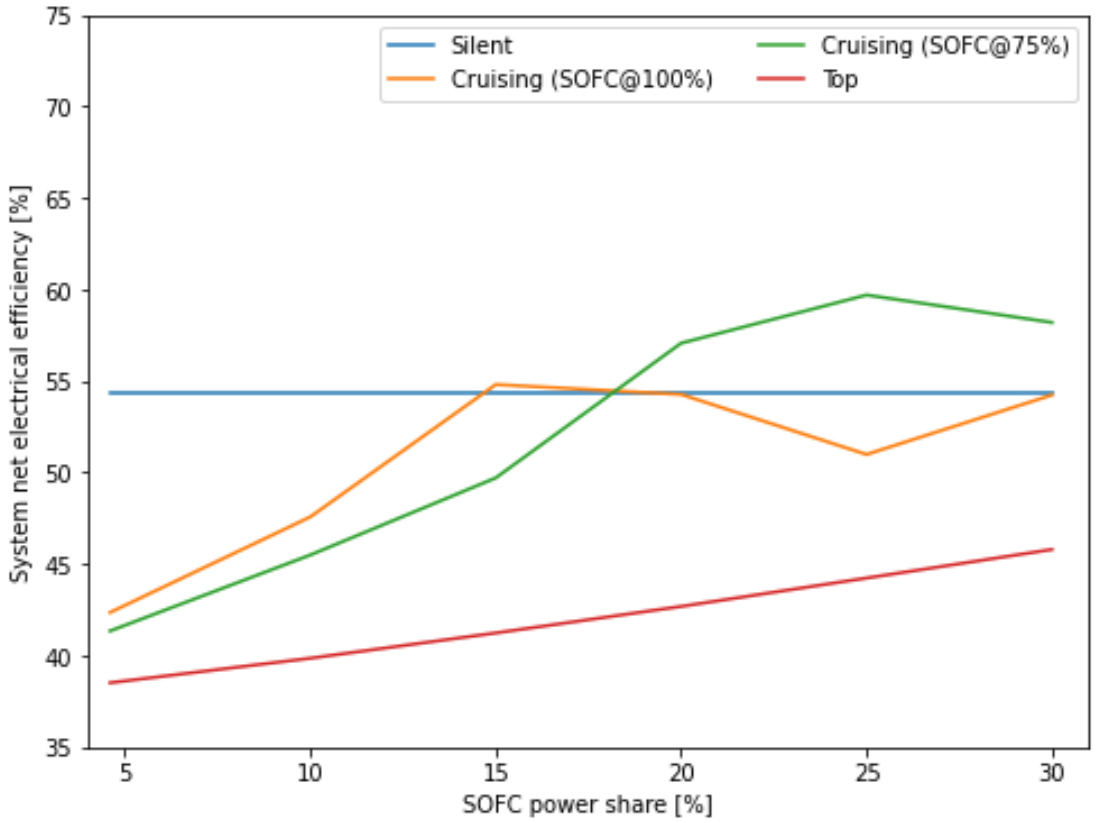

Figure 5.3: Net electrical efficiency for the diesel-fuelled SOFC-GT combined cycle

5.3.3. SOFC-ICE MeOH

The system efficiency for the different operating modes is shown in Figure 5.4. Just like the diesel-fuelled SOFC-ICE, the system efficiency increases at top speed for increasing power splits, and stays constant at silent speed. Again, this is explained by the SOFC always running on 75% load at silent speed, and an increase in AOG combustion in the ICE at top speed.

At cruising speed, the same behaviour as the diesel-fuelled SOFC-ICE combined cycle is observed. Operating the SOFC at 100% load is beneficial for power splits up to 20-80. For larger power splits, the SOFC becomes large enough to produce all the necessary power for cruising speed at full load, which reduces the system efficiency. At 30-70, the SOFC can generate all the necessary power at a load of about 80%, where the SOFC efficiency is higher compared to full load. This in turn increases the system efficiency compared to the 25-75 power split.

When operating the SOFC at 75% load, the system efficiency increases up to a power split of 25-75. At this power split, all the AOG is combusted in the ICE. When the power split is increased to 30-70, only 36% of the

AOG is combusted in the ICE. When more AOG is directed to the ICE, the system produces more power than necessary for cruising speed. This means that part of the unreacted fuel in the AOG is lost as heat in the exhaust gas, lowering the system efficiency.

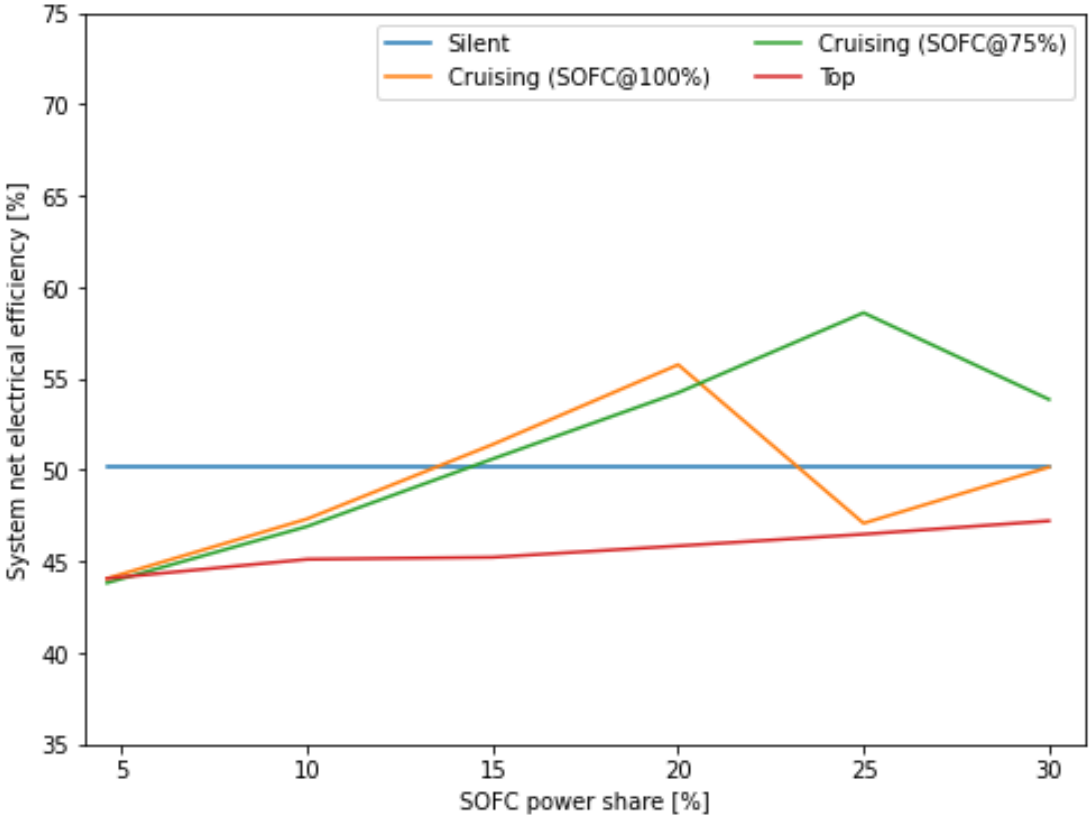

Figure 5.4: Net electrical efficiency for the MeOH-fuelled SOFC-ICE combined cycle

5.3.4. SOFC-GT MeOH

The system efficiency for the different operating modes is shown in Figure 5.5. At silent and top speed the same behaviour as the diesel-fuelled SOFC-GT is observed. This is again explained by the SOFC operating at 75% for each power split at silent speed, and the increase in AOG combustion in the GT at top speed.

Just like the ICE combined cycles, similar behaviour for the different fuel is observed for the GT combined cycles. Up to a power split of 15-85, it is beneficial to operate the SOFC at full load. A higher SOFC load means that more power is generated at the efficiency level of the SOFC, which is higher than the efficiency of the GT. When increasing the power split to 20-80, part of the AOG is needed to heat the inlet streams of the AOG. Together with a low part-load efficiency of the GT, this results in a lower system efficiency compared to operating the SOFC at 75% load. Then, at 25-75, the SOFC becomes large enough to produce all the necessary power, and no additional power is generated by the GT. This results in a system efficiency equal to the SOFC efficiency, which is lower than the combined cycle efficiency.

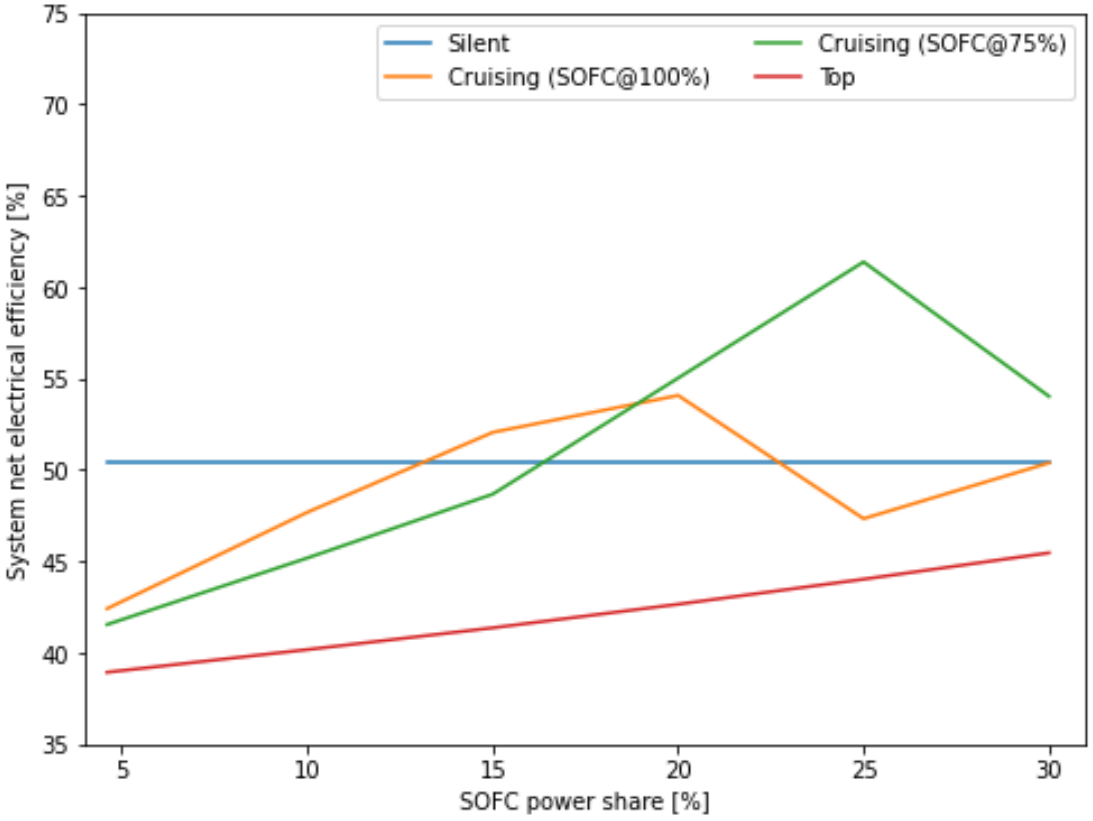

Figure 5.5: Net electrical efficiency for the MeOH-fuelled SOFC-GT combined cycle

5.3.5. Comparison

For each operating mode, the system efficiency of the combined cycles is compared to the current system in Figure 5.6. For cruising speed, only the maximum efficiency is plotted for each power split (i.e. for the diesel-fuelled SOFC-ICE with a power split of 25-75, only the SOFC operation at 75% is plotted, and the operation at 100% is left out). Figure 5.6a shows the system efficiency at silent operation. Here, it can be seen that the diesel-fuelled combined cycles show the highest system efficiency. This is to be expected when looking at the efficiency of the SOFC with the different fuels compared to the efficiency of a diesel-fuelled ICE. The diesel-fuelled SOFC has the highest efficiency at about 54%, and the diesel-fuelled ICE has the lowest efficiency at about 43%.

At top speed (Figure 5.6c), it can be seen that the SOFC-ICE combined cycles always perform better than the current system. The SOFC-GT combined cycles only perform better than the current system for power splits larger than 20-80. The SOFC-ICE combined cycles outperform the current system due to the combustion of AOG in the ICE. This reduces the amount of additional fuel needed for a given power output of the ICE, which increases the system efficiency. Additionally, the SOFC produces power at a higher efficiency than the ICE, which further increases the system efficiency. For increasing power splits, the effect of these two differences increases the gap between the current system and the SOFC-ICE combined cycle. The SOFC-GT combined cycle performs worse than the current system at the lower power splits due to the thermal efficiency of the GT. The GT has a lower thermal efficiency than the ICE. At the lower power splits, the GT power share is large enough to lower the system efficiency compared to the current system. Only for power splits higher than 20-80, the SOFC power share becomes large enough to compensate for the lower GT efficiency, and the system efficiency becomes larger than the current system.

At cruising speed, all the combined cycle outperform the current system, and the diesel-fuelled SOFC-ICE reaches the highest system efficiency of about 64% at a power split of 25-75. This is a combination of the higher efficiency of hte SOFC when running on diesel compared to running on MeOH, and the higher efficiency of the ICE compared to the GT. These two factors result in the diesel-fuelled SOFC-ICE combined cycle having the highest system efficiency.

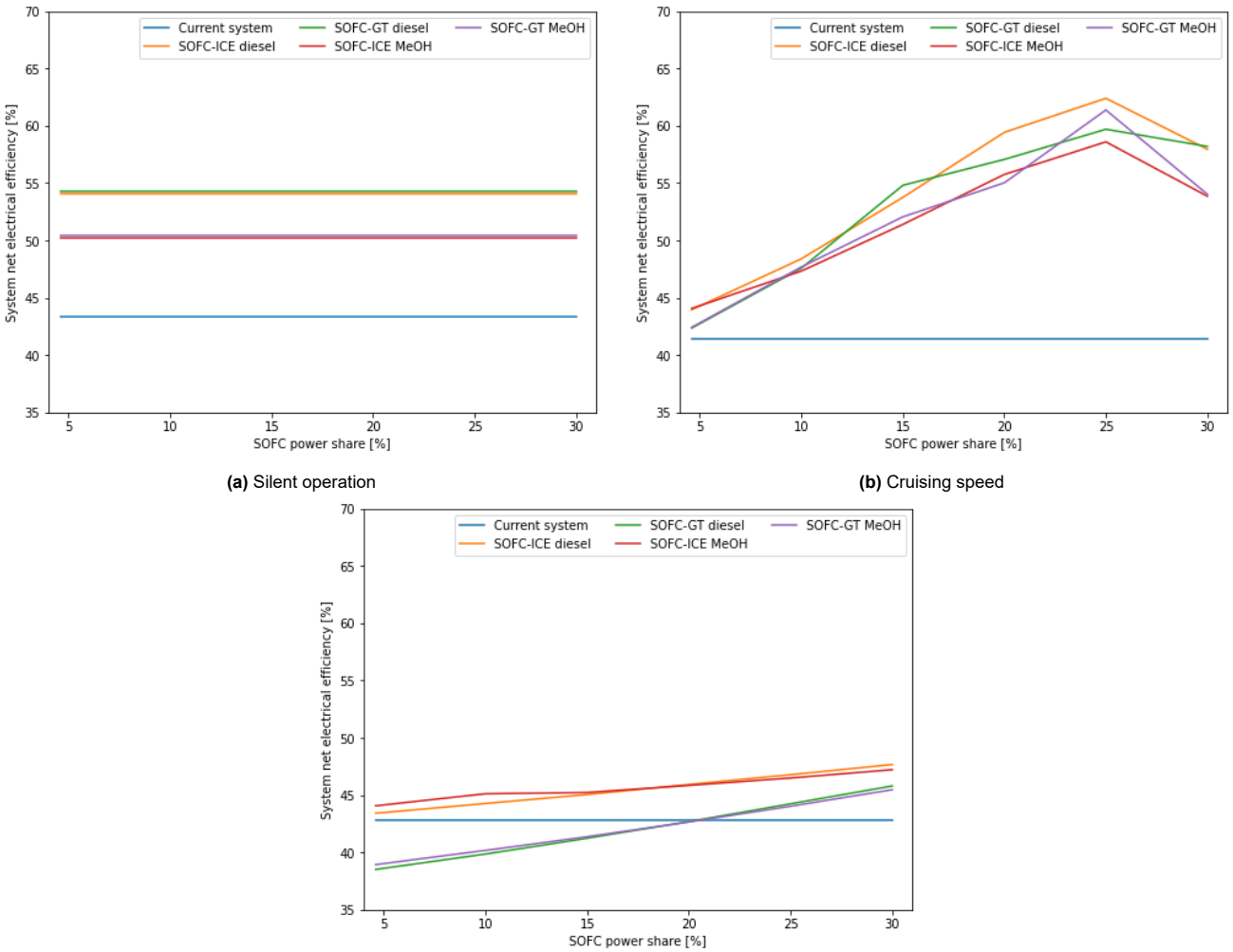

(a) Silent operation

(b) Cruising speed

(c) Top speed

Figure 5.6: Comparison of net system efficiency for silent operation, cruising speed, top speed of each combined cycle

5.4. Energy consumption

The energy consumption is calculated for each combined cycle as discussed in chapter 3. The CT models are run at the power splits discussed in the previous section, and a fuel consumption (in kg/s) is obtained for each power split and operating mode. When comparing the systems based on fuel consumption, the diesel models will always be better. This is due to the higher energy density of diesel compared to MeOH, which results in a higher fuel mass flow for MeOH for the same power output. For this reason, the fuel consumption is transformed into an energy consumption with Equation 5.1. The fuel consumption (in kg/s) is multiplied with the LHV of the fuel (in kJ/kg) to obtain an energy consumption in kJ/s for each operating mode and power split.

$$E_{in} = \dot{m}_{fuel} \cdot LHV_{fuel} \tag{5.1}$$

Next, the annual energy consumption for each power split is calculated by multiplying the energy consumption of an operating mode (resulting from Equation 5.1) with the time spent per year at this operating mode. Equation 5.2 shows this calculation for silent operation, and the annual energy consumption for cruising and top speed are calculated the same. The time spent at the given operating modes is taken from the simplified operational profile discussed in chapter 3, and is equal to 2,280,000 s/year for silent operation, 6,060,000 s/year for cruising speed and 2,460,000 s/year for top speed.

$$E^{year}_{in,silent} = E_{in,silent} \cdot t_{silent} \tag{5.2}$$

5.4.1. SOFC-ICE diesel

First, the fuel consumption for the diesel-fuelled SOFC-ICE model are determined. The fuel consumption is determined for silent speed, cruising speed (where the fuel cell operates at 75% load or 100% load) and top speed. The total net power generated by the CT model is equal to the power demand of the vessel at the different operating modes. The fuel consumption is then converted to an energy consumption using Equation 5.1, and the results are shown in Figure 5.7. In this figure, a few things can be seen. First of all, the energy consumption for silent operation is equal irrespective of the power split. This is because at silent speed, all the power is delivered by the SOFCs. At all power splits, just enough SOFCs are turned on to produce the necessary power at a load of 75%. The energy consumption is therefore not dependent on the power split, and is constant in Figure 5.7.

Secondly, the energy consumption steadily decreases at top speed for increasing power splits. This is to be expected since the efficiency of the SOFC is higher than the efficiency of the ICE. When the power share of the SOFC is increased, more AOG is combusted in the ICE. This means that less diesel needs to be fed into the ICE, resulting in a higher system efficiency at higher power splits. This higher efficiency in turn means that less energy needs to be fed into the system for the same power output, resulting in a lower energy consumption.

Lastly, for cruising speed, an optimum in energy consumption can be observed. The location of this optimum depends on the operating load of the SOFC. If the SOFC is operated at full load, the fuel cell can produce all the necessary power for cruising speed at a power split of 25-75. At this power split, only the fuel cell is operated, which has a lower efficiency compared to the combined cycle operation. This results in the jump in energy consumption at this power split. If the power split is further increased to 30-70, the SOFC can generate the required power at a lower load (80% load), which increases the efficiency of the SOFC compared to full load operation. This is visible in the decrease in energy consumption from 25% to 30%. When operating the SOFC at 75% for every power split, a slightly different behaviour is observed. From 4.6%-25%, the energy consumption decreases linearly. Up until 25% power share, all the AOG can be combusted in the ICE, and less diesel fuel is necessary when the power share of the SOFC is increased. However, for power splits higher than 25-75, the ICE can deliver more power than required when running on pure AOG. At the power share of 30%, only 25% of the AOG is combusted in the ICE. The rest of the unreacted fuel in the AOG is combusted in the combustor of the SOFC system, and is therefore lost as heat in the exhaust gasses. As not all the AOG is combusted in the ICE, the system efficiency decreases, resulting in a higher energy consumption at the 30-70 power split compared to the 25-75 power split, where all of the AOG is directed to the ICE.

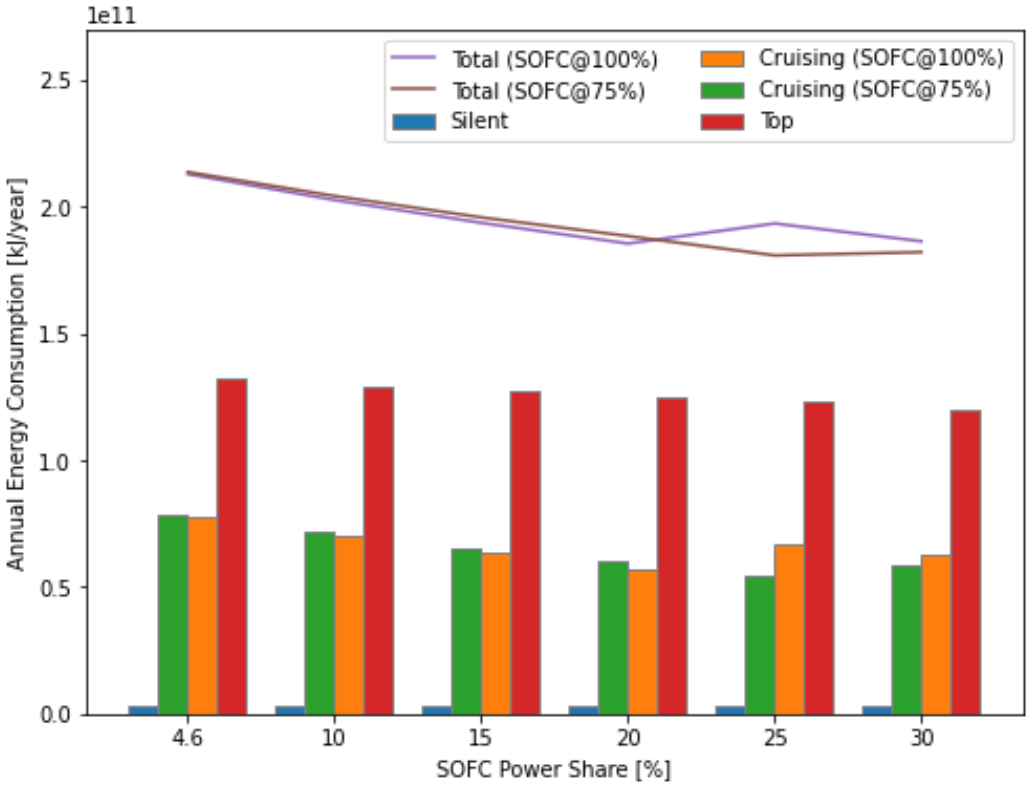

Figure 5.7: Energy consumption of the SOFC-ICE system running on diesel.

5.4.2. SOFC-GT diesel

The energy consumption for the SOFC-GT model running on diesel is calculated in the same manner as the diesel-fuelled SOFC-ICE model. The results for the diesel-fuelled SOFC-GT combined cycle are shown in Figure 5.8. Just like the diesel-fuelled SOFC-ICE combined cycle, the energy consumption for silent operation is constant for the diesel-fuelled SOFC-GT combined cycle, and the energy consumption decreases at top speed for an increase in SOFC power share. Again, this is because at silent speed, the SOFC operates at a constant load (75%), and additional SOFCs are turned of at the higher power splits. At top speed, the higher SOFC power shares mean that more AOG can be combusted in the GT and less additional diesel is needed for the required total power. This increases the system efficiency and decreases the energy consumption at higher power splits.

At cruising speed, two options are evaluated: SOFC at 100% load, and the SOFC at 75% load. For the case where the SOFC is operated at 75%, the energy consumption shows an optimum at the 25-75 power split. At 25% power share, the heat from COG only is not sufficient to heat the incoming streams of the SOFC. At this power share, 80% of the AOG is combusted in the GT, and the remaining AOG is combusted in the SOFC combustor to be used as heat source for the incoming fluid streams. At the SOFC power share of 30%, even less AOG (70%) is combusted in the GT, and 30% of the AOG is needed as a heat source for the SOFC. This reduction in AOG being directed to the GT means that more additional diesel fuel is needed to reach the total power demand, which reduces the system efficiency and increases the energy consumption at cruising speed.

When the SOFC is operated at full load (100%), this problem with heat integration occurs at a lower SOFC power share. At 15%, all the AOG is still directed to the GT, but at 20% power share, already 12% of the AOG is needed for the heating of the incoming streams of the SOFC. Lastly, at 25% power share, the SOFC is large enough to provide all the necessary power for cruising speed when it is operated at full load. The efficiency of the SOFC at full load is lower than the efficiency of the combined cycle operation, which is visible in the figure as an increase in energy consumption at 25% power share compared to 20% power share. Then, at 30% SOFC power share, the energy consumption decreases again. This is explained by the operation of the SOFC. At this power share, the SOFC is large enough to produce all the necessary power at 80% load, which increases the SOFC efficiency compared to full load operation.

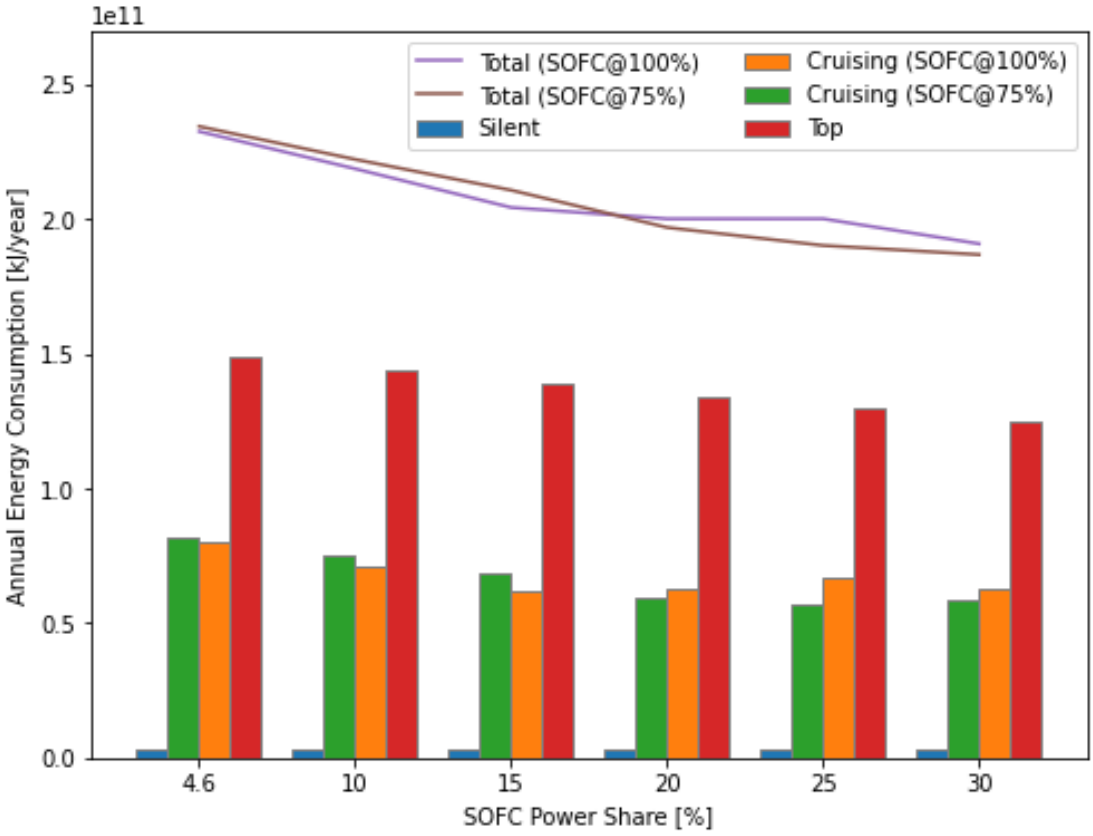

Figure 5.8: Energy consumption of the SOFC-GT system running on diesel.

5.4.3. SOFC-ICE MeOH

The energy consumption for the SOFC-ICE model running on MeOH is calculated in the same manner as the diesel-fuelled SOFC-ICE model. The results for the MeOH-fuelled SOFC-ICE combined cycle are shown in Figure 5.9. The energy consumption of this system shows the same behaviour as the diesel-fuelled SOFC-ICE combined cycle. The main difference is visible for the SOFC power share between 4.6%-20%. For the diesel-fuelled system, running the SOFC at 100% gives an advantage in terms of energy consumption compared to running the SOFC at 75% load. However, for the MeOH-fuelled system, this is no longer the case. Here, the energy consumption is about equal regardless of the operating load of the SOFC. This is explained by the efficiency of the standalone MeOH-fuelled SOFC. The efficiency of the SOFC is 50.6% for 75% load, and 46.5% at 100% load. These efficiencies are only slightly higher than the ICE efficiency, which means that it does not really matter which component produces the power. A higher SOFC power at a lower SOFC efficiency (SOFC at 100% load) does not have a significant influence on the system efficiency compared to a lower SOFC power at a higher efficiency (SOFC at 75%) as the potential gain is diminished by the ICE. For the diesel-fuelled model, the SOFC efficiencies lie significantly higher than the ICE efficiencies, resulting in the gain in system efficiency when running the SOFC at a higher load, and therefore producing more power at a higher efficiency. Just like the diesel-fuelled system, the SOFC running at 100% load is large enough to produce all the necessary power for cruising speed for a power share of 25% and 30%, resulting in the jump in energy consumption at these power shares.

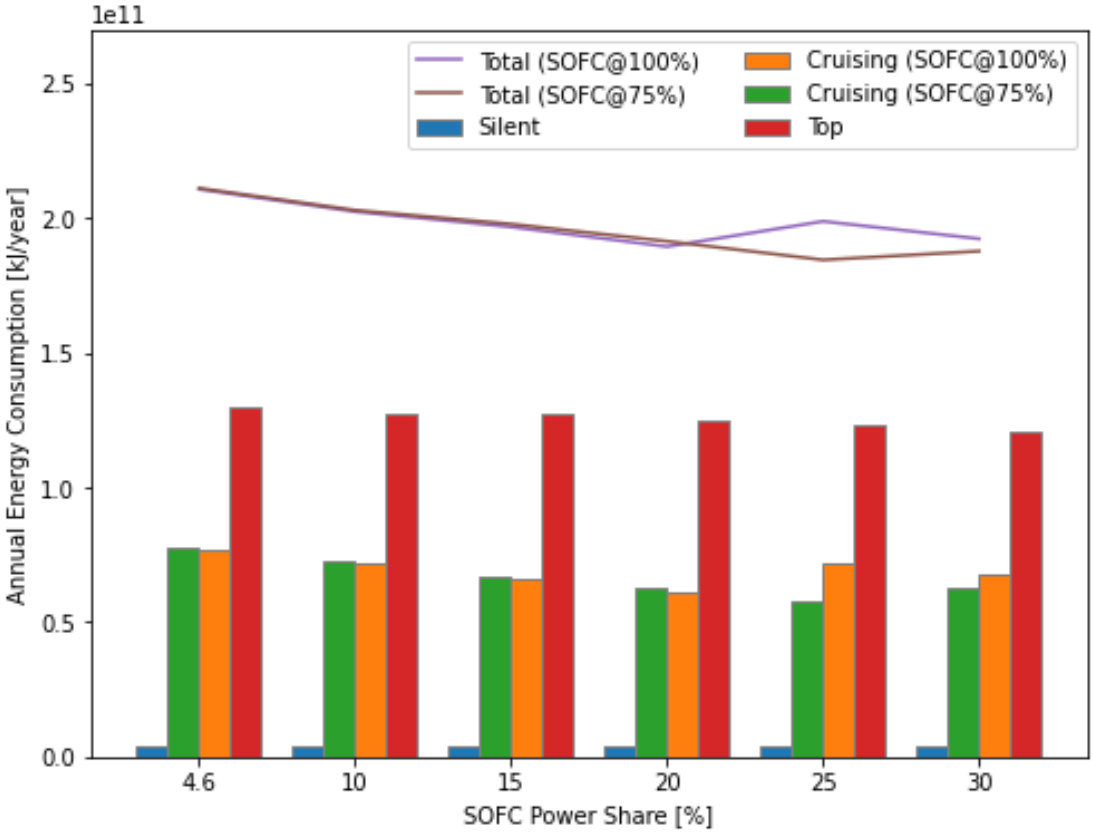

Figure 5.9: Energy consumption of the SOFC-ICE system running on MeOH.

5.4.4. SOFC-GT MeOH

The energy consumption for the SOFC-GT model running on MeOH is calculated in the same manner as the diesel-fuelled SOFC-GT model. The results for the MeOH-fuelled SOFC-GT combined cycle are shown in Figure 5.10. The MeOH-fuelled SOFC-GT combined cycle shows similar behaviour as its diesel-fuelled counterpart. For low power shares (4.6% and 10%), operating the SOFC at 100% load at cruising speed is beneficial for the energy consumption. However, starting at a power share of 15%, AOG needs to be used to heat the incoming streams of the SOFC when running at 100% load. At a power share of 15%, already 40% of the AOG is needed for heating, and the remaining 60% is combusted in the GT. At 20%, only 45% of the AOG is combusted in the GT, and at 25% power share all of the AOG is needed for heating.

When operating the SOFC at 75% load, less AOG is needed for the heating of the incoming streams. At a 15% power share, 80% of the AOG is combusted in the GT. For 20% power share, this drops to 60%, and it further drops to 38% and 40% for respective power shares of 25% and 30%. This higher AOG leads to a lower energy consumption for power shares between 15%-25%. However, at 30% power share, operating the SOFC at full load is again better. This is explained by the fact that the SOFC can produce all the necessary power for this power split. This means that the system efficiency is equal to the SOFC efficiency. For the SOFC at 75% load, a small amount of power is generated by the GT at a very low load (10% load, about 7% efficiency). This lowers the system efficiency compared to operating the SOFC on its own.

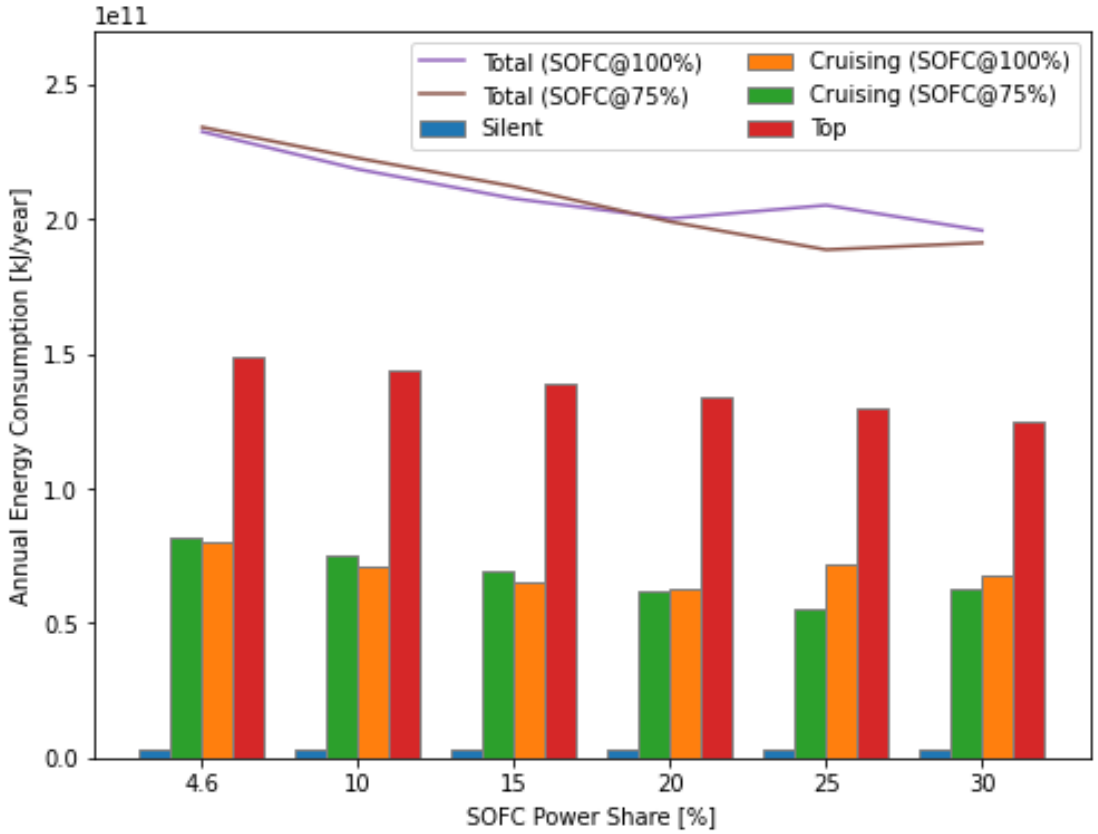

Figure 5.10: Energy consumption of the SOFC-GT system running on MeOH.

5.4.5. Comparison

To compare the different systems, the total energy consumption of each system is plotted in the same figure (Figure 5.11). Here, for each power split, the lowest energy consumption is chosen. This means, that in the case of the SOFC-ICE combined cycle (both diesel- and MeOH-fuelled), the line in Figure 5.11 shows the SOFC running at 100% load at cruising speed for power shares between 4.6%-20%, and the SOFC running at 75% for a power share between 25%-30%. For the diesel-fuelled SOFC-GT combined cycle, the SOFC runs at 100% for power shares between 4.6%-15%, and at 75% load for power shares between 20%-30%. For the MeOH-fuelled SOFC-GT combined cycle, the SOFC runs at 75% for power shares between 15%-25%, and at 100% for a power share of 4.6%, 10% and 30%.

When comparing the different combined cycles with each other, it can be seen that the diesel-fuelled SOFC-ICE combined cycle has the lowest energy consumption for almost every power split. Only at a SOFC power share of 4.6% is the MeOH-fuelled SOFC-ICE combined cycle slightly better. This is because at this power split, most of the power is generated by the ICE. When the ICE runs on MeOH, it has a higher efficiency compared to running on diesel, which results in a slightly higher system efficiency for a powers split of 4.6-95.4. However, at higher power splits, the efficiency of the SOFC becomes more important, and this efficiency is significantly higher when running on diesel compared to MeOH.

The GT combined cycles start at a higher energy consumption compared to the current system. This is explained by the low efficiency of GTs compared to the ICEs of the current system. Starting from a SOFC power share of

about 9%, the SOFC-GT combined cycles become more interesting in terms of energy consumption compared to the current system. For this power split, the SOFC compensates the lower GT efficiency, resulting in a system efficiency comparable to the current system. At higher power splits, the SOFC improves the system efficiency even further, which reduces the energy consumption compared to the current system. When choosing a combined cycle based on energy consumption alone, the diesel-fuelled SOFC-ICE combined cycle with a power split of 25-75 performs the best out of all the combined cycles for power splits higher than 10-90, and the MeOH counterpart performs the best at power splits lower than 10-90.

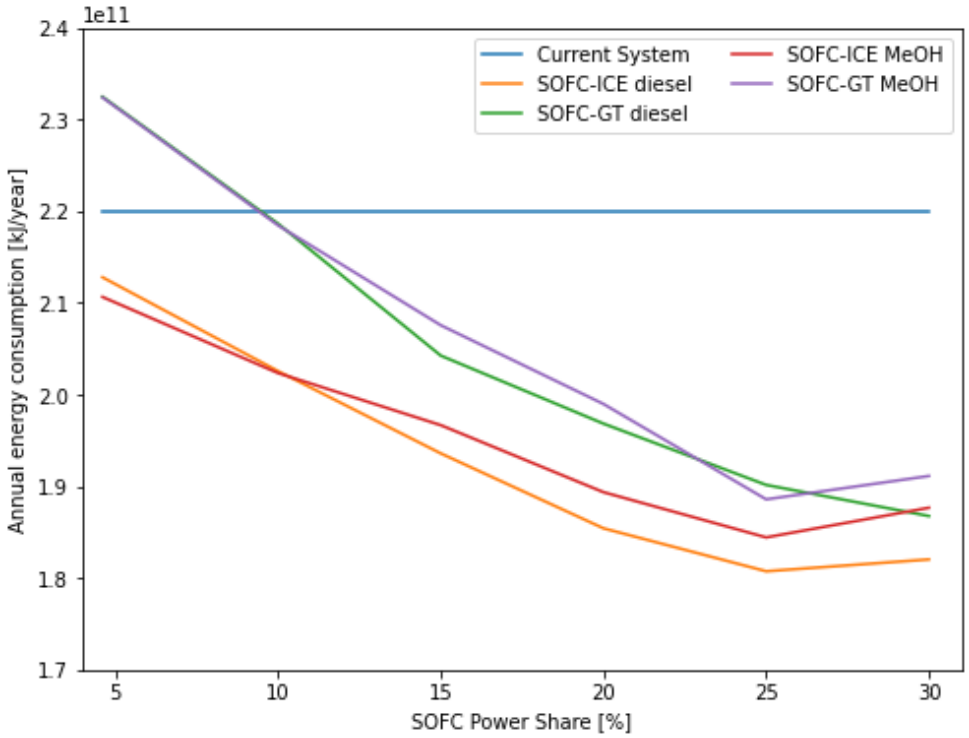

Figure 5.11: Comparison of the annual energy consumption for the different combined cycles

5.5. CO_2 emissions

The CO_2 emissions of the different systems are used to give an indication of the GHG emissions. The CT models assume a full conversion of the fuel into CO_2 and H_2O. The exhaust gas is therefore a mixture of nitrogen (N_2), oxygen (O_2), argon (Ar), CO_2 and H_2O, which is a mixture of standard air and the reaction products from oxidizing the fuel. From the models the exact composition of the exhaust gas is obtained, and the molar fraction for each component is given. The exhaust gas mass flow is also given by the CT models, and these two results are used to calculate the CO_2 emissions of the different systems as discussed in chapter 3.

As the CT model assumes a full conversion of the fuel into CO_2 and H_2O, this means that the annual CO_2 emissions are directly related to the fuel consumption of the system. For cruising speed, the CO_2 emissions are only calculated where the energy consumption is lowest. e.g. for the diesel-fuelled SOFC-ICE combined cycle with a power split of 25-75, operating the SOFC at 100% load has a lower energy consumption than operating the SOFC at 75% load meaning that the CO_2 emissions are calculated for the SOFC at 100% load.

The resulting annual CO_2 emissions are shown in Figure 5.12 for the different combined cycles. These figures are in principle the same figures as the energy consumption of the different combined cycles. This is to be expected, since the model fully converts the fuel into CO_2 and H_2O. A higher fuel consumption will lead to higher CO_2 emissions.

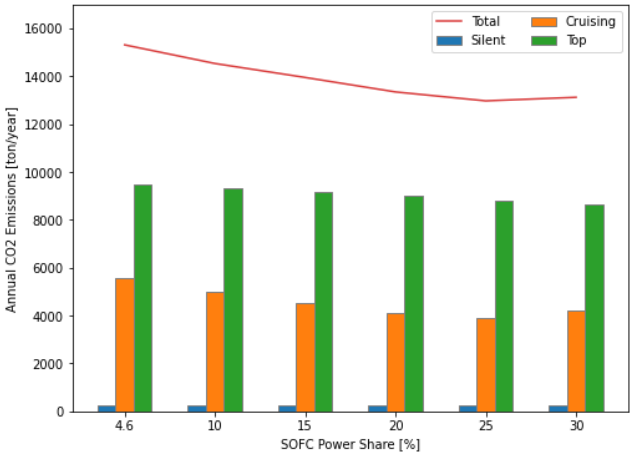

(a) CO_2 emissions of the SOFC-ICE system running on diesel

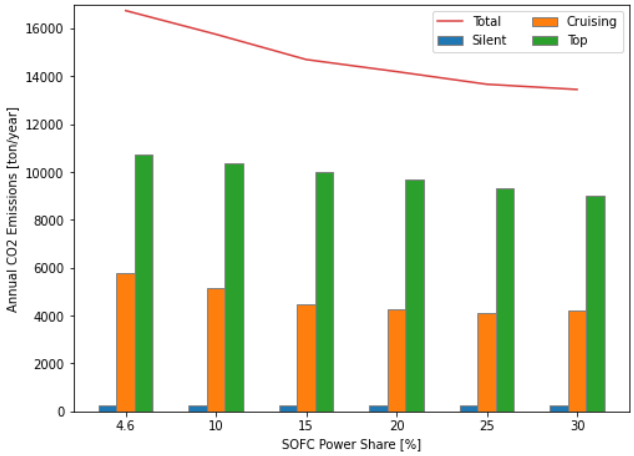

(b) CO_2 emissions of the SOFC-GT system running on diesel

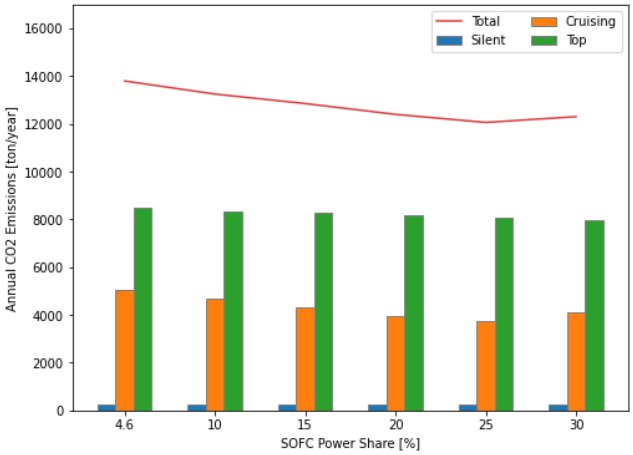

(c) CO_2 emissions of the SOFC-ICE system running on MeOH

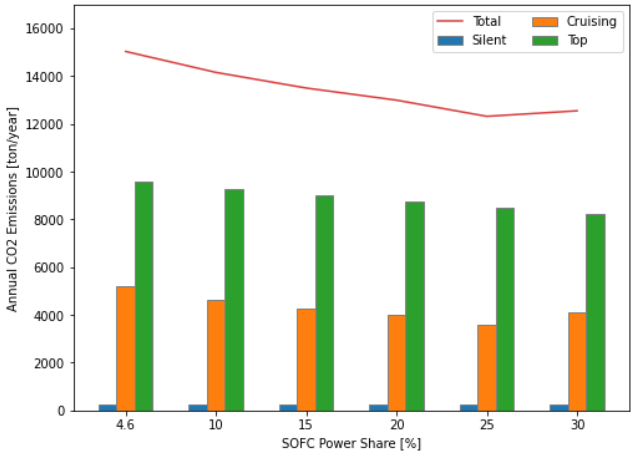

(d) CO_2 emissions of the SOFC-GT system running on MeOH

Figure 5.12: CO_2 emissions of the different combined cycles

5.5.1. Comparison

When comparing the CO_2 emissions of the different combined cycles with each other, there are some differences compared to the energy consumption. As can be seen from Figure 5.13, the CO_2 emissions of the MeOH-fuelled combined cycles are significantly lower than their diesel-fuelled counterpart. This can be explained by the chemical reaction for the conversion of the fuel into CO_2 and H_2O (Equation 5.3 for diesel and Equation 5.4 for MeOH. When fully converting 1 kg of diesel ($C_{14.8}H_{26.9}$), 0.869 kg of CO_2 is produced, whereas only 0.375 kg of CO_2 is produced when converting 1 kg of MeOH (CH_3OH). To make a fair comparison between the two fuels regarding the energy consumption, the CO_2 production in kg/kg fuel is converted to kg/kJ fuel (Equation 5.5). For 1 kJ worth of diesel, 0.0203 grams of CO_2 is emitted, and for 1 kJ of MeOH 0.0178 grams of CO_2 is emitted. When using MeOH as fuel, the CO_2 emissions drop with 12% for the same energy input. This drop in CO_2 emissions is visible when comparing the CO_2 emissions of the different combined cycles in Figure 5.13. Compared to the current system, only the diesel-fuelled SOFC-GT combined cycle performs worse at power shares below 10%, similar to the energy consumption. In this case, the MeOH-fuelled SOFC-GT combined cycle outperforms the current system despite having a higher energy consumption. This is because the MeOH produces less CO_2 compared to the diesel of the current system.

$$4.89C_{14.8}H_{26.9} + 138.14O_2 \rightarrow 72.37CO_2 + 65.77H_2O \tag{5.3}$$

$$31.25CH_3OH + 46.88O_2 \rightarrow 31.25CO_2 + 62.50H_2O \tag{5.4}$$

$$CO_2 \text{ [kg/kJ fuel]} = \frac{CO_2 \text{ [kg/kg fuel]}}{LHV_{fuel} \text{ [kJ/kg]}} \tag{5.5}$$

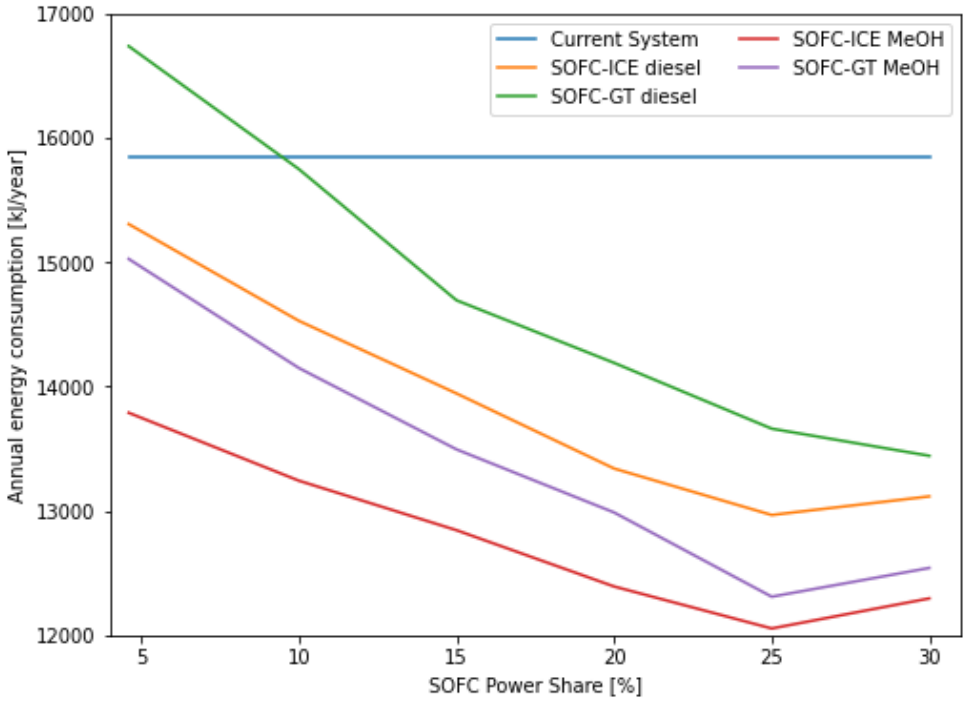

Figure 5.13: Comparison of annual the CO_2 emissions for the different combined cycles

Looking purely at the CO_2 emissions of the systems, the MeOH-fuelled SOFC-ICE combined cycle performs the best, with the minimum emissions occurring at a power split of 25-75. When CO_2 emissions are considered to be the most important factor in choosing a combined cycle, the 25-75 power split for the MeOH-fuelled SOFC-ICE system would be the best choice.

5.6. Exhaust temperature

The exhaust temperature is used to give in indication of the IR-signature of the vessel. The exhaust temperature is given by the CT models, and is taken for the exhaust flow leaving the system. For every combined cycle, power split and operating mode the exhaust temperature is obtained from the CT models, and the results are shown in Figure 5.14. Here, it can be seen that for silent operation the exhaust temperature is constant, and only depends on the used fuel. For diesel-fuelled systems, the exhaust temperature at silent operation is about 153 °C, whereas this is about 208 °C for MeOH-fuelled systems. This is in line with the exhaust temperature of the SOFC model, and is to be expected since at silent speed only the SOFC is running and the exhaust temperature leaving the system should be equal to the exhaust temperature of the SOFC. At top speed, the exhaust temperature decreases with increasing SOFC power shares. This is because the temperature of the SOFC exhaust gas is lower than the temperature of the ICE/GT exhaust gas. A higher SOFC power share means that the exhaust flow of the SOFC increases compared to the exhaust flow of the heat engine, which in turns lowers the temperature of the exhaust gas leaving the vessel.

More interesting results are obtained for cruising speed. Just like the CO_2 emissions, the exhaust temperature is only taken for the SOFC load where the energy consumption is lowest for a given power split. Just like for top speed, it is expected that the exhaust temperature decreases for increasing power splits. While this is also what happens at cruising speed, this decrease is not linearly like the top speed. This is explained by the amount of AOG that is combusted in the heat engine. For low power splits, all the AOG is combusted, and the exhaust temperature linearly decreases with increasing power splits. At the higher power splits, not all of the AOG can be combusted in the heat engine. This is because the heat engine running on pure AOG produces more power than necessary for cruising speed. When this is the case, just enough AOG is directed to the heat engine to produce the necessary power for cruising speed, and the remaining AOG is combusted in the SOFC burner. This leads to a higher SOFC exhaust gas temperature, and the overall exhaust gas temperature of the system rises again.

For both SOFC-ICE combined cycles, this occurs at a power split of 25-75. At this power split, only part of the AOG is used to produce additional power, and the rest produces additional heat, which is lost in the exhaust gas

temperature leaving the system. For the diesel-fuelled SOFC-GT, the usage of AOG for heating already occurs at a power split of 20-80. This results in an equal exhaust gas temperature compared to the 15-85 power split where all of the AOG is combusted in the GT. The exhaust gas temperature then further drops for increasing power shares as the exhaust flow of the SOFC becomes relatively large compared to the GT exhaust flow. Lastly, for the MeOH-fuelled SOFC-GT combined cycle, the exhaust temperature of the 15-85 power split does not follow the expected trend of decreasing exhaust temperature. This is explained by the fact that, at this power split, the switch is made between 75% and 100% SOFC load. This significantly influences the relative exhaust flows of the SOFC and GT. At the 15-85 power split, the GT exhaust flow is relatively larger than for the 10-90 power split. The GT exhaust temperature is higher than the SOFC exhaust temperature, resulting in a higher overall exhaust temperature for the 15-85 power split.

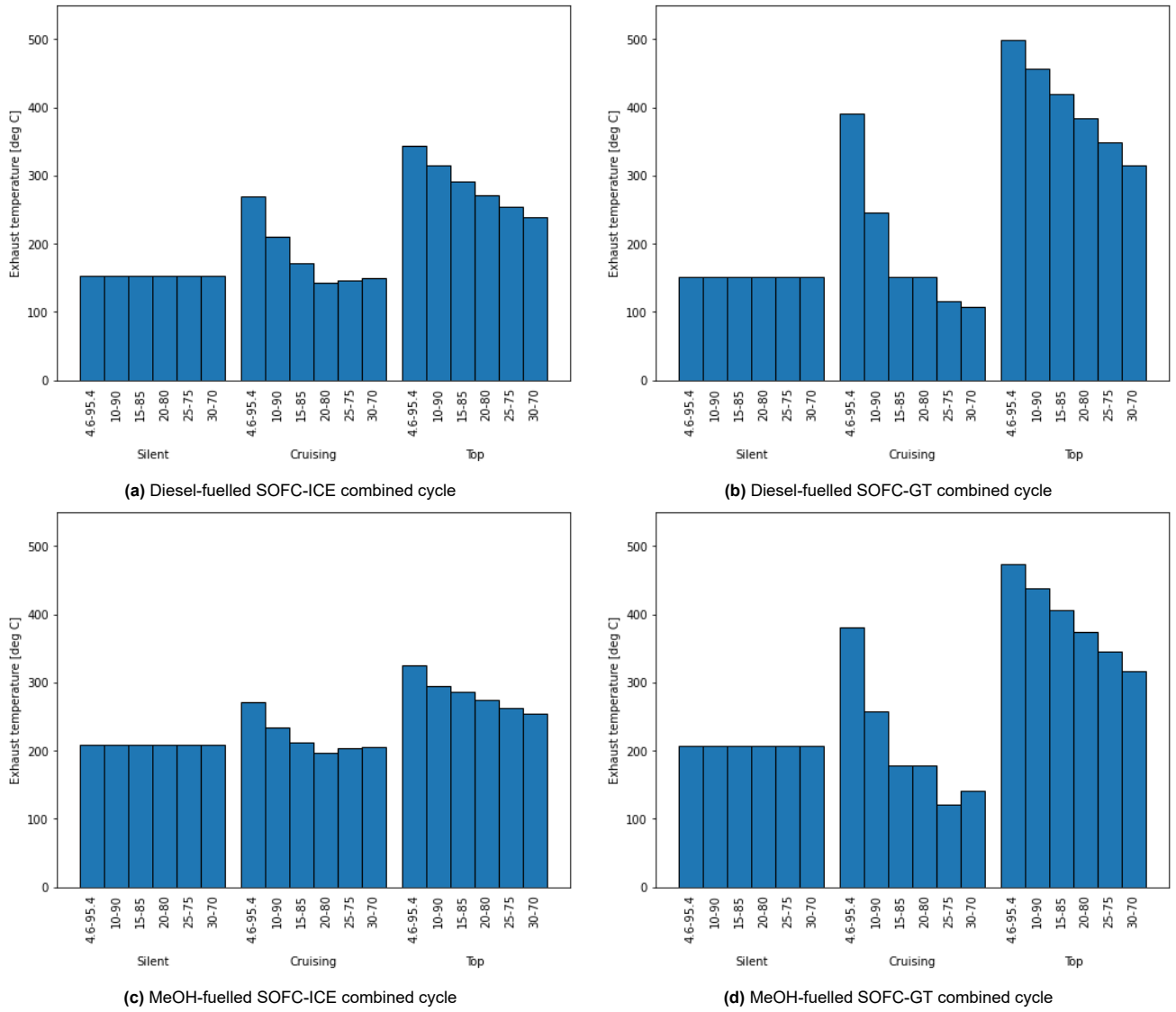

(a) Diesel-fuelled SOFC-ICE combined cycle

(b) Diesel-fuelled SOFC-GT combined cycle

(c) MeOH-fuelled SOFC-ICE combined cycle

(d) MeOH-fuelled SOFC-GT combined cycle

Figure 5.14: Exhaust temperatures of the different combined cycles for silent operation, cruising speed and top speed.

5.6.1. Comparison

To determine the best system in terms of exhaust temperature, the combined cycles are plotted against each other and against the current system in Figure 5.15. Here, it can be seen that at silent operation, the diesel-fuelled systems have the lowest exhaust temperatures. At this operating mode, only the SOFCs are running, and the exhaust temperature is equal to the exhaust temperature of the standalone SOFC. For the standalone SOFC, diesel-operation has a lower exhaust temperature than MeOH-operation, and both SOFCs have a lower exhaust temperature than a diesel-fuelled ICE (which is the current system). This means that in Figure 5.15, it is expected that the diesel-fuelled combined cycles have the lowest exhaust temperature.

At top speed, the exhaust temperature drops with an increase in power split. At higher power splits, the SOFC produces more exhaust gas at a lower temperature than the heat engine. The exhaust temperature in Figure 5.15 is a mixture of the heat engine and SOFC exhaust gasses. When the contribution of the SOFC to the total exhaust flow increases, the temperature drops. The SOFC-ICE combined cycles show lower exhaust temperatures than the SOFC-GT combined cycles. This is explained by the temperature of the exhaust gasses leaving the heat engine. The GT has higher exhaust temperatures than the ICE. At low power splits, the contribution of the heat engine is a significant portion of the total exhaust gas temperature. Since the GT has a higher temperature than the ICE, the combined cycles including the GT also have a higher exhaust temperature than the combined cycles with an ICE. At higher power splits, the exhaust temperatures of the ICE and GT systems lie closer together. This is because the contribution of the SOFC increases, for which the temperature is equal for both the ICE and GT systems.

For cruising speed, something interesting happens. At power splits below 15-85, the SOFC-ICE combined cycles have a lower exhaust temperature than the SOFC-GT combined cycles. This is in line with the results for top speed. However, at higher power splits, the SOFC-GT combined cycles show the lowest exhaust temperatures. This is explained by the integration strategy of the SOFC and GT. In this combined cycle, the GT exhaust gas is used to preheat the incoming streams of the SOFC. This results in exhaust temperatures lower than the ICE exhaust gas, which is leaving the system without cooling from the SOFC inlet streams.

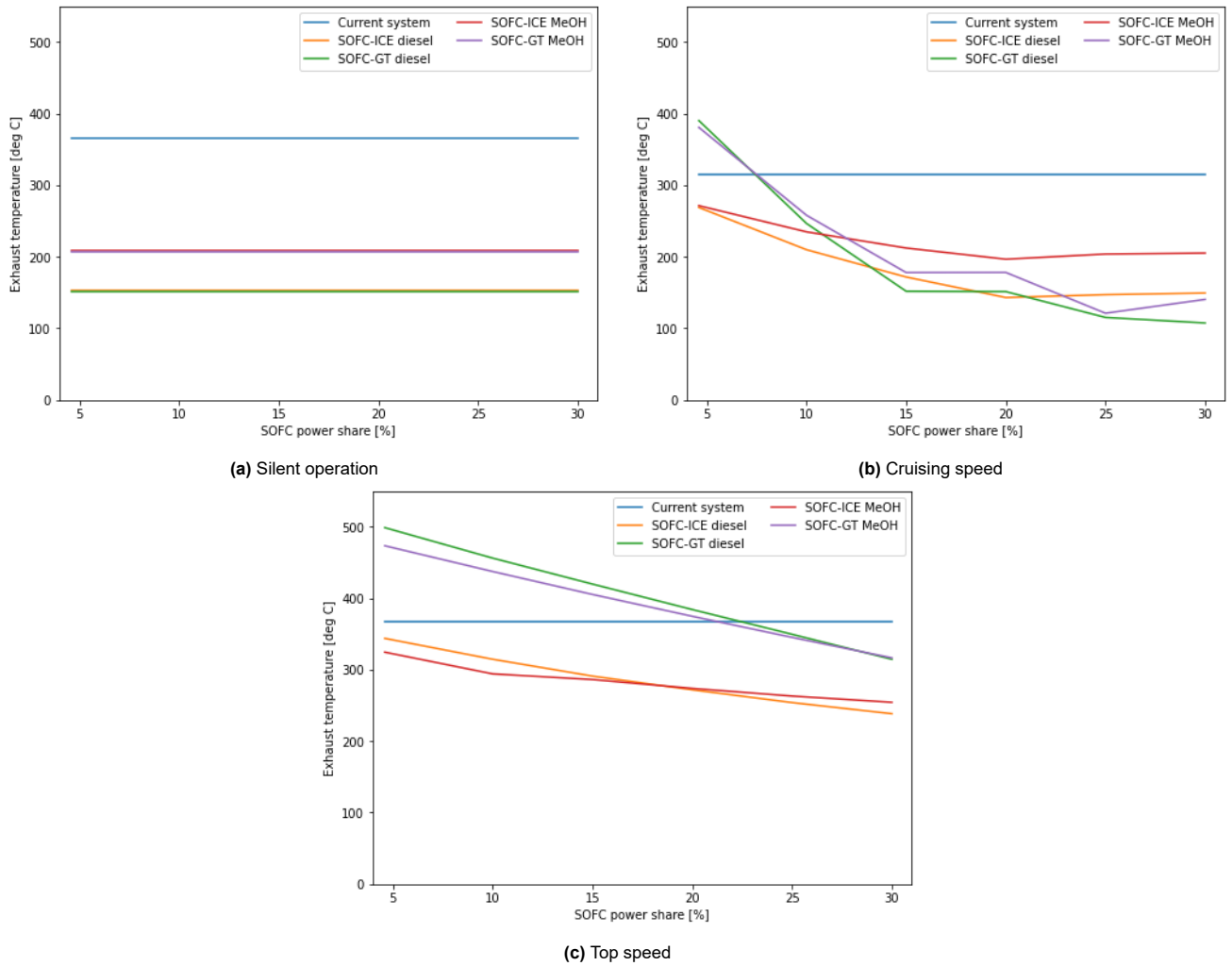

(a) Silent operation

(b) Cruising speed

(c) Top speed

Figure 5.15: Exhaust temperature for silent operation, cruising speed, top speed for each combined cycle

5.7. Size and weight

To evaluate whether the combined cycles could fit onboard of naval surface combatants, the size and weight of the systems is estimated. This estimation is based on the volume and weight of the different components (heat engine, SOFC, e-motor, HEX, gearbox, blowers), as well as the total fuel storage onboard. The sections below discuss the size and weight of each component individually.

5.7.1. Heat engine

To determine the size and weight of the heat engine, commercially available heat engines are considered. Both the ICE and GT can be mechanically connected to the propeller, or electrically through a generator and electric motor.

ICE

For the ICE, marine engines from Wärtsilä and MAN are considered. From these suppliers, an overview of the available ICEs is given in Table 5.2. In this table, the power output, size and weight of the ICEs is given. For the hybrid propulsion plants, the MAN 28/33D STC engine is chosen, and depending on the power share the 16 cylinder (16V) or the 20 cylinder (20V) variant is installed. For the electric propulsion layouts, either the Wärtsilä 34DF or the Wärtsilä 32 are chosen depending on the power split.

Table 5.2: Overview of the available marine ICEs and gensets from MAN and Wärtsilä with a power output larger than 5 MW(e) and a height less than 4.75 m [101, 102]

Engine type	Model	Power output	Length	Width	Height	Weight
ICE	MAN 12V 28/33D STC	6 MW	6.2 m	2.3 m	3.7 m	36.1 ton
	MAN 16V 28/33D STC	8 MW	7.1 m	2.3 m	3.7 m	43.6 ton
	MAN 20V 28/33D STC	10 MW	8.0 m	2.3 m	3.7 m	51.3 ton
	Wärtsilä 10V 31DF	6 MW	6.8 m	3.1 m	4.7 m	66.1 ton
	Wärtsilä 12V 31DF	7.2 MW	7.7 m	3.5 m	4.7 m	77.8 ton
	Wärtsilä 14V 31DF	8.4 MW	8.3 m	3.5 m	4.7 m	85.7 ton
	Wärtsilä 16V 31DF	9.6 MW	9.0 m	3.5 m	4.7 m	93.2 ton
	Wärtsilä 12V 34DF	6 MW	6.8 m	2.9 m	3.7 m	61 ton
	Wärtsilä 16V 34DF	8 MW	7.8 m	2.9 m	3.7 m	77 ton
Genset	Wärtsilä 12V 34DF	5.5 MWe	10.1 m	3.1 m	4.4 m	96 ton
	Wärtsilä 16V 34DF	7.4 MWe	11.2 m	3.1 m	4.5 m	96 ton
	Wärtsilä 12V 32	6.5 MWe	10.7 m	3.1 m	4.1 m	100 ton
	Wärtsilä 16V 32	8.6 MWe	11.5 m	3.4 m	4.4 m	127 ton

GT

For marine GTs, the supply is very limited. There are two manufacturers producing marine GTs; Rolls-Royce and General Electric. Both these manufacturers offer a large (>29MW) and a small (4.6MW) GT which can be used to directly drive a propeller (through a reduction gearbox) or a generator. Table 5.3 shows the size and weight of these GTs as a standalone engine (both Rolls-Royce and General Electric) or as a generating set (only General Electric). As already mentioned in section 5.2, the GT used for the combined cycles is the small GT. In the case of the hybrid propulsion plant, the GE LM500 is chosen due to the availability of size and weight of this GT. For the electric power plant the GE LM500 genset is chosen.

Table 5.3: Overview of the available marine GTs and gensets [103, 104]

Engine type	Model	Power output	Length [m]	Width [m]	Height [m]	Weight [ton]
GT	Rolls-Royce MT7 (without marine base and casing)	4.6 MW	1.6	0.9	0.9	0.46
	Rolls-Royce MT30	36 MW	8.7	2.7	3.6	30
	GE LM500	4.6 MW	3.7	1.7	1.7	2.8
	GE LM2500+	30.2 MW	7.2	2.7	3.1	23
Genset	GE LM500	4.2 MWe	7.1	2.4	2.4	27.3
	GE LM2500+	29 MWe	14.4	3.1	4.0	94.56

5.7.2. SOFC

SOFCs with available dimensions and weights are given in Table 5.4. From these fuel cells, the Bloom Energy Server is chosen due to its highest nominal power and integrated fuel processing unit and DC-AC inverter. This SOFC produces 325 kWe of AC power, and consists of six power modules, one fuel processor and an electric inverter. The power moduls are the fuel cell stacks producing DC power, and this DC power is converted to AC power by the inverter. The fuel processor removes any impurities from NG, mixes it with steam and directs the mixture to the fuel cell stacks. [105]

Table 5.4: Overview of available SOFCs

SOFC	Nominal power	Length [m]	Width [m]	Height [m]	Weight [ton]
Bloom energy server [105]	325 kWe	8.961	1.238	2.494	14.8
Convion C60 [106]	60 kWe	2.78	2.09	2.33	5.9
Elcogen elcoStack® E3000 [107]	3 kWe	0.230	0.190	0.283	0.033
SolydEra G8 stack [83]	1.8 kWe	0.184	0.299	0.250	0.032

In this thesis, the SOFC is operated on either diesel or MeOH. This means that the fuel processor present in the Bloom Energy Server needs to be switched for a diesel or MeOH reformer. For these reformers, no actual data was found in terms of size and weight. It is therefore assumed that the size of the diesel or MeOH reformer is the same as the size of the fuel processor already present in the Bloom Energy Server. Figure 5.16 shows the layout of the Bloom Energy Server including six power modules (PM), one fuel processor (FP) and one inverter (AC). These components are placed on a skid containing the piping to connect them with each other.

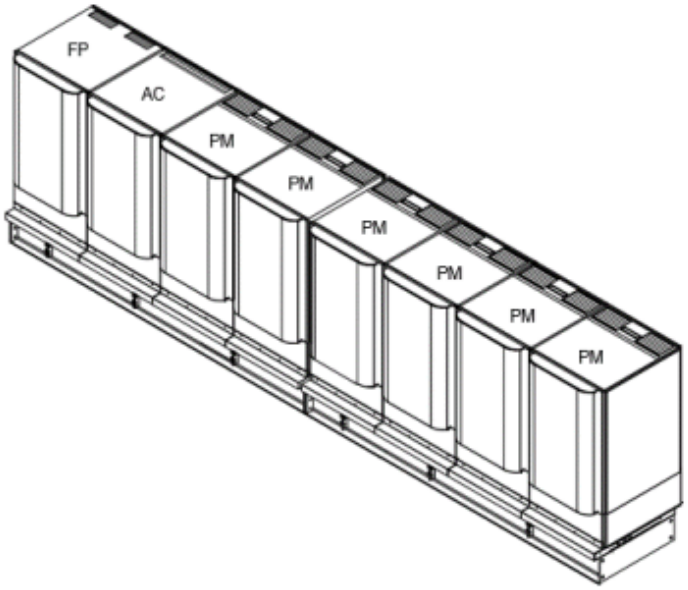

Figure 5.16: 325 kW Bloom Energy Server [105]

5.7.3. E-motor

The size and weight of the electric motors is based on the necessary power output for the different power splits. This power output is determined by taking the net electric power output of the system (only the SOFC for hybrid propulsion, and both SOFC and genset for electric propulsion). This value is then multiplied with an electric conversion efficiency of 95% and an electric motor efficiency of 95% (Equation 5.6). This results in the output power requirement for the electric motor as given in Table 5.5.

$$P_{e-motor} = P_{net,SOFC} * \eta_{conversion} * \eta_{e-motor} \tag{5.6}$$

Table 5.5: Necessary power output (per propeller shaft) for the electric motor for each power split

Propulsion system layout	Power split	$P_{e-motor}$
Electric propulsion	All	10.3 MW
Hybrid propulsion	4.6-95.4	0.332 MW
	10-90	1.060 MW
	15-85	1.790 MW
	20-80	1.973 MW
	25-75	2.996 MW
	30-70	3.642 MW

For the selection of the e-motors, an online configuration tool by Innomotics [108] is used. This configuration tool takes a required e-motor power as input and gives various options for e-motors from SIEMENS [109] that can deliver this power, and the size and weight of these e-motors. Using this configuration tool, e-motors producing the required power from Table 5.5 are selected, and an overview of these e-motors is given in Table 5.6.

Table 5.6: Overview of the selected e-motors from SIEMENS [109]

Model	Rated power [MW]	Length [m]	Width [m]	Height [m]	Volume [m^3]	Weight [ton]
Siemens HV A compact plus	0.36	1.577	0.770	0.695	0.844	1.08
	1.12	1.925	1.385	1.583	4.220	3.55
	1.80	2.149	1.496	1.757	5.649	4.70
	2.50	2.294	1.656	1.907	7.244	5.90
	3.15	2.294	1.656	1.907	7.244	6.65
	4.00	2.555	1.913	2.067	10.103	9.75
Siemens HV-M	10.68	5.580	3.850	3.385	67.181	28.00

5.7.4. Heat exchangers

The size and weight of the different heat exchangers are based on specific power (kW/kg) and power density (kW/m^3) values present in literature. Moon et al. [110] plot the power density and specific power values for different types of HEXs in a single graph. This graph is shown in Figure 5.17, and the average power density and specific power are calculated to obtain reference values, which are used to determine the volume and weight of the HEXs present in the combined cycles. Using the specific power and power density from Figure 5.17, an average power density of 4634.7 kW/m^3 and an average specific power of 2.56 kW/kg are obtained. It should be noted that this average is based on a very large range of power densities (0.01-100 W/cm^3) and specific powers (0.1-100 kW/kg). Additionally, in the average three different types of heat exchangers are included, which may or may not be suitable for usage in fuel cell combined cycles. It is also unclear for which fluid medium these values are (liquid-liquid, gas-gas, liquid-gas). The sizing of the HEX is therefore a rough estimate, and will need to be revisited at a later design iteration of the combined cycles.

A better way of determining the size and weight of the HEX is by calculating the required heat transfer area using Equation 5.7 [111]. Here, the transferred heat (Q) is divided by the overall heat transfer coefficient (U) and the logarithmic mean temperature difference ($\Delta\Theta_{mean}$). This heat transfer area can then be used to select a suitable HEX matching this area. However, manufacturers typically do not specify the heat transfer area and the corresponding HEX dimensions publicly. This makes it difficult to obtain representative values for the size and weight of the HEXs necessary for the fuel cell combined cycles.

$$A_{HEX} = \frac{Q}{U \cdot \Delta\Theta_{mean}} \tag{5.7}$$

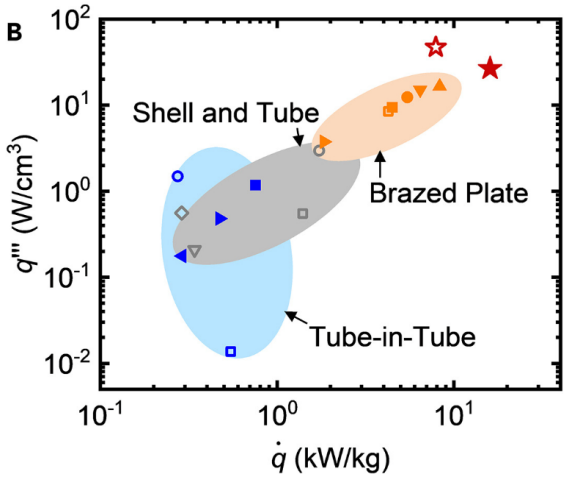

Figure 5.17: Specific power ($\dot{q}$) and power density (q''') for different types of HEXs [110]

Using the average power density and specific power, together with the transferred heat for each HEX, the volume and weight of each HEX is estimated (Equation 5.8 and Equation 5.9). The size and weight of the different HEXs needed for a single 325 kWe Bloom Energy Server are shown in Table 5.7.

$$V_{HEX} = q_{HEX} \cdot Q_{HEX} \tag{5.8}$$

$$m_{HEX} = \dot{q}_{HEX} \cdot Q_{HEX} \tag{5.9}$$

Table 5.7: Size and weight of the different HEXs needed for a single 325 kWe Bloom Energy Server

HEX	Q [kW]	Volume [m^3]	Weight [ton]
LT air heater	447	0.096	0.170
HT air heater	379	0.082	0.147
LT fuel heater	9	0.002	0.004
HT fuel heater	11	0.003	0.005
Economizer	12	0.003	0.005
Evaporator	68	0.015	0.027
Superheater	12	0.003	0.005

Besides the HEXs mentioned in Table 5.7, the SOFC-ICE combined cycles also have an additional HEX: the moisture separator. This HEX cools the AOG until the water in this gas condenses, allowing it to be separated from the AOG. The size of the moisture separator depends on the power split and transmitted heat, and is also calculated using the previously calculated average specific power and power density.

5.7.5. Gearbox

For the gearbox, the only identified supplier that states the dimensions and weight of their gearboxes publicly is Wärtsilä. Wärtsila offers single input/single output (reduction gearbox), double input/single output and custom gearboxes Wärsilä [112]. In the case of the electric propulsion layout, the e-motor is connected to the propeller through a reduction gearbox, and size of this gearbox depends on the transmitted power. For the hybrid solution, a reduction gearbox is not sufficient. In the case of the SOFC-ICE combined cycles, a propeller is driven by a single ICE and an e-motor. This means that a double input/single output gearbox is needed for each propeller shaft. For the SOFC-GT combined cycles, the gearbox becomes more complex. The power output of a single GT (4.6 MW) is too low too power the propeller in combination with the e-motor. To reach the required propulsion power for top speed, multiple GTs need to be connected to a single propeller shaft. This calls for a custom gearbox consisting of three or four inputs (depending on the e-motor size) and a single output for each propeller shaft. With this many inputs, the gearbox becomes very large and heavy. Another option is to install multiple double input/single output gearboxes to connect multiple power sources to the propeller. Table 5.8 shows an

overview of the size and weight of different gearboxes. According to ir. S. Knegt (personal communication), the triple input/single output gearbox would weigh about 80 tons. Using the same ratio between weight and volume as the double input/single output gearbox, the volume of this gearbox would then be about 82 m^3.

Table 5.8: Size and weight of the different gearboxes [112, 113]

Gearbox type	Model	Length [m]	Width [m]	Height [m]	Volume [m^3]	Weight [ton]
Reduction gearbox	SCH105	2.450	2.995	2.429	17.823	30
Double input/single output	TCH270	2.440	3.900	3.020	28.738	28
Triple input/single output	Estimate	-	-	-	82	80

5.7.6. Blowers

The size of the blowers mainly depends on the volume flow through the blower, as well as the pressure increase over the blower. Just like the size of the HEXs, the size of the blower is taken for a single 325 kWe Bloom Energy Server. For this server, the flow through the blower is about 2900 m^3/hr of air for diesel operation, and about 3900 m^3/hr of air for MeOH operation. The power necessary to drive the blowers is about 15 kW for diesel and about 8 kW for MeOH. The company HRBlowers offers positive displacement air blowers in various sizes, and the model that matches these volume flows and powers is the HR43 blower. This blower has a volume flow range between 1199-7530 m^3/hr at a power between 3-73 kW [114]. The size and weight of this blower is shown in Table 5.9.

Table 5.9: Size and weight of the blower needed for a single 325 kWe Bloom Energy Server [114]

Model	Length [m]	Width [m]	Height [m]	Volume [m^3]	Weight [ton]
HR43	1.252	0.510	0.665	0.425	0.68

5.7.7. Fuel storage

Lastly, the weight and volume for fuel storage is determined. For the fuel weight, a vessel range of 5700 NM is used. For the reference vessel, this range equals a fuel storage weight of 350 tons. For the combined cycles, the fuel consumption at cruising speed differs from the fuel consumption of the current system. This means that for an equal range, a different amount of fuel is needed. The fuel storage weight for each combined cycle is calculated using Equation 5.10. The ship speed for this equation is equal to the cruising speed (18 kts), and the fuel consumption is taken from the CT models for cruising speed Next, the volume of the fuel storage is calculated by dividing the fuel weight with the density of the fuel, which is 0.845 ton/m^3 for diesel and 0.792 ton/m^3 for MeOH (Equation 5.11).

$$m_{fuel} = \frac{\dot{m}_{fuel} \cdot 3600 \cdot R}{v_{ship} \cdot 1000} \tag{5.10}$$

$$V_{fuel} = \frac{m_{fuel}}{\rho_{fuel}} \tag{5.11}$$

Using these equations, the fuel weight and volume for the diesel-fuelled SOFC-ICE combined cycle is given in Table 5.10. The fuel storage volume and weight for the other combined cycles are shown in Appendix E.

Table 5.10: Fuel storage volume and weight for the diesel-fuelled SOFC-ICE combined cycle at different power splits

Power split	Volume [m^3]	Weight [ton]
4.6-95.4	388.54	328.32
10-90	349.42	295.26
15-85	312.99	264.48
20-80	279.27	235.98
25-75	267.12	225.72
30-70	300.85	254.22

5.7.8. Total weight and volume

For each combined cycle, the weight and volume of the ICE/GT, genset, SOFC, e-motor, HEXs, gearbox, blowers and fuel are summed to obtain the total weight and volume of the system. Table 5.11 shows a breakdown of the weight and volume of each component, as well as the amount of these components installed in the system for the diesel-fuelled SOFC-ICE combined cycle with a power split of 4.6-95.4. The same table is created for each power split and combined cycle, and these are shown in Appendix E.

Table 5.11: Weight and volume of the components of the diesel-fuelled SOFC-ICE combined cycle with a power split of 4.6-95.4

Component	Variant	Length [m]	Width [m]	Height [m]	Volume [m^3]	Weight [ton]	Amount installed
ICE (hybrid)	MAN 20V 28/33D STC (10 MW)	8.047	2.273	3.982	67.347	51.3	2
Genset (electric)	Wärtsilä 16V 34DF (7.37 MWe)	11.175	3.060	4.515	154.393	121	3
SOFC	Bloom Energy Server (325 kWe)	8.961	1.238	2.494	27.668	14.8	4
E-motor (hybrid)	Siemens HV C (1.17 MW)	2.448	1.030	1.254	3.162	4.7	2
E-motor (electric)	Siemens HV-M (11.65 MW)	5.155	3.85	3.385	67.18	28	2
Gearbox	Wärtsilä SCH105	2.450	2.995	2.429	17.823	30	2
HEX	Low temperature air heater	1.000	0.596	0.596	0.089	0.16	4
	High temperature air heater	1.000	0.552	0.552	0.076	0.138	4
	Low temperature fuel heater	0.300	0.165	0.165	0.002	0.004	4
	High temperature fuel heater	0.300	0.172	0.172	0.002	0.004	4
	Economizer	0.300	0.175	0.175	0.002	0.004	4
	Evaporator	0.500	0.324	0.324	0.013	0.024	4
	Superheater	0.300	0.174	0.174	0.002	0.004	4
	Moisture separator	1.000	0.530	0.530	0.141	126.8	2
Blower	HR43	1.252	0.510	0.665	0.425	0.68	4
Fuel	Diesel	-	-	-	388.54	328.32	-
Total (hybrid)	-	-	-	-	675.78	544.49	-
Total (electric)	-	-	-	-	1098.52	870.59	-

Figure 5.18 shows the contribution of each component to the total weight and volume of the system. In these figures, it can be seen that the main contributor to the weight and volume of the current system is the fuel storage, followed by the ICEs. For the diesel-fuelled combined cycles, the fuel storage has a relatively smaller impact on the total weight and volume of the system, and a large portion is dictated by the SOFC (for the GT combined cycles) and the ICE/GT/Genset (for the ICE combined cycles). For the MeOH-fuelled combined cycles, the fuel storage is still a significant portion of the total weight and volume of the system (about 60%). In the figures, it can also be seen that for an increase in SOFC power share, the total weight and volume of the SOFC increases significantly. Lastly, a stepped decrease is visible for the heat engine for an increase in power split. This is attributed to the fact that the heat engine is available in fixed power outputs, The step in weight and volume corresponds to the point where a smaller engine (lower power output) can be installed to reach the required total power.

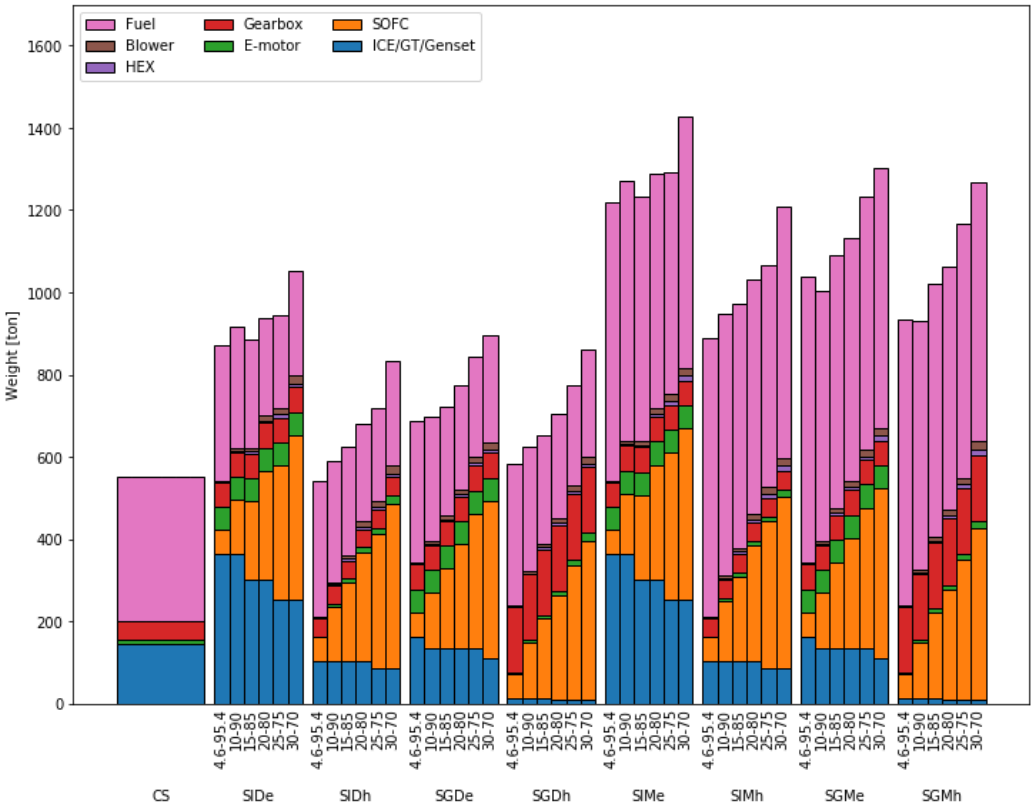

(a) Comparison of total weight

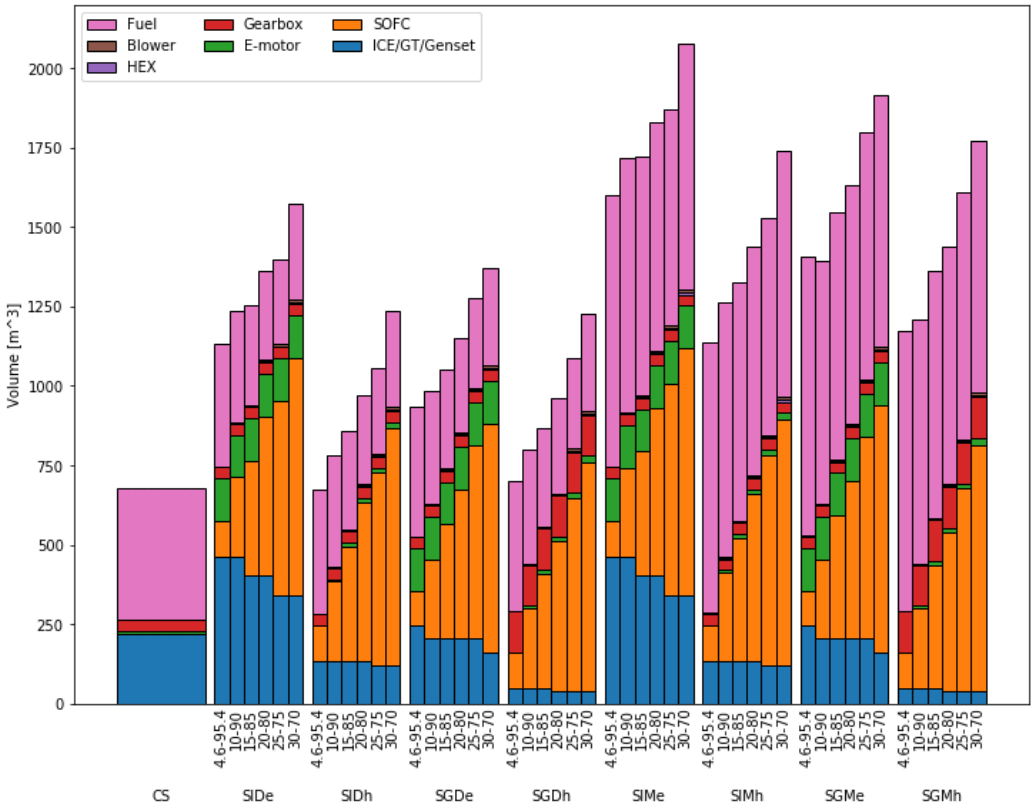

(b) Comparison of total volume

Figure 5.18: Comparison of total weight and volume of the different combined cycles. CS = current system, SIDe = SOFC-ICE diesel electric, SIDh = SOFC-ICE diesel hybrid, SGDe = SOFC-GT diesel electric, SGDh = SOFC-GT diesel hybrid, SIMe = SOFC-ICE MeOH electric, SIMh = SOFC-ICE MeOH hybrid, SGMe = SOFC-GT MeOH electric, SGMh = SOFC-GT MeOH hybrid.

5.8. Best performing system

To see how the different combined cycles perform compared to the reference system, the results for energy consumption, CO_2 emissions, exhaust temperature, component weight, fuel weight and total system weight are normalized with respect to the current system. The current system obtains a baseline score of 100% for each criterion. The combined cycles score relative to this baseline score; e.g. if a system scores 200% for system weight, the system is twice as heavy as the current system, and a score of 50% means it is half the weight of the current system. Table 5.12 shows an overview of the scores for each combined cycle and power split. To easily see which systems score better than the current system, these scores are marked in green. If a system scores worse than the current system, it is marked in red. From this table, it can easily be seen that all the combined cycles (with the exception of the 4.6-95.4 SOFC-GT) outperform the current system in terms of energy consumption, CO_2 emissions and exhaust temperature. However, the downside of the combined cycles is the component weight. Depending on the choice of hybrid or electric propulsion, the weight of the components can be four times heavier compared to the current system. For the diesel-fuelled systems, this increase in component weight can partly be countered by a reduction in fuel weight, but overall the systems are still heavier than the current system (with the exception of the 4.6-95.4 SOFC-ICE combined cycle with hybrid propulsion, which has a slightly lower total weight than the current system).

Interesting to see is that the score for total CO_2 emissions of the diesel-fuelled systems is not exactly equal to the score for energy consumption. In the calculation of the total CO_2 emissions, full conversion of the fuel to CO_2 and H_2 is assumed. This means that the normalized energy consumption and total CO_2 emissions should be equal. The slight difference in normalized scores is attributed to rounding errors in the calculation of the energy consumption. In CT, the fuel consumption is rounded to three decimals. However, for the total CO_2 fraction in CT the fuel consumption is not rounded. This discrepancy leads to the slight difference in normalized scores for the energy consumption and total CO_2 emissions visible in Table 5.12.

Generally, when increasing the power split, the energy consumption, CO_2 emissions and exhaust temperature decrease. However, this increase in power split also leads to an increase in system weight. The CO_2 emissions and energy consumption are directly linked, and an increase in energy consumption leads to an increase in CO_2 emissions. The exhaust temperature is an important factor in the IR-signature of the vessel, but there are other ways of decreasing this temperature.

The energy consumption and system weight and volume are taken as the main selection criteria for the combined cycles. To determine the best system, the energy consumption and total system weight are plotted against each other in Figure 5.19a, and the energy consumption and total system volume are plotted against each other in Figure 5.19b. In these figures, the utopian solution is also plotted. This utopian solution consists of the minimum energy consumption and minimum system weight present in Table 5.12. Unfortunately, it is impossible to reach the utopian solution. However, the utopian solution can help in determining the best combined cycle for naval surface combatants, which is the system that lies closest to the utopian solution. From Figure 5.19a, it can be seen that the SOFC-ICE combined cycle running on diesel fuel with a hybrid propulsion layout lies closest to the utopian solution. This system is therefore chosen as the best combined cycle for naval surface combatants.

To determine the optimal power split based on energy consumption and system weight, a region of equal distance to the utopian solution is plotted in Figure 5.20. Wherever this region intersects with the line for the SOFC-ICE diesel hybrid, is the optimal power split. In Figure 5.20a it can be seen that this region of equal distance intersects the line for the combined cycle close to a power split of 10-90. Figure 5.20b shows the same figure but further zoomed in. The intersection lies between a power split of 4.6-95.4 and 10-90, and the exact power split is obtained by linearly interpolating these two data points. This results in an optimal power split for the SOFC-ICE diesel hybrid system of 8.4-91.6.

When the optimal power split is determined based on system volume instead of system weight, a slightly different solution is found. The diesel-fuelled SOFC-ICE combined cycle with a hybrid power plant is still the best solution, but this time with a power split of 6.1-93.9. This power split is slightly lower than the optimal power split based on system weight.

Table 5.12: Performance of the different combined cycles with respect to the current system. The green cells indicate that the system performs better than the current system, and the red cells indicate that the system performs worse than the current system.

System	Power split	Total energy consumption	Total CO2 emissions	Exhaust temperature silent	Exhaust temperature cruising	Fuel weight (equal range)	Component weight (electric propulsion)	Component weight (hybrid propulsion)	Total weight (electric propulsion)	Total weight (hybrid propulsion)
Current	-	100,00%	100,00%	100,00%	100,00%	100,00%	100,00%	100,00%	100,00%	100,00%
SOFC-ICE diesel	30-70	82,73%	82,79%	41,83%	47,47%	71,10%	399,03%	291,09%	190,70%	151,61%
	25-75	81,82%	81,85%	41,83%	46,75%	65,91%	361,15%	248,10%	172,43%	131,48%
	20-80	84,07%	84,21%	41,83%	45,47%	69,16%	352,29%	223,14%	171,08%	124,30%
	15-85	88,01%	88,02%	41,83%	54,58%	76,62%	312,40%	182,05%	161,60%	114,39%
	10-90	92,16%	91,70%	41,83%	66,69%	85,06%	312,06%	148,96%	166,87%	107,79%
	4.6-95.4	96,63%	96,61%	41,83%	85,43%	93,83%	272,16%	106,57%	158,42%	98,45%
SOFC-GT diesel	30-70	84,88%	84,85%	41,59%	34,20%	70,78%	319,53%	302,24%	161,08%	154,82%
	25-75	86,13%	86,23%	41,59%	36,65%	68,83%	301,42%	267,34%	153,28%	140,93%
	20-80	89,52%	89,57%	41,59%	48,10%	72,08%	261,68%	226,85%	140,54%	127,93%
	15-85	92,73%	92,74%	41,59%	48,26%	75,00%	229,89%	195,25%	131,10%	118,55%
	10-90	99,17%	99,40%	41,59%	78,33%	86,36%	198,10%	162,31%	126,83%	113,87%
	4.6-95.4	105,45%	105,64%	41,59%	123,94%	97,08%	172,04%	120,09%	124,64%	105,83%
SOFC-ICE MeOH	30-70	85,39%	77,62%	57,08%	65,18%	170,78%	408,71%	298,77%	257,58%	217,76%
	25-75	83,73%	76,09%	57,08%	64,77%	155,88%	376,79%	263,74%	229,24%	188,29%
	20-80	85,97%	78,22%	57,08%	62,47%	164,54%	360,04%	230,89%	227,52%	180,75%
	15-85	80,12%	81,08%	57,08%	67,43%	177,01%	320,22%	189,86%	219,73%	172,51%
	10-90	91,89%	83,59%	57,08%	74,60%	190,87%	319,89%	156,78%	228,51%	169,44%
	4.6-95.4	95,65%	87,04%	57,08%	86,22%	203,34%	272,12%	106,54%	219,91%	159,94%
SOFC-GT MeOH	30-70	87,36%	79,16%	56,84%	44,65%	170,08%	335,37%	318,08%	228,73%	222,47%
	25-75	85,80%	77,70%	56,84%	38,51%	149,65%	309,69%	275,61%	202,45%	190,11%
	20-80	90,61%	81,98%	56,84%	56,60%	166,97%	270,69%	235,86%	193,92%	181,30%
	15-85	94,15%	85,18%	56,84%	56,55%	176,67%	238,54%	203,89%	188,49%	175,94%
	10-90	98,68%	89,31%	56,84%	81,96%	192,60%	198,63%	162,84%	185,22%	172,25%
	4.6-95.4	104,82%	94,84%	56,84%	120,91%	216,85%	172,31%	120,35%	191,42%	172,60%

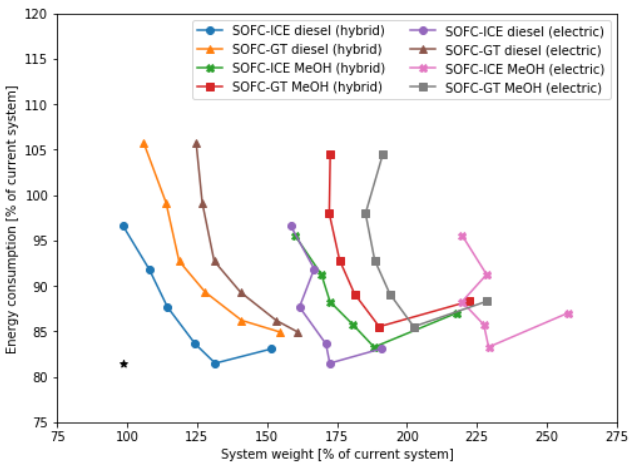

(a) Energy consumption and system weight of the different combined cycles. The black star represents the utopian solution, and corresponds to the minimum weight and energy consumption possible with these systems.

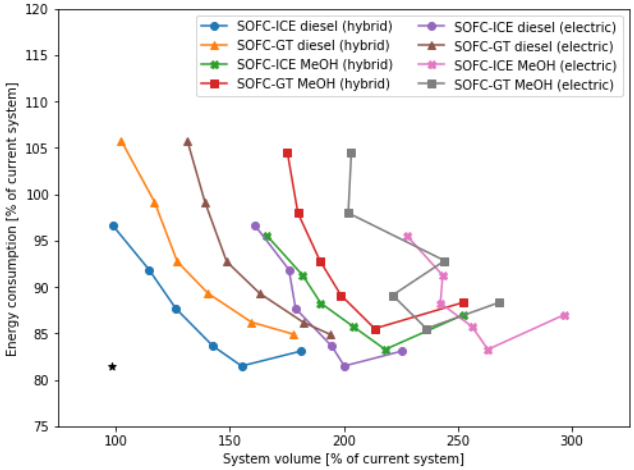

(b) Energy consumption and system volume of the different combined cycles. The black star represents the utopian solution, and corresponds to the minimum volume and energy consumption possible with these systems.

Figure 5.19: Comparison between energy consumption and system weight (a) and comparison between energy consumption and system volume (b) of the different combined cycles.

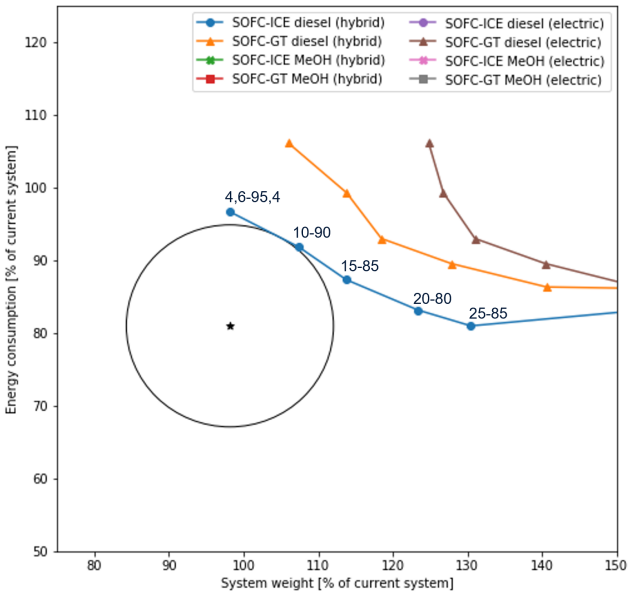

(a) Figure 5.19a zoomed in on the utopian solution. The black circle represents a region of equal distance to this utopian solution.

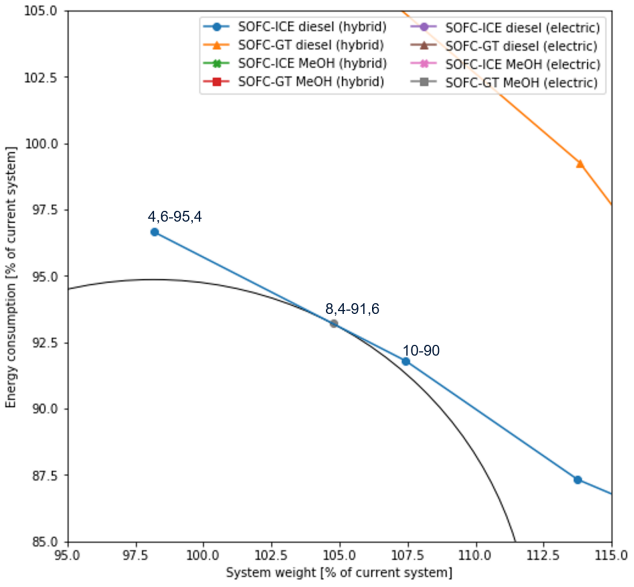

(b) Further zoomed in version of Figure 5.19a, showing the exact intersection of the black circle with the SOFC-ICE diesel hybrid system.

Figure 5.20: Energy consumption and system weight of the different combined cycles. The black star represents the utopian solution, and corresponds to the minimum weight and energy consumption possible with these systems. The black circle is a region of equal distance to the ideal solution, and the intersection with this region represents the best solution.

To determine the performance of the 8.4-91.6 and 6.1-93.9 power splits, all values of Table 5.12 are linearly interpolated between the 10-90 and 4.6-95.4 power splits. This gives the performance parameters for the optimal power split as given in Table 5.13. In this table, it can be seen that the optimal power split of 8.4-91.6 has about 7% less energy consumption and CO_2 emissions, about 58% lower exhaust temperature at silent operation, about 28% lower exhaust temperature at cruising speed, and needs to carry about 13% less fuel for the same range compared to the current power plant of the reference vessel. However, this does come at the cost of about 46% more weight for the necessary components. Most of this extra weight can be countered by the lower fuel storage weight necessary for the same range as the reference vessel. Overall, the system is still about 5% heavier compared to the current power plant. This means that for the same range, the draught of the vessel will increase slightly. Assuming a constant waterplane area, the draught increases with 26 mm. This extra

draught will lead to a slightly higher ship resistance, and therefore to a slightly higher power demand for the different operating modes. This will either lead to a slightly higher fuel consumption (which reduces the energy consumption difference with the current system), or a slightly lower ship speed at the operating modes.

For the 6.1-93.9 power split, the annual energy consumption, CO_2 emissions and exhaust temperature at cruising speed are slightly higher compared to the 8.4-91.6 power split. However, the weight of this lower power split is less, meaning that the draught also increases less compared to the current system. In terms of available space in the vessel, the power split of 6.1-93.9 is preferred due to its lower volume. However, for reducing energy consumption, emissions and exhaust temperature, the 8.4-91.6 power split is preferred. However, this system does have a slightly higher volume, which means that it will be more difficult to retrofit the SIGMA with this system. In chapter 6 it is checked whether this power split is possible in the current design of the SIGMA.

Table 5.13: Performance of the optimal power split of the diesel fuelled SOFC-ICE combined cycle with respect to the current system. The green cells indicate that the system performs better than the current system, and the red cells indicate that the system performs worse than the current system.

System	Power split	Total energy consumption	Total CO_2 emissions	Exhaust temperature silent	Exhaust temperature cruising	Fuel weight (equal range)	Component weight (hybrid propulsion)	Total weight (hybrid propulsion)	Vessel draught [m]
Current	-	100,00%	100,00%	100,00%	100,00%	100,00%	100,00%	100,00%	4.000
SOFC-ICE diesel	10-90	92.16%	91.70%	41.83%	66.69%	85.06%	148.96%	108.21%	4.040
	8.4-91.6	93.45%	93.12%	41.83%	72.10%	87.60%	136.71%	105.39%	4.026
	6.1-93.9	95.42%	95.29%	41.83%	80.37%	91.46%	118.02%	101.08%	4.005
	4.6-95.4	96.63%	96.66%	41.83%	86.03%	93.83%	106.57%	98.45%	3.992

5.9. Conclusion

In this chapter, the results for the different combined cycles are discussed. The annual energy consumption, annual CO_2 emissions, exhaust temperature, system volume and system weight are determined for each combined cycle for various power splits. Using the annual energy consumption and total system weight, the best combined cycle and the optimal power split is determined. The SOFC-ICE combined cycle with a hybrid propulsion layout is determined to be the best system. The optimal power split for this system is obtained by comparing this system to the utopian solution, which corresponds to the minimal possible energy consumption and system weight present for all the combined cycles. When comparing with the utopian solution, a power split of 8.4-91.6 lies closest to this utopian solution. With this power split, the diesel-fuelled SOFC-ICE combined cycle with a hybrid propulsion layout outperforms the current power plant of the reference vessel on annual energy consumption, annual CO_2 emissions, exhaust temperature at silent operation and exhaust temperature at cruising speed. However, this does come at the cost of a slightly higher total system weight (components and fuel storage combined). This slightly higher system weight results in a higher total weight of the vessel, which means that the vessel draught will increase slightly. This draught increase will result in a slightly higher ship resistance, which results in a higher power demand for a given ship speed. To reach the desired speed for the different operating modes, this may indicate that the total power production needs to increase, which has a negative impact on the total weight of the combined cycle. Instead of increasing the power output of the system, it is possible to remove fuel storage from the vessel and keep the total weight of the vessel equal. This will result in a slightly lower vessel range, but this way the reduction in annual energy consumption compared to the current system is not affected by the total weight of the system. The diesel-fuelled SOFC-ICE combined cycle with a power split of 8.4-91.6 and a hybrid propulsion layout is used to test whether this system can fit within the reference vessel in chapter 6.

6

Implementation in the general arrangement

In chapter 5 it is concluded that the SOFC-ICE combined cycle running on diesel is the best solution for a naval surface combatant. Based on the weight of the system and the total energy consumption, the optimal power split is 8.4-91.6. In this chapter, this system is fitted into the general arrangement plan of the reference vessel. The size and weight of the different components is taken equal to the dimensions given in chapter 5, with the exception of the HEXs, blower and burner. These components have a limited height, and can be stacked for more efficient usage of the available space. The stacking of the HEXs, blower and burner is addressed in section 6.1. Next, the system needs water for the steam reforming of the diesel. This water management is briefly discussed in section 6.2. The placement of the different components is addressed in section 6.3, and fuel storage is addressed in section 6.4. Lastly, section 6.5 gives a conclusion regarding the implementation of the combined cycle in the general arrangement of the reference vessel.

6.1. HEX, blower, burner

The Bloom Energy Server has a standard power output of 325 kWe. In order to reach the total SOFC power needed for the combined cycle, multiple Bloom Energy Servers are installed. The HEXs, blowers and burner present in the CT model for the combined cycle, are split into smaller components that can provide for a single Bloom Energy Server. A global bounding box is then determined to fit the HEXs, blowers and burner, and this bounding box is shown in Figure 6.1.

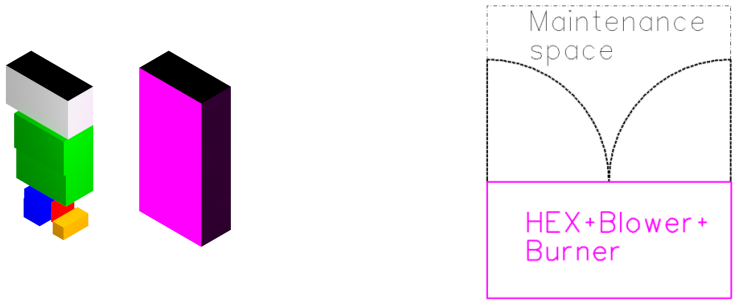

Figure 6.1: Bounding box to fit the HEX, blower and burner for a single Bloom Energy Server. The cathode blower is shown in grey, the air heaters in green, the water heaters in blue, the fuel heaters in red and the burner in orange. The bounding box is shown in purple.

When stacking the HEXs, blower and burner in the bounding box, some room is still available for the piping necessary to connect everything. At this stage in the design, it is still unclear whether this available space is sufficient. For this reason, the maintenance space is taken larger than necessary for the doors to open. This way, the purple bounding box can still grow to accommodate all of the piping.

6.2. Water management

For the steam reforming of the diesel fuel, water needs to be directed to the fuel reformer. To supply the reformer with enough water, the water from the moisture separator can be used. This moisture separator removes water from the AOG, and the amount of water that is removed from the AOG is larger than the necessary water for the steam reforming reaction. This means that when the system is operating, no extra water needs to be fed into the system to keep the system running. Subsequently, no additional water storage tanks need to be integrated in the design of the vessel. This also means that the water created by the reverse osmosis (RO) unit is not necessary for the operation of the fuel cells, and the RO unit can be kept the same as the current one installed on the vessel.

6.3. System layout

The general arrangement plan of the reference vessel is adapted to fit all the components of the hybrid, diesel-fuelled SOFC-ICE combined cycle. From the original general arrangement plan, the diesel generator sets and their exhaust systems and the electric motors are removed. Additionally, holes in the deck above the gensets and e-motors are closed as they are no longer needed. This opens up room for the SOFCs on the 3-deck. Existing components in the general arrangement are kept mostly in place, however, some components need to be moved to allow the SOFC modules to be placed.

First, the new electric motor is placed at the location of the original electric motor. The new e-motor is lower than the original, so no deck cutout is necessary in the deck above the e-motor. Next, the fuel cell modules are placed. Two of the gensets of the original system were located on the 4-deck. This deck is only 2 m high, which means that the SOFCs cannot be placed on the location of the original gensets as the SOFCs have a height of 2.5 m. The SOFCs can thereore only be placed on the 3-deck, which has a height of 2.75 m. The Bloom Energy Server consists of 6 power modules (PM), one fuel processor (FP) and one electric inverter (AC). When placing the Bloom Energy Server in the general arrangement plan, it is assumed that the layout of the PMs, AC and FP can be changed compared to the layout presented by Bloom Energy in [105]. It is also assumed that for a single server, PMs can be removed without a change in FP and AC size. It is also assumed that the AC and FP can accomodate a maximum of 6 PMs; e.g. for three Energy Servers with 5 PMs instead of 6, the system still requires three ACs and FPs.

Relevant sections of the general arrangement plan with the SOFC-ICE combined cycle are shown in Figure 6.2 and Figure 6.3. With this layout, a maximum of 41 PMs are installed on the vessel. Each PM produces one sixth of the total power of the Bloom Energy Server (1 PM produces 54 kWe). This system produces a maximum of $41 \cdot 54 = 2221$kWe of power. This power output is the gross power output of the SOFC. With this gross power output, a maximum net power split of 7.8-92.2 can be obtained inside the reference vessel. This power split is slightly lower than the optimal power split determined in chapter 5 (8.4-91.6 power split).

Compared to the original general arrangement plant, the fuel oil service tanks (SB and PS) are 33% smaller. The size of these tanks are reduced to allow an extra Bloom Energy Server to be installed in the vessel. However, this does reduced service tank size has an implication on the rules regarding the sizing of these tanks. SOLAS regulations dictate that the service tanks have a capacity to operate the main machinery and important auxiliary systems for at least 8 hours [115]. By reducing the size of the service tanks compared to the original size, the new layout may not comply with this regulation. However, the combined cycle sytem consumes less fuel over these 8 hours of operating time, so it may be possible that the reduced tank size still complies with this regulation.

To obtain the performance parameters for the 7.8-92.2 power split, the results for the 4.6-95.4 and 10-90 power split are linearly interpolated. Table 6.1 shows the results for the 7.8-92.2 power split compared to the optimum power split of 8.4-91.6 and the current system. When comparing the 7.8-92.2 power split with the optimal solution, it can be seen that the energy consumption, CO_2 emissions and exhaust temperature at cruising speed are slightly worse. Also slightly more fuel storage is needed to reach the same range. However, the components for the 7.8-92.2 power split are lighter, resulting in a lower overall system weight. Compared to the current system, the 7.8-92.2 power split offers about 6% less energy consumption and CO_2 emissions, about 58% lower exhaust temperature at silent operations, about 25% lower exhaust temperature at cruising speed and a reduction of about 12% in fuel storage weight. This comes at the cost of a 4% increase in total system weight, resulting in a draught increase of 20 mm.

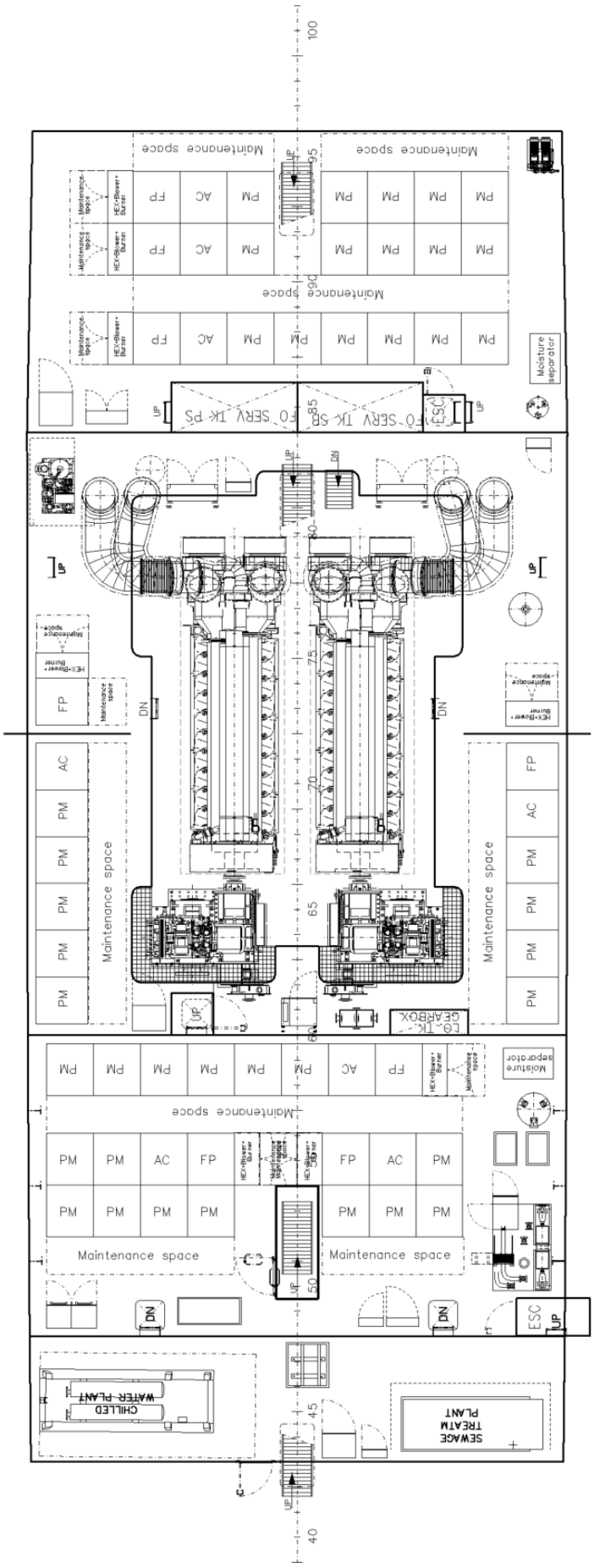

Figure 6.2: Section of the general arrangement plan for Deck 3

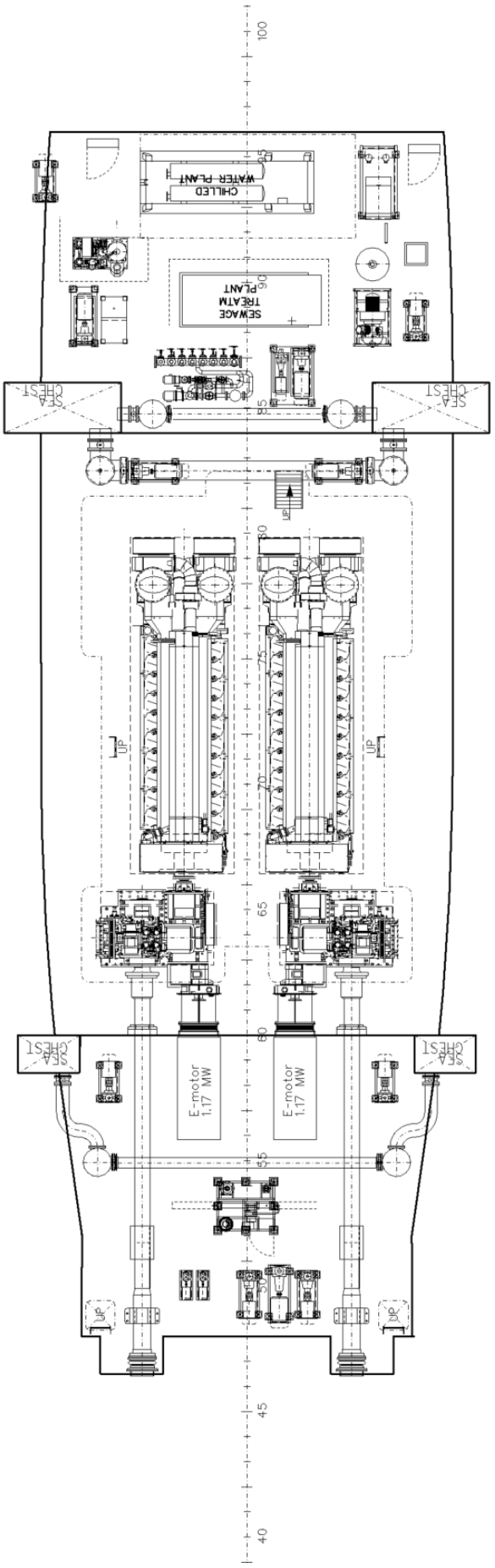

Figure 6.3: Section of the general arrangement plan for Deck 4

Table 6.1: Performance of the maximum power split that still fits in the reference vessel compared to the current system. The green cells indicate that the system performs better than the current system, and the red cells indicate that the system performs worse than the current system.

System	Power split	Total energy consumption	Total CO_2 emissions	Exhaust temperature silent	Exhaust temperature cruising	Fuel weight (equal range)	Component weight (hybrid propulsion)	Total weight (hybrid propulsion)	Vessel draught [m]
Current	-	100,00%	100,00%	100,00%	100,00%	100,00%	100,00%	100,00%	4.000
SOFC-ICE diesel	7.8-92.2	93.81%	93.95%	41.83%	74.27%	88.25%	139.17%	103.98%	4.020

6.4. Fuel tanks

The fuel storage is an important aspect in the layout of the vessel. The optimal power split from chapter 5 (8.4-91.6) needs about 12% less fuel storage weight compared to the current system. This means that for an equal range, the size of the current fuel tanks can be reduced, resulting in possible extra space to fit additional fuel cells. However, in the current design, most of the fuel storage is located in the double bottom of the hull. Reducing these fuel tanks does not lead to an increase in available space for the placement of fuel cells. Besides the double bottom, fuel storage is also located on Deck 4 (between frame 96 and 108 in Figure 6.3). As stated earlier in section 6.3, this deck is too low to for the fuel cells. Just like with the fuel storage in the double bottom, reducing the size of the fuel storage tanks in Deck 4 does not result in usable space for the placement of additional fuel cells.

Instead of keeping the range of the vessel equal, it is possible to keep the fuel storage equal without affecting the possible power split in the vessel. For the maximum fitting power split (7.8-92.2), a fuel storage of 351.1 ton results in a vessel range of 6454 NM (754 NM increase compared to the current system). However, this results in a higher total system weight, which negatively impacts the total weight of the vessel. This higher total vessel weight results in an increase in draught and vessel resistance. Extra resistance means that either the fuel consumption increases for a given ship speed, or the maximum vessel speed decreases for a given power output. For this reason, it is chosen to keep the range of the vessel equal to the current system. This means that the fuel storage weight is reduced, which can compensate the increase of component weight for the combined cycle. Overall, this means that the total weight of the vessel increases less, which is beneficial for the annual energy consumption and GHG emissions. If the fuel storage in Deck 4 is reduced, this space can be converted to storage of e.g. provisions or ammunition (if allowed by the rules and regulations).

6.5. Conclusion

In this chapter, the feasibility of the optimal power split determined in chapter 5 is checked by trying to fit this system in the general arrangement plan of the reference vessel. When removing the generator sets and electric motor from the current system, enough space is freed up to fit SOFCs with a gross power output of 2.2 MWe. This corresponds to a net power split for the reference vessel of 7.8-92.2, which is lower than the optimal power split of 8.4-91.6. Despite the optimal power split not fitting in the reference vessel, the power split that does fit is fairly close to the optimum power split. This means that the benefits of the optimal power split are still present in the maximum fitting power split. However, these benefits are slightly less than the optimal power split. The maximum fit still leads to a reduction in energy consumption, CO_2 emissions and exhaust temperature compared to the current system, with a minimal increase in total system weight. The increase in weight will most likely lead to an increase in power demand for the top speed condition, and whether the combined cycle can still produce enough power to reach the top speed, needs to be checked by determining the power-speed curve for the increased vessel draugth. Additionally, the service tank capacity of the vessel is reduced to fit as much SOFCs as possible in the reference vessel. This reduction in service tank capacity may lead to a violation of the regulation dictating the capacity of these tanks. This tank capacity needs to be checked against this regulation, and if necessary the tank needs to be relocated in the vessel to comply with the regulation.

Besides the reduction in service tank capacity, some components already present in the reference vessel are moved to allow the placement of the SOFCs. When moving these components, the only criteria was that they stay in the same room. Only the sewage treatment plant and chilled water plant are relocated to a different room. The implication of this relocation is that piping and wiring needs to be redirected, and whether or not this is possible is not taken into account. Additonally, the moving of components withing the same room also leads to changes in piping and wiring. Whether the components can actually be placed in the new locations, needs to be checked in an additional iteration of the vessel design.

7

Conclusion

In this thesis, four combinations of fuel, heat engine and SOFC are analyzed, and the relative performance to the current power generation plant of the SIGMA combatants from Damen Naval is determined. The four combinations are:

- Diesel-fuelled SOFC-ICE combined cycle
- Diesel-fuelled SOFC-GT combined cycle
- MeOH-fuelled SOFC-ICE combined cycle
- MeOH-fuelled SOFC-GT combined cycle

The performance of these combined cycles is assessed based on:

- System efficiency
- Annual energy consumption
- Annual CO_2 emissions
- Exhaust temperature
- System weight and volume

The best combined cycle for implementation on the SIGMA depends on the performance parameter. First, in section 7.1, the best system based on system efficiency and energy consumption is selected. Next, the best system is selected based on CO_2 emissions in section 7.2, based on exhaust temperature in section 7.3 and based on system weight and volume in section 7.4. The overall best performing system is selected in section 7.5. Subsequently, the overall best system is drawn in the reference vessel, and the conclusions from this implementation step are stated in section 7.6. Lastly, section 7.7 gives a final conclusion for this thesis.

7.1. System efficiency and energy consumption

Compared to the current power plant of the reference vessel, installing a diesel-fuelled SOFC-ICE combined cycle with a power split of 35-75 can result in a reduction in annual energy consumption of 19.03%. For the other combined cycles, this reduction in annual energy consumption is slightly lower: 13.93% for the diesel-fuelled SOFC-GT (30-70 power split), 14.20% for the MeOH-fuelled SOFC-ICE (25-75 power split) and 11.25% for the MeOH-fuelled SOFC-GT (30-70 power split). To minimize annual energy consumption of the vessel, the diesel-fuelled SOFC-ICE combined cycle with a power split of 25-75 should be installed.

Overall, the best performing systems in terms of system efficiency and energy consumption are the SOFC-ICE combined cycles. From these systems, the diesel-fuelled system performs the best due to a higher electrical efficiency of the SOFC when running on diesel compared ot running on MeOH. The GT combined cycles perform worse than the ICE combined cycles due to the thermal efficiency of the GT. At full load, the GT has a slightly lower thermal efficiency than the ICE (38% compared to 42%). However, at part-load operation, the GT efficiency drops significantly (from 38% to values as low as 15%), whereas the ICE stays around 40% efficiency at part load. This results in a lower system efficiency for the GT combined cycles, and increases the annual energy

consumption of these systems compared to the ICE systems. Similar to the SOFC-ICE combined cycles, the diesel-fuelled SOFC-GT outperforms its MeOH counterpart due to the higher electrical efficiency of the SOFC.

When operating the diesel-fuelled SOFC-ICE combined cycle at a power split of 25-75, the system runs at an efficiency of 54.07% at silent speed, 62.40% at cruising speed and 46.78% at top speed. Compared to the current system of the SIGMA, this is an increase of 10.73 percentage points at silent speed, 20.99 percentage points at cruising speed and 3.98 percentage points at top speed. This means that with this combined cycle, a significant improvement in terms of system efficiency and reduction in annual energy consumption can be achieved.

7.2. CO_2 emissions

Compared to the current system, the combined cycles can reduce the annual CO_2 emissions of the vessel with 21.82% when installing a MeOH-fuelled SOFC-ICE combined cycle with a power split of 25-75. This reduction in annual CO_2 emissions is lower for the other combined cycles: 18.81% for the diesel-fuelled SOFC-ICE (25-75 power split), 13.35% for the diesel-fuelled SOFC-GT (30-70 power split) and 18.90% for the MeOH-fuelled SOFC-GT (30-70 power split). To minimize the annual CO_2 emissions of the vessel, the MeOH-fuelled SOFC-ICE combined cycle with a power split of 25-75 would be the best option.

The annual CO_2 emissions are closely related to the fuel consumption of the combined cycle. In the CT models, a complete conversion of the fuel into CO_2 and H_2 is assumed, meaning that a higher fuel consumption results in higher CO_2 emissions. In the previous section, it is concluded that the diesel-fuelled SOFC-ICE has the lowest annual energy consumption. Despite the direct relation between fuel consumption and CO_2 emissions, the diesel-fuelled system does not have the lowest CO_2 emissions. This is explained by the oxidizing reaction of the fuel: for 1 kJ of diesel 0.0203 gram of CO_2 is produced. For 1 kJ of MeOH this is slightly lower at 0.0178 gram (a reduction of about 12%). This means that despite having a higher energy consumption, the MeOH-fuelled SOFC-ICE can still emit less CO_2 annually. At a power split of 25-75, which is the optimum in terms of energy consumption and CO_2 emissions of the SOFC-ICE combined cycles, the diesel-fuelled system consumes about 4% less energy, but emits about 4% more CO_2 annually than the MeOH-fuelled system.

7.3. Exhaust temperature

The exhaust temperature is used as an indication for the IR-signature of the vessel. For each combined cycle, the exhaust temperature is determined for all three operating modes. At silent operation, the exhaust temperature is equal to the exhaust temperature of the SOFC. This temperature only depends on the fuel type fed into the SOFC, and the diesel-fuelled SOFC has a lower exhaust temperature than the MeOH-fuelled SOFC.

In terms of the best system regarding exhaust temperature, the silent operation is the most important operating mode. At this operating mode, detection is actively being avoided, and the IR-signature of the vessels is one of the giveaways of your presence in the area. For this reason, the diesel-fuelled combined cycles are the best system as they have the lowest exhaust temperature at this operating mode. To differentiate between the ICE and GT combined cycle, the exhaust temperature at cruising speed is considered. For SOFC power shares up to about 12%, the SOFC-ICE combined cycle has a lower exhaust temperature. At higher power splits, the SOFC-GT combined cycle is better. This is because the exhaust gas of the GT is used to preheat the SOFC inlet streams. At higher power splits, more heat is extracted from the GT exhaust gas resulting in a lower system exhaust temperature. In the SOFC-ICE combined cycles, the exhaust gas of the ICE leaves the system directly, which results in a higher exhaust temperature at the higher power splits.

At top speed, the exhaust temperature is mainly determined by the ratio of SOFC exhaust gas and heat engine exhaust gas. The SOFC exhaust gas has a lower temperature than the heat engine exhaust gas, and a higher SOFC power share results in a larger contribution of the SOFC exhaust gas to the exhaust temperature leaving the system. The ICE has a lower exhaust temperature than the GT, which means that for an equal SOFC power share, the SOFC-ICE combined cycles have a lower exhaust temperature than the GT combined cycles. Additionally, the MeOH-fuelled heat engines have a lower exhaust temperature than the diesel-fuelled counterparts. At lower power shares, this results in a lower exhaust temperature for the MeOH-fuelled combined cycles. However, the SOFC exhaust temperature is higher for the MeOH-fuelled systems. When the power split increases, the contribution of the SOFC exhaust gas compensates the lower exhaust temperature of the MeOH-fuelled heat engine, and the temperature of the exhaust gas leaving the system becomes higher for the MeOH-fuelled systems compared to the diesel-fuelled systems. For the SOFC-ICE, this transition occurs at a power split of about 18-82. For the SOFC-GT combined cycle the switch between diesel and MeOH being better occurs at about 28% SOFC power share.

7.4. System weight and volume

The total weight and volume of the different combined cycles is determined based on the weight and volume of the necessary components. These components are the ICE, GT, gensets, SOFC, e-motor, gearbox, HEX, blower and fuel storage. For the sizing, two options for each combined cycle are assessed; fully electric propulsion and hybrid propulsion. In fully electric propulsion, the ICE or GT are installed as genset, and together with the SOFC provide electric power for the propulsion. This electric power is delivered to the propeller with an e-motor and a reduction gearbox. In the hybrid propulsion, the heat engine is coupled to the gearbox with a shaft. This gearbox also receives power from an e-motor, which is powered by the SOFC. The total weight and volume of the system depends mostly on the fuel storage, SOFC and heat engine. For increasing power splits, the size and weight of the heat engine decreases, but the size and weight of the SOFC increases. The fuel storage depends on the energy consumption of the system, and generally decreases for increasing power splits.

Between the diesel- and MeOH-fuelled systems, the main difference lies in the fuel storage. For diesel, the energy density of the fuel is about twice the energy density of MeOH. This means that for an equal energy input, about twice as much MeOH storage weight is necessary. For the diesel-fuelled SOFC-ICE combined cycle with a hybrid propulsion plant, the fuel storage is 328 ton (60% of total weight) for a power split of 4.6-95.4, and this decreases to 254 ton (30% of total weight) for a power split of 30-70. For the MeOH-fuelled counterpart, the fuel storage is 675 ton (74% of total weight) for the 4.6-95.6 power split, and 612 ton (50% of total weight) for the 30-70 power split.

Compared to the current system, only the diesel-fuelled SOFC-ICE combined cycle with a power split of 4.6-95.4 and a hybrid propulsion layout has a slightly lower total weight (-1.78%) and volume (-1.43%). The weight and volume of this system increases compared to the current system (+6.52% for weight and +6.44% for volume), but this increase in component weight and volume is negated due to a lower fuel storage weight (-35.71%) and volume (-35.71%) for an equal range as the current system. At higher power splits, the increase in component weight and volume can no longer be compensated by the reduction in fuel storage, and the system has a higher total weight and volume than the current system.

Out of the different combined cycles, the best system in terms of total weight and volume, is the diesel-fuelled SOFC-ICE combined cycle with a hybrid propulsion layout. Depending on the power split, this system is between 1.78% lighter (4.6-95.4 power split) and 51.46% heavier (30-70 power split) than the current system. If the weight is the only concern, the 4.6-95.4 power split is the best option. However, at higher power splits, the combined cycle performs better in terms of energy consumption and CO_2 emissions. The best system is therefore a trade-off between system weight and annual energy consumption.

7.5. Overall

Depending on the selection criteria, different combined cycles perform the best. The diesel-fuelled SOFC-ICE performs best in terms of annual energy consumption, and system weight and volume. The MeOH-fuelled SOFC-ICE combined cycle performs best in terms of annual CO_2 emissions, and the diesel-fuelled SOFC-GT combined cycle performs best in terms of exhaust temperature. CO_2 emissions are important to reduce the carbon footprint of the maritime sector. However, for naval vessels, this criterion is the least important. If a choice needs to be made between emissions and operational performance of the vessel, the choice will always be operational performance. The exhaust temperature influences the IR-signature of the vessel. Currently, exhaust gasses of the heat engine are cooled before they leave the ship. If the combined cycles have a lower exhaust temperature than the current heat engine, less exhaust cooling is required. At silent operation, the exhaust temperature is especially important. At this operating mode, the vessel is actively trying to stay undetected, and the IR-signature is one of the ways enemy ships can detect your vessel. For this operating mode, the exhaust temperature only depends on the fuel type, as only the SOFC is running. Both fuel types offer a significant reduction in exhaust temperature at silent operation (-212 °C or - 58.4% for diesel and -157 °C or -42.9% for MeOH).

The total weight and volume of the system affect the draught (and therefore total resistance) of the vessel, as well as whether the system can fit in the vessel. These criteria are therefore important for the operational performance of the vessel. A high system volume may mean that the ship needs to increase in size. This in turn increases the total weight of the vessel. A higher vessel weight, as well as a larger vessel, result in a larger ship resistance. This in turn increases the power demand of the power plant and increases the fuel consumption of the vessel. For the combined cycles, the annual energy consumption (and therefore fuel consumption) decreases for an increasing power split. However, this increase in power split also results in an increase in system weight and volume. The energy consumption and system weight and volume are therefore used to select the best

system overall. Annual energy consumption and system weight and volume are plotted against each other, and a utopian solution is determined. This utopian solution consists of the lowest energy consumption (80.97% of current system), system weight (98.45% of current system) and volume (98.78% of current system). It is not possible to reach this utopian solution, but the system that comes closest is deemed the best system.

The best system based on system weight and energy consumption is the hybrid diesel-fuelled SOFC-ICE combined cycle with a power split of 8.4-91.6. Compared to the current system, this power split obtains an annual energy consumption of 93.45%, annual CO_2 emissions of 93.12%, exhaust temperature of 41.83% and 72.10% at silent and cruising speed respectively, and a total system weight of 105.39%. Based on system volume and energy consumption, the hybrid diesel-fuelled SOFC-ICE also lies closest to the utopian solution. However, the ideal power split is slightly lower at 6.1-93.9. Compared to the current system, this power split obtains an annual energy consumption of 93.98%, annual CO_2 emissions of 95.29%, exhaust temperature of 41.83% and 80.37% at silent and cruising speed respectively, and a total system weight of 100.13%. Both power splits show a decrease in annual energy consumption, CO_2 emissions and exhaust temperature at the cost of a slightly higher total system weight. The ideal power split based on weight (8.4-91.6) shows a higher reduction in energy consumption, CO_2 emissions and exhaust temperature, making it the preferred power split for the naval surface combatant. However, this system has a higher system weight and volume compared to the current system, which means that it might not fit in the current vessel design. If this is the case, the maximum power split that still fits in the vessel may be closer to the optimal power split based on volume (6.1-93.9).

7.6. Implementation

The best system overall (hybrid, diesel-fuelled SOFC-ICE) is drawn in the general arrangement plan of the reference vessel, to check whether the ideal power split based on weight (8.4-91.6) actually fits in the reference vessel. For this implementation, the currently present diesel generator sets are removed from the engine room and replaced with SOFCs. Additionally, some components already present in the vessel are relocated to free space for additional SOFCs.

In the available space in the reference vessel, a maximum net power split of 7.8-92.2 can be placed in the vessel. This is slightly lower than the optimal power split based on weight (8.4-91.6) and slightly higher than the optimal power split based on volume (6.1-93.9). Compared to the current system, a power split of 7.8-91.2 results in an annual energy consumption of 93.98%, annual CO_2 emissions of 93.70%, exhaust temperature of 41.83% and 74.32% at silent and cruising speed respectively, and a total system weight of 104.23%. With this increase in weight, the draught of the vessel increases with 20 mm. The maximum power split that still fits in the reference vessel shows an improvement in terms of annual energy consumption, CO_2 emissions and exhaust temperature, at the cost of a slight increase in system weight and vessel draught.

Compared to the maximum possible reduction in energy consumption and CO_2 emissions (-18.2%), the combined cycle that still fits in the current system does not reach its full potential. However, it is still possible to reduce the energy consumption and CO_2 emissions by about 6% compared to the current system, making it a viable solution for naval surface combatants. The maximum fitting power split also gives a significant reduction in exhaust gas temperature (-58% at silent speed and -25% at cruising speed) compared to the current system, which shows the potential for the reduction in IR-signature of the vessel.

7.7. Final conclusion

SOFC combined cycles are an interesting option to reduce the fuel consumption and GHG emissions of the marine sector. However, implementing these combined cycles alone is not enough to reach the IMO goals of net-zero emissions in 2050. Additionally, when fitting a combined cycle in the current design of a reference vessel (in this thesis the SIGMA), the reduction in fuel consumption and CO_2 emissions is relatively small (only about 6%). For naval surface combatants, fuel cell combined cycles do not pose a significant improvement in terms of annual energy consumption and CO_2 emissions. The main benefit of implementing the combined cycles in naval surface combatants lies in the reduction of exhaust gas temperature compared to the current system. With a system that can currently fit in the design of the SIGMA, a significant reduction in exhaust temperature is possible (58% for silent operation and 25% for cruising speed), reducing the risk of detection during the mission of the vessel.

8

Recommendations

In this thesis, the best combined cycle for naval surface combatants is chosen based on annual energy consumption, annual CO_2 emissions, exhaust gas temperature, system weight and system volume. This thesis shows that the diesel-fuelled SOFC-ICE combined cycle shows promising results regarding a reduction of annual energy consumption, CO_2 emissions and exhaust temperature at the cost of an increased system weight and volume. This thesis also shows that it is possible to fit the diesel-fuelled SOFC-ICE combined cycle in the general arrangement plan of a naval surface combatant, albeit with a slightly lower SOFC power share than the optimal solution. In future research, steps need to be taken to give a more realistic result in terms of GHG emissions, IR-signature, which will contribute to the actual implementation of combined cycles in future vessels.

- **Dynamic response of the system:** In this thesis, the system is operated at steady state. However, on an actual ship, the system experiences dynamic load changes. These dynamic load changes are a result of e.g. manoeuvring, acceleration, deceleration, switching equipment on and off, etc. If the combined cycles are to be implemented in future ships, the dynamic response of the system should be evaluated.
- **Operational profile:** In this thesis, a simplified operational profile with only three ship speeds is considered. However, the actual vessel operates at a larger range of ship speeds. Each ship speed has its own power demand and energy consumption contributing to the total annual energy consumption. In future work, a complete operational profile should be considered to give a more accurate depiction of the annual energy consumption of the vessel.
- **Exhaust gas composition:** This thesis assumes that the exhaust gas is a mixture of N_2, O_2, Ar, CO_2 and H_2O. In reality different components, such as CO, UHC, NO_x and SO_x, can be present in the exhaust gas. To determine the GHG emissions of the combined cycles, a more detailed model is needed for the exhaust gas composition. In future work, the GHG emissions of the combined cycles should be evaluated based on a detailed model of the exhaust gas including components such as CO, UHC, NO_x and SO_x, or by experimentally measuring the emissions. While the GHG emissions are not particularly important for naval vessels, they are important for commercial shipping. A detailed analysis of the GHG emissions may therefore contribute to the usage of combined cycles in commercial shipping, and therefore reducing the harmful emissions of the maritime sector.
- **Reformer size:** In this thesis, the size of the reformer is assumed to be equal to the fuel processing unit of the Bloom Energy Server. The actual size of the diesel or MeOH reformer depends on, among others, fuel flow, reaction rate, number of reforming steps, type of catalyst, etc. These parameters may result in a different size reformer than assumed in this thesis, and future work should focus on the actual design and sizing of the reformer for combined cycle power plants. The size of the reformer is an important aspect in the feasibility of onboard fuel reforming for fuel cells. If the reformer needs to be twice the size of the fuel cell, it may not be feasible to implement a combined cycle with onboard fuel reforming. However, if the reformer can be smaller than assumed in this thesis, this may result in the ability to place extra fuel cells, increasing the power split and reducing the annual energy consumption.
- **HEX sizing:** The size of the HEXs are based on average power density (4634.7 kW/m^3) and specific power (2.56 kW/kg). However, these values are based on a large range consisting of different types of HEX. This average value is used due to a lack of publicly available information regarding the size and weight of HEXs.

In a future design iteration, the size of the HEXs, as well as the piping and wiring needed to integrate the HEXs in the combined cycle should be considered in cooperation with HEX manufacturers.

- **Design iteration:** To check whether the placement of the different components in chapter 6 is feasible in terms of vessel operation, a more detailed design needs to be made. This detailed design should include the piping and wiring to the different components to ensure that the placement of all of the components is sensible. Adittionally, the weight distribution along the vessel should be considered in a future design iteration. This thesis only states the total weight of the system, and the impact on the draught of the vessel. However, including heavy fuel cells in the design may influence the weight distribution and center of gravity of the vessel. This may influence the transverse stability and trim angle of the vessel.
- **SOFC:** The implementation of the combined cycles in naval surface combatants is limited by the weight and volume of the SOFC. In the reference vessel, the volume of the SOFC limits the power split to only 7.8-91.2, where the system only reduces the annual energy consumption with about 6%. This reduction in energy consumption can reach about 20% if power splits of 25-75 could be placed in the reference vessel. Future research should focus on reducing the size and weight of SOFCs, to make it possible for a power split of 25-75 (and an energy reduction of 20%) to be placed onboard of naval surface combatants.
- **IR-signature:** The IR-signature is only based on exhaust temperature in this thesis. However, the IR-signature consists of other factors as well. Heat from the components is also radiated to the steel hull surrounding these components. The effect of this heat radiation is neglected in this thesis, and should be included in future work evaluating the IR-signature of combined cycles.
- **Acoustic emissions:** In this thesis, the acoustic emissions of the combined cycle are not taken into account. For silent operation, it is assumed that the SOFC produces less acoustic emissions than a conventional heat engine based on the results of Ezgi et al. [7]. However, the acoustic emissions for cruising speed and top speed are not taken into account in this thesis. In future work, the acoustic emissions for these operating modes should be considered to determine the acoustic emissions of the combined cycle with respect to the current power plant.

Bibliography

[1] Damen Naval. *The Sigma Series*. 2024. URL: https://www.damen.com/vessels/defence-and-security/sigma-frigates#deepdive (visited on 10/09/2024).

[2] IMO. *IMO's work to cut GHG emissions from ships*. URL: https://www.imo.org/en/MediaCentre/HotTopics/Pages/Cutting-GHG-emissions.aspx# (visited on 14/05/2025).

[3] UNCTAD. *Review of maritime transport*. 2024. URL: https://unctad.org/system/files/official-document/rmt2024_en.pdf.

[4] IEA. *International Shipping*. 2023. URL: https://www.iea.org/energy-system/transport/international-shipping (visited on 07/10/2024).

[5] L. van Biert, M. Godjevac, K. Visser and P. Aravind. "A review of fuel cell systems for maritime applications". In: *Journal of Power Sources* 327 (2016), pp. 345–364.

[6] F. Baldi, S. Moret, K. Tammi and F. Maréchal. "The role of solid oxide fuel cells in future ship energy systems". In: *Energy* 194 (2020). 116811.

[7] C. Ezgi, M. T. Çoban and □. Selvi. "Design and Thermodynamic Analysis of an SOFC System for Naval Surface Ship Application". In: *Journal of Fuel Cell Science and Technology* 10 (2013). 031006-1.

[8] P. van Maurik. *An introduction to naval warfare*. 3rd ed. VMA Publishing, 2022. ISBN: 978-90-8250-685-3.

[9] L. K. C. Tse, S. Wilkins, N. McGlashan, B. Urban and R. Martinez-Botas. "Solid oxide fuel cell/gas turbine trigeneration system for marine applications". In: *Journal of Power Sources* 196 (2011), pp. 3149–3162.

[10] H. Sapra, J. Stam, J. Reurings, L. van Biert, W. van Sluijs, P. de Vos, K. Visser, A. P. Vellayani and H. Hopman. "Integration of solid oxide fuel cells and internal combustion engine for maritime applications". In: *Applied Energy* 281 (2021). 115854.

[11] A. F. Massardo and F. Lubelli. "Internal Reforming Solid Oxide Fuel Cell-Gas Turbine Combined Cycles (IRSOFC-GT): Part A - Cell Model and Cycle Thermodynamic Analysis". In: *Journal of Engineering for Gas Turbines and Power* 122 (2000).

[12] F. D. F. Chuahy and S. L. Kokjohn. "Solid oxide fuel cell and advanced combustion engine combined cycle: A pathway to 70% electrical efficiency". In: *Applied Energy* 235 (2019), pp. 391–408.

[13] H. Sapra, J. Stam, L. van Biert, P. de Vos, K. Visser and G.-J. Meijn. "Potential of COmbined drive of Fuel cell And Internal Combustion Engine (COFAICE) for naval ships". In: *International Naval Engineering Conference*. 2020.

[14] B. Babaji and J. W. G. Turner. "Thermodynamic Analysis of a Solid-Oxide Fuel Cell Gas Turbine (SOFC-GT) Hybrid System for Marine Applications". In: *ASME Turbo Expo 2024: Turbomachinery Technical conference and Exposition*. 2024.

[15] C. Li, J. Wang, H. Liu, F. Guo, X. Xiu, C. Wang, J. Qin and L. Wei. "Thermodynamic performance analysis of direct methanol solid oxide fuel cell hybrid power system for ship application". In: *Renewable Energy* 230 (2024). 120809.

[16] Wärtsilä. *Improving ship efficiency*. 2025. URL: https://c2e2.unepccc.org/kms_object/improving-ship-efficiency/ (visited on 24/04/2025).

[17] M. T. Coban and C. Ezgi. "Design and Analysis of Diesel Fueled Solid Oxide Fuel Cell System Onboard Surface Ship". In: *Journal of Naval Science and Engineering* 6(1) (2010), pp. 59–78.

[18] J. Thompson, D. Vaitekunas and A. M. Birk. "IR Signature Suppression of Modern Naval Ships". In: *ASNE 21st Century Combatant Technology Symposium*. 1998.

[19] L. van Biert, T. Woudstra, M. Godjevac, K. Visser and P. V. Aravind. "A thermodynamic comparison of solid oxide fuel cell-combined cycles". In: *Journal of Power Sources* 397 (2018), pp. 382–396.

[20] S. H. Chan, H. K. Ho and Y. Tian. "Multi-level modeling of SOFC-gas turbine hybrid system". In: *International Journal of Hydrogen Energy* 28(8) (2003), pp. 889–900.

[21] S. K. Park and T. S. Kim. “Comparison between pressurized design and ambient pressure design of hybrid solid oxide fuel cell-gas turbine systems”. In: *Journal of Power Sources* 163(1) (2006), pp. 490–499.

[22] P. Aravind, T. Woudstra, N. Woudstra and H. Spliethoff. “Thermodynamic evaluation of small-scale systems with biomass gasifiers, solid oxide fuel cells with Ni/GDC anodes and gas turbines”. In: *Journal of Power Sources* 190.2 (2009), pp. 461–475. URL: https://www.sciencedirect.com/science/article/pii/S0378775309000561.

[23] Y. Zhao, J. Sadhukhan, A. Lanzini, N. Brandon and N. Shah. “Optimal integration strategies for a syngas fuelled SOFC and gas turbine hybrid”. In: *Journal of Power Sources* 196.22 (2011), pp. 9516–9527. ISSN: 0378-7753.

[24] J. Larminie and A. Dicks. *Fuel Cell Systems Explained*. 2nd ed. John Wiley & Sons Ltd, 2003.

[25] M. Gandiglio, A. Lanzini, P. Leone, M. Santarelli and R. Borchiellini. “Thermoeconomic analysis of large solid oxid fuel cell plants: Atmospheric vs. pressurized performance”. In: *Energy* 55 (2013), pp. 142–155.

[26] T. Gechev and P. Punov. “Combined cycles of SOFC/ICE and SOFC/GT –A brief review”. In: *AIP Conference Proceedings* 2557.1 (2022). 060002.

[27] H. Chehrmonavari, A. Kakaee, S. E. Hosseini, U. Desideri, G. Tsatsaronis, G. FLoerchinger, R. Braun and A. Paykani. “Hybridizing solid oxide fuel cells with internal combustion engines for power and propulsion: A review”. In: *Renewable and Sustainable Energy Reviews* 171 (2023). 112982.

[28] Y. Feng, J. Qu, Y. Zhu, B. Wu, Y. Wu, Z. Xiao and J. Liu. “Progress and prospect of the novel integrated SOFC-ICE hybrid power system: System design, mass and heat integration, system optimization and techno-economic analysis”. In: *Energy Conversion and Management: X* 18 (2023), p. 100350.

[29] S. H. Park, Y. D. Lee and K. Y. Ahn. “Performance analysis of an SOFC/HCCI engine hybrid system: System simulation and thermo-economic comparison”. In: *International Journal of Hydrogen Energy* 39 (2014), pp. 1799–1810.

[30] J. E. Freeh, J. W. Pratt and J. Brouwer. “Development of a Solid-Oxide Fuel Cell/Gas Turbine Hybrid System Model for Aerospace Applications”. In: *Proceedings of the ASME Turbo Expo 2004: Power for Land, Sea and Air*. Vol. Volume 7: Turbo Expo 2004. 2004, pp. 371–379.

[31] Q. Hou, H. Zhao and X. Yang. “Thermodynamic performance study of the integrated MR-SOFC-CCHP system”. In: *Energy* 150 (2018), pp. 434–450.

[32] S. Harvey and H. J. Richter. “Gas Turbine Cycles With Solid Oxide Fuel Cells—Part I: Improved Gas Turbine Power Plant Efficiency by Use of Recycled Exhaust Gases and Fuel Cell Technology”. In: *Journal of Energy Resources Technology-transactions of The Asme* 116 (1994), pp. 305–311. URL: https://api.semanticscholar.org/CorpusID:109076694.

[33] T.-H. Lim, R.-H. Song, D.-R. Shin, J.-I. Yang, H. Jung, I. C. Vinke and S.-S. Yang. “Operating characteristics of a 5 kW class anode-supported planar SOFC stack for a fuel cell/gas turbine hybrid system”. In: *International Journal of Hydrogen Energy* 33 (2008), pp. 1076–7083.

[34] P. A. Duong, B. R. Ryu, N. T. H. Hau, J. Jung, J. K. Lee and H. Kang. “A novel designation of LNG solid oxide fuel cells combined system for marine application”. In: *Case Studies in Thermal Engineering* 58 (2024). 104433.

[35] B. R. Ryu, P. A. Duong and H. Kang. “Comparative analysis of the thermodynamic performances of solid oxide fuel cell-gas turbine interated systems for marine vessels using ammonia and hydrogen as fuels”. In: *International Journal of Naval Architecture and Ocean Engineering* 15 (2023). 100524.

[36] Global. *SAFETY DATA SHEET Diesel Fuel*. 2019.

[37] P. S. van Lieshout, V. de Jonge, R. Verbeek, A. W. Vredeveldt and S. Finner. *Green Maritime Methanol: WP3 factsheet and comparison with diesel and LNG*. Tech. rep. TNO, 2020.

[38] Fraunhofer ICT-IMM. *Diesel-powered fuel cell generates green electricity*. July 2015. URL: https://www.imm.fraunhofer.de/en/press-publications/diesel-powered-fuel-cell.html (visited on 11/11/2024).

[39] M. A. Elliot, R. F. Davies and R. A. Friedel. “Products of Combustion from Diesel Fuel”. In: *3rd World Petroleum Congress*. 1951.

[40] R. Laursen, D. Barcarolo, H. Patel, M. Dowling, M. Penfold, J. Faber, J. Király, R. van der Veen, E. Pang and A. van Grinsven. *Potential of Ammonia as fuel in shipping - updated*. Tech. rep. European Maritime Safety Agency, 2023.

[41] M. Hürpekli and A. N. Özsezen. “Determination of combustion and emission characteristics of liquid Fischer-Tropsch diesel fuel synthesized from coal in a diesel engine”. In: *Energy Conversion and Management* 292 (2023). 117351.

[42] Bredenoord. *Quieter, cleaner and sustainable: the opporunities of HVO Diesel*. 2019. URL: https://www.bredenoord.com/en/knowledge/hvo-diesel/ (visited on 27/09/2024).

[43] H. Aatola, M. Larmi and T. Sarjovaara. “Hydrotreated Vegetable Oil (HVO) as a Renewable Diesel Fuel: Trade-off between NOx, Particulate Emission, and Fuel Consumption of a Heavy Duty Engine”. In: *SAE International Journal of Engines* 1(1) (2008).

[44] Watson Fuels. *SAFETY DATA SHEET HVO (Hydrotreated Vegetable OIL)/Renewable Diesel*. 2022.

[45] R. Yadav. *Comparative Study of Marine Biofuels: MGO, HVO, and FAME*. 2024. URL: https://spectrafuels.com/comparative-study-of-marine-biofuels-mgo-hvo-and-fame/ (visited on 11/11/2024).

[46] Nanni Energy. *HVO –The innovative 100% biofuel for the marine sector*. 2023. URL: https://nannienergy.com/hvo-the-innovative-100-biofuel-for-the-marine-sector/ (visited on 11/11/2024).

[47] K. O. P. Bjørgen, D. R. Emberson and T. Løvås. “Combustion and soot characteristics of hydrotreated vegetable oil compression-ignited spray flames”. In: *Fuel* 266 (2020). 116942.

[48] Sigma-Aldrich. *SAFETY DATA SHEET Methanol*. 2024.

[49] G. A. Olah. “Beyond Oil and Gas: The Methanol Economy”. In: *Angewandte Chemie International Edition* 44(18) (2005), pp. 2636–2639.

[50] IMO. *INTERIM GUIDELINES FOR THE SAFETY OF SHIPS USING METHYL/ETHYL ALCOHOL AS FUEL*. 2020. URL: https://www.register-iri.com/wp-content/uploads/MSC.1-Circ.1621.pdf.

[51] N. de Vries. “Ammonia as a Marine Fuel: Safety”. In: *Ammonia Energy Conference*. [Presentation Slides]. 2019. URL: https://www.ammoniaenergy.org/wp-content/uploads/2019/08/20191113.1038-C-Job-Naval-Architects-AEC.pdf.

[52] S. Laselle, H. Hustad, J. Vedeler and H. Abusdal. *Methanol as marine fuel: Environmental benefits, Environmental advisory technology readiness, and economic feasibility*. Tech. rep. DNV-GL, 2016.

[53] PGW. *Safety Data Sheet: Liquified Natural Gas (LNG)*. 2015.

[54] DNV. *LNG as marine fuel*. URL: https://www.dnv.com/maritime/insights/topics/lng-as-marine-fuel/how-to-benefit-from-dnv/ (visited on 25/11/2024).

[55] DNV. *LNG as marine fuel*. URL: https://www.dnv.com/maritime/insights/topics/lng-as-marine-fuel/market-update/ (visited on 25/11/2024).

[56] METGroup. *LNG (liquefied natural gas): definition, storage, transportation and usage*. Aug. 2020. URL: https://group.met.com/en/media/energy-insight/lng-liquefied-natural-gas (visited on 25/11/2024).

[57] The Engineering Toolbox. *Fossil vs. Alternative Fuels - Energy Content*. 2008. URL: https://www.engineeringtoolbox.com/fossil-fuels-energy-content-d_1298.html (visited on 08/11/2024).

[58] C. Bass. *How to be smarter about methane slip –right now*. Oct. 2023. URL: https://www.wartsila.com/insights/article/mind-the-methane-gap (visited on 25/11/2024).

[59] DNV. *Maritime Forecast to 2050: Energy Transition Outlook 2024*. 2024.

[60] B. N. van Veldhuizen, L. van Biert, K. Visser and J. J. Hopman. “Comparative analysis of alternative fuels for marine SOFC systems”. In: *PRADS 2022 Proceedings: 15th International Symposium on Practical Design of Ships and Other Floating Structures*. 2022, pp. 1240–1258.

[61] C. McKinlay, S. R. Turnock and D. A. Hudson. “A Comparison of hydrogen and ammonia for future long distance shipping fuels”. In: *LNG/LPG and Alternative Fuel Ships*. 2020.

[62] Airgas. *SAFETY DATA SHEET Hydrogen*. 2020.

[63] B. Veritas. *An overview of hydrogen as fuel for ships*. 2024. URL: https://marine-offshore.bureauveritas.com/shipping-decarbonization/future-fuels/hydrogen (visited on 25/11/2024).

[64] Y. Demirel. “5.2 Energy Conservation”. In: *Comprehensive Energy Systems*. Ed. by I. Dincer. Oxford: Elsevier, 2018, pp. 45–90. ISBN: 978-0-12-814925-6.

[65] Thunder Said Energy. *DC-DC power converters: efficiency calculations?* URL: https://thundersaidenergy.com/downloads/dc-dc-power-converters-efficiency-calculations/ (visited on 27/11/2024).

[66] Electronic Products. *AC/DC power supplies improve efficiency, cut component count*. Jan. 2020. URL: https://www.electronicproducts.com/ac-dc-power-supplies-improve-efficiency-cut-component-count/?_gl=1%2A1r1fa52%2A_gcl_au%2AODc3ODEwNTUxLjE3MzI3MDQ3OTk.%2A_ga%2ANDk3MDI2MDUuMTczMjcwNDgwMA..%2A_ga_ZLV02RYCZ8%2AMTczMjcwNDc5OS4xLjAuMTczMjcwNDc5OS42MC4wLjA. (visited on 27/11/2024).

[67] Anker. *Understanding the Basics: How a DC to AC Converter Works*. Oct. 2024. URL: https://www.anker.com/blogs/ac-power/understanding-the-basics-how-a-dc-to-ac-converter-works (visited on 27/11/2024).

[68] Wärtsilä. *Wärtsilä generating sets - Tailored to optimize performance*. URL: https://www.wartsila.com/marine/products/engines-and-generating-sets/generating-sets/wartsila-gensets (visited on 27/11/2024).

[69] H. Klein Woud and D. Stapersma. *Design of Propulsion and Electric Power Generation Systems*. IMarEST, 2002.

[70] Asimptote b.v. *Cycle-Tempo Details*. URL: https://asimptote.com/cycle-tempo/cycle-tempo-details/ (visited on 20/11/2024).

[71] B. N. van Veldhuizen, L. van Biert, A. Amladi, T. Woudstra, K. Visser and P. V. Aravind. “The effects of fuel type and cathode off-gas recirculation on combined heat and power generation of marine SOFC systems”. In: *Energy Conversion and Management* 276 (2023). 116498.

[72] R. Geertsma, J. Vollbrandt, R. Negenborn, K. Visser and H. Hopman. “A quantitative comparison of hybrid diesel-electric and gas-turbine-electric propulsion for future frigates”. In: *2017 IEEE Electric Ship Technologies Symposium (ESTS)*. 2017, pp. 451–458.

[73] F. Haglind and B. Elmegaard. “Methodologies for predicting the part-load performance of aero-derivative gas turbines”. In: *Energy* 34.10 (2009), pp. 1484–1492.

[74] SolydEra. *SolydEra Fuel Cell Module (FCM)*. 2023. URL: https://www.solydera.com/media/a2xbob01/solydera_flyer_fcm_sept-2023_web.pdf.

[75] J. B. Heywood. *Internal Combustion Engine Fundamentals*. McGraw-Hill, Inc., 1988. ISBN: 0-07-028637-X.

[76] D. Stapersma. *Diesel Engines Volume 1 Performance Analysis*. [Lecture notes WB4408A]. Jan. 2010.

[77] M. Cho, Y. Kim and H. H. Song. “Solid oxide fuel cell-internal combustion engine hybrid system utilizing an internal combustion engine for anode off-gas recirculation, external reforming, and additional power generation”. In: *Applied Energy* 328 (2022). 120146.

[78] A. G. Elkafas, S. Barberis and M. Rivarolo. “Thermodynamic analysis for SOFC/ICE integration in hybrid systems for maritime application”. In: *E3S Web of Conferences* 414 (2023). 02002.

[79] M. Gallarotti. *Using Dymola for the modelling of fluid machinery: the example of a turbocharger*. 2017. URL: https://www.claytex.com/blog/methods/using-dymola-for-the-modelling-of-fluid-machinery-the-example-of-a-turbocharger/ (visited on 15/05/2025).

[80] “Chapter 5.3.3 - Application of Hydrogen by Use of Chemical Reactions of Hydrogen and Carbon Dioxide”. In: *Science and Engineering of Hydrogen-Based Energy Technologies*. Ed. by P. E. V. de Miranda. Academic Press, 2019, pp. 279–289. ISBN: 978-0-12-814251-6. DOI: https://doi.org/10.1016/B978-0-12-814251-6.00013-7. URL: https://www.sciencedirect.com/science/article/pii/B9780128142516000137.

[81] Y. Hu, C. Han, W. Li, Q. Hu, H. Wu and Z. Luo. “Experimental evaluation of methanol steam reforming reactor heated by catalyst combustion for kW-class SOFC”. In: *International Journal of Hydrogen Energy* 48.12 (2023), pp. 4649–4664. URL: https://www.sciencedirect.com/science/article/pii/S0360319922051576.

[82] T. Tronstad, H. H. Åstrand, G. P. Haugom and L. Langfeldt. *Study on the use of fuel cells in shipping*. Tech. rep. DNV GL, 2017.

[83] SolydEra. *SolydEra G8 Stack*. 2023. URL: https://www.solydera.com/media/xmzfgthh/solydera_flyer_g8-stack_sept-2023_web.pdf.

[84] J. Geng, Q. Guo, J. Pan, B. Chi and J. Pu. "Enhanced stability of co-reforming diesel and methanol into hydrogen-enriched gases for solid oxide fuel cell application". In: *Journal of Power Sources* 564 (2023), p. 232830. URL: https://www.sciencedirect.com/science/article/pii/S0378775323002057.

[85] R. D. Parmar, A. Kundu and K. Karan. "Thermodynamic analysis of diesel reforming process: Mapping of carbon formation boundary and representative independent reactions". In: *Journal of Power Sources* 194.2 (2009), pp. 1007–1020. URL: https://www.sciencedirect.com/science/article/pii/S0378775309010428.

[86] Alfa Laval. *The theory behind heat transfer*. 2004. URL: https://www.alfalaval.com/globalassets/documents/microsites/heating-and-cooling-hub/alfa_laval_heating_and_cooling_hub_the_theory_behind_heat_transfer.pdf (visited on 05/12/2024).

[87] H. Valera and A. K. Agarwal. "Methanol as an Alternative Fuel for Diesel Engines". In: *Methanol and the Alternate Fuel Economy*. Ed. by A. K. Agarwal, A. Gautam, N. Sharma and A. P. Singh. Singapore: Springer Singapore, 2019, pp. 9–33.

[88] Wärtsilä. *Wärtsilä 32 methanol engine*. URL: https://www.wartsila.com/marine/products/engines-and-generating-sets/wartsila-32-methanol-engine (visited on 26/02/2025).

[89] MAN Energy Solutions. *Methanol-ready four-stroke engines*. URL: https://www.man-es.com/marine/products/four-stroke-engines/methanol-ready-engines (visited on 26/02/2025).

[90] Nordhavn Power Solutions. *Methanol*. 2025. URL: https://nordhavn.dk/en/methanol/ (visited on 21/02/2025).

[91] N. P. Solutions. *Methanol Power Marine commercial 13L - 240 kW (325 HP)*. 2025. URL: https://nordhavn.dk/metanol-13l-240-kw-325-hp/.

[92] Scania. *13-Litre Engine*. 2025. URL: https://www.scania.com/content/dam/www/market/master/products/power-solutions/engine-pdfs/marine/marine-propulsion/DI13-080M_249kW.pdf.

[93] R. S. Tol. "Combustion of methanol/diesel blends in a compression ignited engine". MA thesis. Delft University of Technology, 2020.

[94] T. F. Yusaf, I. Hamawand, P. Baker and G. Najafi. "The effect of methanol-diesel blended ratio on CI engine performance". In: *International Journal of Automotive and Mechanical Engineering (IJAME)* 8 (2013), pp. 1385–1395.

[95] Q. H. Hassan, G. Shaker Abdul Ridha, K. A. H. Hafedh and H. A. Alalwan. "The impact of Methanol-Diesel compound on the performance of a Four-Stroke CI engine". In: *Materials Today: Proceedings* 42 (2021). 3rd International Conference on Materials Engineering & Science, pp. 1993–1999. ISSN: 2214-7853.

[96] P. Karvounis, G. Theotokatos, C. Patil, L. Xiang and Y. Ding. "Parametric investigation of diesel–methanol dual fuel marine engines with port and direct injection". In: *Fuel* 381 (2025), p. 133441. ISSN: 0016-2361.

[97] Siemens. *Methanol: a green fuel for gas turbines*. 2023. URL: https://www.netzerotc.com/wp-content/uploads/2023/09/1130-REP-047-R1-SGT-A20-Bio-methanol-demonstration-test-summary-report.pdf.

[98] Y. Hu, C. Han, W. Li, Q. Hu, H. Wu and Z. Luo. "Experimental evaluation of methanol steam reforming reactor heated by catalyst combustion for kW-class SOFC". In: *International Journal of Hydrogen Energy* 48.12 (2023), pp. 4649–4664. URL: https://www.sciencedirect.com/science/article/pii/S0360319922051576.

[99] Y. Wang, R. Zhan, Y. Qin, G. Zhang, Q. Du and K. Jiao. "Three-dimensional modeling of pressure effect on operating characteristics and performance of solid oxide fuel cell". In: *International Journal of Hydrogen Energy* 43.43 (2018), pp. 20059–20076.

[100] H. Liu, J. Qin, X. Xiu, C. Ha and P. Dong. "Comparative study of fuel types on solid oxide fuel cell –gas turbine hybrid system for electric propulsion aircraft". In: *Fuel* 347 (2023), p. 128426. ISSN: 0016-2361.

[101] MAN Energy Solutions. *Strong and smart: Four-stroke propulsion engines*. 2025. URL: https://www.man-es.com/marine/products/four-stroke-engines/propulsion (visited on 04/03/2025).

[102] Wärtsilä. *Diesel Engines*. 2025. URL: https://www.wartsila.com/marine/products/engines-and-generating-sets/diesel-engines (visited on 04/03/2025).

[103] Rolls-Royce. *Marine Gas Turbines*. 2025. URL: https://www.rolls-royce.com/products-and-services/defence/naval/gas-turbines.aspx (visited on 04/03/2025).

[104] GE Aerospace. *Marine Engiens & Systems*. 2025. URL: https://www.geaerospace.com/military-defense/marine (visited on 04/03/2025).

[105] Bloomenergy. *The Bloom Energy Server*. 2024. URL: https://www.bloomenergy.com/wp-content/uploads/bloom-energy-server-brochure-2024.pdf (visited on 23/04/2025).

[106] Convion. *Convion C60 fuel cell co-generation system*. 2023. URL: https://convion.fi/wp/wp-content/uploads/2023/09/Convion_C60_brochure_2023.pdf (visited on 14/05/2025).

[107] Elcogen. *elcoStack®*. 2024. URL: https://elcogen.com/wp-content/uploads/2024/09/elcoStack_product_sheet_09_2024.pdf (visited on 14/05/2025).

[108] Innomotics. *Easy Selection HV motors*. 2025. URL: https://hv-easy.innomotics.com/ (visited on 28/04/2025).

[109] SIEMENS. *Product Configurator*. 2025. URL: https://mall.industry.siemens.com/spice/cloudcm/configurator (visited on 23/04/2025).

[110] H. Moon, D. J. McGregor, N. Miljkovic and W. P. King. "Ultra-power-dense heat exchanger development through genetic algorithm design and additive manufacturing". In: *Joule* 5.11 (2021), pp. 3045–3056.

[111] H. Klein Woud and D. Stapersma. *Selected chapters of Design of Auxiliary Systems, Shafting and Flexible Mounting*. 2016.

[112] Wärsilä. *Wärtsilä Single Input Gear*. 2025. URL: https://www.wartsila.com/marine/products/propulsors-and-gears/gears/wartsila-single-input-gear (visited on 23/04/2025).

[113] Wärsilä. *Wärtsilä Double Input Gear*. 2025. URL: https://www.wartsila.com/marine/products/propulsors-and-gears/gears/wartsila-double-gear (visited on 23/04/2025).

[114] HRblowers. *Positive displacement air blowers: HR41,42,43*. URL: https://hrblowers.co.uk/wp-content/uploads/2019/06/HR41-HR42-HR43.pdf (visited on 23/04/2025).

[115] IMO. *SOLAS Regulation II-1/26.11, Machinery Installations - Service Tank Arrangements*. URL: https://www.imorules.com/GUID-AAD7D0CF-98B7-4386-9E80-F0FFD7F879F9.html (visited on 23/04/2025).

[116] K. Lobachyov and H. Richter. "COmbined Cycle Gas Turbine Power Plant With Coal Gasification and Solid Oxide Fuel Cell". In: *Journal of Energy Resources Tecnology-transactions of the ASME* (1996).

[117] S. Campanari. "Full Load and Part-Load Performance Prediction for Interated SOFC and Microturbine Systems". In: *Journal of engineering for Gas Turbines and Power* 122(2) (2000), pp. 239–246.

[118] J. Palsson, A. Selimovic and L. Sjunnesson. "Combined solid oxide fuel cell and gas turbine systems for efficient power and heat generation". In: *Journal of Power Sources* 86(1-2) (2000), pp. 442–448.

[119] P. Costamagna, L. Magistri and A. F. Massardo. "Design and part-load performance of a hybrid system based on a solid oxide fuel cell reactor and a micro gas turbine". In: *Journal of Power Sources* 96(2) (2001), pp. 352–368.

[120] S. Kimijima and N. Kasagi. "Performance Evaluation of Gas Turbine-Fuel Cell Hybrid Micro Generation System". In: *Proceedings of ASME Turbo Expo 2002*. 2002.

[121] Y. Inui, S. Yanagisawa and T. Ishida. "Proposal of high performance SOFC combined power generation system with carbon dioxide recovery". In: *Energy Conversion and Management* 44(4) (2003), pp. 597–609.

[122] F. Calise, M. Dentice d'Accadia, A. Palombo and L. Vanoli. "Simulation and exery analysis of a hybrid Solid Oxide Fuel Cell (SOFC)-Gas Turbine System". In: *Energy* 31 (2006), pp. 3278–3299.

[123] R. Roberts, J. Brouwer, F. Jabbari, T. Junker and H. Ghezel-Ayagh. "Control design of an atmospheric solid oxide fuel cell/gas turbine hybrid system: Variable versus fixed speed gas turbine operation". In: *Journal of Power Sources* 161(1) (2006), pp. 484–491.

[124] C. Stiller. "Design, Operation and Control Modelling of SOFC/GT Hybrid Systems". PhD thesis. Norwegian University of Science and Technology, 2006.

[125] Y. M. A. Welaya, M. Mosleh and N. R. Ammar. "Thermodynamic analysis of a combined gas turbine power plant with a solid oxide fuel cell for marine applications". In: *International Journal of Naval Architecture and Ocean Engineering* 5 (2013), pp. 529–545.

[126] F. Zabihian and A. S. Fung. “Thermodynamic sensitivity analysis of hybrid system based on solid oxide fuel cell”. In: *Sustainable Energy Technologies and Assessments* 6 (2014), pp. 51–59.

[127] A. S. Martinez, J. Brouwer and G. S. Samuelsen. “Comparative analysis of SOFC-GT freight lcomotive fueled by natural gas and diesel with onboard reformation”. In: *Applied Energy* 148 (2015), pp. 421–438.

[128] P. Saisirirat. “The Solid Oxide Fuel Cell (SOFC) and Gas Turbine (GT) Hybrid System Numerical Model”. In: *Energy Procedia* 79 (2015), pp. 845–850.

[129] S. Campanari, L. Mastropasqua, M. Gazzani, P. Chiesa and M. C. Romano. “Predicting the ultimate potential of natural gas SOFC power cycles with CO_2 capture - Part A: Methodology and reference cases”. In: *Journal of Power Sources* 324 (2016), pp. 598–614.

[130] M. M. Whiston, W. O. Collinge, M. M. Bilec and L. A. Schaefer. “Exergy and economic comparison between kW-scale hybrid and stand-alone solid oxide fuel cell systems”. In: *Journal of Power Sources* 353 (2017), pp. 152–166.

[131] J. Ahn, S. H. Park, Y. Noh, B. I. Choi, J. Ryu, D. Chang and K. L. M. Brendstrup. “Performance and availability of a marine generator-solid oxide fuel cell-gas turbine hybrid system in a very large ethane carrier”. In: *Journal of Power Sources* 399 (2018), pp. 199–206.

[132] K. H. M. Al-Hamed and I. Dincer. “A new direct ammonia solid oxide fuel cell and gas turbine based integrated system for electric rail transportation”. In: *eTransportation* 2 (2019). 100027.

[133] D. Oryshchyn, N. F. Harun, D. tucker, K. M. Bryden and L. Shadle. “Fuel utilization effects on system efficiency in solid oxide fuel cell gas turbine hybrid systems”. In: *Applied Energy* 228 (2018), pp. 1953–1965.

[134] H. J. Kruize. “Improving Methanol Powered Solid Oxide Fuel Cell - Gas Turbine Power Units for Naval Support Vessels through Fuel and Heat Recovery”. MA thesis. University of Twente, 2021.

[135] P. A. Duong, B. Ryu, C. Kim, J. Lee and H. Kang. “Energy and Exergy Analysis of an Ammonia Fuel CellIntegrated System for Marine Vessels”. In: *Energies* 15 (2022). 3331.

[136] S. Serbin, N. Washchilenko, O. Cherednichenko, K. Burunsuz, M. Dzida and D. Chen. “Application analysis of a hybrid solid oxide fuel cell-gas turbine system for marine power plants”. In: *Ships and Offshore Structures* 17(4) (2022), pp. 866–876.

[137] Z. Wang, H. Chen, R. Xia, F. Han, Y. Ji and W. Cai. “Energy, exergy and economy (3E) investigation of a SOFC-GT-ORC waste heat recovery system for green power ships”. In: *Thermal Science and Engineering Progress* 32 (2022). 101342.

[138] S. Seyam, I. Dincer and M. Agelin-Chaab. “Investigation of a hybridized combined cycle engine with SOFC system for marine applications”. In: *Journal of Thermal Analysis and Calorimetry* 148 (2023), pp. 8323–8344.

[139] R. Zeng, J. Gan, B. Guo, X. Zhang, H. Li, W. Yin and G. Zhang. “Thermodynamic performance analysis of solid oxide fuel cell - combined cooling, heating and power system with integrated supercritical CO_2 power cycle - organic Rankine cycle and absorption refrigeration cycle”. In: *Energy* 283 (2023). 129133.

[140] S. Kang and K.-Y. Ahn. “Dynamic modeling of solid oxide fuel cell and engine hybrid system for distributed power generation”. In: *Applied Energy* 195 (2017), pp. 1086–1099.

[141] W. Choi, J. Kim, Y. Kim, S. im, S. Oh and H. H. Song. “Experimental study of homogeneous charge compression ignition engine operation fuelled by emulated solid oxide fuel cell anode off-gas”. In: *Applied Energy* 229 (2018), pp. 42–62.

[142] Y. D. Lee, K. Y. Ahn, T. Morosuk and G. Tsatsaronis. “Exergetic and exergoeconomic evaluation of an SOFC-Engine hybrid power generation system”. In: *Energy* 145 (2018), pp. 810–822.

[143] S. Oh and H. H. Song. “Exergy analysis on non-catalyzed partial oxidation reforming using homogeneous charge compression ignition engine in a solid oxide fuel cell system”. In: *International Jornal of Hydrogen Energy* 43 (2018), pp. 2943–2960.

[144] H. Xu, B. Chen, P. Tan, H. Zhang, J. Yuan, J. T. S. Irvine and M. Ni. “Performance improvement of a direct carbon solid oxide fuel cell through integrating an Otto heat engine”. In: *Energy Conversion and Management* 165 (2018), pp. 761–770.

[145] W. Choi, J. Kim, Y. Kim and H. H. Song. “Solid oxide fuel cell operation in a solid oxide fuel cell-internal combustion engine hybrid system and the design point performance of the hybrid system”. In: *Applied Energy* 254 (2019). 113681.

[146] O. Siddiqui and I. Dincer. “Development and assessment of a novel integrated system using an ammonia internal combustion engine and fuel cells for cogeneration”. In: *Energy&Fuels* 33(3) (2019), pp. 2413–2425.

[147] Z. Wu, P. Tan, P. Zhu, W. Cai, B. Chen, F. Yang, Z. Zhang, E. Perpatham and M. Ni. “Performance analysis of a novel SOFC-HCCI engine hybrid system coupled with metal hydride reactor for H_2 addition by waste heat recovery”. In: *Energy Conversion and Management* 191 (2019), pp. 119–131.

[148] J. Kim, Y. Kim, W. Choi, K. Y. Ahn and H. H. Song. “Analysis on the operating performance of 5-kW class solid oxide fuel cell-internal combustion engine hybrid system using spark-assisted ignition”. In: *Applied Energy* 260 (2020). 114231.

[149] Y. S. Kim, Y. D. Lee and K. Y. Ahn. “System integration and proof-of-concept test results of SOFC-engine hybrid power generation system”. In: *Applied Energy* 277 (2020). 115542.

[150] Z. Wu, P. Zhu, J. Yao, S. Zhang, J. Ren, F. Yang and Z. Zhang. “Combined biomass gasification, SOFC, IC engine, and waste heat recovery system for power and heat generation: energy, exergy, exergoeconomic, environmental (4E) evaluations”. In: *Applied Energy* 279 (2020). 115764.

[151] P. Zhu, J. Yao, C. Qian, F. Yang, E. Porpatham, Z. Zhang and Z. Wu. “High-efficiency conversion of natural gas fuel to power by an integrated system of SOFC, HCCI engine, and waste heat recovery: Thermodynamic and thermo-economic analyses”. In: *Fuel* 275 (2020). 117883.

[152] K. H. M. Al-Hamed and I. Dincer. “Development and optimization of a novel solid oxide fuel cell-engine powering system for cleaner locomotives”. In: *Applied Thermal Engineering* 183 (2021). 116150.

[153] T. Koo, Y. S. Kim, Y. D. Lee, S. Yu, D. K. Lee and K. Y. Ahn. “Exergetic evaluation of operation results of 5-kW-class SOFC-HCCI engine hybrid power generation system”. In: *Applied Energy* 295 (2021). 117037.

[154] T. Ouyang, Z. Zhao, Z. Wang, M. Zhang and B. Liu. “A high-efficiency scheme for waste heat harvesting of solid oxide fuel cell integrated homogeneous charge compression ignition engine”. In: *Engergy* 229 (2021). 120720.

[155] Z. Zhao, Z. Wang, S. Xie, M. Zhang and T. Ouyang. “A novel design of power-cooling cogeneration system driven by solid oxide fuel cell waste heat in ocean-going vessels”. In: *Journal of Cleaner Production* 318 (2021). 128532.

[156] D. Diskin and L. Tartakovsky. “Finite-time energy conversion in a hybrid cycle combining electrochemical, combustion and thermochemical recuperation processes”. In: *Energy Conversion and Management* 262 (2022). 115673.

[157] C. Li, K. Cheng, S. Ma, H. Liu, Z. Ji and J. Qin. “Performance analysis of solid oxide fuel cell/piston engine hybrid system for aviation”. In: *Applied Thermal Engineering* 214 (2022). 118797.

[158] T.-Q. Quach, V.-T. Giap, D. K. Lee, T. P. Israel and K. Y. Ahn. “High-efficiency ammonia-fed solid oxide fuel cell systems for distributed power generation”. In: *Applied Energy* 324 (2022). 119718.

[159] Z. Zhao, X. Shi, M. Zhang and T. Ouyang. “Multi-scale assessment and multi-objective optimization of a novel solid oxide fuel cell hybrid power system fed by bio-syngas”. In: *Journal of Power Sources* 524 (2022). 231047.

[160] Y. Du, Z. yang, Y. Hou, J. Lou and G. He. “Part-load performance prediction of a novel diluted ammonia-fueled solid oxide fuel cell and engine combined system with hydrogen regeneration via data-driven model”. In: *Journal of Cleaner Production* 395 (2023). 136305.

[161] C. Li, Z. W. A. H. Liu, J. Qin and L. Wei. “Comparative study on teh performance of the application of clean alternative fuels in SOFC/ICE hybrid power systems on electric aircraft”. In: *Frontiers in Energy Research* 11 (2023).

[162] J. Qu, Y. Feng, Y. Zhu, B. Wu, Y. Wu, Z. Xiao and S. Zheng. “Assessment of a methanol-fueled integrated hybrid power system of solid oxide fuel cell and low-speed two-stroke engine for maritime application”. In: *Applied Thermal Engineering* 230, Part A (2023). 120735.

[163] J. Qu, Y. Feng, Y. Zhu, B. Wu, J. Liu, H. Jing and Y. Gao. “Thermodynamic analysis and comprehensive system optimization of the near zero emission hybrid power based on SOFC-ICE integrated system fueled with ammonia”. In: *Energy Conversion and Management* 294 (2023). 117553.

[164] J. Qu, Y. Feng, Y. Wu, Y. Zhu, B. Wu and Z. Xiao. “Design and Optimization of an Integrated Power System of Solid Oxide Fuel Cell and Marine Low-Speed Dual-Fuel Engine”. In: *Journal of Marine Science and Application* 22 (2023), pp. 837–849.

[165] B. Wu, Y. Luo, Y. Feng, C. Zhu and P. Yang. “Design and thermodynamic analysis of solid oxide fuel cells-internal combustion engine combined cycle system based on Two-Stage waste heat preheating and EGR”. In: *Fuel* 342 (2023). 127817.

[166] C. Li, Z. Wang, H. Liu, F. Guo, C. Li, xinyan Xiu, C. Wang, J. Qin and L. Wei. “Exergetic and exergoeconomic evaluation of an SOFC-Engine-ORC hybrid power generation system with methanol for ship application”. In: *Fuel* 357(C) (2024). 129944.

[167] Damen Naval. *Sigma Combatants*. 2024. URL: https://www.damen.com/vessels/defence-and-security/sigma-frigates?view=models (visited on 02/10/2024).

[168] S. Abril and L. Goossens. *SIGMA INTRODUCTION*. [Presentation Slides]. Nov. 2019.

[169] Damen Naval. *KRI Raden Eddy Martidinata 331 - SIGMA 10514*. 2021. URL: https://res.cloudinary.com/damen-shipyards2/image/upload/v1631709623/catalogue/defence-and-security/sigma/sigma-multi-mission-frigate-10514/product-sheet-sigma-multi-mission-frigate-10514.pdf.

A

Overview of research on combined cycles

In this appendix, an overview of all the identified research regarding SOFC-GT and SOFC-ICE combined cycles is given. The table below shows the combined cycle, study, used fuel and reported efficiency.

Table A.1: Overview of research on combined cycles

Combined Cycle	Research	Fuel	Reported Efficiency
SOFC-GT	Harvey and Richter [32]	CH_4	77.7% (LHV)
	Lobachyov and Richter [116]	Coal	62%
	Campanari [117]	NG	65%
	Massardo and Lubelli [11]	CH_4	65-70% (atmospheric) 74-76% (pressurized)
	Palsson et al. [118]	CH_4	65%
	Costamagna et al. [119]	CH_4	61.1% (design point) >50% (off-design)
	Kimijima and Kasagi [120]	CH_4	60%
	Chan et al. [20]	NG	86.4% (LHV)
	Inui et al. [121]	CH_4	70.64 (LHV)
	Freeh et al. [30]	Diesel	-
	Calise et al. [122]	CH_4	70%
	Park and Kim [21]	CH_4	66.5% (ambient) 72.5% (pressurized)
	Roberts et al. [123]	-	66% (variable speed operation) 53% (fixed speed operation)
	Stiller [124]	Variable	55-62%
	Lim et al. [33]	LNG	-
	Tse et al. [9]	liquefied petroleum gas (LPG)	53%
	Gandiglio et al. [25]	NG	64.6% (atmospheric) 71.9% (pressurized)
	Welaya et al. [125]	NG	70%
	Zabihian and Fung [126]	CH_4	59-75%
	Martinez et al. [127]	NG	60%

Table A.1: Overview of research on combined cycles

Combined Cycle	Research	Fuel	Reported Efficiency
		Diesel	52.2%
	Saisirirat [128]	NG	58%
	Campanari et al. [129]	NG	78%
	Whiston et al. [130]	CH_4	52.9% (electrical) 80.2% (thermal)
	Ahn et al. [131]	Ethane	61.34
	Al-Hamed and Dincer [132]	NH_3	58.7%
	van Biert et al. [19]	CH_4	59.2% (ambient) 61.6% (pressurized)
	Hou et al. [31]	MeOH	66% (electrical) 90% (thermal)
	Oryshchyn et al. [133]	Syngas	75.6%
	Kruize [134]	MeOH	81%
	Duong et al. [135]	NH_3	64.49%
	Serbin et al. [136]	NG	55%
	Ryu et al. [35]	NH_3 H_2	60.96% 64.46%
	Wang et al. [137]	LNG	-
	Seyam et al. [138]	Variable	61%
	Zeng et al. [139]	CH_4	59.62 %
	Babaji and Turner [14]	CH_4	62% (LHV)
	Duong et al. [34]	LNG	69.32%
SOFC-ICE	Park et al. [29]	LNG	71.2% (thermal) 51.7% (electrical)
	Kang and Ahn [140]	NG	-
	van Biert et al. [19]	CH_4	58%
	Choi et al. [141]	NG	59%
	Lee et al. [142]	NG	58%
	Oh and Song [143]	NG	51.9%
	Xu et al. [144]	Carbon	-
	Chuahy and Kokjohn [12]	Diesel	73.4% (LHV)
	Choi et al. [145]	NG	59%
	Siddiqui and Dincer [146]	NH_3	59.9%
	Wu et al. [147]	NG	58.75%
	Kim et al. [148]	NG	61.6%
	Kim et al. [149]	NG	55.7%
	Sapra et al. [13]	LNG	59.08%
	Wu et al. [150]	Biofuel	68.0%
	Zhu et al. [151]	NG	59.0%
	Al-Hamed and Dincer [152]	NG	80.1%
	Koo et al. [153]	CH_4	-

Table A.1: Overview of research on combined cycles

Combined Cycle	Research	Fuel	Reported Efficiency
	Ouyang et al. [154]	CH_4	63.68% (thermal)
	Sapra et al. [10]	CH_4	43.66%
	Zhao et al. [155]	NG	64.0%
	Cho et al. [77]	CH_4	66.9%
	Diskin and Tartakovsky [156]	MeOH	70%
	Li et al. [157]	CH_4	52.29%
	Quach et al. [158]	NH_3	67.50%
	Zhao et al. [159]	Bio-syngas	59.4%
	Du et al. [160]	NH_3	60.0%
	Elkafas et al. [78]	CH_4	47.3%
	Li et al. [161]	Variable	55.1-61.6%
	Qu et al. [162]	MeOH	55.6% (thermal)
	Qu et al. [163]	NH_3	70.53% (serial) 68.40% (parallel)
	Qu et al. [164]	NG	51.8%
	Wu et al. [165]	NG	56.1%
	Li et al. [15]	MeOH	57.08%
	Li et al. [166]	MeOH	61.86%

B

Survey Results

A survey was conducted to obtain the weight factor for the multi-criteria analysis of the different fuels. A total of 6 representatives from different departments, shown in Table B.1, were asked to fill out the survey. The author also filled out the survey to reach a total 7 possible responses. Only one representative did not find the time to fill in the survey, resulting in a total of 6 responses. While this is a small sample size, it is expected that together with the opinions of these people, the weight factor can be determined sufficiently for the purpose of this report.

Table B.1: Representatives of each department

Department	**Representative**
Research, Development and Innovation	G.J. Meijn
Research, Development and Innovation	S. Knegt
Proposals	S. Bedert
Naval and Technology	P. Maljaars
Engineering	J. van der Vorst
Purchasing	A. Berghuis

These representatives were asked to rate the different criteria between 1 (low importance) and 5 (high importance) for the selection of an alternative fuel. The different criteria are ranked for two different scenarios: peacetime and wartime. In Figure B.1, an overview is given on the number of times a weight factor was chosen for the specific criteria. For operation during wartime (Figure B.1b), the opinions of the respondents regarding the weight factor are fairly similar. Safety, energy density and availability of the fuel are the most important criteria. This is followed by storage and handling conditions and TRL. Emissions are the least important criteria for operation during wartime.

For peacetime operation, the opinions are spread a little further apart. For most criteria, 4 out of 5 weight factors were chosen at least once. For the remaining criteria 3 out of 5 weight factors were chosen. Toxicity and availability are still important criteria for the fuel, but flammability, explosive limits and energy density become less important during peacetime. For peacetime operation, GHG emissions become more important in the selection of the fuel.

While both peacetime and wartime are interesting for the design of a surface combatant, one respondent pointed out that, due to the current geopolitical climate, peacetime scenarios are no longer part of the design of upcoming vessels, and only wartime scenarios are considered. To obtain a peacetime and wartime weight factor for each criterion, the survey results are averaged, and shown in Table B.2.

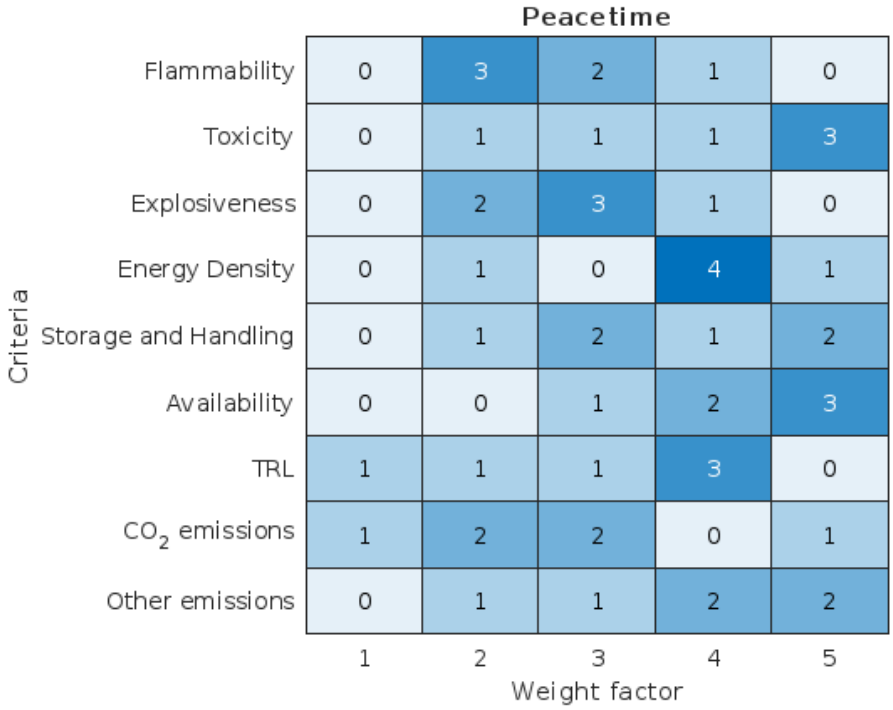

(a) Number of times a weight factor was chosen for peacetime

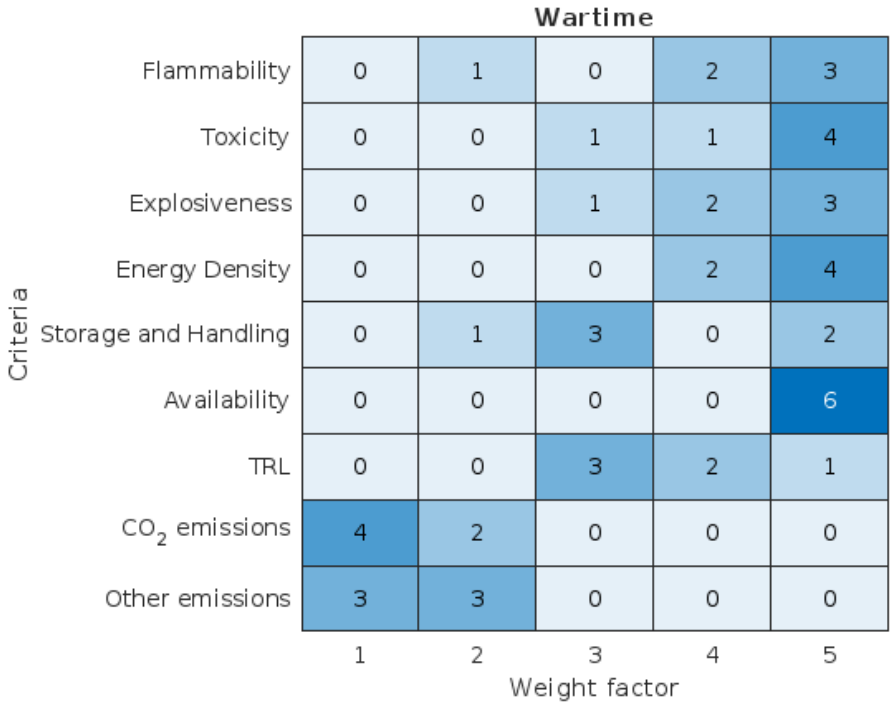

(b) Number of times a weight factor was chosen for wartime

Figure B.1: Results of the survey. Each column represents a weight factor, and the numbers shown inside the column show the number of times this weight factor was chosen for a given criterion.

Table B.2: Average weight factors resulting from the conducted survey

Criteria		Weight factor	
		Peacetime	**Wartime**
Safety	Flammability	2.7	4.2
	Toxicity	4.0	4.5
	Explosiveness	2.8	4.3
Operational	Energy Density	3.8	4.6
	Storage and Handling Conditions	3.7	3.5
	Availability	4.3	5.0
	TRL	3.0	3.7
Environmental	CO2 emissions	2.7	1.3
	Other emissions	3.8	1.5

C

SIGMA class surface combatant

The Ship Integrated Geometrical Modularity Approach (SIGMA) is a range of surface combatants developed by Damen Naval for the export market, ranging from 61 to 125 meters in length. This class of surface combatant is delivered to foreign navies such as Indonesia, Morocco and Mexico [167].

SIGMA is a systematic design series of surface combatants with standardized configurations and systems. This vessel design consists of a modular hull sections, and sections can be added or removed based on the clients needs. The hull is designed based on the layout of these hull sections. First, the necessary modules and systems are selected. The layout of these modules is then determined, and a suitable hull size is selected. [168]

The SIGMA vessels are all designed with global signatures in mind. Radar signature is reduced by using hull flare, tumble home and consistent shaping of the superstructure. IR signature is reduced with insulation and shielding of high temperature parts. Underwater radiated noise is reduced with resiliently mounting and noise abatement at the source of the noise. Lastly, electromagnetic signature is also considered in the design of the vessel. [168]

For this thesis the SIGMA 10514 is used (shown in Figure C.1). This is one of the larger vessels in the SIGMA range, with a length of 105 meters and a beam of 14 meters. The primary functions of this vessel are AAW, anti-surface warfare (ASuW) or anti-submarine warfare (ASW), but it is also capable of doing maritime security & safety, disaster relief and humanitarian aid [169]. Specifications of this vessel are given in Table C.1.

Length:		105.11	m
Beam:		14.02	m
Draught:		3.7	m
Displacement:		2365	t
Installed power:	approx.	20	MW
Top speed:		28	kn
Range (@14 knots):	>	5000	NM
Endurance at sea:	>	20	days

Table C.1: Specifications of the SIGMA 10514 [169]

Figure C.1: SIGMA Multi Mission Frigate 10514 [169]

D

CT model parameters

For all the Cycle-Tempo models that are used in this thesis, the parameters are shown in this appendix. For the standalone ICE models, the parameters are shown in section D.1. Next, in section D.2 the parameters for the standalone GT models are shown. Then in section D.3 the parameters for the standalone SOFC model are given. Lastly, section D.4 and section D.5 show the parameters for the SOFC-ICE and SOFC-GT combined cycle models respectively.

D.1. ICE models

In this section, the parameters for the different components in the CT models for the ICE are given. First, the parameters for diesel operation are given. This is followed by the MeOH operation.

D.1.1. Diesel

In the tables below, the parameters for the ICE model running on diesel are shown for 100% load, 91% load, 85% load, 75% load, 50% load and 25% load.

Table D.1: CT parameters for the diesel-fuelled ICE model at 100% load

Component	Parameter		CT Value		Reference value		Reference
Turbocharger	Isentropic efficiency compressor	$\eta_{is,compr}$	0.79	-	0.8	-	[12]
	Pressure ratio compressor	Π_{compr}	4.752	-	4.752	-	[72]
	Mechanical efficiency compressor	$\eta_{m,compr}$	0.956	-		-	
	Isentropic efficiency turbine	$\eta_{is,turb}$	0.855	-	0.8	-	[12]
	Pressure ratio turbine	Π_{turb}	3.468	-	3.468	-	[72]
	Mechanical efficiency turbine	$\eta_{m,turb}$	0.956	-		-	
Intercooler	Pressure drop	Δp_{loss}	0.049	bar	0.049	bar	[72]
	Temperature drop	ΔT	186	°C	186	°C	[72]
Cylinder	Isentropic efficiency compressor	$\eta_{is,compr}$	1	-	-	-	
	Pressure ratio compressor	Π_{compr}	37.41	-	-	-	
	Mechanical efficiency compressor	$\eta_{m,compr}$	0.8568	-	0.85-0.9	-	[77, 78]
	Air excess ratio combustor	λ	1.95	-	2.4	-	[72]
	Isentropic efficiency turbine	$\eta_{is,turb}$	1	-	-	-	
	Pressure ratio turbine	Π_{turb}	49.29	-	-	-	
	Mechanical efficiency turbine	$\eta_{m,turb}$	0.8568	-	0.85-0.9	-	[77, 78]
Generator	Generator efficiency	η_{gen}	0.97	-	0.95-0.97	-	[68]
Pumps	Isentropic efficiency	η_{is}	0.85	-	0.7-0.85	-	[19, 71]
	Mechanical efficiency	η_m	0.8	-	0.6-0.9	-	[19, 71]
Overall	Power output	P_{out}	9997.7	kW	9997	kW	[72]
	Energy consumption	E_{in}	8403.8	kJ/kWh	8411.9	kJ/kWh	[72]
	Exhaust temperature	T_{exh}	386.79	°C	387	°C	[72]

Table D.2: CT parameters for the diesel-fuelled ICE model at 91% load

Component	Parameter		CT Value		Reference value		Reference
Turbocharger	Isentropic efficiency compressor	$\eta_{is,compr}$	0.8	-	0.8	-	[12]
	Pressure ratio compressor	Π_{compr}	4.492	-	4.492	-	[72]
	Mechanical efficiency compressor	$\eta_{m,compr}$	0.9559	-		-	
	Isentropic efficiency turbine	$\eta_{is,turb}$	0.905	-	0.8	-	[12]
	Pressure ratio turbine	Π_{turb}	3.093	-	3.093	-	[72]
	Mechanical efficiency turbine	$\eta_{m,turb}$	0.9559	-		-	
Intercooler	Pressure drop	Δp_{loss}	0.0375	bar	0.0375	bar	[72]
	Temperature drop	ΔT	176	°C	176	°C	[72]
Cylinder	Isentropic efficiency compressor	$\eta_{is,compr}$	1	-	-	-	
	Pressure ratio compressor	Π_{compr}	37.41	-	-	-	
	Mechanical efficiency compressor	$\eta_{m,compr}$	0.855	-	0.85-0.9	-	[77, 78]
	Air excess ratio combustor	λ	1.88	-	2.4	-	[72]
	Isentropic efficiency turbine	$\eta_{is,turb}$	1	-	-	-	
	Pressure ratio turbine	Π_{turb}	52.3	-	-	-	
	Mechanical efficiency turbine	$\eta_{m,turb}$	0.855	-	0.85-0.9	-	[77, 78]
Generator	Generator efficiency	η_{gen}	0.97	-	0.95-0.97	-	[68]
Pumps	Isentropic efficiency	η_{is}	0.85	-	0.7-0.85	-	[19, 71]
	Mechanical efficiency	η_m	0.8	-	0.6-0.9	-	[19, 71]
Overall	Power output	P_{out}	9112.7	kW	9114	kW	[72]
	Energy consumption	E_{in}	8314.7	kJ/kWh	8309.4	kJ/kWh	[72]
	Exhaust temperature	T_{exh}	371.20	°C	371	°C	[72]

Table D.3: CT parameters for the diesel-fuelled ICE model at 85% load

Component	Parameter		CT Value		Reference value		Reference
Turbocharger	Isentropic efficiency compressor	$\eta_{is,compr}$	0.79	-	0.8	-	[12]
	Pressure ratio compressor	Π_{compr}	4.313	-	4.313	-	[72]
	Mechanical efficiency compressor	$\eta_{m,compr}$	0.9686	-		-	
	Isentropic efficiency turbine	$\eta_{is,turb}$	0.9	-	0.8	-	[12]
	Pressure ratio turbine	Π_{turb}	2.999	-	2.999	-	[72]
	Mechanical efficiency turbine	$\eta_{m,turb}$	0.9686	-		-	
Intercooler	Pressure drop	Δp_{loss}	0.014	bar	0.014	bar	[72]
	Temperature drop	ΔT	173	°C	173	°C	[72]
Cylinder	Isentropic efficiency compressor	$\eta_{is,compr}$	1	-	-	-	
	Pressure ratio compressor	Π_{compr}	37.41	-	-	-	
	Mechanical efficiency compressor	$\eta_{m,compr}$	0.856	-	0.85-0.9	-	[77, 78]
	Air excess ratio combustor	λ	1.93	-	2.65	-	[72]
	Isentropic efficiency turbine	$\eta_{is,turb}$	1	-	-	-	
	Pressure ratio turbine	Π_{turb}	52.1	-	-	-	
	Mechanical efficiency turbine	$\eta_{m,turb}$	0.856	-	0.85-0.9	-	[77, 78]
Generator	Generator efficiency	η_{gen}	0.97	-	0.95-0.97	-	[68]
Pumps	Isentropic efficiency	η_{is}	0.85	-	0.7-0.85	-	[19, 71]
	Mechanical efficiency	η_m	0.8	-	0.6-0.9	-	[19, 71]
Overall	Power output	P_{out}	8492.0	kW	8490	kW	[72]
	Energy consumption	E_{in}	8321.3	kJ/kWh	8330.8	kJ/kWh	[72]
	Exhaust temperature	T_{exh}	365.42	°C	366	°C	[72]

Table D.4: CT parameters for the diesel-fuelled ICE model at 75% load

Component	Parameter		CT Value		Reference value		Reference
Turbocharger	Isentropic efficiency compressor	$\eta_{is,compr}$	0.81	-	0.8	-	[12]
	Pressure ratio compressor	Π_{compr}	3.869	-	3.869	-	[72]
	Mechanical efficiency compressor	$\eta_{m,compr}$	0.958	-		-	
	Isentropic efficiency turbine	$\eta_{is,turb}$	0.925	-	0.8	-	[12]
	Pressure ratio turbine	Π_{turb}	2.63	-		-	[72]
	Mechanical efficiency turbine	$\eta_{m,turb}$	0.958	-		-	
Intercooler	Pressure drop	Δp_{loss}	0.013	bar	0.013	bar	[72]
	Temperature drop	ΔT	154	°C	154	°C	[72]
Cylinder	Isentropic efficiency compressor	$\eta_{is,compr}$	1	-	-	-	
	Pressure ratio compressor	Π_{compr}	37.41	-	-	-	
	Mechanical efficiency compressor	$\eta_{m,compr}$	0.8545	-	0.85-0.9	-	[77, 78]
	Air excess ratio combustor	λ	1.94	-	2.75	-	[72]
	Isentropic efficiency turbine	$\eta_{is,turb}$	1	-	-	-	
	Pressure ratio turbine	Π_{turb}	53.4	-	-	-	
	Mechanical efficiency turbine	$\eta_{m,turb}$	0.8545	-	0.85-0.9	-	[77, 78]
Generator	Generator efficiency	η_{gen}	0.97	-	0.95-0.97	-	[68]
Pumps	Isentropic efficiency	η_{is}	0.85	-	0.7-0.85	-	[19, 71]
	Mechanical efficiency	η_m	0.8	-	0.6-0.9	-	[19, 71]
Overall	Power output	P_{out}	7498.9	kW	7493	kW	[72]
	Energy consumption	E_{in}	8293.5	kJ/kWh	8313.7	kJ/kWh	[72]
	Exhaust temperature	T_{exh}	372.24	°C	372	°C	[72]

Table D.5: CT parameters for the diesel-fuelled ICE model at 50% load

Component	Parameter		CT Value		Reference value		Reference
Turbocharger	Isentropic efficiency compressor	$\eta_{is,compr}$	0.78	-	0.8	-	[12]
	Pressure ratio compressor	Π_{compr}	2.907	-	2.907	-	[72]
	Mechanical efficiency compressor	$\eta_{m,compr}$	0.9446	-		-	
	Isentropic efficiency turbine	$\eta_{is,turb}$	0.97	-	0.8	-	[12]
	Pressure ratio turbine	Π_{turb}	2.172	-	2.172	-	[72]
	Mechanical efficiency turbine	$\eta_{m,turb}$	0.9446	-		-	
Intercooler	Pressure drop	Δp_{loss}	0	bar	0	bar	[72]
	Temperature drop	ΔT	120	°C	120	°C	[72]
Cylinder	Isentropic efficiency compressor	$\eta_{is,compr}$	1	-	-	-	
	Pressure ratio compressor	Π_{compr}	37.41	-	-	-	
	Mechanical efficiency compressor	$\eta_{m,compr}$	0.851	-	0.85-0.9	-	[77, 78]
	Air excess ratio combustor	λ	2.203	-	2.3	-	[72]
	Isentropic efficiency turbine	$\eta_{is,turb}$	1	-	-	-	
	Pressure ratio turbine	Π_{turb}	48.66	-	-	-	
	Mechanical efficiency turbine	$\eta_{m,turb}$	0.851	-	0.85-0.9	-	[77, 78]
Generator	Generator efficiency	η_{gen}	0.97	-	0.95-0.97	-	[68]
Pumps	Isentropic efficiency	η_{is}	0.85	-	0.7-0.85	-	[19, 71]
	Mechanical efficiency	η_m	0.8	-	0.6-0.9	-	[19, 71]
Overall	Power output	P_{out}	4993.1	kW	5013	kW	[72]
	Energy consumption	E_{in}	8865.31	kJ/kWh	8821.8	kJ/kWh	[72]
	Exhaust temperature	T_{exh}	355.08	°C	355	°C	[72]

Table D.6: CT parameters for the diesel-fuelled ICE model at 25% load

Component	Parameter		CT Value		Reference value		Reference
Turbocharger	Isentropic efficiency compressor	$\eta_{is,compr}$	0.7	-	0.8	-	[12]
	Pressure ratio compressor	Π_{compr}	2.234	-	2.234	-	[72]
	Mechanical efficiency compressor	$\eta_{m,compr}$	0.947	-		-	
	Isentropic efficiency turbine	$\eta_{is,turb}$	0.93	-	0.8	-	[12]
	Pressure ratio turbine	Π_{turb}	1.994	-	1.994	-	[72]
	Mechanical efficiency turbine	$\eta_{m,turb}$	0.947	-		-	
Intercooler	Pressure drop	Δp_{loss}	0	bar	0	bar	[72]
	Temperature drop	ΔT	96	°C	96	°C	[72]
Cylinder	Isentropic efficiency compressor	$\eta_{is,compr}$	1	-	-	-	
	Pressure ratio compressor	Π_{compr}	37.41	-	-	-	
	Mechanical efficiency compressor	$\eta_{m,compr}$	0.879	-	0.85-0.9	-	[77, 78]
	Air excess ratio combustor	λ	2.65	-	3.7	-	[72]
	Isentropic efficiency turbine	$\eta_{is,turb}$	1	-	-	-	
	Pressure ratio turbine	Π_{turb}	40.74	-	-	-	
	Mechanical efficiency turbine	$\eta_{m,turb}$	0.879	-	0.85-0.9	-	[77, 78]
Generator	Generator efficiency	η_{gen}	0.97	-	0.95-0.97	-	[68]
Pumps	Isentropic efficiency	η_{is}	0.85	-	0.7-0.85	-	[19, 71]
	Mechanical efficiency	η_m	0.8	-	0.6-0.9	-	[19, 71]
Overall	Power output	P_{out}	2519.5	kW	2520	kW	[72]
	Energy consumption	E_{in}	8735.64	kJ/kWh	8719.3	kJ/kWh	[72]
	Exhaust temperature	T_{exh}	331.10	°C	331	°C	[72]

D.1.2. Methanol

In the tables below, the parameters for the ICE model running on MeOH are shown for 100% load, 91% load, 85% load, 75% load, 50% load and 25% load. The difference with the diesel models is the air-excess ratio (λ), power output, energy consumption and exhaust temperature.

Table D.7: CT parameters for the MeOH-fuelled ICE model at 100% load

Component	Parameter		CT Value	
Turbocharger	Isentropic efficiency compressor	$\eta_{is,compr}$	0.79	
	Pressure ratio compressor	Π_{compr}	4.752	-
	Mechanical efficiency compressor	$\eta_{m,compr}$	0.956	-
	Isentropic efficiency turbine	$\eta_{is,turb}$	0.855	-
	Pressure ratio turbine	Π_{turb}	3.468	-
	Mechanical efficiency turbine	$\eta_{m,turb}$	0.956	-
Intercooler	Pressure drop	Δp_{loss}	0.049	bar
	Temperature drop	ΔT	186	°C
Cylinder	Isentropic efficiency compressor	$\eta_{is,compr}$	1	-
	Pressure ratio compressor	Π_{compr}	37.41	-
	Mechanical efficiency compressor	$\eta_{m,compr}$	0.8568	-
	Air excess ratio combustor	λ	1.96	-
	Isentropic efficiency turbine	$\eta_{is,turb}$	1	-
	Pressure ratio turbine	Π_{turb}	49.29	-
	Mechanical efficiency turbine	$\eta_{m,turb}$	0.8568	-
Generator	Generator efficiency	η_{gen}	0.97	-
Pumps	Isentropic efficiency	η_{is}	0.85	-
	Mechanical efficiency	η_m	0.8	-
Overall	Power output	P_{out}	9997.7	kW
	Energy consumption	E_{in}	8029.1	kJ/kWh
	Exhaust temperature	T_{exh}	334.30	°C

Table D.8: CT parameters for the MeOH-fuelled ICE model at 91% load

Component	Parameter		CT Value	
Turbocharger	Isentropic efficiency compressor	$\eta_{is,compr}$	0.79	-
	Pressure ratio compressor	Π_{compr}	4.752	-
	Mechanical efficiency compressor	$\eta_{m,compr}$	0.956	-
	Isentropic efficiency turbine	$\eta_{is,turb}$	0.855	-
	Pressure ratio turbine	Π_{turb}	3.468	-
	Mechanical efficiency turbine	$\eta_{m,turb}$	0.956	-
Intercooler	Pressure drop	Δp_{loss}	0.049	bar
	Temperature drop	ΔT	186	°C
Cylinder	Isentropic efficiency compressor	$\eta_{is,compr}$	1	-
	Pressure ratio compressor	Π_{compr}	37.41	-
	Mechanical efficiency compressor	$\eta_{m,compr}$	0.8568	-
	Air excess ratio combustor	λ	2.00	-
	Isentropic efficiency turbine	$\eta_{is,turb}$	1	-
	Pressure ratio turbine	Π_{turb}	49.29	-
	Mechanical efficiency turbine	$\eta_{m,turb}$	0.8568	-
Generator	Generator efficiency	η_{gen}	0.97	-
Pumps	Isentropic efficiency	η_{is}	0.85	-
	Mechanical efficiency	η_m	0.8	-
Overall	Power output	P_{out}	9114.6	kW
	Energy consumption	E_{in}	7947.6	kJ/kWh
	Exhaust temperature	T_{exh}	321.13	°C

Table D.9: CT parameters for the MeOH-fuelled ICE model at 85% load

Component	Parameter		CT Value	
Turbocharger	Isentropic efficiency compressor	$\eta_{is,compr}$	0.79	-
	Pressure ratio compressor	Π_{compr}	4.752	-
	Mechanical efficiency compressor	$\eta_{m,compr}$	0.956	-
	Isentropic efficiency turbine	$\eta_{is,turb}$	0.855	-
	Pressure ratio turbine	Π_{turb}	3.468	-
	Mechanical efficiency turbine	$\eta_{m,turb}$	0.956	-
Intercooler	Pressure drop	Δp_{loss}	0.049	bar
	Temperature drop	ΔT	186	°C
Cylinder	Isentropic efficiency compressor	$\eta_{is,compr}$	1	-
	Pressure ratio compressor	Π_{compr}	37.41	-
	Mechanical efficiency compressor	$\eta_{m,compr}$	0.8568	-
	Air excess ratio combustor	λ	2.05	-
	Isentropic efficiency turbine	$\eta_{is,turb}$	1	-
	Pressure ratio turbine	Π_{turb}	49.29	-
	Mechanical efficiency turbine	$\eta_{m,turb}$	0.8568	-
Generator	Generator efficiency	η_{gen}	0.97	-
Pumps	Isentropic efficiency	η_{is}	0.85	-
	Mechanical efficiency	η_m	0.8	-
Overall	Power output	P_{out}	8503.0	kW
	Energy consumption	E_{in}	7949.4	kJ/kWh
	Exhaust temperature	T_{exh}	316.94	°C

Table D.10: CT parameters for the MeOH-fuelled ICE model at 75% load

Component	Parameter		CT Value	
Turbocharger	Isentropic efficiency compressor	$\eta_{is,compr}$	0.79	-
	Pressure ratio compressor	Π_{compr}	4.752	-
	Mechanical efficiency compressor	$\eta_{m,compr}$	0.956	-
	Isentropic efficiency turbine	$\eta_{is,turb}$	0.855	-
	Pressure ratio turbine	Π_{turb}	3.468	-
	Mechanical efficiency turbine	$\eta_{m,turb}$	0.956	-
Intercooler	Pressure drop	Δp_{loss}	0.049	bar
	Temperature drop	ΔT	186	°C
Cylinder	Isentropic efficiency compressor	$\eta_{is,compr}$	1	-
	Pressure ratio compressor	Π_{compr}	37.41	-
	Mechanical efficiency compressor	$\eta_{m,compr}$	0.8568	-
	Air excess ratio combustor	λ	2.06	-
	Isentropic efficiency turbine	$\eta_{is,turb}$	1	-
	Pressure ratio turbine	Π_{turb}	49.29	-
	Mechanical efficiency turbine	$\eta_{m,turb}$	0.8568	-
Generator	Generator efficiency	η_{gen}	0.97	-
Pumps	Isentropic efficiency	η_{is}	0.85	-
	Mechanical efficiency	η_m	0.8	-
Overall	Power output	P_{out}	7506.4	kW
	Energy consumption	E_{in}	7928.9	kJ/kWh
	Exhaust temperature	T_{exh}	324.15	°C

Table D.11: CT parameters for the MeOH-fuelled ICE model at 50% load

Component	Parameter		CT Value	
Turbocharger	Isentropic efficiency compressor	$\eta_{is,compr}$	0.79	-
	Pressure ratio compressor	Π_{compr}	4.752	-
	Mechanical efficiency compressor	$\eta_{m,compr}$	0.956	-
	Isentropic efficiency turbine	$\eta_{is,turb}$	0.855	-
	Pressure ratio turbine	Π_{turb}	3.468	-
	Mechanical efficiency turbine	$\eta_{m,turb}$	0.956	-
Intercooler	Pressure drop	Δp_{loss}	0.049	bar
	Temperature drop	ΔT	186	°C
Cylinder	Isentropic efficiency compressor	$\eta_{is,compr}$	1	-
	Pressure ratio compressor	Π_{compr}	37.41	-
	Mechanical efficiency compressor	$\eta_{m,compr}$	0.8568	-
	Air excess ratio combustor	λ	2.43	-
	Isentropic efficiency turbine	$\eta_{is,turb}$	1	-
	Pressure ratio turbine	Π_{turb}	49.29	-
	Mechanical efficiency turbine	$\eta_{m,turb}$	0.8568	-
Generator	Generator efficiency	η_{gen}	0.97	-
Pumps	Isentropic efficiency	η_{is}	0.85	-
	Mechanical efficiency	η_m	0.8	-
Overall	Power output	P_{out}	4999.6	kW
	Energy consumption	E_{in}	8399.9	kJ/kWh
	Exhaust temperature	T_{exh}	315.46	°C

Table D.12: CT parameters for the MeOH-fuelled ICE model at 25% load

Component	Parameter		CT Value	
Turbocharger	Isentropic efficiency compressor	$\eta_{is,compr}$	0.79	-
	Pressure ratio compressor	Π_{compr}	4.752	-
	Mechanical efficiency compressor	$\eta_{m,compr}$	0.956	-
	Isentropic efficiency turbine	$\eta_{is,turb}$	0.855	-
	Pressure ratio turbine	Π_{turb}	3.468	-
	Mechanical efficiency turbine	$\eta_{m,turb}$	0.956	-
Intercooler	Pressure drop	Δp_{loss}	0.049	bar
	Temperature drop	ΔT	186	°C
Cylinder	Isentropic efficiency compressor	$\eta_{is,compr}$	1	-
	Pressure ratio compressor	Π_{compr}	37.41	-
	Mechanical efficiency compressor	$\eta_{m,compr}$	0.8568	-
	Air excess ratio combustor	λ	2.78	-
	Isentropic efficiency turbine	$\eta_{is,turb}$	1	-
	Pressure ratio turbine	Π_{turb}	49.29	-
	Mechanical efficiency turbine	$\eta_{m,turb}$	0.8568	-
Generator	Generator efficiency	η_{gen}	0.97	-
Pumps	Isentropic efficiency	η_{is}	0.85	-
	Mechanical efficiency	η_m	0.8	-
Overall	Power output	P_{out}	2521.3	kW
	Energy consumption	E_{in}	8295.7	kJ/kWh
	Exhaust temperature	T_{exh}	298.21	°C

D.2. GT models

In this section, the parameters for the different components in the CT models for the GT are given. First, the parameters for diesel operation are given. This is followed by the MeOH operation.

D.2.1. Diesel

In the tables below, the parameters for the GT model running on diesel for loads between 10% and 100% are given in 10% increments.

Table D.13: CT parameters for the diesel-fuelled GT model at 100% load

Component	Parameter		CT Value		Reference value		Reference
Compressor	Isentropic efficiency	η_{is}	0.843	-	0.78	-	[19]
	Pressure ratio	Π	23.54	-	23.54	-	[73]
	Mechanical efficiency	η_m	0.997	-	0.99	-	[73]
Turbine	Isentropic efficiency	η_{is}	0.865	-	0.82	-	[19]
	Pressure ratio	Π	4.80	-		-	
	Mechanical efficiency	η_m	0.997	-	0.99	-	[73]
Power turbine	Isentropic efficiency	η_{is}	0.86	-		-	
	Pressure ratio	Π	4.76	-	-	-	
	Mechanical efficiency	η_m	0.996	-	0.99	-	[73]
Generator	Generator efficiency	η_{gen}	0.975	-	0.975	-	[73]
Pumps	Isentropic efficiency	η_{is}	0.85	-	0.7-0.85	-	[19, 71]
	Mechanical efficiency	η_m	0.8	-	0.6-0.9	-	[19, 71]
Overall	Power output	P_{out}	31.28	MW	31.21	MW	[73]
	Energy consumption	E_{in}	9530.6	kJ/kWh	9549.1	kJ/kWh	[73]
	Exhaust temperature	T_{exh}	533.8	°C	533.8	°C	[73]

Table D.14: CT parameters for the diesel-fuelled GT model at 90% load

Component	Parameter		CT Value		Reference value		Reference
Compressor	Isentropic efficiency	η_{is}	0.85	-	0.78	-	[19]
	Pressure ratio	Π	22.14	-	22.14	-	[73]
	Mechanical efficiency	η_m	0.998	-	0.99	-	[73]
Turbine	Isentropic efficiency	η_{is}	0.86	-	0.82	-	[19]
	Pressure ratio	Π	4.81	-		-	
	Mechanical efficiency	η_m	0.998	-	0.99	-	[73]
Power turbine	Isentropic efficiency	η_{is}	0.86	-		-	
	Pressure ratio	Π	4.46	-	-	-	
	Mechanical efficiency	η_m	0.997	-	0.99	-	[73]
Generator	Generator efficiency	η_{gen}	0.975	-	0.975	-	[73]
Pumps	Isentropic efficiency	η_{is}	0.85	-	0.7-0.85	-	[19, 71]
	Mechanical efficiency	η_m	0.8	-	0.6-0.9	-	[19, 71]
Overall	Power output	P_{out}	28.0	MW	28.1	MW	[73]
	Energy consumption	E_{in}	9682.8	kJ/kWh	9651.5	kJ/kWh	[73]
	Exhaust temperature	T_{exh}	515.8	°C	515.2	°C	[73]

Table D.15: CT parameters for the diesel-fuelled GT model at 80% load

Component	Parameter		CT Value		Reference value		Reference
Compressor	Isentropic efficiency	η_{is}	0.857	-	0.78	-	[19]
	Pressure ratio	Π	20.69	-	20.69	-	[73]
	Mechanical efficiency	η_m	0.997	-	0.99	-	[73]
Turbine	Isentropic efficiency	η_{is}	0.86	-	0.82	-	[19]
	Pressure ratio	Π	4.72	-		-	
	Mechanical efficiency	η_m	0.997	-	0.99	-	[73]
Power turbine	Isentropic efficiency	η_{is}	0.855	-		-	
	Pressure ratio	Π	4.25	-	-	-	
	Mechanical efficiency	η_m	0.997	-	0.99	-	[73]
Generator	Generator efficiency	η_{gen}	0.974	-	0.974	-	[73]
Pumps	Isentropic efficiency	η_{is}	0.85	-	0.7-0.85	-	[19, 71]
	Mechanical efficiency	η_m	0.8	-	0.6-0.9	-	[19, 71]
Overall	Power output	P_{out}	24.9	MW	24.9	MW	[73]
	Energy consumption	E_{in}	9919.1	kJ/kWh	9917.4	kJ/kWh	[73]
	Exhaust temperature	T_{exh}	504.1	°C	503.9	°C	[73]

Table D.16: CT parameters for the diesel-fuelled GT model at 70% load

Component	Parameter		CT Value		Reference value		Reference
Compressor	Isentropic efficiency	η_{is}	0.861	-	0.78	-	[19]
	Pressure ratio	Π	19.17	-	19.17	-	[73]
	Mechanical efficiency	η_m	0.996	-	0.99	-	[73]
Turbine	Isentropic efficiency	η_{is}	0.855	-	0.82	-	[19]
	Pressure ratio	Π	4.69	-		-	
	Mechanical efficiency	η_m	0.996	-	0.99	-	[73]
Power turbine	Isentropic efficiency	η_{is}	0.855	-		-	
	Pressure ratio	Π	3.96	-	-	-	
	Mechanical efficiency	η_m	0.996	-	0.99	-	[73]
Generator	Generator efficiency	η_{gen}	0.973	-	0.975	-	[73]
Pumps	Isentropic efficiency	η_{is}	0.85	-	0.7-0.85	-	[19, 71]
	Mechanical efficiency	η_m	0.8	-	0.6-0.9	-	[19, 71]
Overall	Power output	P_{out}	21.8	MW	21.8	MW	[73]
	Energy consumption	E_{in}	10227.8	kJ/kWh	10227.3	kJ/kWh	[73]
	Exhaust temperature	T_{exh}	492.5	°C	492.6	°C	[73]

Table D.17: CT parameters for the diesel-fuelled GT model at 60% load

Component	Parameter		CT Value		Reference value		Reference
Compressor	Isentropic efficiency	η_{is}	0.862	-	0.78	-	[19]
	Pressure ratio	Π	17.72	-	17.72	-	[73]
	Mechanical efficiency	η_m	0.996	-	0.99	-	[73]
Turbine	Isentropic efficiency	η_{is}	0.85	-	0.82	-	[19]
	Pressure ratio	Π	4.67	-		-	
	Mechanical efficiency	η_m	0.996	-	0.99	-	[73]
Power turbine	Isentropic efficiency	η_{is}	0.845	-		-	
	Pressure ratio	Π	3.68	-	-	-	
	Mechanical efficiency	η_m	0.996	-	0.99	-	[73]
Generator	Generator efficiency	η_{gen}	0.97	-	0.97	-	[73]
Pumps	Isentropic efficiency	η_{is}	0.85	-	0.7-0.85	-	[19, 71]
	Mechanical efficiency	η_m	0.8	-	0.6-0.9	-	[19, 71]
Overall	Power output	P_{out}	18.8	MW	18.6	MW	[73]
	Energy consumption	E_{in}	10715.2	kJ/kWh	10650.9	kJ/kWh	[73]
	Exhaust temperature	T_{exh}	483.1	°C	483.9	°C	[73]

Table D.18: CT parameters for the diesel-fuelled GT model at 50% load

Component	Parameter		CT Value		Reference value		Reference
Compressor	Isentropic efficiency	η_{is}	0.859	-	0.78	-	[19]
	Pressure ratio	Π	16.05	-	23.54	-	[73]
	Mechanical efficiency	η_m	0.997	-	0.99	-	[73]
Turbine	Isentropic efficiency	η_{is}	0.84	-	0.82	-	[19]
	Pressure ratio	Π	4.70	-		-	
	Mechanical efficiency	η_m	0.997	-	0.99	-	[73]
Power turbine	Isentropic efficiency	η_{is}	0.84	-		-	
	Pressure ratio	Π	4.31	-	-	-	
	Mechanical efficiency	η_m	0.997	-	0.99	-	[73]
Generator	Generator efficiency	η_{gen}	0.966	-	0.966	-	[73]
Pumps	Isentropic efficiency	η_{is}	0.85	-	0.7-0.85	-	[19, 71]
	Mechanical efficiency	η_m	0.8	-	0.6-0.9	-	[19, 71]
Overall	Power output	P_{out}	15.3	MW	15.5	MW	[73]
	Energy consumption	E_{in}	11368.7	kJ/kWh	11250.0	kJ/kWh	[73]
	Exhaust temperature	T_{exh}	471.3	°C	474.3	°C	[73]

Component	Parameter		CT Value		Reference value		Reference
Compressor	Isentropic efficiency	η_{is}	0.853	-	0.78	-	[19]
	Pressure ratio	Π	14.46	-	14.46	-	[73]
	Mechanical efficiency	η_m	0.998	-	0.99	-	[73]
Turbine	Isentropic efficiency	η_{is}	0.829	-	0.82	-	[19]
	Pressure ratio	Π	4.75	-		-	
	Mechanical efficiency	η_m	0.998	-	0.99	-	[73]
Power turbine	Isentropic efficiency	η_{is}	0.829	-		-	
	Pressure ratio	Π	2.95	-	-	-	
	Mechanical efficiency	η_m	0.998	-	0.99	-	[73]
Generator	Generator efficiency	η_{gen}	0.96	-	0.975	-	[73]
Pumps	Isentropic efficiency	η_{is}	0.85	-	0.7-0.85	-	[19, 71]
	Mechanical efficiency	η_m	0.8	-	0.6-0.9	-	[19, 71]
Overall	Power output	P_{out}	12.1	MW	12.1	MW	[73]
	Energy consumption	E_{in}	12348.0	kJ/kWh	12121.2	kJ/kWh	[73]
	Exhaust temperature	T_{exh}	460.9	°C	463.9	°C	[73]

Table D.19: CT parameters for the diesel-fuelled GT model at 30% load

Component	Parameter		CT Value		Reference value		Reference
Compressor	Isentropic efficiency	η_{is}	0.84	-	0.78	-	[19]
	Pressure ratio	Π	12.61	-	12.61	-	[73]
	Mechanical efficiency	η_m	0.998	-	0.99	-	[73]
Turbine	Isentropic efficiency	η_{is}	0.817	-	0.82	-	[19]
	Pressure ratio	Π	4.94	-		-	
	Mechanical efficiency	η_m	0.998	-	0.99	-	[73]
Power turbine	Isentropic efficiency	η_{is}	0.817	-		-	
	Pressure ratio	Π	2.58	-	-	-	
	Mechanical efficiency	η_m	0.998	-	0.99	-	[73]
Generator	Generator efficiency	η_{gen}	0.95	-	0.95	-	[73]
Pumps	Isentropic efficiency	η_{is}	0.85	-	0.7-0.85	-	[19, 71]
	Mechanical efficiency	η_m	0.8	-	0.6-0.9	-	[19, 71]
Overall	Power output	P_{out}	8.9	MW	9.1	MW	[73]
	Energy consumption	E_{in}	13933.7	kJ/kWh	13636.4	kJ/kWh	[73]
	Exhaust temperature	T_{exh}	453.9	°C	457.9	°C	[73]

Table D.20: CT parameters for the diesel-fuelled GT model at 20% load

Component	Parameter		CT Value		Reference value		Reference
Compressor	Isentropic efficiency	η_{is}	0.82	-	0.78	-	[19]
	Pressure ratio	Π	10.62	-	10.62	-	[73]
	Mechanical efficiency	η_m	0.998	-	0.99	-	[73]
Turbine	Isentropic efficiency	η_{is}	0.79	-	0.82	-	[19]
	Pressure ratio	Π	5.04	-		-	
	Mechanical efficiency	η_m	0.998	-	0.99	-	[73]
Power turbine	Isentropic efficiency	η_{is}	0.79	-		-	
	Pressure ratio	Π	2.04	-	-	-	
	Mechanical efficiency	η_m	0.998	-	0.99	-	[73]
Generator	Generator efficiency	η_{gen}	0.93	-	0.93	-	[73]
Pumps	Isentropic efficiency	η_{is}	0.85	-	0.7-0.85	-	[19, 71]
	Mechanical efficiency	η_m	0.8	-	0.6-0.9	-	[19, 71]
Overall	Power output	P_{out}	5.3	MW	6.0	MW	[73]
	Energy consumption	E_{in}	18150.8	kJ/kWh	16216.2	kJ/kWh	[73]
	Exhaust temperature	T_{exh}	440.1	°C	446.5	°C	[73]

Table D.21: CT parameters for the diesel-fuelled GT model at 10% load

Component	Parameter		CT Value		Reference value		Reference
Compressor	Isentropic efficiency	η_{is}	0.79	-	0.78	-	[19]
	Pressure ratio	Π	8.38	-	23.54	-	[73]
	Mechanical efficiency	η_m	0.998	-	0.99	-	[73]
Turbine	Isentropic efficiency	η_{is}	0.72	-	0.82	-	[19]
	Pressure ratio	Π	6.38	-		-	
	Mechanical efficiency	η_m	0.998	-	0.99	-	[73]
Power turbine	Isentropic efficiency	η_{is}	0.72	-		-	
	Pressure ratio	Π	1.27	-	-	-	
	Mechanical efficiency	η_m	0.998	-	0.99	-	[73]
Generator	Generator efficiency	η_{gen}	0.874	-	0.874	-	[73]
Pumps	Isentropic efficiency	η_{is}	0.85	-	0.7-0.85	-	[19, 71]
	Mechanical efficiency	η_m	0.8	-	0.6-0.9	-	[19, 71]
Overall	Power output	P_{out}	1.2	MW	2.8	MW	[73]
	Energy consumption	E_{in}	54066.6	kJ/kWh	23076.9	kJ/kWh	[73]
	Exhaust temperature	T_{exh}	420.2	°C	426.4	°C	[73]

D.2.2. Methanol

In the tables below, the parameters for the GT model running on MeOH for loads between 10% and 100% are given in 10% increments. Compared to the diesel models, the MeOH models differ in power output, energy consumption and exhaust temperature.

Table D.22: CT parameters for the MeOH-fuelled GT model at 100% load

Component	Parameter		CT Value	
Compressor	Isentropic efficiency	η_{is}	0.843	-
	Pressure ratio	Π	23.54	-
	Mechanical efficiency	η_m	0.997	-
Turbine	Isentropic efficiency	η_{is}	0.865	-
	Pressure ratio	Π	4.80	-
	Mechanical efficiency	η_m	0.997	-
Power turbine	Isentropic efficiency	η_{is}	0.86	-
	Pressure ratio	Π	4.76	-
	Mechanical efficiency	η_m	0.996	-
Generator	Generator efficiency	η_{gen}	0.975	-
Pumps	Isentropic efficiency	η_{is}	0.85	-
	Mechanical efficiency	η_m	0.8	-
Overall	Power output	P_{out}	31.3	MW
	Energy consumption	E_{in}	9398.5	kJ/kWh
	Exhaust temperature	T_{exh}	503.4	°C

Table D.23: CT parameters for the MeOH-fuelled GT model at 90% load

Component	Parameter		CT Value	
Compressor	Isentropic efficiency	η_{is}	0.85	-
	Pressure ratio	Π	22.14	-
	Mechanical efficiency	η_m	0.998	-
Turbine	Isentropic efficiency	η_{is}	0.86	-
	Pressure ratio	Π	4.81	-
	Mechanical efficiency	η_m	0.998	-
Power turbine	Isentropic efficiency	η_{is}	0.86	-
	Pressure ratio	Π	4.46	-
	Mechanical efficiency	η_m	0.997	-
Generator	Generator efficiency	η_{gen}	0.975	-
Pumps	Isentropic efficiency	η_{is}	0.85	-
	Mechanical efficiency	η_m	0.8	-
Overall	Power output	P_{out}	28.1	MW
	Energy consumption	E_{in}	9547.2	kJ/kWh
	Exhaust temperature	T_{exh}	487.6	°C

Table D.24: CT parameters for the MeOH-fuelled GT model at 80% load

Component	Parameter		CT Value	
Compressor	Isentropic efficiency	η_{is}	0.857	-
	Pressure ratio	Π	20.69	-
	Mechanical efficiency	η_m	0.997	-
Turbine	Isentropic efficiency	η_{is}	0.86	-
	Pressure ratio	Π	4.72	-
	Mechanical efficiency	η_m	0.997	-
Power turbine	Isentropic efficiency	η_{is}	0.855	-
	Pressure ratio	Π	4.25	-
	Mechanical efficiency	η_m	0.997	-
Generator	Generator efficiency	η_{gen}	0.974	-
Pumps	Isentropic efficiency	η_{is}	0.85	-
	Mechanical efficiency	η_m	0.8	-
Overall	Power output	P_{out}	24.9	MW
	Energy consumption	E_{in}	9781.0	kJ/kWh
	Exhaust temperature	T_{exh}	477.3	°C

Table D.25: CT parameters for the MeOH-fuelled GT model at 70% load

Component	Parameter		CT Value	
Compressor	Isentropic efficiency	η_{is}	0.861	-
	Pressure ratio	Π	19.17	-
	Mechanical efficiency	η_m	0.996	-
Turbine	Isentropic efficiency	η_{is}	0.855	-
	Pressure ratio	Π	4.69	-
	Mechanical efficiency	η_m	0.996	-
Power turbine	Isentropic efficiency	η_{is}	0.855	-
	Pressure ratio	Π	3.96	-
	Mechanical efficiency	η_m	0.996	-
Generator	Generator efficiency	η_{gen}	0.973	-
Pumps	Isentropic efficiency	η_{is}	0.85	-
	Mechanical efficiency	η_m	0.8	-
Overall	Power output	P_{out}	21.8	MW
	Energy consumption	E_{in}	10085.7	kJ/kWh
	Exhaust temperature	T_{exh}	467.1	°C

Table D.26: CT parameters for the MeOH-fuelled GT model at 60% load

Component	Parameter		CT Value	
Compressor	Isentropic efficiency	η_{is}	0.862	-
	Pressure ratio	Π	17.72	-
	Mechanical efficiency	η_m	0.996	-
Turbine	Isentropic efficiency	η_{is}	0.85	-
	Pressure ratio	Π	4.67	-
	Mechanical efficiency	η_m	0.996	-
Power turbine	Isentropic efficiency	η_{is}	0.845	-
	Pressure ratio	Π	3.68	-
	Mechanical efficiency	η_m	0.996	-
Generator	Generator efficiency	η_{gen}	0.97	-
Pumps	Isentropic efficiency	η_{is}	0.85	-
	Mechanical efficiency	η_m	0.8	-
Overall	Power output	P_{out}	18.6	MW
	Energy consumption	E_{in}	10568.2	kJ/kWh
	Exhaust temperature	T_{exh}	459.2	°C

Table D.27: CT parameters for the MeOH-fuelled GT model at 50% load

Component	Parameter		CT Value	
Compressor	Isentropic efficiency	η_{is}	0.859	-
	Pressure ratio	Π	16.05	-
	Mechanical efficiency	η_m	0.997	-
Turbine	Isentropic efficiency	η_{is}	0.84	-
	Pressure ratio	Π	4.70	-
	Mechanical efficiency	η_m	0.997	-
Power turbine	Isentropic efficiency	η_{is}	0.84	-
	Pressure ratio	Π	4.31	-
	Mechanical efficiency	η_m	0.997	-
Generator	Generator efficiency	η_{gen}	0.966	-
Pumps	Isentropic efficiency	η_{is}	0.85	-
	Mechanical efficiency	η_m	0.8	-
Overall	Power output	P_{out}	15.5	MW
	Energy consumption	E_{in}	11213.5	kJ/kWh
	Exhaust temperature	T_{exh}	449.0	°C

Table D.28: CT parameters for the MeOH-fuelled GT model at 40% load

Component	Parameter		CT Value	
Compressor	Isentropic efficiency	η_{is}	0.853	-
	Pressure ratio	Π	14.46	-
	Mechanical efficiency	η_m	0.998	-
Turbine	Isentropic efficiency	η_{is}	0.829	-
	Pressure ratio	Π	4.75	-
	Mechanical efficiency	η_m	0.998	-
Power turbine	Isentropic efficiency	η_{is}	0.829	-
	Pressure ratio	Π	2.95	-
	Mechanical efficiency	η_m	0.998	-
Generator	Generator efficiency	η_{gen}	0.96	-
Pumps	Isentropic efficiency	η_{is}	0.85	-
	Mechanical efficiency	η_m	0.8	-
Overall	Power output	P_{out}	12.3	MW
	Energy consumption	E_{in}	12179.8	kJ/kWh
	Exhaust temperature	T_{exh}	440.2	°C

Table D.29: CT parameters for the MeOH-fuelled GT model at 30% load

Component	Parameter		CT Value	
Compressor	Isentropic efficiency	η_{is}	0.84	-
	Pressure ratio	Π	12.61	-
	Mechanical efficiency	η_m	0.998	-
Turbine	Isentropic efficiency	η_{is}	0.817	-
	Pressure ratio	Π	4.94	-
	Mechanical efficiency	η_m	0.998	-
Power turbine	Isentropic efficiency	η_{is}	0.817	-
	Pressure ratio	Π	2.58	-
	Mechanical efficiency	η_m	0.998	-
Generator	Generator efficiency	η_{gen}	0.95	-
Pumps	Isentropic efficiency	η_{is}	0.85	-
	Mechanical efficiency	η_m	0.8	-
Overall	Power output	P_{out}	9.1	MW
	Energy consumption	E_{in}	13746.2	kJ/kWh
	Exhaust temperature	T_{exh}	434.6	°C

Table D.30: CT parameters for the MeOH-fuelled GT model at 20% load

Component	Parameter		CT Value	
Compressor	Isentropic efficiency	η_{is}	0.82	-
	Pressure ratio	Π	10.62	-
	Mechanical efficiency	η_m	0.998	-
Turbine	Isentropic efficiency	η_{is}	0.79	-
	Pressure ratio	Π	5.04	-
	Mechanical efficiency	η_m	0.998	-
Power turbine	Isentropic efficiency	η_{is}	0.79	-
	Pressure ratio	Π	2.04	-
	Mechanical efficiency	η_m	0.998	-
Generator	Generator efficiency	η_{gen}	0.93	-
Pumps	Isentropic efficiency	η_{is}	0.85	-
	Mechanical efficiency	η_m	0.8	-
Overall	Power output	P_{out}	6.0	MW
	Energy consumption	E_{in}	17912.5	kJ/kWh
	Exhaust temperature	T_{exh}	423.3	°C

Table D.31: CT parameters for the MeOH-fuelled GT model at 10% load

Component	Parameter		CT Value	
Compressor	Isentropic efficiency	η_{is}	0.79	-
	Pressure ratio	Π	8.38	-
	Mechanical efficiency	η_m	0.998	-
Turbine	Isentropic efficiency	η_{is}	0.72	-
	Pressure ratio	Π	6.38	-
	Mechanical efficiency	η_m	0.998	-
Power turbine	Isentropic efficiency	η_{is}	0.72	-
	Pressure ratio	Π	1.27	-
	Mechanical efficiency	η_m	0.998	-
Generator	Generator efficiency	η_{gen}	0.874	-
Pumps	Isentropic efficiency	η_{is}	0.85	-
	Mechanical efficiency	η_m	0.8	-
Overall	Power output	P_{out}	2.8	MW
	Energy consumption	E_{in}	53364.8	kJ/kWh
	Exhaust temperature	T_{exh}	407.0	°C

D.3. SOFC models

In this section, the parameters for the different components in the CT models for the SOFC are given. First, the parameters for diesel operation are given. This is followed by the MeOH operation.

D.3.1. Diesel

In the tables below, the parameters for the SOFC model running on diesel for 100% load, 96% load, 80% load and 75% load.

Table D.32: CT parameters for the diesel-fuelled SOFC model at 100% load

Component	Parameter		CT Value		Reference value		Reference
SOFC	Fuel utilization factor	u_f	0.8	-	0.8	-	[71]
	Cell voltage	V_{cell}	0.85	V	0.85	V	[74]
	Stack temperature	T_{stack}	750	°C	750	°C	[74]
	Inlet temperature	T_{in}	700	°C	$T_{stack}-75$ - $T_{stack}-40$	°C	[19, 71]
	Outlet temperature	T_{out}	790	°C	$T_{stack}+25$ - $T_{stack}+40$	°C	[19, 71]
	Anode pressure drop	Δp_{an}	0.02	bar	0.02	bar	[71]
	Cathode pressure drop	Δp_{ca}	0.02	bar	0.015	bar	[71]
Fuel reformer	Reformer temperature	T_{reform}	600	°C	600	°C	[84]
	Steam to carbon ratio	S/C	2	kmol/kmol	2	kmol/kmol	[85]
	Steam to fuel ratio	S/F	2.61	kg/kg	-	-	-
	Pressure drop	Δp	0.01	bar	0.01	bar	[71]
Heat exchangers	Pressure drop	Δp	0.01	bar	0.01	bar	[71]
Pumps	Isentropic efficiency	η_{is}	0.85	-	0.7-0.85	-	[19, 71]
	Mechanical efficiency	η_m	0.8	-	0.6-0.9	-	[19, 71]
Blowers	Isentropic efficiency	η_{is}	0.85	-	0.7-0.85	-	[19, 71]
	Mechanical efficiency	η_m	0.8	-	0.6-0.9	-	[19, 71]

Table D.33: CT parameters for the diesel-fuelled SOFC model at 96% load

Component	Parameter		CT Value		Reference value		Reference
SOFC	Fuel utilization factor	u_f	0.8	-	0.8	-	[71]
	Cell voltage	V_{cell}	0.86	V	0.86	V	[74]
	Stack temperature	T_{stack}	750	°C	750	°C	[74]
	Inlet temperature	T_{in}	700	°C	$T_{stack}-75$ - $T_{stack}-40$	°C	[19, 71]
	Outlet temperature	T_{out}	790	°C	$T_{stack}+25$ - $T_{stack}+40$	°C	[19, 71]
	Anode pressure drop	Δp_{an}	0.02	bar	0.02	bar	[71]
	Cathode pressure drop	Δp_{ca}	0.02	bar	0.015	bar	[71]
Fuel reformer	Reformer temperature	T_{reform}	600	°C	600	°C	[84]
	Steam to carbon ratio	S/C	2	kmol/kmol	2	kmol/kmol	[85]
	Steam to fuel ratio	S/F	2.61	kg/kg	-	-	-
	Pressure drop	Δp	0.01	bar	0.01	bar	[71]
Heat exchangers	Pressure drop	Δp	0.01	bar	0.01	bar	[71]
Pumps	Isentropic efficiency	η_{is}	0.85	-	0.7-0.85	-	[19, 71]
	Mechanical efficiency	η_m	0.8	-	0.6-0.9	-	[19, 71]
Blowers	Isentropic efficiency	η_{is}	0.85	-	0.7-0.85	-	[19, 71]
	Mechanical efficiency	η_m	0.8	-	0.6-0.9	-	[19, 71]

Table D.34: CT parameters for the diesel-fuelled SOFC model at 80% load

Component	Parameter		CT Value		Reference value		Reference
SOFC	Fuel utilization factor	u_f	0.8	-	0.8	-	[71]
	Cell voltage	V_{cell}	0.89	V	0.89	V	[74]
	Stack temperature	T_{stack}	750	°C	750	°C	[74]
	Inlet temperature	T_{in}	700	°C	$T_{stack} - 75$ - $T_{stack} - 40$	°C	[19, 71]
	Outlet temperature	T_{out}	790	°C	$T_{stack} + 25$ - $T_{stack} + 40$	°C	[19, 71]
	Anode pressure drop	Δp_{an}	0.02	bar	0.02	bar	[71]
	Cathode pressure drop	Δp_{ca}	0.02	bar	0.015	bar	[71]
Fuel reformer	Reformer temperature	T_{reform}	600	°C	600	°C	[84]
	Steam to carbon ratio	S/C	2	kmol/kmol	2	kmol/kmol	[85]
	Steam to fuel ratio	S/F	2.61	kg/kg	-	-	-
	Pressure drop	Δp	0.01	bar	0.01	bar	[71]
Heat exchangers	Pressure drop	Δp	0.01	bar	0.01	bar	[71]
Pumps	Isentropic efficiency	η_{is}	0.85	-	0.7-0.85	-	[19, 71]
	Mechanical efficiency	η_m	0.8	-	0.6-0.9	-	[19, 71]
Blowers	Isentropic efficiency	η_{is}	0.85	-	0.7-0.85	-	[19, 71]
	Mechanical efficiency	η_m	0.8	-	0.6-0.9	-	[19, 71]

Table D.35: CT parameters for the diesel-fuelled SOFC model at 75% load

Component	Parameter		CT Value		Reference value		Reference
SOFC	Fuel utilization factor	u_f	0.8	-	0.8	-	[71]
	Cell voltage	V_{cell}	0.89	V	0.89	V	[74]
	Stack temperature	T_{stack}	750	°C	750	°C	[74]
	Inlet temperature	T_{in}	700	°C	$T_{stack} - 75$ - $T_{stack} - 40$	°C	[19, 71]
	Outlet temperature	T_{out}	790	°C	$T_{stack} + 25$ - $T_{stack} + 40$	°C	[19, 71]
	Anode pressure drop	Δp_{an}	0.02	bar	0.02	bar	[71]
	Cathode pressure drop	Δp_{ca}	0.02	bar	0.015	bar	[71]
Fuel reformer	Reformer temperature	T_{reform}	600	°C	600	°C	[84]
	Steam to carbon ratio	S/C	2	kmol/kmol	2	kmol/kmol	[85]
	Steam to fuel ratio	S/F	2.61	kg/kg	-	-	-
	Pressure drop	Δp	0.01	bar	0.01	bar	[71]
Heat exchangers	Pressure drop	Δp	0.01	bar	0.01	bar	[71]
Pumps	Isentropic efficiency	η_{is}	0.85	-	0.7-0.85	-	[19, 71]
	Mechanical efficiency	η_m	0.8	-	0.6-0.9	-	[19, 71]
Blowers	Isentropic efficiency	η_{is}	0.85	-	0.7-0.85	-	[19, 71]
	Mechanical efficiency	η_m	0.8	-	0.6-0.9	-	[19, 71]

D.3.2. Methanol

In the tables below, the parameters for the SOFC model running on MeOH for 100% load, 96% load, 80% load and 75% load.

Table D.36: CT parameters for the MeOH-fuelled SOFC model at 100% load

Component	Parameter		CT Value		Reference value		Reference
SOFC	Fuel utilization factor	u_f	0.8	-	0.8	-	[71]
	Cell voltage	V_{cell}	0.85	V	0.85	V	[74]
	Stack temperature	T_{stack}	750	°C	750	°C	[74]
	Inlet temperature	T_{in}	700	°C	$T_{stack} - 75$ - $T_{stack} - 40$	°C	[19, 71]
	Outlet temperature	T_{out}	790	°C	$T_{stack} + 25$ - $T_{stack} + 40$	°C	[19, 71]
	Anode pressure drop	Δp_{an}	0.02	bar	0.02	bar	[71]
	Cathode pressure drop	Δp_{ca}	0.02	bar	0.015	bar	[71]
Fuel reformer	Reformer temperature	T_{reform}	600	°C	-	-	-
	Steam to carbon ratio	S/C	1.2	kmol/kmol	1.2	kmol/kmol	[98]
	Steam to fuel ratio	S/F	0.68	kg/kg	-	-	-
	Pressure drop	Δp	0.01	bar	0.01	bar	[71]
Heat exchangers	Pressure drop	Δp	0.01	bar	0.01	bar	[71]
Pumps	Isentropic efficiency	η_{is}	0.85	-	0.7-0.85	-	[19, 71]
	Mechanical efficiency	η_m	0.8	-	0.6-0.9	-	[19, 71]
Blowers	Isentropic efficiency	η_{is}	0.85	-	0.7-0.85	-	[19, 71]
	Mechanical efficiency	η_m	0.8	-	0.6-0.9	-	[19, 71]

Table D.37: CT parameters for the MeOH-fuelled SOFC model at 96% load

Component	Parameter		CT Value		Reference value		Reference
SOFC	Fuel utilization factor	u_f	0.8	-	0.8	-	[71]
	Cell voltage	V_{cell}	0.86	V	0.86	V	[74]
	Stack temperature	T_{stack}	750	°C	750	°C	[74]
	Inlet temperature	T_{in}	700	°C	$T_{stack} - 75$ - $T_{stack} - 40$	°C	[19, 71]
	Outlet temperature	T_{out}	790	°C	$T_{stack} + 25$ - $T_{stack} + 40$	°C	[19, 71]
	Anode pressure drop	Δp_{an}	0.02	bar	0.02	bar	[71]
	Cathode pressure drop	Δp_{ca}	0.02	bar	0.015	bar	[71]
Fuel reformer	Reformer temperature	T_{reform}	600	°C	-	-	-
	Steam to carbon ratio	S/C	1.2	kmol/kmol	1.2	kmol/kmol	[98]
	Steam to fuel ratio	S/F	0.68	kg/kg	-	-	-
	Pressure drop	Δp	0.01	bar	0.01	bar	[71]
Heat exchangers	Pressure drop	Δp	0.01	bar	0.01	bar	[71]
Pumps	Isentropic efficiency	η_{is}	0.85	-	0.7-0.85	-	[19, 71]
	Mechanical efficiency	η_m	0.8	-	0.6-0.9	-	[19, 71]
Blowers	Isentropic efficiency	η_{is}	0.85	-	0.7-0.85	-	[19, 71]
	Mechanical efficiency	η_m	0.8	-	0.6-0.9	-	[19, 71]

Table D.38: CT parameters for the MeOH-fuelled SOFC model at 80% load

Component	Parameter		CT Value		Reference value		Reference
SOFC	Fuel utilization factor	u_f	0.8	-	0.8	-	[71]
	Cell voltage	V_{cell}	0.89	V	0.89	V	[74]
	Stack temperature	T_{stack}	750	°C	750	°C	[74]
	Inlet temperature	T_{in}	700	°C	$T_{stack} - 75$ - $T_{stack} - 40$	°C	[19, 71]
	Outlet temperature	T_{out}	790	°C	$T_{stack} + 25$ - $T_{stack} + 40$	°C	[19, 71]
	Anode pressure drop	Δp_{an}	0.02	bar	0.02	bar	[71]
	Cathode pressure drop	Δp_{ca}	0.02	bar	0.015	bar	[71]
Fuel reformer	Reformer temperature	T_{reform}	600	°C	-	-	-
	Steam to carbon ratio	S/C	1.2	kmol/kmol	1.22	kmol/kmol	[98]
	Steam to fuel ratio	S/F	0.68	kg/kg	-	-	-
	Pressure drop	Δp	0.01	bar	0.01	bar	[71]
Heat exchangers	Pressure drop	Δp	0.01	bar	0.01	bar	[71]
Pumps	Isentropic efficiency	η_{is}	0.85	-	0.7-0.85	-	[19, 71]
	Mechanical efficiency	η_m	0.8	-	0.6-0.9	-	[19, 71]
Blowers	Isentropic efficiency	η_{is}	0.85	-	0.7-0.85	-	[19, 71]
	Mechanical efficiency	η_m	0.8	-	0.6-0.9	-	[19, 71]

Table D.39: CT parameters for the MeOH-fuelled SOFC model at 75% load

Component	Parameter		CT Value		Reference value		Reference
SOFC	Fuel utilization factor	u_f	0.8	-	0.8	-	[71]
	Cell voltage	V_{cell}	0.89	V	0.89	V	[74]
	Stack temperature	T_{stack}	750	°C	750	°C	[74]
	Inlet temperature	T_{in}	700	°C	$T_{stack} - 75$ - $T_{stack} - 40$	°C	[19, 71]
	Outlet temperature	T_{out}	790	°C	$T_{stack} + 25$ - $T_{stack} + 40$	°C	[19, 71]
	Anode pressure drop	Δp_{an}	0.02	bar	0.02	bar	[71]
	Cathode pressure drop	Δp_{ca}	0.02	bar	0.015	bar	[71]
Fuel reformer	Reformer temperature	T_{reform}	600	°C	-	-	-
	Steam to carbon ratio	S/C	1.2	kmol/kmol	1.2	kmol/kmol	[98]
	Steam to fuel ratio	S/F	0.68	kg/kg	-	-	-
	Pressure drop	Δp	0.01	bar	0.01	bar	[71]
Heat exchangers	Pressure drop	Δp	0.01	bar	0.01	bar	[71]
Pumps	Isentropic efficiency	η_{is}	0.85	-	0.7-0.85	-	[19, 71]
	Mechanical efficiency	η_m	0.8	-	0.6-0.9	-	[19, 71]
Blowers	Isentropic efficiency	η_{is}	0.85	-	0.7-0.85	-	[19, 71]
	Mechanical efficiency	η_m	0.8	-	0.6-0.9	-	[19, 71]

D.4. SOFC-ICE models

In this section, the parameters for the SOFC-ICE models are given. First, the parameters for silent speed, cruising speed and top speed for the diesel-fuelled models are given. Next, the same parameters are given for the MeOH-fuelled models.

D.4.1. Diesel

The parameters for silent operation are given in Table D.40. Next, Table D.41 to Table D.52 show the parameters for cruising speed. Lastly, Table D.53 to Table D.58 show the parameters for top speed.

Table D.40: CT parameters for the diesel-fuelled SOFC-ICE model at silent speed

Component	Parameter		CT Value	
Turbocharger	Isentropic efficiency compressor	$\eta_{is,compr}$	0.79	-
	Pressure ratio compressor	Π_{compr}	4.752	-
	Mechanical efficiency compressor	$\eta_{m,compr}$	0.956	-
	Isentropic efficiency turbine	$\eta_{is,turb}$	0.855	-
	Pressure ratio turbine	Π_{turb}	3.468	-
	Mechanical efficiency turbine	$\eta_{m,turb}$	0.956	-
Intercooler	Pressure drop	Δp_{loss}	0.049	bar
	Temperature drop	ΔT	186	°C
Cylinder	Isentropic efficiency compressor	$\eta_{is,compr}$	1	-
	Pressure ratio compressor	Π_{compr}	37.41	-
	Mechanical efficiency compressor	$\eta_{m,compr}$	0.8568	-
	Air excess ratio combustor	λ	1.84	-
	Isentropic efficiency turbine	$\eta_{is,turb}$	1	-
	Pressure ratio turbine	Π_{turb}	49.29	-
	Mechanical efficiency turbine	$\eta_{m,turb}$	0.8568	-
Generator	Generator efficiency	η_{gen}	0.97	-
Pumps	Isentropic efficiency	η_{is}	0.85	-
	Mechanical efficiency	η_m	0.8	-
SOFC	Fuel utilization factor	u_f	0.8	-
	Cell voltage	V_{cell}	0.89	V
	Stack temperature	T_{stack}	750	°C
	Inlet temperature	T_{in}	700	°C
	Outlet temperature	T_{out}	790	°C
	Anode pressure drop	Δp_{an}	0.02	bar
	Cathode pressure drop	Δp_{ca}	0.02	bar
Fuel reformer	Reformer temperature	T_{reform}	600	°C
	Steam to fuel ratio	S/F	2.61	kg/kg
	Pressure drop	Δp	0.01	bar
Heat exchangers	Pressure drop	Δp	0.01	bar
Pumps	Isentropic efficiency	η_{is}	0.85	-
	Mechanical efficiency	η_m	0.8	-
Blowers	Isentropic efficiency	η_{is}	0.85	-
	Mechanical efficiency	η_m	0.8	-
Overall	AOG combustion	$\frac{m_{AOG,ICE}}{m_{AOG}}$	0	-
	Gross ICE power	$P_{out,ICE}$	0	MWe
	Gross SOFC power	$P_{out,SOFC}$	0.96	MWe
	Net system power output	P_{out}	0.80	MWe
	ICE load		0	%
	SOFC load		75	%
	Net electrical system efficiency	η_{sys}	54.07	%
	Exhaust temperature	T_{exh}	152.61	°C

Table D.41: CT parameters for the diesel-fuelled SOFC-ICE model at cruising speed for a power split of 4.6-95.4 and an SOFC load of 75%

Component	Parameter		CT Value	
Turbocharger	Isentropic efficiency compressor	$\eta_{is,compr}$	0.78	-
	Pressure ratio compressor	Π_{compr}	2.907	-
	Mechanical efficiency compressor	$\eta_{m,compr}$	0.9446	-
	Isentropic efficiency turbine	$\eta_{is,turb}$	0.97	-
	Pressure ratio turbine	Π_{turb}	2.172	-
	Mechanical efficiency turbine	$\eta_{m,turb}$	0.9446	-
Intercooler	Pressure drop	Δp_{loss}	0	bar
	Temperature drop	ΔT	120	°C
Cylinder	Isentropic efficiency compressor	$\eta_{is,compr}$	1	-
	Pressure ratio compressor	Π_{compr}	37.41	-
	Mechanical efficiency compressor	$\eta_{m,compr}$	0.851	-
	Air excess ratio combustor	λ	2.203	-
	Isentropic efficiency turbine	$\eta_{is,turb}$	1	-
	Pressure ratio turbine	Π_{turb}	49.29	-
	Mechanical efficiency turbine	$\eta_{m,turb}$	0.851	-
Generator	Generator efficiency	η_{gen}	0.97	-
Pumps	Isentropic efficiency	η_{is}	0.85	-
	Mechanical efficiency	η_m	0.8	-
SOFC	Fuel utilization factor	u_f	0.8	-
	Cell voltage	V_{cell}	0.89	V
	Stack temperature	T_{stack}	750	°C
	Inlet temperature	T_{in}	700	°C
	Outlet temperature	T_{out}	790	°C
	Anode pressure drop	Δp_{an}	0.02	bar
	Cathode pressure drop	Δp_{ca}	0.02	bar
Fuel reformer	Reformer temperature	T_{reform}	600	°C
	Steam to fuel ratio	S/F	2.61	kg/kg
	Pressure drop	Δp	0.01	bar
Heat exchangers	Pressure drop	Δp	0.01	bar
Pumps	Isentropic efficiency	η_{is}	0.85	-
	Mechanical efficiency	η_m	0.8	-
Blowers	Isentropic efficiency	η_{is}	0.85	-
	Mechanical efficiency	η_m	0.8	-
Overall	AOG combustion	$\frac{m_{AOG,ICE}}{m_{AOG}}$	1	-
	Gross ICE power	$P_{out,ICE}$	4.82	MWe
	Gross SOFC power	$P_{out,SOFC}$	0.96	MWe
	Net system power output	P_{out}	5.62	MWe
	ICE load		50	%
	SOFC load		75	%
	Net electrical system efficiency	η_{sys}	43.44	%
	Exhaust temperature	T_{exh}	289.34	°C

Table D.42: CT parameters for the diesel-fuelled SOFC-ICE model at cruising speed for a power split of 4.6-95.4 and an SOFC load of 100%

Component	Parameter		CT Value	
Turbocharger	Isentropic efficiency compressor	$\eta_{is,compr}$	0.78	-
	Pressure ratio compressor	Π_{compr}	2.907	-
	Mechanical efficiency compressor	$\eta_{m,compr}$	0.9446	-
	Isentropic efficiency turbine	$\eta_{is,turb}$	0.97	-
	Pressure ratio turbine	Π_{turb}	2.172	-
	Mechanical efficiency turbine	$\eta_{m,turb}$	0.9446	-
Intercooler	Pressure drop	Δp_{loss}	0	bar
	Temperature drop	ΔT	120	°C
Cylinder	Isentropic efficiency compressor	$\eta_{is,compr}$	1	-
	Pressure ratio compressor	Π_{compr}	37.41	-
	Mechanical efficiency compressor	$\eta_{m,compr}$	0.851	-
	Air excess ratio combustor	λ	2.19	-
	Isentropic efficiency turbine	$\eta_{is,turb}$	1	-
	Pressure ratio turbine	Π_{turb}	49.29	-
	Mechanical efficiency turbine	$\eta_{m,turb}$	0.851	-
Generator	Generator efficiency	η_{gen}	0.97	-
Pumps	Isentropic efficiency	η_{is}	0.89	-
	Mechanical efficiency	η_m	0.8	-
SOFC	Fuel utilization factor	u_f	0.8	-
	Cell voltage	V_{cell}	0.89	V
	Stack temperature	T_{stack}	750	°C
	Inlet temperature	T_{in}	700	°C
	Outlet temperature	T_{out}	790	°C
	Anode pressure drop	Δp_{an}	0.02	bar
	Cathode pressure drop	Δp_{ca}	0.02	bar
Fuel reformer	Reformer temperature	T_{reform}	600	°C
	Steam to fuel ratio	S/F	2.61	kg/kg
	Pressure drop	Δp	0.01	bar
Heat exchangers	Pressure drop	Δp	0.01	bar
Pumps	Isentropic efficiency	η_{is}	0.85	-
	Mechanical efficiency	η_m	0.8	-
Blowers	Isentropic efficiency	η_{is}	0.85	-
	Mechanical efficiency	η_m	0.8	-
Overall	AOG combustion	$\frac{m_{AOG,ICE}}{m_{AOG}}$	1	-
	Gross ICE power	$P_{out,ICE}$	4.58	MWe
	Gross SOFC power	$P_{out,SOFC}$	1.28	MWe
	Net system power output	P_{out}	5.61	MWe
	ICE load		50	%
	SOFC load		100	%
	Net electrical system efficiency	η_{sys}	43.96	%
	Exhaust temperature	T_{exh}	268.93	°C

Table D.43: CT parameters for the diesel-fuelled SOFC-ICE model at cruising speed for a power split of 10-90 and an SOFC load of 75%

Component	Parameter		CT Value	
Turbocharger	Isentropic efficiency compressor	$\eta_{is,compr}$	0.78	-
	Pressure ratio compressor	Π_{compr}	2.907	-
	Mechanical efficiency compressor	$\eta_{m,compr}$	0.9446	-
	Isentropic efficiency turbine	$\eta_{is,turb}$	0.97	-
	Pressure ratio turbine	Π_{turb}	2.172	-
	Mechanical efficiency turbine	$\eta_{m,turb}$	0.9446	-
Intercooler	Pressure drop	Δp_{loss}	0	bar
	Temperature drop	ΔT	120	°C
Cylinder	Isentropic efficiency compressor	$\eta_{is,compr}$	1	-
	Pressure ratio compressor	Π_{compr}	37.41	-
	Mechanical efficiency compressor	$\eta_{m,compr}$	0.851	-
	Air excess ratio combustor	λ	2.203	-
	Isentropic efficiency turbine	$\eta_{is,turb}$	1	-
	Pressure ratio turbine	Π_{turb}	49.29	-
	Mechanical efficiency turbine	$\eta_{m,turb}$	0.851	-
Generator	Generator efficiency	η_{gen}	0.97	-
Pumps	Isentropic efficiency	η_{is}	0.85	-
	Mechanical efficiency	η_m	0.8	-
SOFC	Fuel utilization factor	u_f	0.8	-
	Cell voltage	V_{cell}	0.89	V
	Stack temperature	T_{stack}	750	°C
	Inlet temperature	T_{in}	700	°C
	Outlet temperature	T_{out}	790	°C
	Anode pressure drop	Δp_{an}	0.02	bar
	Cathode pressure drop	Δp_{ca}	0.02	bar
Fuel reformer	Reformer temperature	T_{reform}	600	°C
	Steam to fuel ratio	S/F	2.61	kg/kg
	Pressure drop	Δp	0.01	bar
Heat exchangers	Pressure drop	Δp	0.01	bar
Pumps	Isentropic efficiency	η_{is}	0.85	-
	Mechanical efficiency	η_m	0.8	-
Blowers	Isentropic efficiency	η_{is}	0.85	-
	Mechanical efficiency	η_m	0.8	-
Overall	AOG combustion	$\frac{m_{AOG,ICE}}{m_{AOG}}$	1	-
	Gross ICE power	$P_{out,ICE}$	3.85	MWe
	Gross SOFC power	$P_{out,SOFC}$	2.10	MWe
	Net system power output	P_{out}	5.61	MWe
	ICE load		50	%
	SOFC load		75	%
	Net electrical system efficiency	η_{sys}	47.33	%
	Exhaust temperature	T_{exh}	241.47	°C

Table D.44: CT parameters for the diesel-fuelled SOFC-ICE model at cruising speed for a power split of 10-90 and an SOFC load of 100%

Component	Parameter		CT Value	
Turbocharger	Isentropic efficiency compressor	$\eta_{is,compr}$	0.78	-
	Pressure ratio compressor	Π_{compr}	2.907	-
	Mechanical efficiency compressor	$\eta_{m,compr}$	0.9446	-
	Isentropic efficiency turbine	$\eta_{is,turb}$	0.97	-
	Pressure ratio turbine	Π_{turb}	2.172	-
	Mechanical efficiency turbine	$\eta_{m,turb}$	0.9446	-
Intercooler	Pressure drop	Δp_{loss}	0	bar
	Temperature drop	ΔT	120	°C
Cylinder	Isentropic efficiency compressor	$\eta_{is,compr}$	1	-
	Pressure ratio compressor	Π_{compr}	37.41	-
	Mechanical efficiency compressor	$\eta_{m,compr}$	0.851	-
	Air excess ratio combustor	λ	2.203	-
	Isentropic efficiency turbine	$\eta_{is,turb}$	1	-
	Pressure ratio turbine	Π_{turb}	49.29	-
	Mechanical efficiency turbine	$\eta_{m,turb}$	0.851	-
Generator	Generator efficiency	η_{gen}	0.97	-
Pumps	Isentropic efficiency	η_{is}	0.85	-
	Mechanical efficiency	η_m	0.8	-
SOFC	Fuel utilization factor	u_f	0.8	-
	Cell voltage	V_{cell}	0.85	V
	Stack temperature	T_{stack}	750	°C
	Inlet temperature	T_{in}	700	°C
	Outlet temperature	T_{out}	790	°C
	Anode pressure drop	Δp_{an}	0.02	bar
	Cathode pressure drop	Δp_{ca}	0.02	bar
Fuel reformer	Reformer temperature	T_{reform}	600	°C
	Steam to fuel ratio	S/F	2.61	kg/kg
	Pressure drop	Δp	0.01	bar
Heat exchangers	Pressure drop	Δp	0.01	bar
Pumps	Isentropic efficiency	η_{is}	0.89	-
	Mechanical efficiency	η_m	0.8	-
Blowers	Isentropic efficiency	η_{is}	0.85	-
	Mechanical efficiency	η_m	0.8	-
Overall	AOG combustion	$\frac{m_{AOG,ICE}}{m_{AOG}}$	1	-
	Gross ICE power	$P_{out,ICE}$	3.34	MWe
	Gross SOFC power	$P_{out,SOFC}$	2.80	MWe
	Net system power output	P_{out}	5.60	MWe
	ICE load		50	%
	SOFC load		100	%
	Net electrical system efficiency	η_{sys}	48.40	%
	Exhaust temperature	T_{exh}	209.94	°C

Table D.45: CT parameters for the diesel-fuelled SOFC-ICE model at cruising speed for a power split of 15-85 and an SOFC load of 75%

Component	Parameter		CT Value	
Turbocharger	Isentropic efficiency compressor	$\eta_{is,compr}$	0.7	-
	Pressure ratio compressor	Π_{compr}	2.234	-
	Mechanical efficiency compressor	$\eta_{m,compr}$	0.947	-
	Isentropic efficiency turbine	$\eta_{is,turb}$	0.93	-
	Pressure ratio turbine	Π_{turb}	1.994	-
	Mechanical efficiency turbine	$\eta_{m,turb}$	0.947	-
Intercooler	Pressure drop	Δp_{loss}	0	bar
	Temperature drop	ΔT	120	°C
Cylinder	Isentropic efficiency compressor	$\eta_{is,compr}$	1	-
	Pressure ratio compressor	Π_{compr}	37.41	-
	Mechanical efficiency compressor	$\eta_{m,compr}$	0.874	-
	Air excess ratio combustor	λ	2.70	-
	Isentropic efficiency turbine	$\eta_{is,turb}$	1	-
	Pressure ratio turbine	Π_{turb}	40.74	-
	Mechanical efficiency turbine	$\eta_{m,turb}$	0.879	-
Generator	Generator efficiency	η_{gen}	0.97	-
Pumps	Isentropic efficiency	η_{is}	0.85	-
	Mechanical efficiency	η_m	0.8	-
SOFC	Fuel utilization factor	u_f	0.8	-
	Cell voltage	V_{cell}	0.89	V
	Stack temperature	T_{stack}	750	°C
	Inlet temperature	T_{in}	700	°C
	Outlet temperature	T_{out}	790	°C
	Anode pressure drop	Δp_{an}	0.02	bar
	Cathode pressure drop	Δp_{ca}	0.02	bar
Fuel reformer	Reformer temperature	T_{reform}	600	°C
	Steam to fuel ratio	S/F	2.61	kg/kg
	Pressure drop	Δp	0.01	bar
Heat exchangers	Pressure drop	Δp	0.01	bar
Pumps	Isentropic efficiency	η_{is}	0.85	-
	Mechanical efficiency	η_m	0.8	-
Blowers	Isentropic efficiency	η_{is}	0.85	-
	Mechanical efficiency	η_m	0.8	-
Overall	AOG combustion	$\frac{m_{AOG,ICE}}{m_{AOG}}$	1	-
	Gross ICE power	$P_{out,ICE}$	2.96	MWe
	Gross SOFC power	$P_{out,SOFC}$	3.15	MWe
	Net system power output	P_{out}	5.60	MWe
	ICE load		25	%
	SOFC load		75	%
	Net electrical system efficiency	η_{sys}	51.83	%
	Exhaust temperature	T_{exh}	202.25	°C

Table D.46: CT parameters for the diesel-fuelled SOFC-ICE model at cruising speed for a power split of 15-85 and an SOFC load of 100%

Component	Parameter		CT Value	
Turbocharger	Isentropic efficiency compressor	$\eta_{is,compr}$	0.7	-
	Pressure ratio compressor	Π_{compr}	2.234	-
	Mechanical efficiency compressor	$\eta_{m,compr}$	0.947	-
	Isentropic efficiency turbine	$\eta_{is,turb}$	0.93	-
	Pressure ratio turbine	Π_{turb}	1.994	-
	Mechanical efficiency turbine	$\eta_{m,turb}$	0.947	-
Intercooler	Pressure drop	Δp_{loss}	0	bar
	Temperature drop	ΔT	120	°C
Cylinder	Isentropic efficiency compressor	$\eta_{is,compr}$	1	-
	Pressure ratio compressor	Π_{compr}	37.41	-
	Mechanical efficiency compressor	$\eta_{m,compr}$	0.874	-
	Air excess ratio combustor	λ	2.80	-
	Isentropic efficiency turbine	$\eta_{is,turb}$	1	-
	Pressure ratio turbine	Π_{turb}	40.74	-
	Mechanical efficiency turbine	$\eta_{m,turb}$	0.879	-
Generator	Generator efficiency	η_{gen}	0.97	-
Pumps	Isentropic efficiency	η_{is}	0.85	-
	Mechanical efficiency	η_m	0.8	-
SOFC	Fuel utilization factor	u_f	0.8	-
	Cell voltage	V_{cell}	0.85	V
	Stack temperature	T_{stack}	750	°C
	Inlet temperature	T_{in}	700	°C
	Outlet temperature	T_{out}	790	°C
	Anode pressure drop	Δp_{an}	0.02	bar
	Cathode pressure drop	Δp_{ca}	0.02	bar
Fuel reformer	Reformer temperature	T_{reform}	600	°C
	Steam to fuel ratio	S/F	2.61	kg/kg
	Pressure drop	Δp	0.01	bar
Heat exchangers	Pressure drop	Δp	0.01	bar
Pumps	Isentropic efficiency	η_{is}	0.85	-
	Mechanical efficiency	η_m	0.8	-
Blowers	Isentropic efficiency	η_{is}	0.85	-
	Mechanical efficiency	η_m	0.8	-
Overall	AOG combustion	$\frac{m_{AOG,ICE}}{m_{AOG}}$	1	-
	Gross ICE power	$P_{out,ICE}$	2.20	MWe
	Gross SOFC power	$P_{out,SOFC}$	4.21	MWe
	Net system power output	P_{out}	5.60	MWe
	ICE load		25	%
	SOFC load		75	%
	Net electrical system efficiency	η_{sys}	53.71	%
	Exhaust temperature	T_{exh}	171.81	°C

Table D.47: CT parameters for the diesel-fuelled SOFC-ICE model at cruising speed for a power split of 20-80 and an SOFC load of 75%

Component	Parameter		CT Value	
Turbocharger	Isentropic efficiency compressor	$\eta_{is,compr}$	0.7	-
	Pressure ratio compressor	Π_{compr}	2.234	-
	Mechanical efficiency compressor	$\eta_{m,compr}$	0.947	-
	Isentropic efficiency turbine	$\eta_{is,turb}$	0.93	-
	Pressure ratio turbine	Π_{turb}	1.994	-
	Mechanical efficiency turbine	$\eta_{m,turb}$	0.947	-
Intercooler	Pressure drop	Δp_{loss}	0	bar
	Temperature drop	ΔT	120	°C
Cylinder	Isentropic efficiency compressor	$\eta_{is,compr}$	1	-
	Pressure ratio compressor	Π_{compr}	37.41	-
	Mechanical efficiency compressor	$\eta_{m,compr}$	0.874	-
	Air excess ratio combustor	λ	2.80	-
	Isentropic efficiency turbine	$\eta_{is,turb}$	1	-
	Pressure ratio turbine	Π_{turb}	40.74	-
	Mechanical efficiency turbine	$\eta_{m,turb}$	0.879	-
Generator	Generator efficiency	η_{gen}	0.97	-
Pumps	Isentropic efficiency	η_{is}	0.85	-
	Mechanical efficiency	η_m	0.8	-
SOFC	Fuel utilization factor	u_f	0.8	-
	Cell voltage	V_{cell}	0.89	V
	Stack temperature	T_{stack}	750	°C
	Inlet temperature	T_{in}	700	°C
	Outlet temperature	T_{out}	790	°C
	Anode pressure drop	Δp_{an}	0.02	bar
	Cathode pressure drop	Δp_{ca}	0.02	bar
Fuel reformer	Reformer temperature	T_{reform}	600	°C
	Steam to fuel ratio	S/F	2.61	kg/kg
	Pressure drop	Δp	0.01	bar
Heat exchangers	Pressure drop	Δp	0.01	bar
Pumps	Isentropic efficiency	η_{is}	0.85	-
	Mechanical efficiency	η_m	0.8	-
Blowers	Isentropic efficiency	η_{is}	0.85	-
	Mechanical efficiency	η_m	0.8	-
Overall	AOG combustion	$\frac{m_{AOG,ICE}}{m_{AOG}}$	1	-
	Gross ICE power	$P_{out,ICE}$	2.08	MWe
	Gross SOFC power	$P_{out,SOFC}$	4.20	MWe
	Net system power output	P_{out}	5.60	MWe
	ICE load		25	%
	SOFC load		75	%
	Net electrical system efficiency	η_{sys}	56.62	%
	Exhaust temperature	T_{exh}	173.01	°C

Table D.48: CT parameters for the diesel-fuelled SOFC-ICE model at cruising speed for a power split of 20-80 and an SOFC load of 100%

Component	Parameter		CT Value	
Turbocharger	Isentropic efficiency compressor	$\eta_{is,compr}$	0.7	-
	Pressure ratio compressor	Π_{compr}	2.234	-
	Mechanical efficiency compressor	$\eta_{m,compr}$	0.947	-
	Isentropic efficiency turbine	$\eta_{is,turb}$	0.93	-
	Pressure ratio turbine	Π_{turb}	1.994	-
	Mechanical efficiency turbine	$\eta_{m,turb}$	0.947	-
Intercooler	Pressure drop	Δp_{loss}	0	bar
	Temperature drop	ΔT	120	°C
Cylinder	Isentropic efficiency compressor	$\eta_{is,compr}$	1	-
	Pressure ratio compressor	Π_{compr}	37.41	-
	Mechanical efficiency compressor	$\eta_{m,compr}$	0.874	-
	Air excess ratio combustor	λ	2.70	-
	Isentropic efficiency turbine	$\eta_{is,turb}$	1	-
	Pressure ratio turbine	Π_{turb}	40.74	-
	Mechanical efficiency turbine	$\eta_{m,turb}$	0.879	-
Generator	Generator efficiency	η_{gen}	0.97	-
Pumps	Isentropic efficiency	η_{is}	0.85	-
	Mechanical efficiency	η_m	0.8	-
SOFC	Fuel utilization factor	u_f	0.8	-
	Cell voltage	V_{cell}	0.85	V
	Stack temperature	T_{stack}	750	°C
	Inlet temperature	T_{in}	700	°C
	Outlet temperature	T_{out}	790	°C
	Anode pressure drop	Δp_{an}	0.02	bar
	Cathode pressure drop	Δp_{ca}	0.02	bar
Fuel reformer	Reformer temperature	T_{reform}	600	°C
	Steam to fuel ratio	S/F	2.61	kg/kg
	Pressure drop	Δp	0.01	bar
Heat exchangers	Pressure drop	Δp	0.01	bar
Pumps	Isentropic efficiency	η_{is}	0.85	-
	Mechanical efficiency	η_m	0.8	-
Blowers	Isentropic efficiency	η_{is}	0.85	-
	Mechanical efficiency	η_m	0.8	-
Overall	AOG combustion	$\frac{m_{AOG,ICE}}{m_{AOG}}$	1	-
	Gross ICE power	$P_{out,ICE}$	1.09	MWe
	Gross SOFC power	$P_{out,SOFC}$	5.60	MWe
	Net system power output	P_{out}	5.61	MWe
	ICE load		25	%
	SOFC load		75	%
	Net electrical system efficiency	η_{sys}	59.43	%
	Exhaust temperature	T_{exh}	143.15	°C

Table D.49: CT parameters for the diesel-fuelled SOFC-ICE model at cruising speed for a power split of 25-75 and an SOFC load of 75%

Component	Parameter		CT Value	
Turbocharger	Isentropic efficiency compressor	$\eta_{is,compr}$	0.7	-
	Pressure ratio compressor	Π_{compr}	2.234	-
	Mechanical efficiency compressor	$\eta_{m,compr}$	0.947	-
	Isentropic efficiency turbine	$\eta_{is,turb}$	0.93	-
	Pressure ratio turbine	Π_{turb}	1.994	-
	Mechanical efficiency turbine	$\eta_{m,turb}$	0.947	-
Intercooler	Pressure drop	Δp_{loss}	0	bar
	Temperature drop	ΔT	120	°C
Cylinder	Isentropic efficiency compressor	$\eta_{is,compr}$	1	-
	Pressure ratio compressor	Π_{compr}	37.41	-
	Mechanical efficiency compressor	$\eta_{m,compr}$	0.874	-
	Air excess ratio combustor	λ	3.10	-
	Isentropic efficiency turbine	$\eta_{is,turb}$	1	-
	Pressure ratio turbine	Π_{turb}	40.74	-
	Mechanical efficiency turbine	$\eta_{m,turb}$	0.879	-
Generator	Generator efficiency	η_{gen}	0.97	-
Pumps	Isentropic efficiency	η_{is}	0.85	-
	Mechanical efficiency	η_m	0.8	-
SOFC	Fuel utilization factor	u_f	0.8	-
	Cell voltage	V_{cell}	0.89	V
	Stack temperature	T_{stack}	750	°C
	Inlet temperature	T_{in}	700	°C
	Outlet temperature	T_{out}	790	°C
	Anode pressure drop	Δp_{an}	0.02	bar
	Cathode pressure drop	Δp_{ca}	0.02	bar
Fuel reformer	Reformer temperature	T_{reform}	600	°C
	Steam to fuel ratio	S/F	2.61	kg/kg
	Pressure drop	Δp	0.01	bar
Heat exchangers	Pressure drop	Δp	0.01	bar
Pumps	Isentropic efficiency	η_{is}	0.85	-
	Mechanical efficiency	η_m	0.8	-
Blowers	Isentropic efficiency	η_{is}	0.85	-
	Mechanical efficiency	η_m	0.8	-
Overall	AOG combustion	$\frac{m_{AOG,ICE}}{m_{AOG}}$	1	-
	Gross ICE power	$P_{out,ICE}$	1.21	MWe
	Gross SOFC power	$P_{out,SOFC}$	5.25	MWe
	Net system power output	P_{out}	5.60	MWe
	ICE load		25	%
	SOFC load		75	%
	Net electrical system efficiency	η_{sys}	62.40	%
	Exhaust temperature	T_{exh}	147.17	°C

Table D.50: CT parameters for the diesel-fuelled SOFC-ICE model at cruising speed for a power split of 25-75 and an SOFC load of 100%

Component	Parameter		CT Value	
Turbocharger	Isentropic efficiency compressor	$\eta_{is,compr}$	0.7	-
	Pressure ratio compressor	Π_{compr}	2.234	-
	Mechanical efficiency compressor	$\eta_{m,compr}$	0.947	-
	Isentropic efficiency turbine	$\eta_{is,turb}$	0.93	-
	Pressure ratio turbine	Π_{turb}	1.994	-
	Mechanical efficiency turbine	$\eta_{m,turb}$	0.947	-
Intercooler	Pressure drop	Δp_{loss}	0	bar
	Temperature drop	ΔT	120	°C
Cylinder	Isentropic efficiency compressor	$\eta_{is,compr}$	1	-
	Pressure ratio compressor	Π_{compr}	37.41	-
	Mechanical efficiency compressor	$\eta_{m,compr}$	0.874	-
	Air excess ratio combustor	λ	2.70	-
	Isentropic efficiency turbine	$\eta_{is,turb}$	1	-
	Pressure ratio turbine	Π_{turb}	40.74	-
	Mechanical efficiency turbine	$\eta_{m,turb}$	0.879	-
Generator	Generator efficiency	η_{gen}	0.97	-
Pumps	Isentropic efficiency	η_{is}	0.85	-
	Mechanical efficiency	η_m	0.8	-
SOFC	Fuel utilization factor	u_f	0.8	-
	Cell voltage	V_{cell}	0.85	V
	Stack temperature	T_{stack}	750	°C
	Inlet temperature	T_{in}	700	°C
	Outlet temperature	T_{out}	790	°C
	Anode pressure drop	Δp_{an}	0.02	bar
	Cathode pressure drop	Δp_{ca}	0.02	bar
Fuel reformer	Reformer temperature	T_{reform}	600	°C
	Steam to fuel ratio	S/F	2.61	kg/kg
	Pressure drop	Δp	0.01	bar
Heat exchangers	Pressure drop	Δp	0.01	bar
Pumps	Isentropic efficiency	η_{is}	0.85	-
	Mechanical efficiency	η_m	0.8	-
Blowers	Isentropic efficiency	η_{is}	0.85	-
	Mechanical efficiency	η_m	0.8	-
Overall	AOG combustion	$\frac{m_{AOG,ICE}}{m_{AOG}}$	0	-
	Gross ICE power	$P_{out,ICE}$	0	MWe
	Gross SOFC power	$P_{out,SOFC}$	6.96	MWe
	Net system power output	P_{out}	5.60	MWe
	ICE load		0	%
	SOFC load		75	%
	Net electrical system efficiency	η_{sys}	50.72	%
	Exhaust temperature	T_{exh}	153.07	°C

Table D.51: CT parameters for the diesel-fuelled SOFC-ICE model at cruising speed for a power split of 30-70 and an SOFC load of 75%

Component	Parameter		CT Value	
Turbocharger	Isentropic efficiency compressor	$\eta_{is,compr}$	0.7	-
	Pressure ratio compressor	Π_{compr}	2.234	-
	Mechanical efficiency compressor	$\eta_{m,compr}$	0.947	-
	Isentropic efficiency turbine	$\eta_{is,turb}$	0.93	-
	Pressure ratio turbine	Π_{turb}	1.994	-
	Mechanical efficiency turbine	$\eta_{m,turb}$	0.947	-
Intercooler	Pressure drop	Δp_{loss}	0	bar
	Temperature drop	ΔT	120	°C
Cylinder	Isentropic efficiency compressor	$\eta_{is,compr}$	1	-
	Pressure ratio compressor	Π_{compr}	37.41	-
	Mechanical efficiency compressor	$\eta_{m,compr}$	0.874	-
	Air excess ratio combustor	λ	2.65	-
	Isentropic efficiency turbine	$\eta_{is,turb}$	1	-
	Pressure ratio turbine	Π_{turb}	40.74	-
	Mechanical efficiency turbine	$\eta_{m,turb}$	0.879	-
Generator	Generator efficiency	η_{gen}	0.97	-
Pumps	Isentropic efficiency	η_{is}	0.85	-
	Mechanical efficiency	η_m	0.8	-
SOFC	Fuel utilization factor	u_f	0.8	-
	Cell voltage	V_{cell}	0.89	V
	Stack temperature	T_{stack}	750	°C
	Inlet temperature	T_{in}	700	°C
	Outlet temperature	T_{out}	790	°C
	Anode pressure drop	Δp_{an}	0.02	bar
	Cathode pressure drop	Δp_{ca}	0.02	bar
Fuel reformer	Reformer temperature	T_{reform}	600	°C
	Steam to fuel ratio	S/F	2.61	kg/kg
	Pressure drop	Δp	0.01	bar
Heat exchangers	Pressure drop	Δp	0.01	bar
Pumps	Isentropic efficiency	η_{is}	0.85	-
	Mechanical efficiency	η_m	0.8	-
Blowers	Isentropic efficiency	η_{is}	0.85	-
	Mechanical efficiency	η_m	0.8	-
Overall	AOG combustion	$\frac{m_{AOG,ICE}}{m_{AOG}}$	0.34	-
	Gross ICE power	$P_{out,ICE}$	0.35	MWe
	Gross SOFC power	$P_{out,SOFC}$	6.30	MWe
	Net system power output	P_{out}	5.60	MWe
	ICE load		25	%
	SOFC load		75	%
	Net electrical system efficiency	η_{sys}	57.96	%
	Exhaust temperature	T_{exh}	149.44	°C

Table D.52: CT parameters for the diesel-fuelled SOFC-ICE model at cruising speed for a power split of 30-70 and an SOFC load of 100%

Component	Parameter		CT Value	
Turbocharger	Isentropic efficiency compressor	$\eta_{is,compr}$	0.7	-
	Pressure ratio compressor	Π_{compr}	2.234	-
	Mechanical efficiency compressor	$\eta_{m,compr}$	0.947	-
	Isentropic efficiency turbine	$\eta_{is,turb}$	0.93	-
	Pressure ratio turbine	Π_{turb}	1.994	-
	Mechanical efficiency turbine	$\eta_{m,turb}$	0.947	-
Intercooler	Pressure drop	Δp_{loss}	0	bar
	Temperature drop	ΔT	120	°C
Cylinder	Isentropic efficiency compressor	$\eta_{is,compr}$	1	-
	Pressure ratio compressor	Π_{compr}	37.41	-
	Mechanical efficiency compressor	$\eta_{m,compr}$	0.874	-
	Air excess ratio combustor	λ	2.70	-
	Isentropic efficiency turbine	$\eta_{is,turb}$	1	-
	Pressure ratio turbine	Π_{turb}	40.74	-
	Mechanical efficiency turbine	$\eta_{m,turb}$	0.879	-
Generator	Generator efficiency	η_{gen}	0.97	-
Pumps	Isentropic efficiency	η_{is}	0.85	-
	Mechanical efficiency	η_m	0.8	-
SOFC	Fuel utilization factor	u_f	0.8	-
	Cell voltage	V_{cell}	0.89	V
	Stack temperature	T_{stack}	750	°C
	Inlet temperature	T_{in}	700	°C
	Outlet temperature	T_{out}	790	°C
	Anode pressure drop	Δp_{an}	0.02	bar
	Cathode pressure drop	Δp_{ca}	0.02	bar
Fuel reformer	Reformer temperature	T_{reform}	600	°C
	Steam to fuel ratio	S/F	2.61	kg/kg
	Pressure drop	Δp	0.01	bar
Heat exchangers	Pressure drop	Δp	0.01	bar
Pumps	Isentropic efficiency	η_{is}	0.85	-
	Mechanical efficiency	η_m	0.8	-
Blowers	Isentropic efficiency	η_{is}	0.85	-
	Mechanical efficiency	η_m	0.8	-
Overall	AOG combustion	$\frac{m_{AOG,ICE}}{m_{AOG}}$	0	-
	Gross ICE power	$P_{out,ICE}$	0	MWe
	Gross SOFC power	$P_{out,SOFC}$	6.77	MWe
	Net system power output	P_{out}	5.60	MWe
	ICE load		0	%
	SOFC load		80	%
	Net electrical system efficiency	η_{sys}	54.02	%
	Exhaust temperature	T_{exh}	153.06	°C

Table D.53: CT parameters for the diesel-fuelled SOFC-ICE model at top speed for a power split of 4.6-95.4

Component	Parameter		CT Value	
Turbocharger	Isentropic efficiency compressor	$\eta_{is,compr}$	0.79	-
	Pressure ratio compressor	Π_{compr}	4.752	-
	Mechanical efficiency compressor	$\eta_{m,compr}$	0.956	-
	Isentropic efficiency turbine	$\eta_{is,turb}$	0.855	-
	Pressure ratio turbine	Π_{turb}	3.468	-
	Mechanical efficiency turbine	$\eta_{m,turb}$	0.956	-
Intercooler	Pressure drop	Δp_{loss}	0.049	bar
	Temperature drop	ΔT	186	°C
Cylinder	Isentropic efficiency compressor	$\eta_{is,compr}$	1	-
	Pressure ratio compressor	Π_{compr}	37.41	-
	Mechanical efficiency compressor	$\eta_{m,compr}$	0.8568	-
	Air excess ratio combustor	λ	1.825	-
	Isentropic efficiency turbine	$\eta_{is,turb}$	1	-
	Pressure ratio turbine	Π_{turb}	49.29	-
	Mechanical efficiency turbine	$\eta_{m,turb}$	0.8568	-
Generator	Generator efficiency	η_{gen}	0.97	-
Pumps	Isentropic efficiency	η_{is}	0.85	-
	Mechanical efficiency	η_m	0.8	-
SOFC	Fuel utilization factor	u_f	0.8	-
	Cell voltage	V_{cell}	0.85	V
	Stack temperature	T_{stack}	750	°C
	Inlet temperature	T_{in}	700	°C
	Outlet temperature	T_{out}	790	°C
	Anode pressure drop	Δp_{an}	0.02	bar
	Cathode pressure drop	Δp_{ca}	0.02	bar
Fuel reformer	Reformer temperature	T_{reform}	600	°C
	Steam to fuel ratio	S/F	2.61	kg/kg
	Pressure drop	Δp	0.01	bar
Heat exchangers	Pressure drop	Δp	0.01	bar
Pumps	Isentropic efficiency	η_{is}	0.85	-
	Mechanical efficiency	η_m	0.8	-
Blowers	Isentropic efficiency	η_{is}	0.85	-
	Mechanical efficiency	η_m	0.8	-
Overall	AOG combustion	$\frac{m_{AOG,ICE}}{m_{AOG}}$	1	-
	Gross ICE power	$P_{out,ICE}$	22.30	MWe
	Gross SOFC power	$P_{out,SOFC}$	1.28	MWe
	Net system power output	P_{out}	23.31	MWe
	ICE load		100	%
	SOFC load		100	%
	Net electrical system efficiency	η_{sys}	43.42	%
	Exhaust temperature	T_{exh}	343.82	°C

Table D.54: CT parameters for the diesel-fuelled SOFC-ICE model at top speed for a power split of 10-90

Component	Parameter		CT Value	
Turbocharger	Isentropic efficiency compressor	$\eta_{is,compr}$	0.79	-
	Pressure ratio compressor	Π_{compr}	4.752	-
	Mechanical efficiency compressor	$\eta_{m,compr}$	0.956	-
	Isentropic efficiency turbine	$\eta_{is,turb}$	0.855	-
	Pressure ratio turbine	Π_{turb}	3.468	-
	Mechanical efficiency turbine	$\eta_{m,turb}$	0.956	-
Intercooler	Pressure drop	Δp_{loss}	0.049	bar
	Temperature drop	ΔT	186	°C
Cylinder	Isentropic efficiency compressor	$\eta_{is,compr}$	1	-
	Pressure ratio compressor	Π_{compr}	37.41	-
	Mechanical efficiency compressor	$\eta_{m,compr}$	0.8568	-
	Air excess ratio combustor	λ	1.83	-
	Isentropic efficiency turbine	$\eta_{is,turb}$	1	-
	Pressure ratio turbine	Π_{turb}	49.29	-
	Mechanical efficiency turbine	$\eta_{m,turb}$	0.8568	-
Generator	Generator efficiency	η_{gen}	0.97	-
Pumps	Isentropic efficiency	η_{is}	0.85	-
	Mechanical efficiency	η_m	0.8	-
SOFC	Fuel utilization factor	u_f	0.8	-
	Cell voltage	V_{cell}	0.85	V
	Stack temperature	T_{stack}	750	°C
	Inlet temperature	T_{in}	700	°C
	Outlet temperature	T_{out}	790	°C
	Anode pressure drop	Δp_{an}	0.02	bar
	Cathode pressure drop	Δp_{ca}	0.02	bar
Fuel reformer	Reformer temperature	T_{reform}	600	°C
	Steam to fuel ratio	S/F	2.61	kg/kg
	Pressure drop	Δp	0.01	bar
Heat exchangers	Pressure drop	Δp	0.01	bar
Pumps	Isentropic efficiency	η_{is}	0.85	-
	Mechanical efficiency	η_m	0.8	-
Blowers	Isentropic efficiency	η_{is}	0.85	-
	Mechanical efficiency	η_m	0.8	-
Overall	AOG combustion	$\frac{m_{AOG,ICE}}{m_{AOG}}$	1	-
	Gross ICE power	$P_{out,ICE}$	21.05	MWe
	Gross SOFC power	$P_{out,SOFC}$	2.80	MWe
	Net system power output	P_{out}	23.30	MWe
	ICE load		100	%
	SOFC load		100	%
	Net electrical system efficiency	η_{sys}	44.27	%
	Exhaust temperature	T_{exh}	314.60	°C

Table D.55: CT parameters for the diesel-fuelled SOFC-ICE model at top speed for a power split of 15-85

Component	Parameter		CT Value	
Turbocharger	Isentropic efficiency compressor	$\eta_{is,compr}$	0.79	-
	Pressure ratio compressor	Π_{compr}	4.752	-
	Mechanical efficiency compressor	$\eta_{m,compr}$	0.956	-
	Isentropic efficiency turbine	$\eta_{is,turb}$	0.855	-
	Pressure ratio turbine	Π_{turb}	3.468	-
	Mechanical efficiency turbine	$\eta_{m,turb}$	0.956	-
Intercooler	Pressure drop	Δp_{loss}	0.049	bar
	Temperature drop	ΔT	186	°C
Cylinder	Isentropic efficiency compressor	$\eta_{is,compr}$	1	-
	Pressure ratio compressor	Π_{compr}	37.41	-
	Mechanical efficiency compressor	$\eta_{m,compr}$	0.8568	-
	Air excess ratio combustor	λ	1.84	-
	Isentropic efficiency turbine	$\eta_{is,turb}$	1	-
	Pressure ratio turbine	Π_{turb}	49.29	-
	Mechanical efficiency turbine	$\eta_{m,turb}$	0.8568	-
Generator	Generator efficiency	η_{gen}	0.97	-
Pumps	Isentropic efficiency	η_{is}	0.85	-
	Mechanical efficiency	η_{m}	0.8	-
SOFC	Fuel utilization factor	u_f	0.8	-
	Cell voltage	V_{cell}	0.85	V
	Stack temperature	T_{stack}	750	°C
	Inlet temperature	T_{in}	700	°C
	Outlet temperature	T_{out}	790	°C
	Anode pressure drop	Δp_{an}	0.02	bar
	Cathode pressure drop	Δp_{ca}	0.02	bar
Fuel reformer	Reformer temperature	T_{reform}	600	°C
	Steam to fuel ratio	S/F	2.61	kg/kg
	Pressure drop	Δp	0.01	bar
Heat exchangers	Pressure drop	Δp	0.01	bar
Pumps	Isentropic efficiency	η_{is}	0.85	-
	Mechanical efficiency	η_{m}	0.8	-
Blowers	Isentropic efficiency	η_{is}	0.85	-
	Mechanical efficiency	η_{m}	0.8	-
Overall	AOG combustion	$\frac{m_{AOG,ICE}}{m_{AOG}}$	1	-
	Gross ICE power	$P_{out,ICE}$	19.93	MWe
	Gross SOFC power	$P_{out,SOFC}$	4.20	MWe
	Net system power output	P_{out}	23.30	MWe
	ICE load		100	%
	SOFC load		100	%
	Net electrical system efficiency	η_{sys}	45.05	%
	Exhaust temperature	T_{exh}	291.03	°C

Table D.56: CT parameters for the diesel-fuelled SOFC-ICE model at top speed for a power split of 20-80

Component	Parameter		CT Value	
Turbocharger	Isentropic efficiency compressor	$\eta_{is,compr}$	0.79	-
	Pressure ratio compressor	Π_{compr}	4.752	-
	Mechanical efficiency compressor	$\eta_{m,compr}$	0.956	-
	Isentropic efficiency turbine	$\eta_{is,turb}$	0.855	-
	Pressure ratio turbine	Π_{turb}	3.468	-
	Mechanical efficiency turbine	$\eta_{m,turb}$	0.956	-
Intercooler	Pressure drop	Δp_{loss}	0.049	bar
	Temperature drop	ΔT	186	°C
Cylinder	Isentropic efficiency compressor	$\eta_{is,compr}$	1	-
	Pressure ratio compressor	Π_{compr}	37.41	-
	Mechanical efficiency compressor	$\eta_{m,compr}$	0.8568	-
	Air excess ratio combustor	λ	1.84	-
	Isentropic efficiency turbine	$\eta_{is,turb}$	1	-
	Pressure ratio turbine	Π_{turb}	49.29	-
	Mechanical efficiency turbine	$\eta_{m,turb}$	0.8568	-
Generator	Generator efficiency	η_{gen}	0.97	-
Pumps	Isentropic efficiency	η_{is}	0.85	-
	Mechanical efficiency	η_m	0.8	-
SOFC	Fuel utilization factor	u_f	0.8	-
	Cell voltage	V_{cell}	0.85	V
	Stack temperature	T_{stack}	750	°C
	Inlet temperature	T_{in}	700	°C
	Outlet temperature	T_{out}	790	°C
	Anode pressure drop	Δp_{an}	0.02	bar
	Cathode pressure drop	Δp_{ca}	0.02	bar
Fuel reformer	Reformer temperature	T_{reform}	600	°C
	Steam to fuel ratio	S/F	2.61	kg/kg
	Pressure drop	Δp	0.01	bar
Heat exchangers	Pressure drop	Δp	0.01	bar
Pumps	Isentropic efficiency	η_{is}	0.85	-
	Mechanical efficiency	η_m	0.8	-
Blowers	Isentropic efficiency	η_{is}	0.85	-
	Mechanical efficiency	η_m	0.8	-
Overall	AOG combustion	$\frac{m_{AOG,ICE}}{m_{AOG}}$	1	-
	Gross ICE power	$P_{out,ICE}$	18.79	MWe
	Gross SOFC power	$P_{out,SOFC}$	5.60	MWe
	Net system power output	P_{out}	23.31	MWe
	ICE load		100	%
	SOFC load		100	%
	Net electrical system efficiency	η_{sys}	45.93	%
	Exhaust temperature	T_{exh}	271.82	°C

Table D.57: CT parameters for the diesel-fuelled SOFC-ICE model at top speed for a power split of 25-75

Component	Parameter		CT Value	
Turbocharger	Isentropic efficiency compressor	$\eta_{is,compr}$	0.79	-
	Pressure ratio compressor	Π_{compr}	4.752	-
	Mechanical efficiency compressor	$\eta_{m,compr}$	0.956	-
	Isentropic efficiency turbine	$\eta_{is,turb}$	0.855	-
	Pressure ratio turbine	Π_{turb}	3.468	-
	Mechanical efficiency turbine	$\eta_{m,turb}$	0.956	-
Intercooler	Pressure drop	Δp_{loss}	0.049	bar
	Temperature drop	ΔT	186	°C
Cylinder	Isentropic efficiency compressor	$\eta_{is,compr}$	1	-
	Pressure ratio compressor	Π_{compr}	37.41	-
	Mechanical efficiency compressor	$\eta_{m,compr}$	0.8568	-
	Air excess ratio combustor	λ	1.85	-
	Isentropic efficiency turbine	$\eta_{is,turb}$	1	-
	Pressure ratio turbine	Π_{turb}	49.29	-
	Mechanical efficiency turbine	$\eta_{m,turb}$	0.8568	-
Generator	Generator efficiency	η_{gen}	0.97	-
Pumps	Isentropic efficiency	η_{is}	0.85	-
	Mechanical efficiency	η_m	0.8	-
SOFC	Fuel utilization factor	u_f	0.8	-
	Cell voltage	V_{cell}	0.85	V
	Stack temperature	T_{stack}	750	°C
	Inlet temperature	T_{in}	700	°C
	Outlet temperature	T_{out}	790	°C
	Anode pressure drop	Δp_{an}	0.02	bar
	Cathode pressure drop	Δp_{ca}	0.02	bar
Fuel reformer	Reformer temperature	T_{reform}	600	°C
	Steam to fuel ratio	S/F	2.61	kg/kg
	Pressure drop	Δp	0.01	bar
Heat exchangers	Pressure drop	Δp	0.01	bar
Pumps	Isentropic efficiency	η_{is}	0.85	-
	Mechanical efficiency	η_m	0.8	-
Blowers	Isentropic efficiency	η_{is}	0.85	-
	Mechanical efficiency	η_m	0.8	-
Overall	AOG combustion	$\frac{m_{AOG,ICE}}{m_{AOG}}$	1	-
	Gross ICE power	$P_{out,ICE}$	17.66	MWe
	Gross SOFC power	$P_{out,SOFC}$	7.00	MWe
	Net system power output	P_{out}	23.30	MWe
	ICE load		100	%
	SOFC load		100	%
	Net electrical system efficiency	η_{sys}	46.78	%
	Exhaust temperature	T_{exh}	253.99	°C

Table D.58: CT parameters for the diesel-fuelled SOFC-ICE model at top speed for a power split of 30-70

Component	Parameter		CT Value	
Turbocharger	Isentropic efficiency compressor	$\eta_{is,compr}$	0.79	-
	Pressure ratio compressor	Π_{compr}	4.752	-
	Mechanical efficiency compressor	$\eta_{m,compr}$	0.956	-
	Isentropic efficiency turbine	$\eta_{is,turb}$	0.855	-
	Pressure ratio turbine	Π_{turb}	3.468	-
	Mechanical efficiency turbine	$\eta_{m,turb}$	0.956	-
Intercooler	Pressure drop	Δp_{loss}	0.049	bar
	Temperature drop	ΔT	186	°C
Cylinder	Isentropic efficiency compressor	$\eta_{is,compr}$	1	-
	Pressure ratio compressor	Π_{compr}	37.41	-
	Mechanical efficiency compressor	$\eta_{m,compr}$	0.8568	-
	Air excess ratio combustor	λ	1.86	-
	Isentropic efficiency turbine	$\eta_{is,turb}$	1	-
	Pressure ratio turbine	Π_{turb}	49.29	-
	Mechanical efficiency turbine	$\eta_{m,turb}$	0.8568	-
Generator	Generator efficiency	η_{gen}	0.97	-
Pumps	Isentropic efficiency	η_{is}	0.85	-
	Mechanical efficiency	η_m	0.8	-
SOFC	Fuel utilization factor	u_f	0.8	-
	Cell voltage	V_{cell}	0.85	V
	Stack temperature	T_{stack}	750	°C
	Inlet temperature	T_{in}	700	°C
	Outlet temperature	T_{out}	790	°C
	Anode pressure drop	Δp_{an}	0.02	bar
	Cathode pressure drop	Δp_{ca}	0.02	bar
Fuel reformer	Reformer temperature	T_{reform}	600	°C
	Steam to fuel ratio	S/F	2.61	kg/kg
	Pressure drop	Δp	0.01	bar
Heat exchangers	Pressure drop	Δp	0.01	bar
Pumps	Isentropic efficiency	η_{is}	0.85	-
	Mechanical efficiency	η_m	0.8	-
Blowers	Isentropic efficiency	η_{is}	0.85	-
	Mechanical efficiency	η_m	0.8	-
Overall	AOG combustion	$\frac{m_{AOG,ICE}}{m_{AOG}}$	1	-
	Gross ICE power	$P_{out,ICE}$	16.53	MWe
	Gross SOFC power	$P_{out,SOFC}$	8.40	MWe
	Net system power output	P_{out}	23.30	MWe
	ICE load		100	%
	SOFC load		100	%
	Net electrical system efficiency	η_{sys}	47.67	%
	Exhaust temperature	T_{exh}	238.38	°C

D.4.2. Methanol

The parameters for silent operation are given in Table D.59. Next, Table D.60 to Table D.71 show the parameters for cruising speed. Lastly, Table D.72 to Table D.77 show the parameters for top speed.

Table D.59: CT parameters for the MeOH-fuelled SOFC-ICE model at silent speed

Component	Parameter		CT Value	
Turbocharger	Isentropic efficiency compressor	$\eta_{is,compr}$	0.79	-
	Pressure ratio compressor	Π_{compr}	4.752	-
	Mechanical efficiency compressor	$\eta_{m,compr}$	0.956	-
	Isentropic efficiency turbine	$\eta_{is,turb}$	0.855	-
	Pressure ratio turbine	Π_{turb}	3.468	-
	Mechanical efficiency turbine	$\eta_{m,turb}$	0.956	-
Intercooler	Pressure drop	Δp_{loss}	0.049	bar
	Temperature drop	ΔT	186	°C
Cylinder	Isentropic efficiency compressor	$\eta_{is,compr}$	1	-
	Pressure ratio compressor	Π_{compr}	37.41	-
	Mechanical efficiency compressor	$\eta_{m,compr}$	0.8568	-
	Air excess ratio combustor	λ	1.84	-
	Isentropic efficiency turbine	$\eta_{is,turb}$	1	-
	Pressure ratio turbine	Π_{turb}	49.29	-
	Mechanical efficiency turbine	$\eta_{m,turb}$	0.8568	-
Generator	Generator efficiency	η_{gen}	0.97	-
Pumps	Isentropic efficiency	η_{is}	0.85	-
	Mechanical efficiency	η_m	0.8	-
SOFC	Fuel utilization factor	u_f	0.8	-
	Cell voltage	V_{cell}	0.89	V
	Stack temperature	T_{stack}	750	°C
	Inlet temperature	T_{in}	700	°C
	Outlet temperature	T_{out}	790	°C
	Anode pressure drop	Δp_{an}	0.02	bar
	Cathode pressure drop	Δp_{ca}	0.02	bar
Fuel reformer	Reformer temperature	T_{reform}	600	°C
	Steam to fuel ratio	S/F	0.68	kg/kg
	Pressure drop	Δp	0.01	bar
Heat exchangers	Pressure drop	Δp	0.01	bar
Pumps	Isentropic efficiency	η_{is}	0.85	-
	Mechanical efficiency	η_m	0.8	-
Blowers	Isentropic efficiency	η_{is}	0.85	-
	Mechanical efficiency	η_m	0.8	-
Overall	AOG combustion	$\frac{m_{AOG,ICE}}{m_{AOG}}$	0	-
	Gross ICE power	$P_{out,ICE}$	0	MWe
	Gross SOFC power	$P_{out,SOFC}$	0.97	MWe
	Net system power output	P_{out}	0.80	MWe
	ICE load		0	%
	SOFC load		75	%
	Net electrical system efficiency	η_{sys}	50.22	%
	Exhaust temperature	T_{exh}	208.22	°C

Table D.60: CT parameters for the MeOH-fuelled SOFC-ICE model at cruising speed for a power split of 4.6-95.4 and an SOFC load of 75%

Component	Parameter		CT Value	
Turbocharger	Isentropic efficiency compressor	$\eta_{is,compr}$	0.78	-
	Pressure ratio compressor	Π_{compr}	2.907	-
	Mechanical efficiency compressor	$\eta_{m,compr}$	0.9446	-
	Isentropic efficiency turbine	$\eta_{is,turb}$	0.97	-
	Pressure ratio turbine	Π_{turb}	2.172	-
	Mechanical efficiency turbine	$\eta_{m,turb}$	0.9446	-
Intercooler	Pressure drop	Δp_{loss}	0	bar
	Temperature drop	ΔT	120	°C
Cylinder	Isentropic efficiency compressor	$\eta_{is,compr}$	1	-
	Pressure ratio compressor	Π_{compr}	37.41	-
	Mechanical efficiency compressor	$\eta_{m,compr}$	0.851	-
	Air excess ratio combustor	λ	2.33	-
	Isentropic efficiency turbine	$\eta_{is,turb}$	1	-
	Pressure ratio turbine	Π_{turb}	49.29	-
	Mechanical efficiency turbine	$\eta_{m,turb}$	0.851	-
Generator	Generator efficiency	η_{gen}	0.97	-
Pumps	Isentropic efficiency	η_{is}	0.85	-
	Mechanical efficiency	η_{m}	0.8	-
SOFC	Fuel utilization factor	u_f	0.8	-
	Cell voltage	V_{cell}	0.89	V
	Stack temperature	T_{stack}	750	°C
	Inlet temperature	T_{in}	700	°C
	Outlet temperature	T_{out}	790	°C
	Anode pressure drop	Δp_{an}	0.02	bar
	Cathode pressure drop	Δp_{ca}	0.02	bar
Fuel reformer	Reformer temperature	T_{reform}	600	°C
	Steam to fuel ratio	S/F	0.68	kg/kg
	Pressure drop	Δp	0.01	bar
Heat exchangers	Pressure drop	Δp	0.01	bar
Pumps	Isentropic efficiency	η_{is}	0.85	-
	Mechanical efficiency	η_{m}	0.8	-
Blowers	Isentropic efficiency	η_{is}	0.85	-
	Mechanical efficiency	η_{m}	0.8	-
Overall	AOG combustion	$\frac{m_{AOG,ICE}}{m_{AOG}}$	1	-
	Gross ICE power	$P_{out,ICE}$	4.79	MWe
	Gross SOFC power	$P_{out,SOFC}$	0.97	MWe
	Net system power output	P_{out}	5.60	MWe
	ICE load		50	%
	SOFC load		75	%
	Net electrical system efficiency	η_{sys}	43.83	%
	Exhaust temperature	T_{exh}	285.63	°C

Table D.61: CT parameters for the MeOH-fuelled SOFC-ICE model at cruising speed for a power split of 4.6-95.4 and an SOFC load of 100%

Component	Parameter		CT Value	
Turbocharger	Isentropic efficiency compressor	$\eta_{is,compr}$	0.78	-
	Pressure ratio compressor	Π_{compr}	2.907	-
	Mechanical efficiency compressor	$\eta_{m,compr}$	0.9446	-
	Isentropic efficiency turbine	$\eta_{is,turb}$	0.97	-
	Pressure ratio turbine	Π_{turb}	2.172	-
	Mechanical efficiency turbine	$\eta_{m,turb}$	0.9446	-
Intercooler	Pressure drop	Δp_{loss}	0	bar
	Temperature drop	ΔT	120	°C
Cylinder	Isentropic efficiency compressor	$\eta_{is,compr}$	1	-
	Pressure ratio compressor	Π_{compr}	37.41	-
	Mechanical efficiency compressor	$\eta_{m,compr}$	0.851	-
	Air excess ratio combustor	λ	2.33	-
	Isentropic efficiency turbine	$\eta_{is,turb}$	1	-
	Pressure ratio turbine	Π_{turb}	49.29	-
	Mechanical efficiency turbine	$\eta_{m,turb}$	0.851	-
Generator	Generator efficiency	η_{gen}	0.97	-
Pumps	Isentropic efficiency	η_{is}	0.89	-
	Mechanical efficiency	η_m	0.8	-
SOFC	Fuel utilization factor	u_f	0.8	-
	Cell voltage	V_{cell}	0.89	V
	Stack temperature	T_{stack}	750	°C
	Inlet temperature	T_{in}	700	°C
	Outlet temperature	T_{out}	790	°C
	Anode pressure drop	Δp_{an}	0.02	bar
	Cathode pressure drop	Δp_{ca}	0.02	bar
Fuel reformer	Reformer temperature	T_{reform}	600	°C
	Steam to fuel ratio	S/F	0.68	kg/kg
	Pressure drop	Δp	0.01	bar
Heat exchangers	Pressure drop	Δp	0.01	bar
Pumps	Isentropic efficiency	η_{is}	0.85	-
	Mechanical efficiency	η_m	0.8	-
Blowers	Isentropic efficiency	η_{is}	0.85	-
	Mechanical efficiency	η_m	0.8	-
Overall	AOG combustion	$\frac{m_{AOG,ICE}}{m_{AOG}}$	1	-
	Gross ICE power	$P_{out,ICE}$	4.57	MWe
	Gross SOFC power	$P_{out,SOFC}$	1.29	MWe
	Net system power output	P_{out}	5.60	MWe
	ICE load		50	%
	SOFC load		100	%
	Net electrical system efficiency	η_{sys}	44.07	%
	Exhaust temperature	T_{exh}	271.42	°C

Table D.62: CT parameters for the MeOH-fuelled SOFC-ICE model at cruising speed for a power split of 10-90 and an SOFC load of 75%

Component	Parameter		CT Value	
Turbocharger	Isentropic efficiency compressor	$\eta_{is,compr}$	0.78	-
	Pressure ratio compressor	Π_{compr}	2.907	-
	Mechanical efficiency compressor	$\eta_{m,compr}$	0.9446	-
	Isentropic efficiency turbine	$\eta_{is,turb}$	0.97	-
	Pressure ratio turbine	Π_{turb}	2.172	-
	Mechanical efficiency turbine	$\eta_{m,turb}$	0.9446	-
Intercooler	Pressure drop	Δp_{loss}	0	bar
	Temperature drop	ΔT	120	°C
Cylinder	Isentropic efficiency compressor	$\eta_{is,compr}$	1	-
	Pressure ratio compressor	Π_{compr}	37.41	-
	Mechanical efficiency compressor	$\eta_{m,compr}$	0.851	-
	Air excess ratio combustor	λ	2.35	-
	Isentropic efficiency turbine	$\eta_{is,turb}$	1	-
	Pressure ratio turbine	Π_{turb}	49.29	-
	Mechanical efficiency turbine	$\eta_{m,turb}$	0.851	-
Generator	Generator efficiency	η_{gen}	0.97	-
Pumps	Isentropic efficiency	η_{is}	0.85	-
	Mechanical efficiency	η_m	0.8	-
SOFC	Fuel utilization factor	u_f	0.8	-
	Cell voltage	V_{cell}	0.89	V
	Stack temperature	T_{stack}	750	°C
	Inlet temperature	T_{in}	700	°C
	Outlet temperature	T_{out}	790	°C
	Anode pressure drop	Δp_{an}	0.02	bar
	Cathode pressure drop	Δp_{ca}	0.02	bar
Fuel reformer	Reformer temperature	T_{reform}	600	°C
	Steam to fuel ratio	S/F	0.68	kg/kg
	Pressure drop	Δp	0.01	bar
Heat exchangers	Pressure drop	Δp	0.01	bar
Pumps	Isentropic efficiency	η_{is}	0.85	-
	Mechanical efficiency	η_m	0.8	-
Blowers	Isentropic efficiency	η_{is}	0.85	-
	Mechanical efficiency	η_m	0.8	-
Overall	AOG combustion	$\frac{m_{AOG,ICE}}{m_{AOG}}$	1	-
	Gross ICE power	$P_{out,ICE}$	3.84	MWe
	Gross SOFC power	$P_{out,SOFC}$	2.12	MWe
	Net system power output	P_{out}	5.61	MWe
	ICE load		50	%
	SOFC load		75	%
	Net electrical system efficiency	η_{sys}	46.92	%
	Exhaust temperature	T_{exh}	257.50	°C

Table D.63: CT parameters for the MeOH-fuelled SOFC-ICE model at cruising speed for a power split of 10-90 and an SOFC load of 100%

Component	Parameter		CT Value	
Turbocharger	Isentropic efficiency compressor	$\eta_{is,compr}$	0.78	-
	Pressure ratio compressor	Π_{compr}	2.907	-
	Mechanical efficiency compressor	$\eta_{m,compr}$	0.9446	-
	Isentropic efficiency turbine	$\eta_{is,turb}$	0.97	-
	Pressure ratio turbine	Π_{turb}	2.172	-
	Mechanical efficiency turbine	$\eta_{m,turb}$	0.9446	-
Intercooler	Pressure drop	Δp_{loss}	0	bar
	Temperature drop	ΔT	120	°C
Cylinder	Isentropic efficiency compressor	$\eta_{is,compr}$	1	-
	Pressure ratio compressor	Π_{compr}	37.41	-
	Mechanical efficiency compressor	$\eta_{m,compr}$	0.851	-
	Air excess ratio combustor	λ	2.203	-
	Isentropic efficiency turbine	$\eta_{is,turb}$	1	-
	Pressure ratio turbine	Π_{turb}	49.29	-
	Mechanical efficiency turbine	$\eta_{m,turb}$	0.851	-
Generator	Generator efficiency	η_{gen}	0.97	-
Pumps	Isentropic efficiency	η_{is}	0.85	-
	Mechanical efficiency	η_m	0.8	-
SOFC	Fuel utilization factor	u_f	0.8	-
	Cell voltage	V_{cell}	0.85	V
	Stack temperature	T_{stack}	750	°C
	Inlet temperature	T_{in}	700	°C
	Outlet temperature	T_{out}	790	°C
	Anode pressure drop	Δp_{an}	0.02	bar
	Cathode pressure drop	Δp_{ca}	0.02	bar
Fuel reformer	Reformer temperature	T_{reform}	600	°C
	Steam to fuel ratio	S/F	0.68	kg/kg
	Pressure drop	Δp	0.01	bar
Heat exchangers	Pressure drop	Δp	0.01	bar
Pumps	Isentropic efficiency	η_{is}	0.89	-
	Mechanical efficiency	η_m	0.8	-
Blowers	Isentropic efficiency	η_{is}	0.85	-
	Mechanical efficiency	η_m	0.8	-
Overall	AOG combustion	$\frac{m_{AOG,ICE}}{m_{AOG}}$	1	-
	Gross ICE power	$P_{out,ICE}$	3.35	MWe
	Gross SOFC power	$P_{out,SOFC}$	2.82	MWe
	Net system power output	P_{out}	5.61	MWe
	ICE load		50	%
	SOFC load		100	%
	Net electrical system efficiency	η_{sys}	47.33	%
	Exhaust temperature	T_{exh}	234.84	°C

Table D.64: CT parameters for the MeOH-fuelled SOFC-ICE model at cruising speed for a power split of 15-85 and an SOFC load of 75%

Component	Parameter		CT Value	
Turbocharger	Isentropic efficiency compressor	$\eta_{is,compr}$	0.7	-
	Pressure ratio compressor	Π_{compr}	2.234	-
	Mechanical efficiency compressor	$\eta_{m,compr}$	0.947	-
	Isentropic efficiency turbine	$\eta_{is,turb}$	0.93	-
	Pressure ratio turbine	Π_{turb}	1.994	-
	Mechanical efficiency turbine	$\eta_{m,turb}$	0.947	-
Intercooler	Pressure drop	Δp_{loss}	0	bar
	Temperature drop	ΔT	120	°C
Cylinder	Isentropic efficiency compressor	$\eta_{is,compr}$	1	-
	Pressure ratio compressor	Π_{compr}	37.41	-
	Mechanical efficiency compressor	$\eta_{m,compr}$	0.874	-
	Air excess ratio combustor	λ	2.85	-
	Isentropic efficiency turbine	$\eta_{is,turb}$	1	-
	Pressure ratio turbine	Π_{turb}	40.74	-
	Mechanical efficiency turbine	$\eta_{m,turb}$	0.879	-
Generator	Generator efficiency	η_{gen}	0.97	-
Pumps	Isentropic efficiency	η_{is}	0.85	-
	Mechanical efficiency	η_m	0.8	-
SOFC	Fuel utilization factor	u_f	0.8	-
	Cell voltage	V_{cell}	0.89	V
	Stack temperature	T_{stack}	750	°C
	Inlet temperature	T_{in}	700	°C
	Outlet temperature	T_{out}	790	°C
	Anode pressure drop	Δp_{an}	0.02	bar
	Cathode pressure drop	Δp_{ca}	0.02	bar
Fuel reformer	Reformer temperature	T_{reform}	600	°C
	Steam to fuel ratio	S/F	0.68	kg/kg
	Pressure drop	Δp	0.01	bar
Heat exchangers	Pressure drop	Δp	0.01	bar
Pumps	Isentropic efficiency	η_{is}	0.85	-
	Mechanical efficiency	η_m	0.8	-
Blowers	Isentropic efficiency	η_{is}	0.85	-
	Mechanical efficiency	η_m	0.8	-
Overall	AOG combustion	$\frac{m_{AOG,ICE}}{m_{AOG}}$	1	-
	Gross ICE power	$P_{out,ICE}$	2.95	MWe
	Gross SOFC power	$P_{out,SOFC}$	3.17	MWe
	Net system power output	P_{out}	5.60	MWe
	ICE load		25	%
	SOFC load		75	%
	Net electrical system efficiency	η_{sys}	50.61	%
	Exhaust temperature	T_{exh}	233.89	°C

Table D.65: CT parameters for the MeOH-fuelled SOFC-ICE model at cruising speed for a power split of 15-85 and an SOFC load of 100%

Component	Parameter		CT Value	
Turbocharger	Isentropic efficiency compressor	$\eta_{is,compr}$	0.7	-
	Pressure ratio compressor	Π_{compr}	2.234	-
	Mechanical efficiency compressor	$\eta_{m,compr}$	0.947	-
	Isentropic efficiency turbine	$\eta_{is,turb}$	0.93	-
	Pressure ratio turbine	Π_{turb}	1.994	-
	Mechanical efficiency turbine	$\eta_{m,turb}$	0.947	-
Intercooler	Pressure drop	Δp_{loss}	0	bar
	Temperature drop	ΔT	120	°C
Cylinder	Isentropic efficiency compressor	$\eta_{is,compr}$	1	-
	Pressure ratio compressor	Π_{compr}	37.41	-
	Mechanical efficiency compressor	$\eta_{m,compr}$	0.874	-
	Air excess ratio combustor	λ	2.95	-
	Isentropic efficiency turbine	$\eta_{is,turb}$	1	-
	Pressure ratio turbine	Π_{turb}	40.74	-
	Mechanical efficiency turbine	$\eta_{m,turb}$	0.879	-
Generator	Generator efficiency	η_{gen}	0.97	-
Pumps	Isentropic efficiency	η_{is}	0.85	-
	Mechanical efficiency	η_m	0.8	-
SOFC	Fuel utilization factor	u_f	0.8	-
	Cell voltage	V_{cell}	0.85	V
	Stack temperature	T_{stack}	750	°C
	Inlet temperature	T_{in}	700	°C
	Outlet temperature	T_{out}	790	°C
	Anode pressure drop	Δp_{an}	0.02	bar
	Cathode pressure drop	Δp_{ca}	0.02	bar
Fuel reformer	Reformer temperature	T_{reform}	600	°C
	Steam to fuel ratio	S/F	0.68	kg/kg
	Pressure drop	Δp	0.01	bar
Heat exchangers	Pressure drop	Δp	0.01	bar
Pumps	Isentropic efficiency	η_{is}	0.85	-
	Mechanical efficiency	η_m	0.8	-
Blowers	Isentropic efficiency	η_{is}	0.85	-
	Mechanical efficiency	η_m	0.8	-
Overall	AOG combustion	$\frac{m_{AOG,ICE}}{m_{AOG}}$	1	-
	Gross ICE power	$P_{out,ICE}$	2.21	MWe
	Gross SOFC power	$P_{out,SOFC}$	4.23	MWe
	Net system power output	P_{out}	5.60	MWe
	ICE load		25	%
	SOFC load		75	%
	Net electrical system efficiency	η_{sys}	51.40	%
	Exhaust temperature	T_{exh}	212.28	°C

Table D.66: CT parameters for the MeOH-fuelled SOFC-ICE model at cruising speed for a power split of 20-80 and an SOFC load of 75%

Component	Parameter		CT Value	
Turbocharger	Isentropic efficiency compressor	$\eta_{is,compr}$	0.7	-
	Pressure ratio compressor	Π_{compr}	2.234	-
	Mechanical efficiency compressor	$\eta_{m,compr}$	0.947	-
	Isentropic efficiency turbine	$\eta_{is,turb}$	0.93	-
	Pressure ratio turbine	Π_{turb}	1.994	-
	Mechanical efficiency turbine	$\eta_{m,turb}$	0.947	-
Intercooler	Pressure drop	Δp_{loss}	0	bar
	Temperature drop	ΔT	120	°C
Cylinder	Isentropic efficiency compressor	$\eta_{is,compr}$	1	-
	Pressure ratio compressor	Π_{compr}	37.41	-
	Mechanical efficiency compressor	$\eta_{m,compr}$	0.874	-
	Air excess ratio combustor	λ	2.95	-
	Isentropic efficiency turbine	$\eta_{is,turb}$	1	-
	Pressure ratio turbine	Π_{turb}	40.74	-
	Mechanical efficiency turbine	$\eta_{m,turb}$	0.879	-
Generator	Generator efficiency	η_{gen}	0.97	-
Pumps	Isentropic efficiency	η_{is}	0.85	-
	Mechanical efficiency	η_m	0.8	-
SOFC	Fuel utilization factor	u_f	0.8	-
	Cell voltage	V_{cell}	0.89	V
	Stack temperature	T_{stack}	750	°C
	Inlet temperature	T_{in}	700	°C
	Outlet temperature	T_{out}	790	°C
	Anode pressure drop	Δp_{an}	0.02	bar
	Cathode pressure drop	Δp_{ca}	0.02	bar
Fuel reformer	Reformer temperature	T_{reform}	600	°C
	Steam to fuel ratio	S/F	0.68	kg/kg
	Pressure drop	Δp	0.01	bar
Heat exchangers	Pressure drop	Δp	0.01	bar
Pumps	Isentropic efficiency	η_{is}	0.85	-
	Mechanical efficiency	η_m	0.8	-
Blowers	Isentropic efficiency	η_{is}	0.85	-
	Mechanical efficiency	η_m	0.8	-
Overall	AOG combustion	$\frac{m_{AOG,ICE}}{m_{AOG}}$	1	-
	Gross ICE power	$P_{out,ICE}$	2.08	MWe
	Gross SOFC power	$P_{out,SOFC}$	4.23	MWe
	Net system power output	P_{out}	5.60	MWe
	ICE load		25	%
	SOFC load		75	%
	Net electrical system efficiency	η_{sys}	54.23	%
	Exhaust temperature	T_{exh}	217.60	°C

Table D.67: CT parameters for the MeOH-fuelled SOFC-ICE model at cruising speed for a power split of 20-80 and an SOFC load of 100%

Component	Parameter		CT Value	
Turbocharger	Isentropic efficiency compressor	$\eta_{is,compr}$	0.7	-
	Pressure ratio compressor	Π_{compr}	2.234	-
	Mechanical efficiency compressor	$\eta_{m,compr}$	0.947	-
	Isentropic efficiency turbine	$\eta_{is,turb}$	0.93	-
	Pressure ratio turbine	Π_{turb}	1.994	-
	Mechanical efficiency turbine	$\eta_{m,turb}$	0.947	-
Intercooler	Pressure drop	Δp_{loss}	0	bar
	Temperature drop	ΔT	120	°C
Cylinder	Isentropic efficiency compressor	$\eta_{is,compr}$	1	-
	Pressure ratio compressor	Π_{compr}	37.41	-
	Mechanical efficiency compressor	$\eta_{m,compr}$	0.874	-
	Air excess ratio combustor	λ	3.20	-
	Isentropic efficiency turbine	$\eta_{is,turb}$	1	-
	Pressure ratio turbine	Π_{turb}	40.74	-
	Mechanical efficiency turbine	$\eta_{m,turb}$	0.879	-
Generator	Generator efficiency	η_{gen}	0.97	-
Pumps	Isentropic efficiency	η_{is}	0.85	-
	Mechanical efficiency	η_m	0.8	-
SOFC	Fuel utilization factor	u_f	0.8	-
	Cell voltage	V_{cell}	0.85	V
	Stack temperature	T_{stack}	750	°C
	Inlet temperature	T_{in}	700	°C
	Outlet temperature	T_{out}	790	°C
	Anode pressure drop	Δp_{an}	0.02	bar
	Cathode pressure drop	Δp_{ca}	0.02	bar
Fuel reformer	Reformer temperature	T_{reform}	600	°C
	Steam to fuel ratio	S/F	0.68	kg/kg
	Pressure drop	Δp	0.01	bar
Heat exchangers	Pressure drop	Δp	0.01	bar
Pumps	Isentropic efficiency	η_{is}	0.85	-
	Mechanical efficiency	η_m	0.8	-
Blowers	Isentropic efficiency	η_{is}	0.85	-
	Mechanical efficiency	η_m	0.8	-
Overall	AOG combustion	$\frac{m_{AOG,ICE}}{m_{AOG}}$	1	-
	Gross ICE power	$P_{out,ICE}$	1.08	MWe
	Gross SOFC power	$P_{out,SOFC}$	5.64	MWe
	Net system power output	P_{out}	5.60	MWe
	ICE load		25	%
	SOFC load		75	%
	Net electrical system efficiency	η_{sys}	55.76	%
	Exhaust temperature	T_{exh}	196.66	°C

Table D.68: CT parameters for the MeOH-fuelled SOFC-ICE model at cruising speed for a power split of 25-75 and an SOFC load of 75%

Component	Parameter		CT Value	
Turbocharger	Isentropic efficiency compressor	$\eta_{is,compr}$	0.7	-
	Pressure ratio compressor	Π_{compr}	2.234	-
	Mechanical efficiency compressor	$\eta_{m,compr}$	0.947	-
	Isentropic efficiency turbine	$\eta_{is,turb}$	0.93	-
	Pressure ratio turbine	Π_{turb}	1.994	-
	Mechanical efficiency turbine	$\eta_{m,turb}$	0.947	-
Intercooler	Pressure drop	Δp_{loss}	0	bar
	Temperature drop	ΔT	120	°C
Cylinder	Isentropic efficiency compressor	$\eta_{is,compr}$	1	-
	Pressure ratio compressor	Π_{compr}	37.41	-
	Mechanical efficiency compressor	$\eta_{m,compr}$	0.874	-
	Air excess ratio combustor	λ	3.15	-
	Isentropic efficiency turbine	$\eta_{is,turb}$	1	-
	Pressure ratio turbine	Π_{turb}	40.74	-
	Mechanical efficiency turbine	$\eta_{m,turb}$	0.879	-
Generator	Generator efficiency	η_{gen}	0.97	-
Pumps	Isentropic efficiency	η_{is}	0.85	-
	Mechanical efficiency	η_m	0.8	-
SOFC	Fuel utilization factor	u_f	0.8	-
	Cell voltage	V_{cell}	0.89	V
	Stack temperature	T_{stack}	750	°C
	Inlet temperature	T_{in}	700	°C
	Outlet temperature	T_{out}	790	°C
	Anode pressure drop	Δp_{an}	0.02	bar
	Cathode pressure drop	Δp_{ca}	0.02	bar
Fuel reformer	Reformer temperature	T_{reform}	600	°C
	Steam to fuel ratio	S/F	0.68	kg/kg
	Pressure drop	Δp	0.01	bar
Heat exchangers	Pressure drop	Δp	0.01	bar
Pumps	Isentropic efficiency	η_{is}	0.85	-
	Mechanical efficiency	η_m	0.8	-
Blowers	Isentropic efficiency	η_{is}	0.85	-
	Mechanical efficiency	η_m	0.8	-
Overall	AOG combustion	$\frac{m_{AOG,ICE}}{m_{AOG}}$	1	-
	Gross ICE power	$P_{out,ICE}$	1.19	MWe
	Gross SOFC power	$P_{out,SOFC}$	5.29	MWe
	Net system power output	P_{out}	5.60	MWe
	ICE load		25	%
	SOFC load		75	%
	Net electrical system efficiency	η_{sys}	58.60	%
	Exhaust temperature	T_{exh}	203.89	°C

Table D.69: CT parameters for the MeOH-fuelled SOFC-ICE model at cruising speed for a power split of 25-75 and an SOFC load of 100%

Component	Parameter		CT Value	
Turbocharger	Isentropic efficiency compressor	$\eta_{is,compr}$	0.7	-
	Pressure ratio compressor	Π_{compr}	2.234	-
	Mechanical efficiency compressor	$\eta_{m,compr}$	0.947	-
	Isentropic efficiency turbine	$\eta_{is,turb}$	0.93	-
	Pressure ratio turbine	Π_{turb}	1.994	-
	Mechanical efficiency turbine	$\eta_{m,turb}$	0.947	-
Intercooler	Pressure drop	Δp_{loss}	0	bar
	Temperature drop	ΔT	120	°C
Cylinder	Isentropic efficiency compressor	$\eta_{is,compr}$	1	-
	Pressure ratio compressor	Π_{compr}	37.41	-
	Mechanical efficiency compressor	$\eta_{m,compr}$	0.874	-
	Air excess ratio combustor	λ	2.65	-
	Isentropic efficiency turbine	$\eta_{is,turb}$	1	-
	Pressure ratio turbine	Π_{turb}	40.74	-
	Mechanical efficiency turbine	$\eta_{m,turb}$	0.879	-
Generator	Generator efficiency	η_{gen}	0.97	-
Pumps	Isentropic efficiency	η_{is}	0.85	-
	Mechanical efficiency	η_m	0.8	-
SOFC	Fuel utilization factor	u_f	0.8	-
	Cell voltage	V_{cell}	0.85	V
	Stack temperature	T_{stack}	750	°C
	Inlet temperature	T_{in}	700	°C
	Outlet temperature	T_{out}	790	°C
	Anode pressure drop	Δp_{an}	0.02	bar
	Cathode pressure drop	Δp_{ca}	0.02	bar
Fuel reformer	Reformer temperature	T_{reform}	600	°C
	Steam to fuel ratio	S/F	0.68	kg/kg
	Pressure drop	Δp	0.01	bar
Heat exchangers	Pressure drop	Δp	0.01	bar
Pumps	Isentropic efficiency	η_{is}	0.85	-
	Mechanical efficiency	η_m	0.8	-
Blowers	Isentropic efficiency	η_{is}	0.85	-
	Mechanical efficiency	η_m	0.8	-
Overall	AOG combustion	$\frac{m_{AOG,ICE}}{m_{AOG}}$	0	-
	Gross ICE power	$P_{out,ICE}$	0	MWe
	Gross SOFC power	$P_{out,SOFC}$	7.01	MWe
	Net system power output	P_{out}	5.60	MWe
	ICE load		0	%
	SOFC load		75	%
	Net electrical system efficiency	η_{sys}	47.09	%
	Exhaust temperature	T_{exh}	203.43	°C

Table D.70: CT parameters for the MeOH-fuelled SOFC-ICE model at cruising speed for a power split of 30-70 and an SOFC load of 75%

Component	Parameter		CT Value	
Turbocharger	Isentropic efficiency compressor	$\eta_{is,compr}$	0.7	-
	Pressure ratio compressor	Π_{compr}	2.234	-
	Mechanical efficiency compressor	$\eta_{m,compr}$	0.947	-
	Isentropic efficiency turbine	$\eta_{is,turb}$	0.93	-
	Pressure ratio turbine	Π_{turb}	1.994	-
	Mechanical efficiency turbine	$\eta_{m,turb}$	0.947	-
Intercooler	Pressure drop	Δp_{loss}	0	bar
	Temperature drop	ΔT	120	°C
Cylinder	Isentropic efficiency compressor	$\eta_{is,compr}$	1	-
	Pressure ratio compressor	Π_{compr}	37.41	-
	Mechanical efficiency compressor	$\eta_{m,compr}$	0.874	-
	Air excess ratio combustor	λ	3.20	-
	Isentropic efficiency turbine	$\eta_{is,turb}$	1	-
	Pressure ratio turbine	Π_{turb}	40.74	-
	Mechanical efficiency turbine	$\eta_{m,turb}$	0.879	-
Generator	Generator efficiency	η_{gen}	0.97	-
Pumps	Isentropic efficiency	η_{is}	0.85	-
	Mechanical efficiency	η_m	0.8	-
SOFC	Fuel utilization factor	u_f	0.8	-
	Cell voltage	V_{cell}	0.89	V
	Stack temperature	T_{stack}	750	°C
	Inlet temperature	T_{in}	700	°C
	Outlet temperature	T_{out}	790	°C
	Anode pressure drop	Δp_{an}	0.02	bar
	Cathode pressure drop	Δp_{ca}	0.02	bar
Fuel reformer	Reformer temperature	T_{reform}	600	°C
	Steam to fuel ratio	S/F	0.68	kg/kg
	Pressure drop	Δp	0.01	bar
Heat exchangers	Pressure drop	Δp	0.01	bar
Pumps	Isentropic efficiency	η_{is}	0.85	-
	Mechanical efficiency	η_m	0.8	-
Blowers	Isentropic efficiency	η_{is}	0.85	-
	Mechanical efficiency	η_m	0.8	-
Overall	AOG combustion	$\frac{m_{AOG,ICE}}{m_{AOG}}$	0.36	-
	Gross ICE power	$P_{out,ICE}$	0.36	MWe
	Gross SOFC power	$P_{out,SOFC}$	6.35	MWe
	Net system power output	P_{out}	5.61	MWe
	ICE load		25	%
	SOFC load		75	%
	Net electrical system efficiency	η_{sys}	53.86	%
	Exhaust temperature	T_{exh}	205.20	°C

Table D.71: CT parameters for the MeOH-fuelled SOFC-ICE model at cruising speed for a power split of 30-70 and an SOFC load of 100%

Component	Parameter		CT Value	
Turbocharger	Isentropic efficiency compressor	$\eta_{is,compr}$	0.7	-
	Pressure ratio compressor	Π_{compr}	2.234	-
	Mechanical efficiency compressor	$\eta_{m,compr}$	0.947	-
	Isentropic efficiency turbine	$\eta_{is,turb}$	0.93	-
	Pressure ratio turbine	Π_{turb}	1.994	-
	Mechanical efficiency turbine	$\eta_{m,turb}$	0.947	-
Intercooler	Pressure drop	Δp_{loss}	0	bar
	Temperature drop	ΔT	120	°C
Cylinder	Isentropic efficiency compressor	$\eta_{is,compr}$	1	-
	Pressure ratio compressor	Π_{compr}	37.41	-
	Mechanical efficiency compressor	$\eta_{m,compr}$	0.874	-
	Air excess ratio combustor	λ	2.70	-
	Isentropic efficiency turbine	$\eta_{is,turb}$	1	-
	Pressure ratio turbine	Π_{turb}	40.74	-
	Mechanical efficiency turbine	$\eta_{m,turb}$	0.879	-
Generator	Generator efficiency	η_{gen}	0.97	-
Pumps	Isentropic efficiency	η_{is}	0.85	-
	Mechanical efficiency	η_m	0.8	-
SOFC	Fuel utilization factor	u_f	0.8	-
	Cell voltage	V_{cell}	0.89	V
	Stack temperature	T_{stack}	750	°C
	Inlet temperature	T_{in}	700	°C
	Outlet temperature	T_{out}	790	°C
	Anode pressure drop	Δp_{an}	0.02	bar
	Cathode pressure drop	Δp_{ca}	0.02	bar
Fuel reformer	Reformer temperature	T_{reform}	600	°C
	Steam to fuel ratio	S/F	0.68	kg/kg
	Pressure drop	Δp	0.01	bar
Heat exchangers	Pressure drop	Δp	0.01	bar
Pumps	Isentropic efficiency	η_{is}	0.85	-
	Mechanical efficiency	η_m	0.8	-
Blowers	Isentropic efficiency	η_{is}	0.85	-
	Mechanical efficiency	η_m	0.8	-
Overall	AOG combustion	$\frac{m_{AOG,ICE}}{m_{AOG}}$	0	-
	Gross ICE power	$P_{out,ICE}$	0	MWe
	Gross SOFC power	$P_{out,SOFC}$	6.81	MWe
	Net system power output	P_{out}	5.60	MWe
	ICE load		0	%
	SOFC load		80	%
	Net electrical system efficiency	η_{sys}	50.16	%
	Exhaust temperature	T_{exh}	207.92	°C

Table D.72: CT parameters for the MeOH-fuelled SOFC-ICE model at top speed for a power split of 4.6-95.4

Component	Parameter		CT Value	
Turbocharger	Isentropic efficiency compressor	$\eta_{is,compr}$	0.79	-
	Pressure ratio compressor	Π_{compr}	4.752	-
	Mechanical efficiency compressor	$\eta_{m,compr}$	0.956	-
	Isentropic efficiency turbine	$\eta_{is,turb}$	0.855	-
	Pressure ratio turbine	Π_{turb}	3.468	-
	Mechanical efficiency turbine	$\eta_{m,turb}$	0.956	-
Intercooler	Pressure drop	Δp_{loss}	0.049	bar
	Temperature drop	ΔT	186	°C
Cylinder	Isentropic efficiency compressor	$\eta_{is,compr}$	1	-
	Pressure ratio compressor	Π_{compr}	37.41	-
	Mechanical efficiency compressor	$\eta_{m,compr}$	0.8568	-
	Air excess ratio combustor	λ	1.96	-
	Isentropic efficiency turbine	$\eta_{is,turb}$	1	-
	Pressure ratio turbine	Π_{turb}	49.29	-
	Mechanical efficiency turbine	$\eta_{m,turb}$	0.8568	-
Generator	Generator efficiency	η_{gen}	0.97	-
Pumps	Isentropic efficiency	η_{is}	0.85	-
	Mechanical efficiency	η_m	0.8	-
SOFC	Fuel utilization factor	u_f	0.8	-
	Cell voltage	V_{cell}	0.85	V
	Stack temperature	T_{stack}	750	°C
	Inlet temperature	T_{in}	700	°C
	Outlet temperature	T_{out}	790	°C
	Anode pressure drop	Δp_{an}	0.02	bar
	Cathode pressure drop	Δp_{ca}	0.02	bar
Fuel reformer	Reformer temperature	T_{reform}	600	°C
	Steam to fuel ratio	S/F	0.68	kg/kg
	Pressure drop	Δp	0.01	bar
Heat exchangers	Pressure drop	Δp	0.01	bar
Pumps	Isentropic efficiency	η_{is}	0.85	-
	Mechanical efficiency	η_m	0.8	-
Blowers	Isentropic efficiency	η_{is}	0.85	-
	Mechanical efficiency	η_m	0.8	-
Overall	AOG combustion	$\frac{m_{AOG,ICE}}{m_{AOG}}$	1	-
	Gross ICE power	$P_{out,ICE}$	22.28	MWe
	Gross SOFC power	$P_{out,SOFC}$	1.29	MWe
	Net system power output	P_{out}	23.30	MWe
	ICE load		100	%
	SOFC load		100	%
	Net electrical system efficiency	η_{sys}	43.95	%
	Exhaust temperature	T_{exh}	317.33	°C

Table D.73: CT parameters for the MeOH-fuelled SOFC-ICE model at top speed for a power split of 10-90

Component	Parameter		CT Value	
Turbocharger	Isentropic efficiency compressor	$\eta_{is,compr}$	0.79	-
	Pressure ratio compressor	Π_{compr}	4.752	-
	Mechanical efficiency compressor	$\eta_{m,compr}$	0.956	-
	Isentropic efficiency turbine	$\eta_{is,turb}$	0.855	-
	Pressure ratio turbine	Π_{turb}	3.468	-
	Mechanical efficiency turbine	$\eta_{m,turb}$	0.956	-
Intercooler	Pressure drop	Δp_{loss}	0.049	bar
	Temperature drop	ΔT	186	°C
Cylinder	Isentropic efficiency compressor	$\eta_{is,compr}$	1	-
	Pressure ratio compressor	Π_{compr}	37.41	-
	Mechanical efficiency compressor	$\eta_{m,compr}$	0.8568	-
	Air excess ratio combustor	λ	1.97	-
	Isentropic efficiency turbine	$\eta_{is,turb}$	1	-
	Pressure ratio turbine	Π_{turb}	49.29	-
	Mechanical efficiency turbine	$\eta_{m,turb}$	0.8568	-
Generator	Generator efficiency	η_{gen}	0.97	-
Pumps	Isentropic efficiency	η_{is}	0.85	-
	Mechanical efficiency	η_m	0.8	-
SOFC	Fuel utilization factor	u_f	0.8	-
	Cell voltage	V_{cell}	0.85	V
	Stack temperature	T_{stack}	750	°C
	Inlet temperature	T_{in}	700	°C
	Outlet temperature	T_{out}	790	°C
	Anode pressure drop	Δp_{an}	0.02	bar
	Cathode pressure drop	Δp_{ca}	0.02	bar
Fuel reformer	Reformer temperature	T_{reform}	600	°C
	Steam to fuel ratio	S/F	0.68	kg/kg
	Pressure drop	Δp	0.01	bar
Heat exchangers	Pressure drop	Δp	0.01	bar
Pumps	Isentropic efficiency	η_{is}	0.85	-
	Mechanical efficiency	η_m	0.8	-
Blowers	Isentropic efficiency	η_{is}	0.85	-
	Mechanical efficiency	η_m	0.8	-
Overall	AOG combustion	$\frac{m_{AOG,ICE}}{m_{AOG}}$	1	-
	Gross ICE power	$P_{out,ICE}$	20.79	MWe
	Gross SOFC power	$P_{out,SOFC}$	2.82	MWe
	Net system power output	P_{out}	23.30	MWe
	ICE load		100	%
	SOFC load		100	%
	Net electrical system efficiency	η_{sys}	45.12	%
	Exhaust temperature	T_{exh}	294.14	°C

Table D.74: CT parameters for the MeOH-fuelled SOFC-ICE model at top speed for a power split of 15-85

Component	Parameter		CT Value	
Turbocharger	Isentropic efficiency compressor	$\eta_{is,compr}$	0.79	-
	Pressure ratio compressor	Π_{compr}	4.752	-
	Mechanical efficiency compressor	$\eta_{m,compr}$	0.956	-
	Isentropic efficiency turbine	$\eta_{is,turb}$	0.855	-
	Pressure ratio turbine	Π_{turb}	3.468	-
	Mechanical efficiency turbine	$\eta_{m,turb}$	0.956	-
Intercooler	Pressure drop	Δp_{loss}	0.049	bar
	Temperature drop	ΔT	186	°C
Cylinder	Isentropic efficiency compressor	$\eta_{is,compr}$	1	-
	Pressure ratio compressor	Π_{compr}	37.41	-
	Mechanical efficiency compressor	$\eta_{m,compr}$	0.8568	-
	Air excess ratio combustor	λ	1.97	-
	Isentropic efficiency turbine	$\eta_{is,turb}$	1	-
	Pressure ratio turbine	Π_{turb}	49.29	-
	Mechanical efficiency turbine	$\eta_{m,turb}$	0.8568	-
Generator	Generator efficiency	η_{gen}	0.97	-
Pumps	Isentropic efficiency	η_{is}	0.85	-
	Mechanical efficiency	η_m	0.8	-
SOFC	Fuel utilization factor	u_f	0.8	-
	Cell voltage	V_{cell}	0.85	V
	Stack temperature	T_{stack}	750	°C
	Inlet temperature	T_{in}	700	°C
	Outlet temperature	T_{out}	790	°C
	Anode pressure drop	Δp_{an}	0.02	bar
	Cathode pressure drop	Δp_{ca}	0.02	bar
Fuel reformer	Reformer temperature	T_{reform}	600	°C
	Steam to fuel ratio	S/F	0.68	kg/kg
	Pressure drop	Δp	0.01	bar
Heat exchangers	Pressure drop	Δp	0.01	bar
Pumps	Isentropic efficiency	η_{is}	0.85	-
	Mechanical efficiency	η_m	0.8	-
Blowers	Isentropic efficiency	η_{is}	0.85	-
	Mechanical efficiency	η_m	0.8	-
Overall	AOG combustion	$\frac{m_{AOG,ICE}}{m_{AOG}}$	1	-
	Gross ICE power	$P_{out,ICE}$	19.92	MWe
	Gross SOFC power	$P_{out,SOFC}$	4.23	MWe
	Net system power output	P_{out}	23.30	MWe
	ICE load		100	%
	SOFC load		100	%
	Net electrical system efficiency	η_{sys}	45.23	%
	Exhaust temperature	T_{exh}	286.19	°C

Table D.75: CT parameters for the MeOH-fuelled SOFC-ICE model at top speed for a power split of 20-80

Component	Parameter		CT Value	
Turbocharger	Isentropic efficiency compressor	$\eta_{is,compr}$	0.79	-
	Pressure ratio compressor	Π_{compr}	4.752	-
	Mechanical efficiency compressor	$\eta_{m,compr}$	0.956	-
	Isentropic efficiency turbine	$\eta_{is,turb}$	0.855	-
	Pressure ratio turbine	Π_{turb}	3.468	-
	Mechanical efficiency turbine	$\eta_{m,turb}$	0.956	-
Intercooler	Pressure drop	Δp_{loss}	0.049	bar
	Temperature drop	ΔT	186	°C
Cylinder	Isentropic efficiency compressor	$\eta_{is,compr}$	1	-
	Pressure ratio compressor	Π_{compr}	37.41	-
	Mechanical efficiency compressor	$\eta_{m,compr}$	0.8568	-
	Air excess ratio combustor	λ	1.98	-
	Isentropic efficiency turbine	$\eta_{is,turb}$	1	-
	Pressure ratio turbine	Π_{turb}	49.29	-
	Mechanical efficiency turbine	$\eta_{m,turb}$	0.8568	-
Generator	Generator efficiency	η_{gen}	0.97	-
Pumps	Isentropic efficiency	η_{is}	0.85	-
	Mechanical efficiency	η_m	0.8	-
SOFC	Fuel utilization factor	u_f	0.8	-
	Cell voltage	V_{cell}	0.85	V
	Stack temperature	T_{stack}	750	°C
	Inlet temperature	T_{in}	700	°C
	Outlet temperature	T_{out}	790	°C
	Anode pressure drop	Δp_{an}	0.02	bar
	Cathode pressure drop	Δp_{ca}	0.02	bar
Fuel reformer	Reformer temperature	T_{reform}	600	°C
	Steam to fuel ratio	S/F	0.68	kg/kg
	Pressure drop	Δp	0.01	bar
Heat exchangers	Pressure drop	Δp	0.01	bar
Pumps	Isentropic efficiency	η_{is}	0.85	-
	Mechanical efficiency	η_m	0.8	-
Blowers	Isentropic efficiency	η_{is}	0.85	-
	Mechanical efficiency	η_m	0.8	-
Overall	AOG combustion	$\frac{m_{AOG,ICE}}{m_{AOG}}$	1	-
	Gross ICE power	$P_{out,ICE}$	18.80	MWe
	Gross SOFC power	$P_{out,SOFC}$	5.64	MWe
	Net system power output	P_{out}	23.30	MWe
	ICE load		100	%
	SOFC load		100	%
	Net electrical system efficiency	η_{sys}	45.85	%
	Exhaust temperature	T_{exh}	273.83	°C

Table D.76: CT parameters for the MeOH-fuelled SOFC-ICE model at top speed for a power split of 25-75

Component	Parameter		CT Value	
Turbocharger	Isentropic efficiency compressor	$\eta_{is,compr}$	0.79	-
	Pressure ratio compressor	Π_{compr}	4.752	-
	Mechanical efficiency compressor	$\eta_{m,compr}$	0.956	-
	Isentropic efficiency turbine	$\eta_{is,turb}$	0.855	-
	Pressure ratio turbine	Π_{turb}	3.468	-
	Mechanical efficiency turbine	$\eta_{m,turb}$	0.956	-
Intercooler	Pressure drop	Δp_{loss}	0.049	bar
	Temperature drop	ΔT	186	°C
Cylinder	Isentropic efficiency compressor	$\eta_{is,compr}$	1	-
	Pressure ratio compressor	Π_{compr}	37.41	-
	Mechanical efficiency compressor	$\eta_{m,compr}$	0.8568	-
	Air excess ratio combustor	λ	1.99	-
	Isentropic efficiency turbine	$\eta_{is,turb}$	1	-
	Pressure ratio turbine	Π_{turb}	49.29	-
	Mechanical efficiency turbine	$\eta_{m,turb}$	0.8568	-
Generator	Generator efficiency	η_{gen}	0.97	-
Pumps	Isentropic efficiency	η_{is}	0.85	-
	Mechanical efficiency	η_m	0.8	-
SOFC	Fuel utilization factor	u_f	0.8	-
	Cell voltage	V_{cell}	0.85	V
	Stack temperature	T_{stack}	750	°C
	Inlet temperature	T_{in}	700	°C
	Outlet temperature	T_{out}	790	°C
	Anode pressure drop	Δp_{an}	0.02	bar
	Cathode pressure drop	Δp_{ca}	0.02	bar
Fuel reformer	Reformer temperature	T_{reform}	600	°C
	Steam to fuel ratio	S/F	0.68	kg/kg
	Pressure drop	Δp	0.01	bar
Heat exchangers	Pressure drop	Δp	0.01	bar
Pumps	Isentropic efficiency	η_{is}	0.85	-
	Mechanical efficiency	η_m	0.8	-
Blowers	Isentropic efficiency	η_{is}	0.85	-
	Mechanical efficiency	η_m	0.8	-
Overall	AOG combustion	$\frac{m_{AOG,ICE}}{m_{AOG}}$	1	-
	Gross ICE power	$P_{out,ICE}$	17.67	MWe
	Gross SOFC power	$P_{out,SOFC}$	7.05	MWe
	Net system power output	P_{out}	23.30	MWe
	ICE load		100	%
	SOFC load		100	%
	Net electrical system efficiency	η_{sys}	46.49	%
	Exhaust temperature	T_{exh}	263.08	°C

Table D.77: CT parameters for the MeOH-fuelled SOFC-ICE model at top speed for a power split of 30-70

Component	Parameter		CT Value	
Turbocharger	Isentropic efficiency compressor	$\eta_{is,compr}$	0.79	-
	Pressure ratio compressor	Π_{compr}	4.752	-
	Mechanical efficiency compressor	$\eta_{m,compr}$	0.956	-
	Isentropic efficiency turbine	$\eta_{is,turb}$	0.855	-
	Pressure ratio turbine	Π_{turb}	3.468	-
	Mechanical efficiency turbine	$\eta_{m,turb}$	0.956	-
Intercooler	Pressure drop	Δp_{loss}	0.049	bar
	Temperature drop	ΔT	186	°C
Cylinder	Isentropic efficiency compressor	$\eta_{is,compr}$	1	-
	Pressure ratio compressor	Π_{compr}	37.41	-
	Mechanical efficiency compressor	$\eta_{m,compr}$	0.8568	-
	Air excess ratio combustor	λ	1.99	-
	Isentropic efficiency turbine	$\eta_{is,turb}$	1	-
	Pressure ratio turbine	Π_{turb}	49.29	-
	Mechanical efficiency turbine	$\eta_{m,turb}$	0.8568	-
Generator	Generator efficiency	η_{gen}	0.97	-
Pumps	Isentropic efficiency	η_{is}	0.85	-
	Mechanical efficiency	η_m	0.8	-
SOFC	Fuel utilization factor	u_f	0.8	-
	Cell voltage	V_{cell}	0.85	V
	Stack temperature	T_{stack}	750	°C
	Inlet temperature	T_{in}	700	°C
	Outlet temperature	T_{out}	790	°C
	Anode pressure drop	Δp_{an}	0.02	bar
	Cathode pressure drop	Δp_{ca}	0.02	bar
Fuel reformer	Reformer temperature	T_{reform}	600	°C
	Steam to fuel ratio	S/F	0.68	kg/kg
	Pressure drop	Δp	0.01	bar
Heat exchangers	Pressure drop	Δp	0.01	bar
Pumps	Isentropic efficiency	η_{is}	0.85	-
	Mechanical efficiency	η_m	0.8	-
Blowers	Isentropic efficiency	η_{is}	0.85	-
	Mechanical efficiency	η_m	0.8	-
Overall	AOG combustion	$\frac{m_{AOG,ICE}}{m_{AOG}}$	1	-
	Gross ICE power	$P_{out,ICE}$	16.53	MWe
	Gross SOFC power	$P_{out,SOFC}$	8.46	MWe
	Net system power output	P_{out}	23.30	MWe
	ICE load		100	%
	SOFC load		100	%
	Net electrical system efficiency	η_{sys}	47.22	%
	Exhaust temperature	T_{exh}	254.38	°C

D.5. SOFC-GT models

In this section, the parameters for the SOFC-GT models are given. First, the parameters for silent speed, cruising speed and top speed for the diesel-fuelled models are given. Next, the same parameters are given for the MeOH-fuelled models.

D.5.1. Diesel

The parameters for silent operation are given in Table D.97. Next, Table D.98 to Table D.109 show the parameters for cruising speed. Lastly, Table D.110 to Table D.115 show the parameters for top speed.

Table D.78: CT parameters for the diesel-fuelled SOFC-GT model at silent speed

Component	Parameter		CT Value	
Compressor	Isentropic efficiency	η_{is}	0.843	-
	Pressure ratio	Π	23.54	-
	Mechanical efficiency	η_m	0.997	-
Turbine	Isentropic efficiency	η_{is}	0.865	-
	Pressure ratio	Π	4.80	-
	Mechanical efficiency	η_m	0.997	-
Power turbine	Isentropic efficiency	η_{is}	0.86	-
	Pressure ratio	Π	4.76	-
	Mechanical efficiency	η_m	0.996	-
Generator	Generator efficiency	η_{gen}	0.975	
Pumps	Isentropic efficiency	η_{is}	0.85	-
	Mechanical efficiency	η_m	0.8	-
SOFC	Fuel utilization factor	u_f	0.8	-
	Cell voltage	V_{cell}	0.89	V
	Stack temperature	T_{stack}	750	°C
	Inlet temperature	T_{in}	700	°C
	Outlet temperature	T_{out}	790	°C
	Anode pressure drop	Δp_{an}	0.02	bar
	Cathode pressure drop	Δp_{ca}	0.02	bar
Fuel reformer	Reformer temperature	T_{reform}	600	°C
	Steam to fuel ratio	S/F	2.61	kg/kg
	Pressure drop	Δp	0.01	bar
Heat exchangers	Pressure drop	Δp	0.01	bar
Pumps	Isentropic efficiency	η_{is}	0.85	-
	Mechanical efficiency	η_m	0.8	-
Blowers	Isentropic efficiency	η_{is}	0.85	-
	Mechanical efficiency	η_m	0.8	-
Overall	AOG combustion	$\frac{m_{AOG,GT}}{m_{AOG}}$	0	-
	Gross GT power	$P_{out,GT}$	0	MWe
	Gross SOFC power	$P_{out,SOFC}$	0.96	MWe
	Net system power output	P_{out}	0.80	MWe
	GT load		0	%
	SOFC load		75	%
	Net electrical system efficiency	η_{sys}	54.31	%
	Exhaust temperature	T_{exh}	151.72	°C

Table D.79: CT parameters for the diesel-fuelled SOFC-GT model at cruising speed for a power split of 4.6-95.4 and an SOFC load of 75%

Component	Parameter		CT Value	
Compressor	Isentropic efficiency	η_{is}	0.843	-
	Pressure ratio	Π	23.54	-
	Mechanical efficiency	η_m	0.997	-
Turbine	Isentropic efficiency	η_{is}	0.865	-
	Pressure ratio	Π	4.80	-
	Mechanical efficiency	η_m	0.997	-
Power turbine	Isentropic efficiency	η_{is}	0.86	-
	Pressure ratio	Π	4.76	-
	Mechanical efficiency	η_m	0.996	-
Generator	Generator efficiency	η_{gen}	0.975	
Pumps	Isentropic efficiency	η_{is}	0.85	-
	Mechanical efficiency	η_m	0.8	-
SOFC	Fuel utilization factor	u_f	0.8	-
	Cell voltage	V_{cell}	0.89	V
	Stack temperature	T_{stack}	750	°C
	Inlet temperature	T_{in}	700	°C
	Outlet temperature	T_{out}	790	°C
	Anode pressure drop	Δp_{an}	0.02	bar
	Cathode pressure drop	Δp_{ca}	0.02	bar
Fuel reformer	Reformer temperature	T_{reform}	600	°C
	Steam to fuel ratio	S/F	2.61	kg/kg
	Pressure drop	Δp	0.01	bar
Heat exchangers	Pressure drop	Δp	0.01	bar
Pumps	Isentropic efficiency	η_{is}	0.85	-
	Mechanical efficiency	η_m	0.8	-
Blowers	Isentropic efficiency	η_{is}	0.85	-
	Mechanical efficiency	η_m	0.8	-
Overall	AOG combustion	$\frac{m_{AOG,GT}}{m_{AOG}}$	1	-
	Gross GT power	$P_{out,GT}$	4.77	MWe
	Gross SOFC power	$P_{out,SOFC}$	0.96	MWe
	Net system power output	P_{out}	5.60	MWe
	GT load		100	%
	SOFC load		75	%
	Net electrical system efficiency	η_{sys}	41.35	%
	Exhaust temperature	T_{exh}	434.20	°C

Table D.80: CT parameters for the diesel-fuelled SOFC-GT model at cruising speed for a power split of 4.6-95.4 and an SOFC load of 100%

Component	Parameter		CT Value	
Compressor	Isentropic efficiency	η_{is}	0.843	-
	Pressure ratio	Π	23.54	-
	Mechanical efficiency	η_m	0.997	-
Turbine	Isentropic efficiency	η_{is}	0.865	-
	Pressure ratio	Π	4.80	-
	Mechanical efficiency	η_m	0.997	-
Power turbine	Isentropic efficiency	η_{is}	0.86	-
	Pressure ratio	Π	4.76	-
	Mechanical efficiency	η_m	0.996	-
Generator	Generator efficiency	η_{gen}	0.975	
Pumps	Isentropic efficiency	η_{is}	0.85	-
	Mechanical efficiency	η_m	0.8	-
SOFC	Fuel utilization factor	u_f	0.8	-
	Cell voltage	V_{cell}	0.85	V
	Stack temperature	T_{stack}	750	°C
	Inlet temperature	T_{in}	700	°C
	Outlet temperature	T_{out}	790	°C
	Anode pressure drop	Δp_{an}	0.02	bar
	Cathode pressure drop	Δp_{ca}	0.02	bar
Fuel reformer	Reformer temperature	T_{reform}	600	°C
	Steam to fuel ratio	S/F	2.61	kg/kg
	Pressure drop	Δp	0.01	bar
Heat exchangers	Pressure drop	Δp	0.01	bar
Pumps	Isentropic efficiency	η_{is}	0.85	-
	Mechanical efficiency	η_m	0.8	-
Blowers	Isentropic efficiency	η_{is}	0.85	-
	Mechanical efficiency	η_m	0.8	-
Overall	AOG combustion	$\frac{m_{AOG,GT}}{m_{AOG}}$	1	-
	Gross GT power	$P_{out,GT}$	4.54	MWe
	Gross SOFC power	$P_{out,SOFC}$	1.28	MWe
	Net system power output	P_{out}	5.61	MWe
	GT load		100	%
	SOFC load		100	%
	Net electrical system efficiency	η_{sys}	42.36	%
	Exhaust temperature	T_{exh}	390.19	°C

Table D.81: CT parameters for the diesel-fuelled SOFC-GT model at cruising speed for a power split of 10-90 and an SOFC load of 75%

Component	Parameter		CT Value	
Compressor	Isentropic efficiency	η_{is}	0.857	-
	Pressure ratio	Π	20.69	-
	Mechanical efficiency	η_m	0.997	-
Turbine	Isentropic efficiency	η_{is}	0.86	-
	Pressure ratio	Π	4.72	-
	Mechanical efficiency	η_m	0.997	-
Power turbine	Isentropic efficiency	η_{is}	0.855	-
	Pressure ratio	Π	4.25	-
	Mechanical efficiency	η_m	0.997	-
Generator	Generator efficiency	η_{gen}	0.974	
Pumps	Isentropic efficiency	η_{is}	0.85	-
	Mechanical efficiency	η_m	0.8	-
SOFC	Fuel utilization factor	u_f	0.8	-
	Cell voltage	V_{cell}	0.89	V
	Stack temperature	T_{stack}	750	°C
	Inlet temperature	T_{in}	700	°C
	Outlet temperature	T_{out}	790	°C
	Anode pressure drop	Δp_{an}	0.02	bar
	Cathode pressure drop	Δp_{ca}	0.02	bar
Fuel reformer	Reformer temperature	T_{reform}	600	°C
	Steam to fuel ratio	S/F	2.61	kg/kg
	Pressure drop	Δp	0.01	bar
Heat exchangers	Pressure drop	Δp	0.01	bar
Pumps	Isentropic efficiency	η_{is}	0.85	-
	Mechanical efficiency	η_m	0.8	-
Blowers	Isentropic efficiency	η_{is}	0.85	-
	Mechanical efficiency	η_m	0.8	-
Overall	AOG combustion	$\frac{m_{AOG,GT}}{m_{AOG}}$	1	-
	Gross GT power	$P_{out,GT}$	3.80	MWe
	Gross SOFC power	$P_{out,SOFC}$	2.09	MWe
	Net system power output	P_{out}	5.61	MWe
	GT load		80	%
	SOFC load		75	%
	Net electrical system efficiency	η_{sys}	45.50	%
	Exhaust temperature	T_{exh}	319.30	°C

Table D.82: CT parameters for the diesel-fuelled SOFC-GT model at cruising speed for a power split of 10-90 and an SOFC load of 100%

Component	Parameter		CT Value	
Compressor	Isentropic efficiency	η_{is}	0.861	-
	Pressure ratio	Π	19.17	-
	Mechanical efficiency	η_m	0.996	-
Turbine	Isentropic efficiency	η_{is}	0.855	-
	Pressure ratio	Π	4.69	-
	Mechanical efficiency	η_m	0.996	-
Power turbine	Isentropic efficiency	η_{is}	0.855	-
	Pressure ratio	Π	3.96	-
	Mechanical efficiency	η_m	0.996	-
Generator	Generator efficiency	η_{gen}	0.973	
Pumps	Isentropic efficiency	η_{is}	0.85	-
	Mechanical efficiency	η_m	0.8	-
SOFC	Fuel utilization factor	u_f	0.8	-
	Cell voltage	V_{cell}	0.85	V
	Stack temperature	T_{stack}	750	°C
	Inlet temperature	T_{in}	700	°C
	Outlet temperature	T_{out}	790	°C
	Anode pressure drop	Δp_{an}	0.02	bar
	Cathode pressure drop	Δp_{ca}	0.02	bar
Fuel reformer	Reformer temperature	T_{reform}	600	°C
	Steam to fuel ratio	S/F	2.61	kg/kg
	Pressure drop	Δp	0.01	bar
Heat exchangers	Pressure drop	Δp	0.01	bar
Pumps	Isentropic efficiency	η_{is}	0.85	-
	Mechanical efficiency	η_m	0.8	-
Blowers	Isentropic efficiency	η_{is}	0.85	-
	Mechanical efficiency	η_m	0.8	-
Overall	AOG combustion	$\frac{m_{AOG,GT}}{m_{AOG}}$	1	-
	Gross GT power	$P_{out,GT}$	3.28	MWe
	Gross SOFC power	$P_{out,SOFC}$	2.79	MWe
	Net system power output	P_{out}	5.60	MWe
	GT load		70	%
	SOFC load		100	%
	Net electrical system efficiency	η_{sys}	47.58	%
	Exhaust temperature	T_{exh}	246.60	°C

Table D.83: CT parameters for the diesel-fuelled SOFC-GT model at cruising speed for a power split of 15-85 and an SOFC load of 75%

Component	Parameter		CT Value	
Compressor	Isentropic efficiency	η_{is}	0.862	-
	Pressure ratio	Π	17.72	-
	Mechanical efficiency	η_m	0.996	-
Turbine	Isentropic efficiency	η_{is}	0.85	-
	Pressure ratio	Π	4.67	-
	Mechanical efficiency	η_m	0.996	-
Power turbine	Isentropic efficiency	η_{is}	0.845	-
	Pressure ratio	Π	3.68	-
	Mechanical efficiency	η_m	0.996	-
Generator	Generator efficiency	η_{gen}	0.97	
Pumps	Isentropic efficiency	η_{is}	0.85	-
	Mechanical efficiency	η_m	0.8	-
SOFC	Fuel utilization factor	u_f	0.8	-
	Cell voltage	V_{cell}	0.89	V
	Stack temperature	T_{stack}	750	°C
	Inlet temperature	T_{in}	700	°C
	Outlet temperature	T_{out}	790	°C
	Anode pressure drop	Δp_{an}	0.02	bar
	Cathode pressure drop	Δp_{ca}	0.02	bar
Fuel reformer	Reformer temperature	T_{reform}	600	°C
	Steam to fuel ratio	S/F	2.61	kg/kg
	Pressure drop	Δp	0.01	bar
Heat exchangers	Pressure drop	Δp	0.01	bar
Pumps	Isentropic efficiency	η_{is}	0.85	-
	Mechanical efficiency	η_m	0.8	-
Blowers	Isentropic efficiency	η_{is}	0.85	-
	Mechanical efficiency	η_m	0.8	-
Overall	AOG combustion	$\frac{m_{AOG,GT}}{m_{AOG}}$	1	-
	Gross GT power	$P_{out,GT}$	4.18	MWe
	Gross SOFC power	$P_{out,SOFC}$	2.12	MWe
	Net system power output	P_{out}	5.60	MWe
	GT load		60	%
	SOFC load		75	%
	Net electrical system efficiency	η_{sys}	49.71	%
	Exhaust temperature	T_{exh}	232.29	°C

Table D.84: CT parameters for the diesel-fuelled SOFC-GT model at cruising speed for a power split of 15-85 and an SOFC load of 100%

Component	Parameter		CT Value	
Compressor	Isentropic efficiency	η_{is}	0.859	-
	Pressure ratio	Π	16.05	-
	Mechanical efficiency	η_m	0.997	-
Turbine	Isentropic efficiency	η_{is}	0.84	-
	Pressure ratio	Π	4.70	-
	Mechanical efficiency	η_m	0.997	-
Power turbine	Isentropic efficiency	η_{is}	0.84	-
	Pressure ratio	Π	4.31	-
	Mechanical efficiency	η_m	0.997	-
Generator	Generator efficiency	η_{gen}	0.966	
Pumps	Isentropic efficiency	η_{is}	0.85	-
	Mechanical efficiency	η_m	0.8	-
SOFC	Fuel utilization factor	u_f	0.8	-
	Cell voltage	V_{cell}	0.85	V
	Stack temperature	T_{stack}	750	°C
	Inlet temperature	T_{in}	700	°C
	Outlet temperature	T_{out}	790	°C
	Anode pressure drop	Δp_{an}	0.02	bar
	Cathode pressure drop	Δp_{ca}	0.02	bar
Fuel reformer	Reformer temperature	T_{reform}	600	°C
	Steam to fuel ratio	S/F	2.61	kg/kg
	Pressure drop	Δp	0.01	bar
Heat exchangers	Pressure drop	Δp	0.01	bar
Pumps	Isentropic efficiency	η_{is}	0.85	-
	Mechanical efficiency	η_m	0.8	-
Blowers	Isentropic efficiency	η_{is}	0.85	-
	Mechanical efficiency	η_m	0.8	-
Overall	AOG combustion	$\frac{m_{AOG,GT}}{m_{AOG}}$	1	-
	Gross GT power	$P_{out,GT}$	3.14	MWe
	Gross SOFC power	$P_{out,SOFC}$	2.89	MWe
	Net system power output	P_{out}	5.60	MWe
	GT load		50	%
	SOFC load		100	%
	Net electrical system efficiency	η_{sys}	54.81	%
	Exhaust temperature	T_{exh}	151.93	°C

Table D.85: CT parameters for the diesel-fuelled SOFC-GT model at cruising speed for a power split of 20-80 and an SOFC load of 75%

Component	Parameter		CT Value	
Compressor	Isentropic efficiency	η_{is}	0.859	-
	Pressure ratio	Π	16.05	-
	Mechanical efficiency	η_m	0.997	-
Turbine	Isentropic efficiency	η_{is}	0.84	-
	Pressure ratio	Π	4.70	-
	Mechanical efficiency	η_m	0.997	-
Power turbine	Isentropic efficiency	η_{is}	0.84	-
	Pressure ratio	Π	4.31	-
	Mechanical efficiency	η_m	0.997	-
Generator	Generator efficiency	η_{gen}	0.966	
Pumps	Isentropic efficiency	η_{is}	0.85	-
	Mechanical efficiency	η_m	0.8	-
SOFC	Fuel utilization factor	u_f	0.8	-
	Cell voltage	V_{cell}	0.89	V
	Stack temperature	T_{stack}	750	°C
	Inlet temperature	T_{in}	700	°C
	Outlet temperature	T_{out}	790	°C
	Anode pressure drop	Δp_{an}	0.02	bar
	Cathode pressure drop	Δp_{ca}	0.02	bar
Fuel reformer	Reformer temperature	T_{reform}	600	°C
	Steam to fuel ratio	S/F	2.61	kg/kg
	Pressure drop	Δp	0.01	bar
Heat exchangers	Pressure drop	Δp	0.01	bar
Pumps	Isentropic efficiency	η_{is}	0.85	-
	Mechanical efficiency	η_m	0.8	-
Blowers	Isentropic efficiency	η_{is}	0.85	-
	Mechanical efficiency	η_m	0.8	-
Overall	AOG combustion	$\frac{m_{AOG,GT}}{m_{AOG}}$	1	-
	Gross GT power	$P_{out,GT}$	2.01	MWe
	Gross SOFC power	$P_{out,SOFC}$	4.18	MWe
	Net system power output	P_{out}	5.61	MWe
	GT load		50	%
	SOFC load		75	%
	Net electrical system efficiency	η_{sys}	57.07	%
	Exhaust temperature	T_{exh}	151.43	°C

Table D.86: CT parameters for the diesel-fuelled SOFC-GT model at cruising speed for a power split of 20-80 and an SOFC load of 100%

Component	Parameter		CT Value	
Compressor	Isentropic efficiency	η_{is}	0.82	-
	Pressure ratio	Π	10.62	-
	Mechanical efficiency	η_m	0.998	-
Turbine	Isentropic efficiency	η_{is}	0.79	-
	Pressure ratio	Π	5.04	-
	Mechanical efficiency	η_m	0.998	-
Power turbine	Isentropic efficiency	η_{is}	0.79	-
	Pressure ratio	Π	2.04	-
	Mechanical efficiency	η_m	0.998	-
Generator	Generator efficiency	η_{gen}	0.93	
Pumps	Isentropic efficiency	η_{is}	0.85	-
	Mechanical efficiency	η_m	0.8	-
SOFC	Fuel utilization factor	u_f	0.8	-
	Cell voltage	V_{cell}	0.85	V
	Stack temperature	T_{stack}	750	°C
	Inlet temperature	T_{in}	700	°C
	Outlet temperature	T_{out}	790	°C
	Anode pressure drop	Δp_{an}	0.02	bar
	Cathode pressure drop	Δp_{ca}	0.02	bar
Fuel reformer	Reformer temperature	T_{reform}	600	°C
	Steam to fuel ratio	S/F	2.61	kg/kg
	Pressure drop	Δp	0.01	bar
Heat exchangers	Pressure drop	Δp	0.01	bar
Pumps	Isentropic efficiency	η_{is}	0.85	-
	Mechanical efficiency	η_m	0.8	-
Blowers	Isentropic efficiency	η_{is}	0.85	-
	Mechanical efficiency	η_m	0.8	-
Overall	AOG combustion	$\frac{m_{AOG,GT}}{m_{AOG}}$	0.9	-
	Gross GT power	$P_{out,GT}$	1.01	MWe
	Gross SOFC power	$P_{out,SOFC}$	5.58	MWe
	Net system power output	P_{out}	0.80	MWe
	GT load		20	%
	SOFC load		100	%
	Net electrical system efficiency	η_{sys}	54.27	%
	Exhaust temperature	T_{exh}	117.16	°C

Table D.87: CT parameters for the diesel-fuelled SOFC-GT model at cruising speed for a power split of 25-75 and an SOFC load of 75%

Component	Parameter		CT Value	
Compressor	Isentropic efficiency	η_{is}	0.84	-
	Pressure ratio	Π	12.61	-
	Mechanical efficiency	η_m	0.998	-
Turbine	Isentropic efficiency	η_{is}	0.817	-
	Pressure ratio	Π	4.94	-
	Mechanical efficiency	η_m	0.998	-
Power turbine	Isentropic efficiency	η_{is}	0.817	-
	Pressure ratio	Π	2.58	-
	Mechanical efficiency	η_m	0.998	-
Generator	Generator efficiency	η_{gen}	0.95	
Pumps	Isentropic efficiency	η_{is}	0.85	-
	Mechanical efficiency	η_m	0.8	-
SOFC	Fuel utilization factor	u_f	0.8	-
	Cell voltage	V_{cell}	0.89	V
	Stack temperature	T_{stack}	750	°C
	Inlet temperature	T_{in}	700	°C
	Outlet temperature	T_{out}	790	°C
	Anode pressure drop	Δp_{an}	0.02	bar
	Cathode pressure drop	Δp_{ca}	0.02	bar
Fuel reformer	Reformer temperature	T_{reform}	600	°C
	Steam to fuel ratio	S/F	2.61	kg/kg
	Pressure drop	Δp	0.01	bar
Heat exchangers	Pressure drop	Δp	0.01	bar
Pumps	Isentropic efficiency	η_{is}	0.85	-
	Mechanical efficiency	η_m	0.8	-
Blowers	Isentropic efficiency	η_{is}	0.85	-
	Mechanical efficiency	η_m	0.8	-
Overall	AOG combustion	$\frac{m_{AOG,GT}}{m_{AOG}}$	0.82	-
	Gross GT power	$P_{out,GT}$	1.13	MWe
	Gross SOFC power	$P_{out,SOFC}$	5.23	MWe
	Net system power output	P_{out}	5.61	MWe
	GT load		30	%
	SOFC load		75	%
	Net electrical system efficiency	η_{sys}	59.70	%
	Exhaust temperature	T_{exh}	115.37	°C

Table D.88: CT parameters for the diesel-fuelled SOFC-GT model at cruising speed for a power split of 25-75 and an SOFC load of 100%

Component	Parameter		CT Value	
Compressor	Isentropic efficiency	η_{is}	0.843	-
	Pressure ratio	Π	23.54	-
	Mechanical efficiency	η_m	0.997	-
Turbine	Isentropic efficiency	η_{is}	0.865	-
	Pressure ratio	Π	4.80	-
	Mechanical efficiency	η_m	0.997	-
Power turbine	Isentropic efficiency	η_{is}	0.86	-
	Pressure ratio	Π	4.76	-
	Mechanical efficiency	η_m	0.996	-
Generator	Generator efficiency	η_{gen}	0.975	
Pumps	Isentropic efficiency	η_{is}	0.85	-
	Mechanical efficiency	η_m	0.8	-
SOFC	Fuel utilization factor	u_f	0.8	-
	Cell voltage	V_{cell}	0.85	V
	Stack temperature	T_{stack}	750	°C
	Inlet temperature	T_{in}	700	°C
	Outlet temperature	T_{out}	790	°C
	Anode pressure drop	Δp_{an}	0.02	bar
	Cathode pressure drop	Δp_{ca}	0.02	bar
Fuel reformer	Reformer temperature	T_{reform}	600	°C
	Steam to fuel ratio	S/F	2.61	kg/kg
	Pressure drop	Δp	0.01	bar
Heat exchangers	Pressure drop	Δp	0.01	bar
Pumps	Isentropic efficiency	η_{is}	0.85	-
	Mechanical efficiency	η_m	0.8	-
Blowers	Isentropic efficiency	η_{is}	0.86	-
	Mechanical efficiency	η_m	0.8	-
Overall	AOG combustion	$\frac{m_{AOG,GT}}{m_{AOG}}$	0	-
	Gross GT power	$P_{out,GT}$	0	MWe
	Gross SOFC power	$P_{out,SOFC}$	6.93	MWe
	Net system power output	P_{out}	5.61	MWe
	GT load		0	%
	SOFC load		96	%
	Net electrical system efficiency	η_{sys}	50.99	%
	Exhaust temperature	T_{exh}	152.71	°C

Table D.89: CT parameters for the diesel-fuelled SOFC-GT model at cruising speed for a power split of 30-70 and an SOFC load of 75%

Component	Parameter		CT Value	
Compressor	Isentropic efficiency	η_{is}	0.79	-
	Pressure ratio	Π	8.38	-
	Mechanical efficiency	η_m	0.998	-
Turbine	Isentropic efficiency	η_{is}	0.72	-
	Pressure ratio	Π	6.38	-
	Mechanical efficiency	η_m	0.998	-
Power turbine	Isentropic efficiency	η_{is}	0.72	-
	Pressure ratio	Π	1.27	-
	Mechanical efficiency	η_m	0.998	-
Generator	Generator efficiency	η_{gen}	0.874	
Pumps	Isentropic efficiency	η_{is}	0.85	-
	Mechanical efficiency	η_m	0.8	-
SOFC	Fuel utilization factor	u_f	0.8	-
	Cell voltage	V_{cell}	0.89	V
	Stack temperature	T_{stack}	750	°C
	Inlet temperature	T_{in}	700	°C
	Outlet temperature	T_{out}	790	°C
	Anode pressure drop	Δp_{an}	0.02	bar
	Cathode pressure drop	Δp_{ca}	0.02	bar
Fuel reformer	Reformer temperature	T_{reform}	600	°C
	Steam to fuel ratio	S/F	2.61	kg/kg
	Pressure drop	Δp	0.01	bar
Heat exchangers	Pressure drop	Δp	0.01	bar
Pumps	Isentropic efficiency	η_{is}	0.85	-
	Mechanical efficiency	η_m	0.8	-
Blowers	Isentropic efficiency	η_{is}	0.85	-
	Mechanical efficiency	η_m	0.8	-
Overall	AOG combustion	$\frac{m_{AOG,GT}}{m_{AOG}}$	0.65	-
	Gross GT power	$P_{out,GT}$	0.17	MWe
	Gross SOFC power	$P_{out,SOFC}$	6.28	MWe
	Net system power output	P_{out}	5.60	MWe
	GT load		10	%
	SOFC load		75	%
	Net electrical system efficiency	η_{sys}	58.20	%
	Exhaust temperature	T_{exh}	107.66	°C

Table D.90: CT parameters for the diesel-fuelled SOFC-GT model at cruising speed for a power split of 30-70 and an SOFC load of 100%

Component	Parameter		CT Value	
Compressor	Isentropic efficiency	η_{is}	0.843	-
	Pressure ratio	Π	23.54	-
	Mechanical efficiency	η_m	0.997	-
Turbine	Isentropic efficiency	η_{is}	0.865	-
	Pressure ratio	Π	4.80	-
	Mechanical efficiency	η_m	0.997	-
Power turbine	Isentropic efficiency	η_{is}	0.86	-
	Pressure ratio	Π	4.76	-
	Mechanical efficiency	η_m	0.996	-
Generator	Generator efficiency	η_{gen}	0.975	
Pumps	Isentropic efficiency	η_{is}	0.85	-
	Mechanical efficiency	η_m	0.8	-
SOFC	Fuel utilization factor	u_f	0.8	-
	Cell voltage	V_{cell}	0.89	V
	Stack temperature	T_{stack}	750	°C
	Inlet temperature	T_{in}	700	°C
	Outlet temperature	T_{out}	790	°C
	Anode pressure drop	Δp_{an}	0.02	bar
	Cathode pressure drop	Δp_{ca}	0.02	bar
Fuel reformer	Reformer temperature	T_{reform}	600	°C
	Steam to fuel ratio	S/F	2.61	kg/kg
	Pressure drop	Δp	0.01	bar
Heat exchangers	Pressure drop	Δp	0.01	bar
Pumps	Isentropic efficiency	η_{is}	0.85	-
	Mechanical efficiency	η_m	0.8	-
Blowers	Isentropic efficiency	η_{is}	0.85	-
	Mechanical efficiency	η_m	0.8	-
Overall	AOG combustion	$\frac{m_{AOG,GT}}{m_{AOG}}$	0	-
	Gross GT power	$P_{out,GT}$	0	MWe
	Gross SOFC power	$P_{out,SOFC}$	6.73	MWe
	Net system power output	P_{out}	5.60	MWe
	GT load		0	%
	SOFC load		80	%
	Net electrical system efficiency	η_{sys}	54.24	%
	Exhaust temperature	T_{exh}	151.75	°C

Table D.91: CT parameters for the diesel-fuelled SOFC-GT model at top speed for a power split of 4.6-95.4

Component	Parameter		CT Value	
Compressor	Isentropic efficiency	η_{is}	0.843	-
	Pressure ratio	Π	23.54	-
	Mechanical efficiency	η_m	0.997	-
Turbine	Isentropic efficiency	η_{is}	0.865	-
	Pressure ratio	Π	4.80	-
	Mechanical efficiency	η_m	0.997	-
Power turbine	Isentropic efficiency	η_{is}	0.86	-
	Pressure ratio	Π	4.76	-
	Mechanical efficiency	η_m	0.996	-
Generator	Generator efficiency	η_{gen}	0.975	
Pumps	Isentropic efficiency	η_{is}	0.85	-
	Mechanical efficiency	η_m	0.8	-
SOFC	Fuel utilization factor	u_f	0.8	-
	Cell voltage	V_{cell}	0.89	V
	Stack temperature	T_{stack}	750	°C
	Inlet temperature	T_{in}	700	°C
	Outlet temperature	T_{out}	790	°C
	Anode pressure drop	Δp_{an}	0.02	bar
	Cathode pressure drop	Δp_{ca}	0.02	bar
Fuel reformer	Reformer temperature	T_{reform}	600	°C
	Steam to fuel ratio	S/F	2.61	kg/kg
	Pressure drop	Δp	0.01	bar
Heat exchangers	Pressure drop	Δp	0.01	bar
Pumps	Isentropic efficiency	η_{is}	0.85	-
	Mechanical efficiency	η_m	0.8	-
Blowers	Isentropic efficiency	η_{is}	0.85	-
	Mechanical efficiency	η_m	0.8	-
Overall	AOG combustion	$\frac{m_{AOG,GT}}{m_{AOG}}$	1	-
	Gross GT power	$P_{out,GT}$	22.22	MWe
	Gross SOFC power	$P_{out,SOFC}$	1.28	MWe
	Net system power output	P_{out}	23.31	MWe
	GT load		100	%
	SOFC load		100	%
	Net electrical system efficiency	η_{sys}	38.52	%
	Exhaust temperature	T_{exh}	498.72	°C

Table D.92: CT parameters for the diesel-fuelled SOFC-GT model at top speed for a power split of 10-90

Component	Parameter		CT Value	
Compressor	Isentropic efficiency	η_{is}	0.843	-
	Pressure ratio	Π	23.54	-
	Mechanical efficiency	η_m	0.997	-
Turbine	Isentropic efficiency	η_{is}	0.865	-
	Pressure ratio	Π	4.80	-
	Mechanical efficiency	η_m	0.997	-
Power turbine	Isentropic efficiency	η_{is}	0.86	-
	Pressure ratio	Π	4.76	-
	Mechanical efficiency	η_m	0.996	-
Generator	Generator efficiency	η_{gen}	0.975	
Pumps	Isentropic efficiency	η_{is}	0.85	-
	Mechanical efficiency	η_m	0.8	-
SOFC	Fuel utilization factor	u_f	0.8	-
	Cell voltage	V_{cell}	0.89	V
	Stack temperature	T_{stack}	750	°C
	Inlet temperature	T_{in}	700	°C
	Outlet temperature	T_{out}	790	°C
	Anode pressure drop	Δp_{an}	0.02	bar
	Cathode pressure drop	Δp_{ca}	0.02	bar
Fuel reformer	Reformer temperature	T_{reform}	600	°C
	Steam to fuel ratio	S/F	2.61	kg/kg
	Pressure drop	Δp	0.01	bar
Heat exchangers	Pressure drop	Δp	0.01	bar
Pumps	Isentropic efficiency	η_{is}	0.85	-
	Mechanical efficiency	η_m	0.8	-
Blowers	Isentropic efficiency	η_{is}	0.85	-
	Mechanical efficiency	η_m	0.8	-
Overall	AOG combustion	$\frac{m_{AOG,GT}}{m_{AOG}}$	1	-
	Gross GT power	$P_{out,GT}$	20.98	MWe
	Gross SOFC power	$P_{out,SOFC}$	2.79	MWe
	Net system power output	P_{out}	23.31	MWe
	GT load		100	%
	SOFC load		100	%
	Net electrical system efficiency	η_{sys}	39.86	%
	Exhaust temperature	T_{exh}	456.12	°C

Table D.93: CT parameters for the diesel-fuelled SOFC-GT model at top speed for a power split of 15-85

Component	Parameter		CT Value	
Compressor	Isentropic efficiency	η_{is}	0.843	-
	Pressure ratio	Π	23.54	-
	Mechanical efficiency	η_m	0.997	-
Turbine	Isentropic efficiency	η_{is}	0.865	-
	Pressure ratio	Π	4.80	-
	Mechanical efficiency	η_m	0.997	-
Power turbine	Isentropic efficiency	η_{is}	0.86	-
	Pressure ratio	Π	4.76	-
	Mechanical efficiency	η_m	0.996	-
Generator	Generator efficiency	η_{gen}	0.975	
Pumps	Isentropic efficiency	η_{is}	0.85	-
	Mechanical efficiency	η_m	0.8	-
SOFC	Fuel utilization factor	u_f	0.8	-
	Cell voltage	V_{cell}	0.89	V
	Stack temperature	T_{stack}	750	°C
	Inlet temperature	T_{in}	700	°C
	Outlet temperature	T_{out}	790	°C
	Anode pressure drop	Δp_{an}	0.02	bar
	Cathode pressure drop	Δp_{ca}	0.02	bar
Fuel reformer	Reformer temperature	T_{reform}	600	°C
	Steam to fuel ratio	S/F	2.61	kg/kg
	Pressure drop	Δp	0.01	bar
Heat exchangers	Pressure drop	Δp	0.01	bar
Pumps	Isentropic efficiency	η_{is}	0.85	-
	Mechanical efficiency	η_m	0.8	-
Blowers	Isentropic efficiency	η_{is}	0.85	-
	Mechanical efficiency	η_m	0.8	-
Overall	AOG combustion	$\frac{m_{AOG,GT}}{m_{AOG}}$	1	-
	Gross GT power	$P_{out,GT}$	19.75	MWe
	Gross SOFC power	$P_{out,SOFC}$	4.18	MWe
	Net system power output	P_{out}	23.31	MWe
	GT load		100	%
	SOFC load		100	%
	Net electrical system efficiency	η_{sys}	41.24	%
	Exhaust temperature	T_{exh}	419.79	°C

Table D.94: CT parameters for the diesel-fuelled SOFC-GT model at top speed for a power split of 20-80

Component	Parameter		CT Value	
Compressor	Isentropic efficiency	η_{is}	0.843	-
	Pressure ratio	Π	23.54	-
	Mechanical efficiency	η_m	0.997	-
Turbine	Isentropic efficiency	η_{is}	0.865	-
	Pressure ratio	Π	4.80	-
	Mechanical efficiency	η_m	0.997	-
Power turbine	Isentropic efficiency	η_{is}	0.86	-
	Pressure ratio	Π	4.76	-
	Mechanical efficiency	η_m	0.996	-
Generator	Generator efficiency	η_{gen}	0.975	
Pumps	Isentropic efficiency	η_{is}	0.85	-
	Mechanical efficiency	η_m	0.8	-
SOFC	Fuel utilization factor	u_f	0.8	-
	Cell voltage	V_{cell}	0.89	V
	Stack temperature	T_{stack}	750	°C
	Inlet temperature	T_{in}	700	°C
	Outlet temperature	T_{out}	790	°C
	Anode pressure drop	Δp_{an}	0.02	bar
	Cathode pressure drop	Δp_{ca}	0.02	bar
Fuel reformer	Reformer temperature	T_{reform}	600	°C
	Steam to fuel ratio	S/F	2.61	kg/kg
	Pressure drop	Δp	0.01	bar
Heat exchangers	Pressure drop	Δp	0.01	bar
Pumps	Isentropic efficiency	η_{is}	0.85	-
	Mechanical efficiency	η_m	0.8	-
Blowers	Isentropic efficiency	η_{is}	0.85	-
	Mechanical efficiency	η_m	0.8	-
Overall	AOG combustion	$\frac{m_{AOG,GT}}{m_{AOG}}$	1	-
	Gross GT power	$P_{out,GT}$	18.55	MWe
	Gross SOFC power	$P_{out,SOFC}$	5.58	MWe
	Net system power output	P_{out}	23.31	MWe
	GT load		100	%
	SOFC load		100	%
	Net electrical system efficiency	η_{sys}	42.69	%
	Exhaust temperature	T_{exh}	384.14	°C

Table D.95: CT parameters for the diesel-fuelled SOFC-GT model at top speed for a power split of 25-75

Component	Parameter		CT Value	
Compressor	Isentropic efficiency	η_{is}	0.843	-
	Pressure ratio	Π	23.54	-
	Mechanical efficiency	η_m	0.997	-
Turbine	Isentropic efficiency	η_{is}	0.865	-
	Pressure ratio	Π	4.80	-
	Mechanical efficiency	η_m	0.997	-
Power turbine	Isentropic efficiency	η_{is}	0.86	-
	Pressure ratio	Π	4.76	-
	Mechanical efficiency	η_m	0.996	-
Generator	Generator efficiency	η_{gen}	0.975	
Pumps	Isentropic efficiency	η_{is}	0.85	-
	Mechanical efficiency	η_m	0.8	-
SOFC	Fuel utilization factor	u_f	0.8	-
	Cell voltage	V_{cell}	0.89	V
	Stack temperature	T_{stack}	750	°C
	Inlet temperature	T_{in}	700	°C
	Outlet temperature	T_{out}	790	°C
	Anode pressure drop	Δp_{an}	0.02	bar
	Cathode pressure drop	Δp_{ca}	0.02	bar
Fuel reformer	Reformer temperature	T_{reform}	600	°C
	Steam to fuel ratio	S/F	2.61	kg/kg
	Pressure drop	Δp	0.01	bar
Heat exchangers	Pressure drop	Δp	0.01	bar
Pumps	Isentropic efficiency	η_{is}	0.85	-
	Mechanical efficiency	η_m	0.8	-
Blowers	Isentropic efficiency	η_{is}	0.85	-
	Mechanical efficiency	η_m	0.8	-
Overall	AOG combustion	$\frac{m_{AOG,GT}}{m_{AOG}}$	1	-
	Gross GT power	$P_{out,GT}$	17.37	MWe
	Gross SOFC power	$P_{out,SOFC}$	6.97	MWe
	Net system power output	P_{out}	23.31	MWe
	GT load		100	%
	SOFC load		100	%
	Net electrical system efficiency	η_{sys}	44.24	%
	Exhaust temperature	T_{exh}	349.52	°C

Table D.96: CT parameters for the diesel-fuelled SOFC-GT model at top speed for a power split of 30-70

Component	Parameter		CT Value	
Compressor	Isentropic efficiency	η_{is}	0.843	-
	Pressure ratio	Π	23.54	-
	Mechanical efficiency	η_m	0.997	-
Turbine	Isentropic efficiency	η_{is}	0.865	-
	Pressure ratio	Π	4.80	-
	Mechanical efficiency	η_m	0.997	-
Power turbine	Isentropic efficiency	η_{is}	0.86	-
	Pressure ratio	Π	4.76	-
	Mechanical efficiency	η_m	0.996	-
Generator	Generator efficiency	η_{gen}	0.975	
Pumps	Isentropic efficiency	η_{is}	0.85	-
	Mechanical efficiency	η_m	0.8	-
SOFC	Fuel utilization factor	u_f	0.8	-
	Cell voltage	V_{cell}	0.89	V
	Stack temperature	T_{stack}	750	°C
	Inlet temperature	T_{in}	700	°C
	Outlet temperature	T_{out}	790	°C
	Anode pressure drop	Δp_{an}	0.02	bar
	Cathode pressure drop	Δp_{ca}	0.02	bar
Fuel reformer	Reformer temperature	T_{reform}	600	°C
	Steam to fuel ratio	S/F	2.61	kg/kg
	Pressure drop	Δp	0.01	bar
Heat exchangers	Pressure drop	Δp	0.01	bar
Pumps	Isentropic efficiency	η_{is}	0.85	-
	Mechanical efficiency	η_m	0.8	-
Blowers	Isentropic efficiency	η_{is}	0.85	-
	Mechanical efficiency	η_m	0.8	-
Overall	AOG combustion	$\frac{m_{AOG,GT}}{m_{AOG}}$	1	-
	Gross GT power	$P_{out,GT}$	16.35	MWe
	Gross SOFC power	$P_{out,SOFC}$	8.37	MWe
	Net system power output	P_{out}	23.31	MWe
	GT load		100	%
	SOFC load		100	%
	Net electrical system efficiency	η_{sys}	45.80	%
	Exhaust temperature	T_{exh}	314.48	°C

D.5.2. Methanol

The parameters for silent operation are given in Table D.97. Next, Table D.98 to Table D.109 show the parameters for cruising speed. Lastly, Table D.110 to Table D.115 show the parameters for top speed.

Table D.97: CT parameters for the MeOH-fuelled SOFC-GT model at silent speed

Component	Parameter		CT Value	
Compressor	Isentropic efficiency	η_{is}	0.843	-
	Pressure ratio	Π	23.54	-
	Mechanical efficiency	η_m	0.997	-
Turbine	Isentropic efficiency	η_{is}	0.865	-
	Pressure ratio	Π	4.80	-
	Mechanical efficiency	η_m	0.997	-
Power turbine	Isentropic efficiency	η_{is}	0.86	-
	Pressure ratio	Π	4.76	-
	Mechanical efficiency	η_m	0.996	-
Generator	Generator efficiency	η_{gen}	0.975	
Pumps	Isentropic efficiency	η_{is}	0.85	-
	Mechanical efficiency	η_m	0.8	-
SOFC	Fuel utilization factor	u_f	0.8	-
	Cell voltage	V_{cell}	0.89	V
	Stack temperature	T_{stack}	750	°C
	Inlet temperature	T_{in}	700	°C
	Outlet temperature	T_{out}	790	°C
	Anode pressure drop	Δp_{an}	0.02	bar
	Cathode pressure drop	Δp_{ca}	0.02	bar
Fuel reformer	Reformer temperature	T_{reform}	600	°C
	Steam to fuel ratio	S/F	0.68	kg/kg
	Pressure drop	Δp	0.01	bar
Heat exchangers	Pressure drop	Δp	0.01	bar
Pumps	Isentropic efficiency	η_{is}	0.85	-
	Mechanical efficiency	η_m	0.8	-
Blowers	Isentropic efficiency	η_{is}	0.85	-
	Mechanical efficiency	η_m	0.8	-
Overall	AOG combustion	$\frac{m_{AOG,GT}}{m_{AOG}}$	0	-
	Gross GT power	$P_{out,GT}$	0	MWe
	Gross SOFC power	$P_{out,SOFC}$	0.97	MWe
	Net system power output	P_{out}	0.80	MWe
	GT load		0	%
	SOFC load		75	%
	Net electrical system efficiency	η_{sys}	50.44	%
	Exhaust temperature	T_{exh}	207.34	°C

Table D.98: CT parameters for the MeOH-fuelled SOFC-GT model at cruising speed for a power split of 4.6-95.4 and an SOFC load of 75%

Component	Parameter		CT Value	
Compressor	Isentropic efficiency	η_{is}	0.843	-
	Pressure ratio	Π	23.54	-
	Mechanical efficiency	η_m	0.997	-
Turbine	Isentropic efficiency	η_{is}	0.865	-
	Pressure ratio	Π	4.80	-
	Mechanical efficiency	η_m	0.997	-
Power turbine	Isentropic efficiency	η_{is}	0.86	-
	Pressure ratio	Π	4.76	-
	Mechanical efficiency	η_m	0.996	-
Generator	Generator efficiency	η_{gen}	0.975	
Pumps	Isentropic efficiency	η_{is}	0.85	-
	Mechanical efficiency	η_m	0.8	-
SOFC	Fuel utilization factor	u_f	0.8	-
	Cell voltage	V_{cell}	0.89	V
	Stack temperature	T_{stack}	750	°C
	Inlet temperature	T_{in}	700	°C
	Outlet temperature	T_{out}	790	°C
	Anode pressure drop	Δp_{an}	0.02	bar
	Cathode pressure drop	Δp_{ca}	0.02	bar
Fuel reformer	Reformer temperature	T_{reform}	600	°C
	Steam to fuel ratio	S/F	0.68	kg/kg
	Pressure drop	Δp	0.01	bar
Heat exchangers	Pressure drop	Δp	0.01	bar
Pumps	Isentropic efficiency	η_{is}	0.85	-
	Mechanical efficiency	η_m	0.8	-
Blowers	Isentropic efficiency	η_{is}	0.85	-
	Mechanical efficiency	η_m	0.8	-
Overall	AOG combustion	$\frac{m_{AOG,GT}}{m_{AOG}}$	1	-
	Gross GT power	$P_{out,GT}$	4.78	MWe
	Gross SOFC power	$P_{out,SOFC}$	0.96	MWe
	Net system power output	P_{out}	5.60	MWe
	GT load		100	%
	SOFC load		75	%
	Net electrical system efficiency	η_{sys}	41.55	%
	Exhaust temperature	T_{exh}	418.75	°C

Table D.99: CT parameters for the MeOH-fuelled SOFC-GT model at cruising speed for a power split of 4.6-95.4 and an SOFC load of 100%

Component	Parameter		CT Value	
Compressor	Isentropic efficiency	η_{is}	0.843	-
	Pressure ratio	Π	23.54	-
	Mechanical efficiency	η_m	0.997	-
Turbine	Isentropic efficiency	η_{is}	0.865	-
	Pressure ratio	Π	4.80	-
	Mechanical efficiency	η_m	0.997	-
Power turbine	Isentropic efficiency	η_{is}	0.86	-
	Pressure ratio	Π	4.76	-
	Mechanical efficiency	η_m	0.996	-
Generator	Generator efficiency	η_{gen}	0.975	
Pumps	Isentropic efficiency	η_{is}	0.85	-
	Mechanical efficiency	η_m	0.8	-
SOFC	Fuel utilization factor	u_f	0.8	-
	Cell voltage	V_{cell}	0.85	V
	Stack temperature	T_{stack}	750	°C
	Inlet temperature	T_{in}	700	°C
	Outlet temperature	T_{out}	790	°C
	Anode pressure drop	Δp_{an}	0.02	bar
	Cathode pressure drop	Δp_{ca}	0.02	bar
Fuel reformer	Reformer temperature	T_{reform}	600	°C
	Steam to fuel ratio	S/F	0.68	kg/kg
	Pressure drop	Δp	0.01	bar
Heat exchangers	Pressure drop	Δp	0.01	bar
Pumps	Isentropic efficiency	η_{is}	0.85	-
	Mechanical efficiency	η_m	0.8	-
Blowers	Isentropic efficiency	η_{is}	0.85	-
	Mechanical efficiency	η_m	0.8	-
Overall	AOG combustion	$\frac{m_{AOG,GT}}{m_{AOG}}$	1	-
	Gross GT power	$P_{out,GT}$	4.54	MWe
	Gross SOFC power	$P_{out,SOFC}$	1.29	MWe
	Net system power output	P_{out}	5.60	MWe
	GT load		100	%
	SOFC load		100	%
	Net electrical system efficiency	η_{sys}	42.42	%
	Exhaust temperature	T_{exh}	380.64	°C

Table D.100: CT parameters for the MeOH-fuelled SOFC-GT model at cruising speed for a power split of 10-90 and an SOFC load of 75%

Component	Parameter		CT Value	
Compressor	Isentropic efficiency	η_{is}	0.857	-
	Pressure ratio	Π	20.69	-
	Mechanical efficiency	η_m	0.997	-
Turbine	Isentropic efficiency	η_{is}	0.86	-
	Pressure ratio	Π	4.72	-
	Mechanical efficiency	η_m	0.997	-
Power turbine	Isentropic efficiency	η_{is}	0.855	-
	Pressure ratio	Π	4.25	-
	Mechanical efficiency	η_m	0.997	-
Generator	Generator efficiency	η_{gen}	0.974	
Pumps	Isentropic efficiency	η_{is}	0.85	-
	Mechanical efficiency	η_m	0.8	-
SOFC	Fuel utilization factor	u_f	0.8	-
	Cell voltage	V_{cell}	0.89	V
	Stack temperature	T_{stack}	750	°C
	Inlet temperature	T_{in}	700	°C
	Outlet temperature	T_{out}	790	°C
	Anode pressure drop	Δp_{an}	0.02	bar
	Cathode pressure drop	Δp_{ca}	0.02	bar
Fuel reformer	Reformer temperature	T_{reform}	600	°C
	Steam to fuel ratio	S/F	0.68	kg/kg
	Pressure drop	Δp	0.01	bar
Heat exchangers	Pressure drop	Δp	0.01	bar
Pumps	Isentropic efficiency	η_{is}	0.85	-
	Mechanical efficiency	η_m	0.8	-
Blowers	Isentropic efficiency	η_{is}	0.85	-
	Mechanical efficiency	η_m	0.8	-
Overall	AOG combustion	$\frac{m_{AOG,GT}}{m_{AOG}}$	1	-
	Gross GT power	$P_{out,GT}$	3.81	MWe
	Gross SOFC power	$P_{out,SOFC}$	2.11	MWe
	Net system power output	P_{out}	5.60	MWe
	GT load		80	%
	SOFC load		75	%
	Net electrical system efficiency	η_{sys}	45.19	%
	Exhaust temperature	T_{exh}	321.13	°C

Table D.101: CT parameters for the MeOH-fuelled SOFC-GT model at cruising speed for a power split of 10-90 and an SOFC load of 100%

Component	Parameter		CT Value	
Compressor	Isentropic efficiency	η_{is}	0.861	-
	Pressure ratio	Π	19.17	-
	Mechanical efficiency	η_m	0.996	-
Turbine	Isentropic efficiency	η_{is}	0.855	-
	Pressure ratio	Π	4.69	-
	Mechanical efficiency	η_m	0.996	-
Power turbine	Isentropic efficiency	η_{is}	0.855	-
	Pressure ratio	Π	3.96	-
	Mechanical efficiency	η_m	0.996	-
Generator	Generator efficiency	η_{gen}	0.973	
Pumps	Isentropic efficiency	η_{is}	0.85	-
	Mechanical efficiency	η_m	0.8	-
SOFC	Fuel utilization factor	u_f	0.8	-
	Cell voltage	V_{cell}	0.85	V
	Stack temperature	T_{stack}	750	°C
	Inlet temperature	T_{in}	700	°C
	Outlet temperature	T_{out}	790	°C
	Anode pressure drop	Δp_{an}	0.02	bar
	Cathode pressure drop	Δp_{ca}	0.02	bar
Fuel reformer	Reformer temperature	T_{reform}	600	°C
	Steam to fuel ratio	S/F	0.68	kg/kg
	Pressure drop	Δp	0.01	bar
Heat exchangers	Pressure drop	Δp	0.01	bar
Pumps	Isentropic efficiency	η_{is}	0.85	-
	Mechanical efficiency	η_m	0.8	-
Blowers	Isentropic efficiency	η_{is}	0.85	-
	Mechanical efficiency	η_m	0.8	-
Overall	AOG combustion	$\frac{m_{AOG,GT}}{m_{AOG}}$	1	-
	Gross GT power	$P_{out,GT}$	3.16	MWe
	Gross SOFC power	$P_{out,SOFC}$	2.92	MWe
	Net system power output	P_{out}	5.60	MWe
	GT load		70	%
	SOFC load		100	%
	Net electrical system efficiency	η_{sys}	48.68	%
	Exhaust temperature	T_{exh}	246.87	°C

Table D.102: CT parameters for the MeOH-fuelled SOFC-GT model at cruising speed for a power split of 15-85 and an SOFC load of 75%

Component	Parameter		CT Value	
Compressor	Isentropic efficiency	η_{is}	0.862	-
	Pressure ratio	Π	17.72	-
	Mechanical efficiency	η_m	0.996	-
Turbine	Isentropic efficiency	η_{is}	0.85	-
	Pressure ratio	Π	4.67	-
	Mechanical efficiency	η_m	0.996	-
Power turbine	Isentropic efficiency	η_{is}	0.845	-
	Pressure ratio	Π	3.68	-
	Mechanical efficiency	η_m	0.996	-
Generator	Generator efficiency	η_{gen}	0.97	
Pumps	Isentropic efficiency	η_{is}	0.85	-
	Mechanical efficiency	η_m	0.8	-
SOFC	Fuel utilization factor	u_f	0.8	-
	Cell voltage	V_{cell}	0.89	V
	Stack temperature	T_{stack}	750	°C
	Inlet temperature	T_{in}	700	°C
	Outlet temperature	T_{out}	790	°C
	Anode pressure drop	Δp_{an}	0.02	bar
	Cathode pressure drop	Δp_{ca}	0.02	bar
Fuel reformer	Reformer temperature	T_{reform}	600	°C
	Steam to fuel ratio	S/F	0.68	kg/kg
	Pressure drop	Δp	0.01	bar
Heat exchangers	Pressure drop	Δp	0.01	bar
Pumps	Isentropic efficiency	η_{is}	0.85	-
	Mechanical efficiency	η_m	0.8	-
Blowers	Isentropic efficiency	η_{is}	0.85	-
	Mechanical efficiency	η_m	0.8	-
Overall	AOG combustion	$\frac{m_{AOG,GT}}{m_{AOG}}$	1	-
	Gross GT power	$P_{out,GT}$	4.21	MWe
	Gross SOFC power	$P_{out,SOFC}$	2.15	MWe
	Net system power output	P_{out}	5.60	MWe
	GT load		60	%
	SOFC load		75	%
	Net electrical system efficiency	η_{sys}	52.06	%
	Exhaust temperature	T_{exh}	246.87	°C

Table D.103: CT parameters for the MeOH-fuelled SOFC-GT model at cruising speed for a power split of 15-85 and an SOFC load of 100%

Component	Parameter		CT Value	
Compressor	Isentropic efficiency	η_{is}	0.859	-
	Pressure ratio	Π	16.05	-
	Mechanical efficiency	η_m	0.997	-
Turbine	Isentropic efficiency	η_{is}	0.84	-
	Pressure ratio	Π	4.70	-
	Mechanical efficiency	η_m	0.997	-
Power turbine	Isentropic efficiency	η_{is}	0.84	-
	Pressure ratio	Π	4.31	-
	Mechanical efficiency	η_m	0.997	-
Generator	Generator efficiency	η_{gen}	0.966	
Pumps	Isentropic efficiency	η_{is}	0.85	-
	Mechanical efficiency	η_m	0.8	-
SOFC	Fuel utilization factor	u_f	0.8	-
	Cell voltage	V_{cell}	0.85	V
	Stack temperature	T_{stack}	750	°C
	Inlet temperature	T_{in}	700	°C
	Outlet temperature	T_{out}	790	°C
	Anode pressure drop	Δp_{an}	0.02	bar
	Cathode pressure drop	Δp_{ca}	0.02	bar
Fuel reformer	Reformer temperature	T_{reform}	600	°C
	Steam to fuel ratio	S/F	0.68	kg/kg
	Pressure drop	Δp	0.01	bar
Heat exchangers	Pressure drop	Δp	0.01	bar
Pumps	Isentropic efficiency	η_{is}	0.85	-
	Mechanical efficiency	η_m	0.8	-
Blowers	Isentropic efficiency	η_{is}	0.85	-
	Mechanical efficiency	η_m	0.8	-
Overall	AOG combustion	$\frac{m_{AOG,GT}}{m_{AOG}}$	1	-
	Gross GT power	$P_{out,GT}$	4.21	MWe
	Gross SOFC power	$P_{out,SOFC}$	2.15	MWe
	Net system power output	P_{out}	5.60	MWe
	GT load		50	%
	SOFC load		100	%
	Net electrical system efficiency	η_{sys}	52.06	%
	Exhaust temperature	T_{exh}	178.03	°C

Table D.104: CT parameters for the MeOH-fuelled SOFC-GT model at cruising speed for a power split of 20-80 and an SOFC load of 75%

Component	Parameter		CT Value	
Compressor	Isentropic efficiency	η_{is}	0.859	-
	Pressure ratio	Π	16.05	-
	Mechanical efficiency	η_m	0.997	-
Turbine	Isentropic efficiency	η_{is}	0.84	-
	Pressure ratio	Π	4.70	-
	Mechanical efficiency	η_m	0.997	-
Power turbine	Isentropic efficiency	η_{is}	0.84	-
	Pressure ratio	Π	4.31	-
	Mechanical efficiency	η_m	0.997	-
Generator	Generator efficiency	η_{gen}	0.966	
Pumps	Isentropic efficiency	η_{is}	0.85	-
	Mechanical efficiency	η_m	0.8	-
SOFC	Fuel utilization factor	u_f	0.8	-
	Cell voltage	V_{cell}	0.89	V
	Stack temperature	T_{stack}	750	°C
	Inlet temperature	T_{in}	700	°C
	Outlet temperature	T_{out}	790	°C
	Anode pressure drop	Δp_{an}	0.02	bar
	Cathode pressure drop	Δp_{ca}	0.02	bar
Fuel reformer	Reformer temperature	T_{reform}	600	°C
	Steam to fuel ratio	S/F	0.68	kg/kg
	Pressure drop	Δp	0.01	bar
Heat exchangers	Pressure drop	Δp	0.01	bar
Pumps	Isentropic efficiency	η_{is}	0.85	-
	Mechanical efficiency	η_m	0.8	-
Blowers	Isentropic efficiency	η_{is}	0.85	-
	Mechanical efficiency	η_m	0.8	-
Overall	AOG combustion	$\frac{m_{AOG,GT}}{m_{AOG}}$	1	-
	Gross GT power	$P_{out,GT}$	2.02	MWe
	Gross SOFC power	$P_{out,SOFC}$	4.21	MWe
	Net system power output	P_{out}	5.61	MWe
	GT load		50	%
	SOFC load		75	%
	Net electrical system efficiency	η_{sys}	55.03	%
	Exhaust temperature	T_{exh}	178.19	°C

Table D.105: CT parameters for the MeOH-fuelled SOFC-GT model at cruising speed for a power split of 20-80 and an SOFC load of 100%

Component	Parameter		CT Value	
Compressor	Isentropic efficiency	η_{is}	0.82	-
	Pressure ratio	Π	10.62	-
	Mechanical efficiency	η_m	0.998	-
Turbine	Isentropic efficiency	η_{is}	0.79	-
	Pressure ratio	Π	5.04	-
	Mechanical efficiency	η_m	0.998	-
Power turbine	Isentropic efficiency	η_{is}	0.79	-
	Pressure ratio	Π	2.04	-
	Mechanical efficiency	η_m	0.998	-
Generator	Generator efficiency	η_{gen}	0.93	
Pumps	Isentropic efficiency	η_{is}	0.85	-
	Mechanical efficiency	η_m	0.8	-
SOFC	Fuel utilization factor	u_f	0.8	-
	Cell voltage	V_{cell}	0.85	V
	Stack temperature	T_{stack}	750	°C
	Inlet temperature	T_{in}	700	°C
	Outlet temperature	T_{out}	790	°C
	Anode pressure drop	Δp_{an}	0.02	bar
	Cathode pressure drop	Δp_{ca}	0.02	bar
Fuel reformer	Reformer temperature	T_{reform}	600	°C
	Steam to fuel ratio	S/F	0.68	kg/kg
	Pressure drop	Δp	0.01	bar
Heat exchangers	Pressure drop	Δp	0.01	bar
Pumps	Isentropic efficiency	η_{is}	0.85	-
	Mechanical efficiency	η_m	0.8	-
Blowers	Isentropic efficiency	η_{is}	0.85	-
	Mechanical efficiency	η_m	0.8	-
Overall	AOG combustion	$\frac{m_{AOG,GT}}{m_{AOG}}$	1	-
	Gross GT power	$P_{out,GT}$	0.99	MWe
	Gross SOFC power	$P_{out,SOFC}$	5.62	MWe
	Net system power output	P_{out}	5.60	MWe
	GT load		20	%
	SOFC load		100	%
	Net electrical system efficiency	η_{sys}	54.08	%
	Exhaust temperature	T_{exh}	133.50	°C

Table D.106: CT parameters for the MeOH-fuelled SOFC-GT model at cruising speed for a power split of 25-75 and an SOFC load of 75%

Component	Parameter		CT Value	
Compressor	Isentropic efficiency	η_{is}	0.84	-
	Pressure ratio	Π	12.61	-
	Mechanical efficiency	η_m	0.998	-
Turbine	Isentropic efficiency	η_{is}	0.817	-
	Pressure ratio	Π	4.94	-
	Mechanical efficiency	η_m	0.998	-
Power turbine	Isentropic efficiency	η_{is}	0.817	-
	Pressure ratio	Π	2.58	-
	Mechanical efficiency	η_m	0.998	-
Generator	Generator efficiency	η_{gen}	0.95	
Pumps	Isentropic efficiency	η_{is}	0.85	-
	Mechanical efficiency	η_m	0.8	-
SOFC	Fuel utilization factor	u_f	0.8	-
	Cell voltage	V_{cell}	0.89	V
	Stack temperature	T_{stack}	750	°C
	Inlet temperature	T_{in}	700	°C
	Outlet temperature	T_{out}	790	°C
	Anode pressure drop	Δp_{an}	0.02	bar
	Cathode pressure drop	Δp_{ca}	0.02	bar
Fuel reformer	Reformer temperature	T_{reform}	600	°C
	Steam to fuel ratio	S/F	0.68	kg/kg
	Pressure drop	Δp	0.01	bar
Heat exchangers	Pressure drop	Δp	0.01	bar
Pumps	Isentropic efficiency	η_{is}	0.85	-
	Mechanical efficiency	η_m	0.8	-
Blowers	Isentropic efficiency	η_{is}	0.85	-
	Mechanical efficiency	η_m	0.8	-
Overall	AOG combustion	$\frac{m_{AOG,GT}}{m_{AOG}}$	1	-
	Gross GT power	$P_{out,GT}$	1.12	MWe
	Gross SOFC power	$P_{out,SOFC}$	5.26	MWe
	Net system power output	P_{out}	5.61	MWe
	GT load		30	%
	SOFC load		75	%
	Net electrical system efficiency	η_{sys}	61.38	%
	Exhaust temperature	T_{exh}	121.24	°C

Table D.107: CT parameters for the MeOH-fuelled SOFC-GT model at cruising speed for a power split of 25-75 and an SOFC load of 100%

Component	Parameter		CT Value	
Compressor	Isentropic efficiency	η_{is}	0.843	-
	Pressure ratio	Π	23.54	-
	Mechanical efficiency	η_m	0.997	-
Turbine	Isentropic efficiency	η_{is}	0.865	-
	Pressure ratio	Π	4.80	-
	Mechanical efficiency	η_m	0.997	-
Power turbine	Isentropic efficiency	η_{is}	0.86	-
	Pressure ratio	Π	4.76	-
	Mechanical efficiency	η_m	0.996	-
Generator	Generator efficiency	η_{gen}	0.975	
Pumps	Isentropic efficiency	η_{is}	0.85	-
	Mechanical efficiency	η_m	0.8	-
SOFC	Fuel utilization factor	u_f	0.8	-
	Cell voltage	V_{cell}	0.85	V
	Stack temperature	T_{stack}	750	°C
	Inlet temperature	T_{in}	700	°C
	Outlet temperature	T_{out}	790	°C
	Anode pressure drop	Δp_{an}	0.02	bar
	Cathode pressure drop	Δp_{ca}	0.02	bar
Fuel reformer	Reformer temperature	T_{reform}	600	°C
	Steam to fuel ratio	S/F	0.68	kg/kg
	Pressure drop	Δp	0.01	bar
Heat exchangers	Pressure drop	Δp	0.01	bar
Pumps	Isentropic efficiency	η_{is}	0.85	-
	Mechanical efficiency	η_m	0.8	-
Blowers	Isentropic efficiency	η_{is}	0.86	-
	Mechanical efficiency	η_m	0.8	-
Overall	AOG combustion	$\frac{m_{AOG,GT}}{m_{AOG}}$	0	-
	Gross GT power	$P_{out,GT}$	0	MWe
	Gross SOFC power	$P_{out,SOFC}$	6.97	MWe
	Net system power output	P_{out}	5.60	MWe
	GT load		0	%
	SOFC load		96	%
	Net electrical system efficiency	η_{sys}	47.34	%
	Exhaust temperature	T_{exh}	202.54	°C

Table D.108: CT parameters for the MeOH-fuelled SOFC-GT model at cruising speed for a power split of 30-70 and an SOFC load of 75%

Component	Parameter		CT Value	
Compressor	Isentropic efficiency	η_{is}	0.79	-
	Pressure ratio	Π	8.38	-
	Mechanical efficiency	η_m	0.998	-
Turbine	Isentropic efficiency	η_{is}	0.72	-
	Pressure ratio	Π	6.38	-
	Mechanical efficiency	η_m	0.998	-
Power turbine	Isentropic efficiency	η_{is}	0.72	-
	Pressure ratio	Π	1.27	-
	Mechanical efficiency	η_m	0.998	-
Generator	Generator efficiency	η_{gen}	0.874	
Pumps	Isentropic efficiency	η_{is}	0.85	-
	Mechanical efficiency	η_m	0.8	-
SOFC	Fuel utilization factor	u_f	0.8	-
	Cell voltage	V_{cell}	0.89	V
	Stack temperature	T_{stack}	750	°C
	Inlet temperature	T_{in}	700	°C
	Outlet temperature	T_{out}	790	°C
	Anode pressure drop	Δp_{an}	0.02	bar
	Cathode pressure drop	Δp_{ca}	0.02	bar
Fuel reformer	Reformer temperature	T_{reform}	600	°C
	Steam to fuel ratio	S/F	0.68	kg/kg
	Pressure drop	Δp	0.01	bar
Heat exchangers	Pressure drop	Δp	0.01	bar
Pumps	Isentropic efficiency	η_{is}	0.85	-
	Mechanical efficiency	η_m	0.8	-
Blowers	Isentropic efficiency	η_{is}	0.85	-
	Mechanical efficiency	η_m	0.8	-
Overall	AOG combustion	$\frac{m_{AOG,GT}}{m_{AOG}}$	0.82	-
	Gross GT power	$P_{out,GT}$	0.24	MWe
	Gross SOFC power	$P_{out,SOFC}$	6.32	MWe
	Net system power output	P_{out}	5.60	MWe
	GT load		10	%
	SOFC load		75	%
	Net electrical system efficiency	η_{sys}	54.03	%
	Exhaust temperature	T_{exh}	140.56	°C

Table D.109: CT parameters for the MeOH-fuelled SOFC-GT model at cruising speed for a power split of 30-70 and an SOFC load of 100%

Component	Parameter		CT Value	
Compressor	Isentropic efficiency	η_{is}	0.843	-
	Pressure ratio	Π	23.54	-
	Mechanical efficiency	η_m	0.997	-
Turbine	Isentropic efficiency	η_{is}	0.865	-
	Pressure ratio	Π	4.80	-
	Mechanical efficiency	η_m	0.997	-
Power turbine	Isentropic efficiency	η_{is}	0.86	-
	Pressure ratio	Π	4.76	-
	Mechanical efficiency	η_m	0.996	-
Generator	Generator efficiency	η_{gen}	0.975	
Pumps	Isentropic efficiency	η_{is}	0.85	-
	Mechanical efficiency	η_m	0.8	-
SOFC	Fuel utilization factor	u_f	0.8	-
	Cell voltage	V_{cell}	0.89	V
	Stack temperature	T_{stack}	750	°C
	Inlet temperature	T_{in}	700	°C
	Outlet temperature	T_{out}	790	°C
	Anode pressure drop	Δp_{an}	0.02	bar
	Cathode pressure drop	Δp_{ca}	0.02	bar
Fuel reformer	Reformer temperature	T_{reform}	600	°C
	Steam to fuel ratio	S/F	0.68	kg/kg
	Pressure drop	Δp	0.01	bar
Heat exchangers	Pressure drop	Δp	0.01	bar
Pumps	Isentropic efficiency	η_{is}	0.85	-
	Mechanical efficiency	η_m	0.8	-
Blowers	Isentropic efficiency	η_{is}	0.85	-
	Mechanical efficiency	η_m	0.8	-
Overall	AOG combustion	$\frac{m_{AOG,GT}}{m_{AOG}}$	0	-
	Gross GT power	$P_{out,GT}$	0	MWe
	Gross SOFC power	$P_{out,SOFC}$	6.78	MWe
	Net system power output	P_{out}	5.60	MWe
	GT load		0	%
	SOFC load		80	%
	Net electrical system efficiency	η_{sys}	50.39	%
	Exhaust temperature	T_{exh}	207.05	°C

Table D.110: CT parameters for the MeOH-fuelled SOFC-GT model at top speed for a power split of 4.6-95.4

Component	Parameter		CT Value	
Compressor	Isentropic efficiency	η_{is}	0.843	-
	Pressure ratio	Π	23.54	-
	Mechanical efficiency	η_m	0.997	-
Turbine	Isentropic efficiency	η_{is}	0.865	-
	Pressure ratio	Π	4.80	-
	Mechanical efficiency	η_m	0.997	-
Power turbine	Isentropic efficiency	η_{is}	0.86	-
	Pressure ratio	Π	4.76	-
	Mechanical efficiency	η_m	0.996	-
Generator	Generator efficiency	η_{gen}	0.975	
Pumps	Isentropic efficiency	η_{is}	0.85	-
	Mechanical efficiency	η_m	0.8	-
SOFC	Fuel utilization factor	u_f	0.8	-
	Cell voltage	V_{cell}	0.89	V
	Stack temperature	T_{stack}	750	°C
	Inlet temperature	T_{in}	700	°C
	Outlet temperature	T_{out}	790	°C
	Anode pressure drop	Δp_{an}	0.02	bar
	Cathode pressure drop	Δp_{ca}	0.02	bar
Fuel reformer	Reformer temperature	T_{reform}	600	°C
	Steam to fuel ratio	S/F	0.68	kg/kg
	Pressure drop	Δp	0.01	bar
Heat exchangers	Pressure drop	Δp	0.01	bar
Pumps	Isentropic efficiency	η_{is}	0.85	-
	Mechanical efficiency	η_m	0.8	-
Blowers	Isentropic efficiency	η_{is}	0.85	-
	Mechanical efficiency	η_m	0.8	-
Overall	AOG combustion	$\frac{m_{AOG,GT}}{m_{AOG}}$	1	-
	Gross GT power	$P_{out,GT}$	22.24	MWe
	Gross SOFC power	$P_{out,SOFC}$	1.29	MWe
	Net system power output	P_{out}	23.31	MWe
	GT load		100	%
	SOFC load		100	%
	Net electrical system efficiency	η_{sys}	38.94	%
	Exhaust temperature	T_{exh}	473.37	°C

Table D.111: CT parameters for the MeOH-fuelled SOFC-GT model at top speed for a power split of 10-90

Component	Parameter		CT Value	
Compressor	Isentropic efficiency	η_{is}	0.843	-
	Pressure ratio	Π	23.54	-
	Mechanical efficiency	η_m	0.997	-
Turbine	Isentropic efficiency	η_{is}	0.865	-
	Pressure ratio	Π	4.80	-
	Mechanical efficiency	η_m	0.997	-
Power turbine	Isentropic efficiency	η_{is}	0.86	-
	Pressure ratio	Π	4.76	-
	Mechanical efficiency	η_m	0.996	-
Generator	Generator efficiency	η_{gen}	0.975	
Pumps	Isentropic efficiency	η_{is}	0.85	-
	Mechanical efficiency	η_m	0.8	-
SOFC	Fuel utilization factor	u_f	0.8	-
	Cell voltage	V_{cell}	0.89	V
	Stack temperature	T_{stack}	750	°C
	Inlet temperature	T_{in}	700	°C
	Outlet temperature	T_{out}	790	°C
	Anode pressure drop	Δp_{an}	0.02	bar
	Cathode pressure drop	Δp_{ca}	0.02	bar
Fuel reformer	Reformer temperature	T_{reform}	600	°C
	Steam to fuel ratio	S/F	0.68	kg/kg
	Pressure drop	Δp	0.01	bar
Heat exchangers	Pressure drop	Δp	0.01	bar
Pumps	Isentropic efficiency	η_{is}	0.85	-
	Mechanical efficiency	η_m	0.8	-
Blowers	Isentropic efficiency	η_{is}	0.85	-
	Mechanical efficiency	η_m	0.8	-
Overall	AOG combustion	$\frac{m_{AOG,GT}}{m_{AOG}}$	1	-
	Gross GT power	$P_{out,GT}$	20.97	MWe
	Gross SOFC power	$P_{out,SOFC}$	2.81	MWe
	Net system power output	P_{out}	23.31	MWe
	GT load		100	%
	SOFC load		100	%
	Net electrical system efficiency	η_{sys}	40.18	%
	Exhaust temperature	T_{exh}	437.47	°C

Table D.112: CT parameters for the MeOH-fuelled SOFC-GT model at top speed for a power split of 15-85

Component	Parameter		CT Value	
Compressor	Isentropic efficiency	η_{is}	0.843	-
	Pressure ratio	Π	23.54	-
	Mechanical efficiency	η_m	0.997	-
Turbine	Isentropic efficiency	η_{is}	0.865	-
	Pressure ratio	Π	4.80	-
	Mechanical efficiency	η_m	0.997	-
Power turbine	Isentropic efficiency	η_{is}	0.86	-
	Pressure ratio	Π	4.76	-
	Mechanical efficiency	η_m	0.996	-
Generator	Generator efficiency	η_{gen}	0.975	
Pumps	Isentropic efficiency	η_{is}	0.85	-
	Mechanical efficiency	η_m	0.8	-
SOFC	Fuel utilization factor	u_f	0.8	-
	Cell voltage	V_{cell}	0.89	V
	Stack temperature	T_{stack}	750	°C
	Inlet temperature	T_{in}	700	°C
	Outlet temperature	T_{out}	790	°C
	Anode pressure drop	Δp_{an}	0.02	bar
	Cathode pressure drop	Δp_{ca}	0.02	bar
Fuel reformer	Reformer temperature	T_{reform}	600	°C
	Steam to fuel ratio	S/F	0.68	kg/kg
	Pressure drop	Δp	0.01	bar
Heat exchangers	Pressure drop	Δp	0.01	bar
Pumps	Isentropic efficiency	η_{is}	0.85	-
	Mechanical efficiency	η_m	0.8	-
Blowers	Isentropic efficiency	η_{is}	0.85	-
	Mechanical efficiency	η_m	0.8	-
Overall	AOG combustion	$\frac{m_{AOG,GT}}{m_{AOG}}$	1	-
	Gross GT power	$P_{out,GT}$	19.84	MWe
	Gross SOFC power	$P_{out,SOFC}$	4.21	MWe
	Net system power output	P_{out}	23.31	MWe
	GT load		100	%
	SOFC load		100	%
	Net electrical system efficiency	η_{sys}	41.37	%
	Exhaust temperature	T_{exh}	405.28	°C

Table D.113: CT parameters for the MeOH-fuelled SOFC-GT model at top speed for a power split of 20-80

Component	Parameter		CT Value	
Compressor	Isentropic efficiency	η_{is}	0.843	-
	Pressure ratio	Π	23.54	-
	Mechanical efficiency	η_m	0.997	-
Turbine	Isentropic efficiency	η_{is}	0.865	-
	Pressure ratio	Π	4.80	-
	Mechanical efficiency	η_m	0.997	-
Power turbine	Isentropic efficiency	η_{is}	0.86	-
	Pressure ratio	Π	4.76	-
	Mechanical efficiency	η_m	0.996	-
Generator	Generator efficiency	η_{gen}	0.975	
Pumps	Isentropic efficiency	η_{is}	0.85	-
	Mechanical efficiency	η_m	0.8	-
SOFC	Fuel utilization factor	u_f	0.8	-
	Cell voltage	V_{cell}	0.89	V
	Stack temperature	T_{stack}	750	°C
	Inlet temperature	T_{in}	700	°C
	Outlet temperature	T_{out}	790	°C
	Anode pressure drop	Δp_{an}	0.02	bar
	Cathode pressure drop	Δp_{ca}	0.02	bar
Fuel reformer	Reformer temperature	T_{reform}	600	°C
	Steam to fuel ratio	S/F	0.68	kg/kg
	Pressure drop	Δp	0.01	bar
Heat exchangers	Pressure drop	Δp	0.01	bar
Pumps	Isentropic efficiency	η_{is}	0.85	-
	Mechanical efficiency	η_m	0.8	-
Blowers	Isentropic efficiency	η_{is}	0.85	-
	Mechanical efficiency	η_m	0.8	-
Overall	AOG combustion	$\frac{m_{AOG,GT}}{m_{AOG}}$	1	-
	Gross GT power	$P_{out,GT}$	18.68	MWe
	Gross SOFC power	$P_{out,SOFC}$	5.62	MWe
	Net system power output	P_{out}	23.31	MWe
	GT load		100	%
	SOFC load		100	%
	Net electrical system efficiency	η_{sys}	42.66	%
	Exhaust temperature	T_{exh}	374.72	°C

Table D.114: CT parameters for the MeOH-fuelled SOFC-GT model at top speed for a power split of 25-75

Component	Parameter		CT Value	
Compressor	Isentropic efficiency	η_{is}	0.843	-
	Pressure ratio	Π	23.54	-
	Mechanical efficiency	η_m	0.997	-
Turbine	Isentropic efficiency	η_{is}	0.865	-
	Pressure ratio	Π	4.80	-
	Mechanical efficiency	η_m	0.997	-
Power turbine	Isentropic efficiency	η_{is}	0.86	-
	Pressure ratio	Π	4.76	-
	Mechanical efficiency	η_m	0.996	-
Generator	Generator efficiency	η_{gen}	0.975	
Pumps	Isentropic efficiency	η_{is}	0.85	-
	Mechanical efficiency	η_m	0.8	-
SOFC	Fuel utilization factor	u_f	0.8	-
	Cell voltage	V_{cell}	0.89	V
	Stack temperature	T_{stack}	750	°C
	Inlet temperature	T_{in}	700	°C
	Outlet temperature	T_{out}	790	°C
	Anode pressure drop	Δp_{an}	0.02	bar
	Cathode pressure drop	Δp_{ca}	0.02	bar
Fuel reformer	Reformer temperature	T_{reform}	600	°C
	Steam to fuel ratio	S/F	0.68	kg/kg
	Pressure drop	Δp	0.01	bar
Heat exchangers	Pressure drop	Δp	0.01	bar
Pumps	Isentropic efficiency	η_{is}	0.85	-
	Mechanical efficiency	η_m	0.8	-
Blowers	Isentropic efficiency	η_{is}	0.85	-
	Mechanical efficiency	η_m	0.8	-
Overall	AOG combustion	$\frac{m_{AOG,GT}}{m_{AOG}}$	1	-
	Gross GT power	$P_{out,GT}$	17.52	MWe
	Gross SOFC power	$P_{out,SOFC}$	7.02	MWe
	Net system power output	P_{out}	23.31	MWe
	GT load		100	%
	SOFC load		100	%
	Net electrical system efficiency	η_{sys}	44.03	%
	Exhaust temperature	T_{exh}	345.21	°C

Table D.115: CT parameters for the MeOH-fuelled SOFC-GT model at top speed for a power split of 30-70

Component	Parameter		CT Value	
Compressor	Isentropic efficiency	η_{is}	0.843	-
	Pressure ratio	Π	23.54	-
	Mechanical efficiency	η_m	0.997	-
Turbine	Isentropic efficiency	η_{is}	0.865	-
	Pressure ratio	Π	4.80	-
	Mechanical efficiency	η_m	0.997	-
Power turbine	Isentropic efficiency	η_{is}	0.86	-
	Pressure ratio	Π	4.76	-
	Mechanical efficiency	η_m	0.996	-
Generator	Generator efficiency	η_{gen}	0.975	
Pumps	Isentropic efficiency	η_{is}	0.85	-
	Mechanical efficiency	η_m	0.8	-
SOFC	Fuel utilization factor	u_f	0.8	-
	Cell voltage	V_{cell}	0.89	V
	Stack temperature	T_{stack}	750	°C
	Inlet temperature	T_{in}	700	°C
	Outlet temperature	T_{out}	790	°C
	Anode pressure drop	Δp_{an}	0.02	bar
	Cathode pressure drop	Δp_{ca}	0.02	bar
Fuel reformer	Reformer temperature	T_{reform}	600	°C
	Steam to fuel ratio	S/F	0.68	kg/kg
	Pressure drop	Δp	0.01	bar
Heat exchangers	Pressure drop	Δp	0.01	bar
Pumps	Isentropic efficiency	η_{is}	0.85	-
	Mechanical efficiency	η_m	0.8	-
Blowers	Isentropic efficiency	η_{is}	0.85	-
	Mechanical efficiency	η_m	0.8	-
Overall	AOG combustion	$\frac{m_{AOG,GT}}{m_{AOG}}$	1	-
	Gross GT power	$P_{out,GT}$	16.39	MWe
	Gross SOFC power	$P_{out,SOFC}$	8.42	MWe
	Net system power output	P_{out}	23.31	MWe
	GT load		100	%
	SOFC load		100	%
	Net electrical system efficiency	η_{sys}	45.47	%
	Exhaust temperature	T_{exh}	316.52	°C

E

Weight and volume breakdown

This appendix gives a breakdown of the total weight and volume of the current power plant and the different combined cycles. The current system is given in section E.1, and the diesel-fuelled systems are given in section E.2 (SOFC-ICE) and section E.3 (SOFC-GT). Lastly, the MeOH-fuelled systems are given in section E.4 (SOFC-ICE) and section E.5 (SOFC-GT).

E.1. Current system

The weight and volume of the current system is shown in the table below. The current system consists of a mixture of ICEs and gensets producing the total power demand of the vessel. Additionally, the system consists of e-motors, gearboxes and fuel storage.

Table E.1: Weight and volume of the components of the current power plant of the reference vessel

Component	Variant	Length [m]	Width [m]	Height [m]	Volume [m^3]	Weight [ton]	Amount installed
ICE	-	-	-	-	67.347	51.3	2
Genset	-	-	-	-	21.435	10.15	4
E-motor	-	-	-	-	4.091	5.02	2
Gearbox	-	-	-	-	17.33	22.05	2
Fuel	Diesel	-	-	-	415.53	351.12	-
Total	-	-	-	-	679.79	550.50	-

E.2. SOFC-ICE diesel

This section shows the weight and volume of each component in the diesel-fuelled SOFC-ICE combined cycle. For hybrid and electric propulsion the differences lie in the ICE/genset, e-motor and gearbox. The total weight and volume for each power split is also given in the tables.

Table E.2: Weight and volume of the components of the diesel-fuelled SOFC-ICE combined cycle with a power split of 4.6-95.4

Component	Variant	Length [m]	Width [m]	Height [m]	Volume [m^3]	Weight [ton]	Amount installed
ICE (hybrid)	MAN 20V 28/33D STC (10 MW)	8.047	2.273	3.982	67.347	51.3	2
Genset (electric)	Wärtsilä 16V 34DF (7.37 MWe)	11.175	3.060	4.515	154.393	121	3
SOFC	Bloom Energy Server (325 kWe)	8.961	1.238	2.494	27.668	14.8	4
E-motor (hybrid)	Siemens HV A compact plus (0.355 MW)	1.577	0.770	0.695	0.844	1.08	2
E-motor (electric)	Siemens HV-M (10.68 MW)	5.580	3.85	3.385	67.18	28	2
Gearbox (hybrid)	Wärtsilä TCH270	2.440	3.900	3.020	28.738	28	2
Gearbox (electric)	Wärtsilä SCH105	2.450	2.995	2.429	17.823	30	2
HEX	Low temperature air heater	1.000	0.621	0.621	0.096	0.174	4
	High temperature air heater	1.000	0.572	0.572	0.082	0.147	4
	Low temperature fuel heater	0.300	0.165	0.165	0.002	0.004	4
	High temperature fuel heater	0.300	0.179	0.179	0.002	0.004	4
	Economizer	0.300	0.186	0.186	0.003	0.005	4
	Evaporator	0.500	0.345	0.345	0.015	0.027	4
	Superheater	0.300	0.185	0.185	0.003	0.005	4
	Moisture separator	1.000	0.530	0.530	0.070	0.127	2
Blower	HR43	1.252	0.510	0.665	0.425	0.68	4
Fuel	Diesel	-	-	-	388.54	328.32	-
Total (hybrid)	-	-	-	-	673.14	540.70	-
Total (electric)	-	-	-	-	1098.66	870.84	-

Table E.3: Weight and volume of the components of the diesel-fuelled SOFC-ICE combined cycle with a power split of 10-90

Component	Variant	Length [m]	Width [m]	Height [m]	Volume [m^3]	Weight [ton]	Amount installed
ICE (hybrid)	MAN 20V 28/33D STC (10 MW)	8.047	2.273	3.982	67.347	51.3	2
Genset (electric)	Wärtsilä 16V 34DF (7.37 MWe)	11.175	3.060	4.515	154.393	121	3
SOFC	Bloom Energy Server (325 kWe)	8.961	1.238	2.494	27.668	14.8	9
E-motor (hybrid)	Siemens HV A compact plus (1.12 MW)	1.925	1.385	1.583	4.22	3.55	2
E-motor (electric)	Siemens HV-M (10.68 MW)	5.580	3.85	3.385	67.18	28	2
Gearbox (hybrid)	Wärtsilä TCH270	2.440	3.900	3.020	28.738	28	2
Gearbox (electric)	Wärtsilä SCH105	2.450	2.995	2.429	17.823	30	2
HEX	Low temperature air heater	1.000	0.621	0.621	0.096	0.174	9
	High temperature air heater	1.000	0.572	0.572	0.082	0.147	9
	Low temperature fuel heater	0.300	0.165	0.165	0.002	0.004	9
	High temperature fuel heater	0.300	0.179	0.179	0.002	0.004	9
	Economizer	0.300	0.186	0.186	0.003	0.005	9
	Evaporator	0.500	0.345	0.345	0.015	0.027	9
	Superheater	0.300	0.185	0.185	0.003	0.005	9
	Moisture separator	1.25	0.720	0.720	0.162	0.293	2
Blower	HR43	1.252	0.510	0.665	0.425	0.68	9
Fuel	Diesel	-	-	-	349.42	295.26	-
Total (hybrid)	-	-	-	-	781.49	592.00	-
Total (electric)	-	-	-	-	1200.25	917.20	-

Table E.4: Weight and volume of the components of the diesel-fuelled SOFC-ICE combined cycle with a power split of 15-85

Component	Variant	Length [m]	Width [m]	Height [m]	Volume [m^3]	Weight [ton]	Amount installed
ICE (hybrid)	MAN 20V 28/33D STC (10 MW)	8.047	2.273	3.982	67.347	51.3	2
Genset (electric)	Wärtsilä 12V 32 (6.5 MWe)	10.7	3.06	4.13	135.224	100	3
SOFC	Bloom Energy Server (325 kWe)	8.961	1.238	2.494	27.668	14.8	13
E-motor (hybrid)	Siemens HV A compact plus (1.80 MW)	2.149	1.496	1.757	5.649	4.70	2
E-motor (electric)	Siemens HV-M (10.68 MW)	5.580	3.85	3.385	67.18	28	2
Gearbox (hybrid)	Wärtsilä TCH270	2.440	3.900	3.020	28.738	28	2
Gearbox (electric)	Wärtsilä SCH105	2.450	2.995	2.429	17.823	30	2
HEX	Low temperature air heater	1.000	0.621	0.621	0.096	0.174	13
	High temperature air heater	1.000	0.572	0.572	0.082	0.147	13
	Low temperature fuel heater	0.300	0.165	0.165	0.002	0.004	13
	High temperature fuel heater	0.300	0.179	0.179	0.002	0.004	13
	Economizer	0.300	0.186	0.186	0.003	0.005	13
	Evaporator	0.500	0.345	0.345	0.015	0.027	13
	Superheater	0.300	0.185	0.185	0.003	0.005	13
	Moisture separator	1.50	0.805	0.805	0.244	0.439	2
Blower	HR43	1.252	0.510	0.665	0.425	0.68	13
Fuel	Diesel	-	-	-	313.00	264.48	-
Total (hybrid)	-	-	-	-	860.52	627.08	-
Total (electric)	-	-	-	-	1218.92	886.98	-

Table E.5: Weight and volume of the components of the diesel-fuelled SOFC-ICE combined cycle with a power split of 20-80

Component	Variant	Length [m]	Width [m]	Height [m]	Volume [m^3]	Weight [ton]	Amount installed
ICE (hybrid)	MAN 20V 28/33D STC (10 MW)	8.047	2.273	3.982	67.347	51.3	2
Genset (electric)	Wärtsilä 12V 32 (6.5 MWe)	10.7	3.06	4.13	135.224	100	3
SOFC	Bloom Energy Server (325 kWe)	8.961	1.238	2.494	27.668	14.8	18
E-motor (hybrid)	Siemens HV A compact plus (2.50 MW)	2.294	1.656	1.907	7.244	5.90	2
E-motor (electric)	Siemens HV-M (10.68 MW)	5.580	3.85	3.385	67.18	28	2
Gearbox (hybrid)	Wärtsilä TCH270	2.440	3.900	3.020	28.738	28	2
Gearbox (electric)	Wärtsilä SCH105	2.450	2.995	2.429	17.823	30	2
HEX	Low temperature air heater	1.000	0.621	0.621	0.096	0.174	18
	High temperature air heater	1.000	0.572	0.572	0.082	0.147	18
	Low temperature fuel heater	0.300	0.165	0.165	0.002	0.004	18
	High temperature fuel heater	0.300	0.179	0.179	0.002	0.004	18
	Economizer	0.300	0.186	0.186	0.003	0.005	18
	Evaporator	0.500	0.345	0.345	0.015	0.027	18
	Superheater	0.300	0.185	0.185	0.003	0.005	18
	Moisture separator	1.500	0.931	0.931	0.325	0.586	2
Blower	HR43	1.252	0.510	0.665	0.425	0.68	18
Fuel	Diesel	-	-	-	279.27	235.98	-
Total (hybrid)	-	-	-	-	970.68	680.36	-
Total (electric)	-	-	-	-	1325.89	937.86	-

Table E.6: Weight and volume of the components of the diesel-fuelled SOFC-ICE combined cycle with a power split of 25-75

Component	Variant	Length [m]	Width [m]	Height [m]	Volume [m^3]	Weight [ton]	Amount installed
ICE (hybrid)	MAN 16V 28/33D STC (8 MW)	7.127	2.273	3.982	59.647	43.6	2
Genset (electric)	Wärtsilä 16V 32 (8.6 MWe)	11.465	3.36	4.445	171.232	127	2
SOFC	Bloom Energy Server (325 kWe)	8.961	1.238	2.494	27.668	14.8	22
E-motor (hybrid)	Siemens HV A compact plus (3.15 MW)	2.294	1.656	1.907	7.244	6.65	2
E-motor (electric)	Siemens HV-M (10.68 MW)	5.580	3.85	3.385	67.18	28	2
Gearbox (hybrid)	Wärtsilä TCH270	2.440	3.900	3.020	28.738	28	2
Gearbox (electric)	Wärtsilä SCH105	2.450	2.995	2.429	17.823	30	2
HEX	Low temperature air heater	1.000	0.621	0.621	0.096	0.174	22
	High temperature air heater	1.000	0.572	0.572	0.082	0.147	22
	Low temperature fuel heater	0.300	0.165	0.165	0.002	0.004	22
	High temperature fuel heater	0.300	0.179	0.179	0.002	0.004	22
	Economizer	0.300	0.186	0.186	0.003	0.005	22
	Evaporator	0.500	0.345	0.345	0.015	0.027	22
	Superheater	0.300	0.185	0.185	0.003	0.005	22
	Moisture separator	1.500	1.040	1.040	0.406	0.733	2
Blower	HR43	1.252	0.510	0.665	0.425	0.68	22
Fuel	Diesel	-	-	-	267.12	225.72	-
Total (hybrid)	-	-	-	-	1054.92	718.29	-
Total (electric)	-	-	-	-	1363.13	945.16	-

Table E.7: Weight and volume of the components of the diesel-fuelled SOFC-ICE combined cycle with a power split of 30-70

Component	Variant	Length [m]	Width [m]	Height [m]	Volume [m^3]	Weight [ton]	Amount installed
ICE (hybrid)	MAN 16V 28/33D STC (8 MW)	7.127	2.273	3.982	59.647	43.6	2
Genset (electric)	Wärtsilä 16V 32 (8.6 MWe)	11.465	3.36	4.445	171.232	127	2
SOFC	Bloom Energy Server (325 kWe)	8.961	1.238	2.494	27.668	14.8	27
E-motor (hybrid)	Siemens HV A compact plus (4.00 MW)	2.555	1.913	2.067	10.103	9.75	2
E-motor (electric)	Siemens HV-M (10.68 MW)	5.580	3.85	3.385	67.18	28	2
Gearbox (hybrid)	Wärtsilä TCH270	2.440	3.900	3.020	28.738	28	2
Gearbox (electric)	Wärtsilä SCH105	2.450	2.995	2.429	17.823	30	2
HEX	Low temperature air heater	1.000	0.621	0.621	0.096	0.174	27
	High temperature air heater	1.000	0.572	0.572	0.082	0.147	27
	Low temperature fuel heater	0.300	0.165	0.165	0.002	0.004	27
	High temperature fuel heater	0.300	0.179	0.179	0.002	0.004	27
	Economizer	0.300	0.186	0.186	0.003	0.005	27
	Evaporator	0.500	0.345	0.345	0.015	0.027	27
	Superheater	0.300	0.185	0.185	0.003	0.005	27
	Moisture separator	1.750	1.050	1.050	0.488	0.880	2
Blower	HR43	1.252	0.510	0.665	0.425	0.68	27
Fuel	Diesel	-	-	-	300.85	254.22	-
Total (hybrid)	-	-	-	-	1235.88	833.84	-
Total (electric)	-	-	-	-	1537.56	1049.04	-

E.3. SOFC-GT diesel

This section shows the weight and volume of each component in the diesel-fuelled SOFC-GT combined cycle. For hybrid and electric propulsion the differences lie in the GT/genset, e-motor and gearbox. The total weight and volume for each power split is also given in the tables.

Table E.8: Weight and volume of the components of the diesel-fuelled SOFC-GT combined cycle with a power split of 4.6-95.4

Component	Variant	Length [m]	Width [m]	Height [m]	Volume [m^3]	Weight [ton]	Amount installed
GT (hybrid)	GE LM500 (4.6 MW)	3.660	1.650	1.650	9.964	2.779	5
Genset (electric)	GE LM500 (4.2 MWe)	7.140	2.390	2.390	40.784	27.273	6
SOFC	Bloom Energy Server (325 kWe)	8.961	1.238	2.494	27.668	14.8	4
E-motor (hybrid)	Siemens HV A (0.355 MW)	1.577	0.770	0.695	0.844	1.43	2
E-motor (electric)	Siemens HV-M (10.68 MW)	5.580	3.85	3.385	67.18	28	2
Gearbox (hybrid)	Triple input/single output	-	-	-	82	80	2
Gearbox (electric)	Wärtsilä SCH105	2.450	2.995	2.429	17.823	30	2
HEX	Low + intermediate temperature air heater	1.000	0.621	0.621	0.097	0.174	4
	High temperature air heater	1.000	0.572	0.572	0.082	0.147	4
	Low temperature fuel heater	0.300	0.165	0.165	0.002	0.004	4
	High temperature fuel heater	0.300	0.179	0.179	0.002	0.004	4
	Economizer	0.300	0.186	0.186	0.003	0.005	4
	Evaporator	0.500	0.345	0.345	0.015	0.027	4
	Superheater	0.300	0.185	0.185	0.003	0.005	4
Blower	HR43	1.252	0.510	0.665	0.425	0.68	4
Fuel	Diesel	-	-	-	407.43	344.28	-
Total (hybrid)	-	-	-	-	700.72	583.64	-
Total (electric)	-	-	-	-	898.95	687.23	-

Table E.9: Weight and volume of the components of the diesel-fuelled SOFC-GT combined cycle with a power split of 10-90

Component	Variant	Length [m]	Width [m]	Height [m]	Volume [m^3]	Weight [ton]	Amount installed
GT (hybrid)	GE LM500 (4.6 MW)	3.660	1.650	1.650	9.964	2.779	5
Genset (electric)	GE LM500 (4.2 MWe)	7.140	2.390	2.390	40.784	27.273	5
SOFC	Bloom Energy Server (325 kWe)	8.961	1.238	2.494	27.668	14.8	9
E-motor (hybrid)	Siemens HV A compact plus (1.12 MW)	1.925	1.385	1.583	4.22	3.55	2
E-motor (electric)	Siemens HV-M (10.68 MW)	5.580	3.85	3.385	67.18	28	2
Gearbox (hybrid)	Triple input/single output	-	-	-	82	80	2
Gearbox (electric)	Wärtsilä SCH105	2.450	2.995	2.429	17.823	30	2
HEX	Low + intermediate temperature air heater	1.000	0.621	0.621	0.097	0.174	9
	High temperature air heater	1.000	0.572	0.572	0.082	0.147	9
	Low temperature fuel heater	0.300	0.165	0.165	0.002	0.004	9
	High temperature fuel heater	0.300	0.179	0.179	0.002	0.004	9
	Economizer	0.300	0.186	0.186	0.003	0.005	9
	Evaporator	0.500	0.345	0.345	0.015	0.027	9
	Superheater	0.300	0.185	0.185	0.003	0.005	9
Blower	HR43	1.252	0.510	0.665	0.425	0.68	9
Fuel	Diesel	-	-	-	358.86	303.24	-
Total (hybrid)	-	-	-	-	799.48	626.68	-
Total (electric)	-	-	-	-	950.17	698.05	-

Table E.10: Weight and volume of the components of the diesel-fuelled SOFC-GT combined cycle with a power split of 15-85

Component	Variant	Length [m]	Width [m]	Height [m]	Volume [m^3]	Weight [ton]	Amount installed
GT (hybrid)	GE LM500 (4.6 MW)	3.660	1.650	1.650	9.964	2.779	5
Genset (electric)	GE LM500 (4.2 MWe)	7.140	2.390	2.390	40.784	27.273	5
SOFC	Bloom Energy Server (325 kWe)	8.961	1.238	2.494	27.668	14.8	13
E-motor (hybrid)	Siemens HV A compact plus (1.80 MW)	2.149	1.496	1.757	5.649	4.70	2
E-motor (electric)	Siemens HV-M (10.68 MW)	5.580	3.85	3.385	67.18	28	2
Gearbox (hybrid)	Triple input/single output	-	-	-	82	80	2
Gearbox (electric)	Wärtsilä SCH105	2.450	2.995	2.429	17.823	30	2
HEX	Low + intermediate temperature air heater	1.000	0.621	0.621	0.097	0.174	13
	High temperature air heater	1.000	0.572	0.572	0.082	0.147	13
	Low temperature fuel heater	0.300	0.165	0.165	0.002	0.004	13
	High temperature fuel heater	0.300	0.179	0.179	0.002	0.004	13
	Economizer	0.300	0.186	0.186	0.003	0.005	13
	Evaporator	0.500	0.345	0.345	0.015	0.027	13
	Superheater	0.300	0.185	0.185	0.003	0.005	13
Blower	HR43	1.252	0.510	0.665	0.425	0.68	13
Fuel	Diesel	-	-	-	358.86	303.24	-
Total (hybrid)	-	-	-	-	867.57	652.39	-
Total (electric)	-	-	-	-	1015.40	721.46	-

Table E.11: Weight and volume of the components of the diesel-fuelled SOFC-GT combined cycle with a power split of 20-80

Component	Variant	Length [m]	Width [m]	Height [m]	Volume [m^3]	Weight [ton]	Amount installed
GT (hybrid)	GE LM500 (4.6 MW)	3.660	1.650	1.650	9.964	2.779	5
Genset (electric)	GE LM500 (4.2 MWe)	7.140	2.390	2.390	40.784	27.273	4
SOFC	Bloom Energy Server (325 kWe)	8.961	1.238	2.494	27.668	14.8	17
E-motor (hybrid)	Siemens HV A compact plus (2.50 MW)	2.294	1.656	1.907	7.244	5.90	2
E-motor (electric)	Siemens HV-M (10.68 MW)	5.580	3.85	3.385	67.18	28	2
Gearbox (hybrid)	Triple input/single output	-	-	-	82	80	2
Gearbox (electric)	Wärtsilä SCH105	2.450	2.995	2.429	17.823	30	2
HEX	Low + intermediate temperature air heater	1.000	0.621	0.621	0.097	0.174	17
	High temperature air heater	1.000	0.572	0.572	0.082	0.147	17
	Low temperature fuel heater	0.300	0.165	0.165	0.002	0.004	17
	High temperature fuel heater	0.300	0.179	0.179	0.002	0.004	17
	Economizer	0.300	0.186	0.186	0.003	0.005	17
	Evaporator	0.500	0.345	0.345	0.015	0.027	17
	Superheater	0.300	0.185	0.185	0.003	0.005	17
Blower	HR43	1.252	0.510	0.665	0.425	0.68	17
Fuel	Diesel	-	-	-	298.15	251.94	-
Total (hybrid)	-	-	-	-	959.75	703.92	-
Total (electric)	-	-	-	-	1114.36	773.37	-

Table E.12: Weight and volume of the components of the diesel-fuelled SOFC-GT combined cycle with a power split of 25-75

Component	Variant	Length [m]	Width [m]	Height [m]	Volume [m^3]	Weight [ton]	Amount installed
GT (hybrid)	GE LM500 (4.6 MW)	3.660	1.650	1.650	9.964	2.779	5
Genset (electric)	GE LM500 (4.2 MWe)	7.140	2.390	2.390	40.784	27.273	4
SOFC	Bloom Energy Server (325 kWe)	8.961	1.238	2.494	27.668	14.8	22
E-motor (hybrid)	Siemens HV A compact plus (3.15 MW)	2.294	1.656	1.907	7.244	6.65	2
E-motor (electric)	Siemens HV-M (10.68 MW)	5.580	3.85	3.385	67.18	28	2
Gearbox (hybrid)	Triple input/single output	-	-	-	82	80	2
Gearbox (electric)	Wärtsilä SCH105	2.450	2.995	2.429	17.823	30	2
HEX	Low + intermediate temperature air heater	1.000	0.621	0.621	0.097	0.174	22
	High temperature air heater	1.000	0.572	0.572	0.082	0.147	22
	Low temperature fuel heater	0.300	0.165	0.165	0.002	0.004	22
	High temperature fuel heater	0.300	0.179	0.179	0.002	0.004	22
	Economizer	0.300	0.186	0.186	0.003	0.005	22
	Evaporator	0.500	0.345	0.345	0.015	0.027	22
	Superheater	0.300	0.185	0.185	0.003	0.005	22
Blower	HR43	1.252	0.510	0.665	0.425	0.68	22
Fuel	Diesel	-	-	-	286.01	241.68	-
Total (hybrid)	-	-	-	-	1088.18	774.29	-
Total (electric)	-	-	-	-	1242.79	842.24	-

Table E.13: Weight and volume of the components of the diesel-fuelled SOFC-GT combined cycle with a power split of 30-70

Component	Variant	Length [m]	Width [m]	Height [m]	Volume [m^3]	Weight [ton]	Amount installed
GT (hybrid)	GE LM500 (4.6 MW)	3.660	1.650	1.650	9.964	2.779	4
Genset (electric)	GE LM500 (4.2 MWe)	7.140	2.390	2.390	40.784	27.273	4
SOFC	Bloom Energy Server (325 kWe)	8.961	1.238	2.494	27.668	14.8	26
E-motor (hybrid)	Siemens HV A compact plus (4.00 MW)	2.555	1.913	2.067	10.103	9.75	2
E-motor (electric)	Siemens HV-M (10.68 MW)	5.580	3.85	3.385	67.18	28	2
Gearbox (hybrid)	Triple input/single output	-	-	-	82	80	2
Gearbox (electric)	Wärtsilä SCH105	2.450	2.995	2.429	17.823	30	2
HEX	Low + intermediate temperature air heater	1.000	0.621	0.621	0.097	0.174	26
	High temperature air heater	1.000	0.572	0.572	0.082	0.147	26
	Low temperature fuel heater	0.300	0.165	0.165	0.002	0.004	26
	High temperature fuel heater	0.300	0.179	0.179	0.002	0.004	26
	Economizer	0.300	0.186	0.186	0.003	0.005	26
	Evaporator	0.500	0.345	0.345	0.015	0.027	26
	Superheater	0.300	0.185	0.185	0.003	0.005	26
Blower	HR43	1.252	0.510	0.665	0.425	0.68	26
Fuel	Diesel	-	-	-	306.25	258.78	-
Total (hybrid)	-	-	-	-	1226.58	860.90	-
Total (electric)	-	-	-	-	1334.69	895.38	-

E.4. SOFC-ICE MeOH

This section shows the weight and volume of each component in the MeOH-fuelled SOFC-ICE combined cycle. For hybrid and electric propulsion the differences lie in the ICE/genset, e-motor and gearbox. The total weight and volume for each power split is also given in the tables.

Table E.14: Weight and volume of the components of the MeOH-fuelled SOFC-ICE combined cycle with a power split of 4.6-95.4

Component	Variant	Length [m]	Width [m]	Height [m]	Volume [m^3]	Weight [ton]	Amount installed
ICE (hybrid)	MAN 20V 28/33D STC (10 MW)	8.047	2.273	3.982	67.347	51.3	2
Genset (electric)	Wärtsilä 16V 34DF (7.37 MWe)	11.175	3.060	4.515	154.393	121	3
SOFC	Bloom Energy Server (325 kWe)	8.961	1.238	2.494	27.668	14.8	4
E-motor (hybrid)	Siemens HV A compact plus (0.355 MW)	1.577	0.770	0.695	0.844	1.08	2
E-motor (electric)	Siemens HV-M (10.68 MW)	5.580	3.85	3.385	67.18	28	2
Gearbox (hybrid)	Wärtsilä TCH270	2.440	3.900	3.020	28.738	28	2
Gearbox (electric)	Wärtsilä SCH105	2.450	2.995	2.429	17.823	30	2
HEX	Low temperature air heater	1.250	0.560	0.560	0.116	0.209	4
	High temperature air heater	1.250	0.560	0.560	0.098	0.177	4
	Low temperature fuel heater	0.300	0.191	0.191	0.003	0.005	4
	High temperature fuel heater	0.500	0.194	0.194	0.005	0.008	4
	Economizer	0.500	0.203	0.203	0.005	0.009	4
	Evaporator	0.750	0.395	0.395	0.029	0.053	4
	Superheater	0.500	0.201	0.201	0.005	0.009	4
	Moisture separator	1.250	0.719	0.719	0.162	0.292	2
Blower	HR43	1.252	0.510	0.665	0.425	0.68	4
Fuel	Methanol	-	-	-	852.12	674.88	-
Total (hybrid)	-	-	-	-	1143.95	888.12	-
Total (electric)	-	-	-	-	1562.71	1218.26	-

Table E.15: Weight and volume of the components of the MeOH-fuelled SOFC-ICE combined cycle with a power split of 10-90

Component	Variant	Length [m]	Width [m]	Height [m]	Volume [m^3]	Weight [ton]	Amount installed
ICE (hybrid)	MAN 20V 28/33D STC (10 MW)	8.047	2.273	3.982	67.347	51.3	2
Genset (electric)	Wärtsilä 16V 34DF (7.37 MWe)	11.175	3.060	4.515	154.393	121	3
SOFC	Bloom Energy Server (325 kWe)	8.961	1.238	2.494	27.668	14.8	10
E-motor (hybrid)	Siemens HV A compact plus (1.12 MW)	1.925	1.385	1.583	4.22	3.55	2
E-motor (electric)	Siemens HV-M (10.68 MW)	5.580	3.85	3.385	67.18	28	2
Gearbox (hybrid)	Wärtsilä TCH270	2.440	3.900	3.020	28.738	28	2
Gearbox (electric)	Wärtsilä SCH105	2.450	2.995	2.429	17.823	30	2
HEX	Low temperature air heater	1.250	0.560	0.560	0.116	0.209	10
	High temperature air heater	1.250	0.560	0.560	0.098	0.177	10
	Low temperature fuel heater	0.300	0.191	0.191	0.003	0.005	10
	High temperature fuel heater	0.500	0.194	0.194	0.005	0.008	10
	Economizer	0.500	0.203	0.203	0.005	0.009	10
	Evaporator	0.750	0.395	0.395	0.029	0.053	10
	Superheater	0.500	0.201	0.201	0.005	0.009	10
	Moisture separator	1.500	0.997	0.997	0.373	0.673	2
Blower	HR43	1.252	0.510	0.665	0.425	0.68	10
Fuel	Methanol	-	-	-	800.30	633.84	-
Total (hybrid)	-	-	-	-	1261.64	948.49	-
Total (electric)	-	-	-	-	1680.40	1273.69	-

Table E.16: Weight and volume of the components of the MeOIH-fuelled SOFC-ICE combined cycle with a power split of 15-85

Component	Variant	Length [m]	Width [m]	Height [m]	Volume [m^3]	Weight [ton]	Amount installed
ICE (hybrid)	MAN 20V 28/33D STC (10 MW)	8.047	2.273	3.982	67.347	51.3	2
Genset (electric)	Wärtsilä 12V 32 (6.5 MWe)	10.7	3.06	4.13	135.224	100	3
SOFC	Bloom Energy Server (325 kWe)	8.961	1.238	2.494	27.668	14.8	14
E-motor (hybrid)	Siemens HV A compact plus (1.80 MW)	2.149	1.496	1.757	5.649	4.70	2
E-motor (electric)	Siemens HV-M (10.68 MW)	5.580	3.85	3.385	67.18	28	2
Gearbox (hybrid)	Wärtsilä TCH270	2.440	3.900	3.020	28.738	28	2
Gearbox (electric)	Wärtsilä SCH105	2.450	2.995	2.429	17.823	30	2
HEX	Low temperature air heater	1.250	0.560	0.560	0.116	0.209	14
	High temperature air heater	1.250	0.560	0.560	0.098	0.177	14
	Low temperature fuel heater	0.300	0.191	0.191	0.003	0.005	14
	High temperature fuel heater	0.500	0.194	0.194	0.005	0.008	14
	Economizer	0.500	0.203	0.203	0.005	0.009	14
	Evaporator	0.750	0.395	0.395	0.029	0.053	14
	Superheater	0.500	0.201	0.201	0.005	0.009	14
	Moisture separator	1.750	1.132	1.132	0.560	1.010	2
Blower	HR43	1.252	0.510	0.665	0.425	0.68	14
Fuel	Methanol	-	-	-	749.92	593.94	-
Total (hybrid)	-	-	-	-	1327.22	975.36	-
Total (electric)	-	-	-	-	1685.62	1235.26	-

Table E.17: Weight and volume of the components of the MeOH-fuelled SOFC-ICE combined cycle with a power split of 20-80

Component	Variant	Length [m]	Width [m]	Height [m]	Volume [m^3]	Weight [ton]	Amount installed
ICE (hybrid)	MAN 20V 28/33D STC (10 MW)	8.047	2.273	3.982	67.347	51.3	2
Genset (electric)	Wärtsilä 12V 32 (6.5 MWe)	10.7	3.06	4.13	135.224	100	3
SOFC	Bloom Energy Server (325 kWe)	8.961	1.238	2.494	27.668	14.8	19
E-motor (hybrid)	Siemens HV A compact plus (2.50 MW)	2.294	1.656	1.907	7.244	5.90	2
E-motor (electric)	Siemens HV-M (10.68 MW)	5.580	3.85	3.385	67.18	28	2
Gearbox (hybrid)	Wärtsilä TCH270	2.440	3.900	3.020	28.738	28	2
Gearbox (electric)	Wärtsilä SCH105	2.450	2.995	2.429	17.823	30	2
HEX	Low temperature air heater	1.250	0.560	0.560	0.116	0.209	19
	High temperature air heater	1.250	0.560	0.560	0.098	0.177	19
	Low temperature fuel heater	0.300	0.191	0.191	0.003	0.005	19
	High temperature fuel heater	0.500	0.194	0.194	0.005	0.008	19
	Economizer	0.500	0.203	0.203	0.005	0.009	19
	Evaporator	0.750	0.395	0.395	0.029	0.053	19
	Superheater	0.500	0.201	0.201	0.005	0.009	19
	Moisture separator	2.000	1.221	1.221	0.746	1.346	2
Blower	HR43	1.252	0.510	0.665	0.425	0.68	19
Fuel	Methanol	-	-	-	718.26	568.86	-
Total (hybrid)	-	-	-	-	1440.02	1033.10	-
Total (electric)	-	-	-	-	1795.23	1290.60	-

Table E.18: Weight and volume of the components of the MeOH-fuelled SOFC-ICE combined cycle with a power split of 25-75

Component	Variant	Length [m]	Width [m]	Height [m]	Volume [m^3]	Weight [ton]	Amount installed
ICE (hybrid)	MAN 16V 28/33D STC (8 MW)	7.127	2.273	3.982	59.647	43.6	2
Genset (electric)	Wärtsilä 16V 32 (8.6 MWe)	11.465	3.36	4.445	171.232	127	2
SOFC	Bloom Energy Server (325 kWe)	8.961	1.238	2.494	27.668	14.8	24
E-motor (hybrid)	Siemens HV A compact plus (3.15 MW)	2.294	1.656	1.907	7.244	6.65	2
E-motor (electric)	Siemens HV-M (10.68 MW)	5.580	3.85	3.385	67.18	28	2
Gearbox (hybrid)	Wärtsilä TCH270	2.440	3.900	3.020	28.738	28	2
Gearbox (electric)	Wärtsilä SCH105	2.450	2.995	2.429	17.823	30	2
HEX	Low temperature air heater	1.250	0.560	0.560	0.116	0.209	24
	High temperature air heater	1.250	0.560	0.560	0.098	0.177	24
	Low temperature fuel heater	0.300	0.191	0.191	0.003	0.005	24
	High temperature fuel heater	0.500	0.194	0.194	0.005	0.008	24
	Economizer	0.500	0.203	0.203	0.005	0.009	24
	Evaporator	0.750	0.395	0.395	0.029	0.053	24
	Superheater	0.500	0.201	0.201	0.005	0.009	24
	Moisture separator	2.000	1.366	1.366	0.933	1.683	2
Blower	HR43	1.252	0.510	0.665	0.425	0.68	24
Fuel	Methanol	-	-	-	682.27	540.36	-
Total (hybrid)	-	-	-	-	1529.92	1071.13	-
Total (electric)	-	-	-	-	1837.32	1296.53	-

Table E.19: Weight and volume of the components of the MeOH-fuelled SOFC-ICE combined cycle with a power split of 30-70

Component	Variant	Length [m]	Width [m]	Height [m]	Volume [m^3]	Weight [ton]	Amount installed
ICE (hybrid)	MAN 16V 28/33D STC (8 MW)	7.127	2.273	3.982	59.647	43.6	2
Genset (electric)	Wärtsilä 16V 32 (8.6 MWe)	11.465	3.36	4.445	171.232	127	2
SOFC	Bloom Energy Server (325 kWe)	8.961	1.238	2.494	27.668	14.8	28
E-motor (hybrid)	Siemens HV A compact plus (4.00 MW)	2.555	1.913	2.067	10.103	9.75	2
E-motor (electric)	Siemens HV-M (10.68 MW)	5.580	3.85	3.385	67.18	28	2
Gearbox (hybrid)	Wärtsilä TCH270	2.440	3.900	3.020	28.738	28	2
Gearbox (electric)	Wärtsilä SCH105	2.450	2.995	2.429	17.823	30	2
HEX	Low temperature air heater	1.250	0.560	0.560	0.116	0.209	28
	High temperature air heater	1.250	0.560	0.560	0.098	0.177	28
	Low temperature fuel heater	0.300	0.191	0.191	0.003	0.005	28
	High temperature fuel heater	0.500	0.194	0.194	0.005	0.008	28
	Economizer	0.500	0.203	0.203	0.005	0.009	28
	Evaporator	0.750	0.395	0.395	0.029	0.053	28
	Superheater	0.500	0.201	0.201	0.005	0.009	28
	Moisture separator	2.250	1.410	1.410	1.119	2.019	2
Blower	HR43	1.252	0.510	0.665	0.425	0.68	28
Fuel	Methanol	-	-	-	772.95	612.18	-
Total (hybrid)	-	-	-	-	1739.42	1213.62	-
Total (electric)	-	-	-	-	2041.10	1432.82	-

E.5. SOFC-GT MeOH

This section shows the weight and volume of each component in the MeOH-fuelled SOFC-GT combined cycle. For hybrid and electric propulsion the differences lie in the GT/genset, e-motor and gearbox. The total weight and volume for each power split is also given in the tables.

Table E.20: Weight and volume of the components of the MeOH-fuelled SOFC-GT combined cycle with a power split of 4.6-95.4

Component	Variant	Length [m]	Width [m]	Height [m]	Volume [m^3]	Weight [ton]	Amount installed
GT (hybrid)	GE LM500 (4.6 MW)	3.660	1.650	1.650	9.964	2.779	5
Genset (electric)	GE LM500 (4.2 MWe)	7.140	2.390	2.390	40.784	27.273	6
SOFC	Bloom Energy Server (325 kWe)	8.961	1.238	2.494	27.668	14.8	4
E-motor (hybrid)	Siemens HV A (0.355 MW)	1.577	0.770	0.695	0.844	1.43	2
E-motor (electric)	Siemens HV-M (10.68 MW)	5.580	3.85	3.385	67.18	28	2
Gearbox (hybrid)	Triple input/single output	-	-	-	82	80	2
Gearbox (electric)	Wärtsilä SCH105	2.450	2.995	2.429	17.823	30	2
HEX	Low + intermediate temperature air heater	1.000	0.608	0.608	0.092	0.17	4
	High temperature air heater	1.000	0.559	0.559	0.078	0.141	4
	Low temperature fuel heater	0.300	0.191	0.191	0.003	0.005	4
	High temperature fuel heater	0.500	0.194	0.194	0.005	0.008	4
	Economizer	0.500	0.203	0.203	0.005	0.009	4
	Evaporator	0.750	0.395	0.395	0.029	0.053	4
	Superheater	0.500	0.201	0.201	0.005	0.009	4
Blower	HR43	1.252	0.510	0.665	0.425	0.68	4
Fuel	Methanol	-	-	-	878.03	695.40	-
Total (hybrid)	-	-	-	-	1178.41	935.36	-
Total (electric)	-	-	-	-	1369.88	1038.95	-

Table E.21: Weight and volume of the components of the MeOH-fuelled SOFC-GT combined cycle with a power split of 10-90

Component	Variant	Length [m]	Width [m]	Height [m]	Volume [m^3]	Weight [ton]	Amount installed
GT (hybrid)	GE LM500 (4.6 MW)	3.660	1.650	1.650	9.964	2.779	5
Genset (electric)	GE LM500 (4.2 MWe)	7.140	2.390	2.390	40.784	27.273	5
SOFC	Bloom Energy Server (325 kWe)	8.961	1.238	2.494	27.668	14.8	9
E-motor (hybrid)	Siemens HV A compact plus (1.12 MW)	1.925	1.385	1.583	4.22	3.55	2
E-motor (electric)	Siemens HV-M (10.68 MW)	5.580	3.85	3.385	67.18	28	2
Gearbox (hybrid)	Triple input/single output	-	-	-	82	80	2
Gearbox (electric)	Wärtsilä SCH105	2.450	2.995	2.429	17.823	30	2
HEX	Low + intermediate temperature air heater	1.000	0.608	0.608	0.092	0.17	9
	High temperature air heater	1.000	0.559	0.559	0.078	0.141	9
	Low temperature fuel heater	0.300	0.191	0.191	0.003	0.005	9
	High temperature fuel heater	0.500	0.194	0.194	0.005	0.008	9
	Economizer	0.500	0.203	0.203	0.005	0.009	9
	Evaporator	0.750	0.395	0.395	0.029	0.053	9
	Superheater	0.500	0.201	0.201	0.005	0.009	9
Blower	HR43	1.252	0.510	0.665	0.425	0.68	9
Fuel	Methanol	-	-	-	765.76	606.48	-
Total (hybrid)	-	-	-	-	1207.05	931.15	-
Total (electric)	-	-	-	-	1357.74	1002.52	-

Table E.22: Weight and volume of the components of the MeOH-fuelled SOFC-GT combined cycle with a power split of 15-85

Component	Variant	Length [m]	Width [m]	Height [m]	Volume [m^3]	Weight [ton]	Amount installed
GT (hybrid)	GE LM500 (4.6 MW)	3.660	1.650	1.650	9.964	2.779	5
Genset (electric)	GE LM500 (4.2 MWe)	7.140	2.390	2.390	40.784	27.273	5
SOFC	Bloom Energy Server (325 kWe)	8.961	1.238	2.494	27.668	14.8	14
E-motor (hybrid)	Siemens HV A compact plus (1.80 MW)	2.149	1.496	1.757	5.649	4.70	2
E-motor (electric)	Siemens HV-M (10.68 MW)	5.580	3.85	3.385	67.18	28	2
Gearbox (hybrid)	Triple input/single output	-	-	-	82	80	2
Gearbox (electric)	Wärtsilä SCH105	2.450	2.995	2.429	17.823	30	2
HEX	Low + intermediate temperature air heater	1.000	0.608	0.608	0.092	0.17	14
	High temperature air heater	1.000	0.559	0.559	0.078	0.141	14
	Low temperature fuel heater	0.300	0.191	0.191	0.003	0.005	14
	High temperature fuel heater	0.500	0.194	0.194	0.005	0.008	14
	Economizer	0.500	0.203	0.203	0.005	0.009	14
	Evaporator	0.750	0.395	0.395	0.029	0.053	14
	Superheater	0.500	0.201	0.201	0.005	0.009	14
Blower	HR43	1.252	0.510	0.665	0.425	0.68	14
Fuel	Methanol	-	-	-	775.83	614.46	-
Total (hybrid)	-	-	-	-	1360.78	1020.98	-
Total (electric)	-	-	-	-	1508.62	1090.05	-

Table E.23: Weight and volume of the components of the MeOH-fuelled SOFC-GT combined cycle with a power split of 20-80

Component	Variant	Length [m]	Width [m]	Height [m]	Volume [m^3]	Weight [ton]	Amount installed
GT (hybrid)	GE LM500 (4.6 MW)	3.660	1.650	1.650	9.964	2.779	5
Genset (electric)	GE LM500 (4.2 MWe)	7.140	2.390	2.390	40.784	27.273	4
SOFC	Bloom Energy Server (325 kWe)	8.961	1.238	2.494	27.668	14.8	18
E-motor (hybrid)	Siemens HV A compact plus (2.50 MW)	2.294	1.656	1.907	7.244	5.90	2
E-motor (electric)	Siemens HV-M (10.68 MW)	5.580	3.85	3.385	67.18	28	2
Gearbox (hybrid)	Triple input/single output	-	-	-	82	80	2
Gearbox (electric)	Wärtsilä SCH105	2.450	2.995	2.429	17.823	30	2
HEX	Low + intermediate temperature air heater	1.000	0.608	0.608	0.092	0.17	18
	High temperature air heater	1.000	0.559	0.559	0.078	0.141	18
	Low temperature fuel heater	0.300	0.191	0.191	0.003	0.005	18
	High temperature fuel heater	0.500	0.194	0.194	0.005	0.008	18
	Economizer	0.500	0.203	0.203	0.005	0.009	18
	Evaporator	0.750	0.395	0.395	0.029	0.053	18
	Superheater	0.500	0.201	0.201	0.005	0.009	18
Blower	HR43	1.252	0.510	0.665	0.425	0.68	18
Fuel	Methanol	-	-	-	748.49	592.80	-
Total (hybrid)	-	-	-	-	1439.56	1063.05	-
Total (electric)	-	-	-	-	1594.16	1132.50	-

Table E.24: Weight and volume of the components of the MeOH-fuelled SOFC-GT combined cycle with a power split of 25-75

Component	Variant	Length [m]	Width [m]	Height [m]	Volume [m^3]	Weight [ton]	Amount installed
GT (hybrid)	GE LM500 (4.6 MW)	3.660	1.650	1.650	9.964	2.779	5
Genset (electric)	GE LM500 (4.2 MWe)	7.140	2.390	2.390	40.784	27.273	4
SOFC	Bloom Energy Server (325 kWe)	8.961	1.238	2.494	27.668	14.8	23
E-motor (hybrid)	Siemens HV A compact plus (3.15 MW)	2.294	1.656	1.907	7.244	6.65	2
E-motor (electric)	Siemens HV-M (10.68 MW)	5.580	3.85	3.385	67.18	28	2
Gearbox (hybrid)	Triple input/single output	-	-	-	82	80	2
Gearbox (electric)	Wärtsilä SCH105	2.450	2.995	2.429	17.823	30	2
HEX	Low + intermediate temperature air heater	1.000	0.608	0.608	0.092	0.17	23
	High temperature air heater	1.000	0.559	0.559	0.078	0.141	23
	Low temperature fuel heater	0.300	0.191	0.191	0.003	0.005	23
	High temperature fuel heater	0.500	0.194	0.194	0.005	0.008	23
	Economizer	0.500	0.203	0.203	0.005	0.009	23
	Evaporator	0.750	0.395	0.395	0.029	0.053	23
	Superheater	0.500	0.201	0.201	0.005	0.009	23
Blower	HR43	1.252	0.510	0.665	0.425	0.68	23
Fuel	Methanol	-	-	-	777.27	615.60	-
Total (hybrid)	-	-	-	-	1608.15	1165.12	-
Total (electric)	-	-	-	-	1762.76	1233.07	-

Table E.25: Weight and volume of the components of the MeOH-fuelled SOFC-GT combined cycle with a power split of 30-70

Component	Variant	Length [m]	Width [m]	Height [m]	Volume [m^3]	Weight [ton]	Amount installed
GT (hybrid)	GE LM500 (4.6 MW)	3.660	1.650	1.650	9.964	2.779	4
Genset (electric)	GE LM500 (4.2 MWe)	7.140	2.390	2.390	40.784	27.273	4
SOFC	Bloom Energy Server (325 kWe)	8.961	1.238	2.494	27.668	14.8	28
E-motor (hybrid)	Siemens HV A compact plus (4.00 MW)	2.555	1.913	2.067	10.103	9.75	2
E-motor (electric)	Siemens HV-M (10.68 MW)	5.580	3.85	3.385	67.18	28	2
Gearbox (hybrid)	Triple input/single output	-	-	-	82	80	2
Gearbox (electric)	Wärtsilä SCH105	2.450	2.995	2.429	17.823	30	2
HEX	Low + intermediate temperature air heater	1.250	0.609	0.609	0.116	0.209	28
	High temperature air heater	1.250	0.560	0.560	0.098	0.177	28
	Low temperature fuel heater	0.300	0.191	0.191	0.003	0.005	28
	High temperature fuel heater	0.500	0.194	0.194	0.005	0.008	28
	Economizer	0.500	0.203	0.203	0.005	0.009	28
	Evaporator	0.750	0.395	0.395	0.029	0.053	28
	Superheater	0.500	0.201	0.201	0.005	0.009	28
Blower	HR43	1.252	0.510	0.665	0.425	0.68	28
Fuel	Methanol	-	-	-	794.55	629.28	-
Total (hybrid)	-	-	-	-	1773.02	1266.51	-
Total (electric)	-	-	-	-	1881.13	1300.99	-